The Active Control of Low Frequency Room Modes

M.R.Avis

School of Acoustics and Electronic Engineering
University of Salford
Salford
M5 4WT

Submitted in part fulfilment of the regulations governing the degree of Ph.D.

November 2000

'...My Child, there is something else to watch out for. There is no end to the writing of books, and too much study will wear you out...'

Ecclesiastes 12v12, GNB

Contents

Acknowledgements

The author would like to acknowledge the Engineering and Physical Sciences Research Council for the financial support given to this work in its early stages, and the subsequent funding provided by Genelec OY and the Department of Applied Acoustics.

The support and encouragement provided by RB, Dr David Saunders, Dr Paul Darlington, family, friends and colleagues at the Department has, of course, been invaluable.

Glossary of Symbols

a	source radius (m)
Bl	electrodynamic force factor (NA^{-1})
c	speed of sound in air at STP (ms^{-1})
$c(z)$	z-domain controller transfer function
C	electrical capacitance (F), plant transfer function
C_{AB}	acoustic compliance of air volume in sealed cabinet (m^5N^{-1})
C_{MD}	loudspeaker mechanical suspension compliance (mN^{-1})
D	sample delay
d_k	desired filter output
e	voltage (V)
e_k	adaptive filter error
F	force (N)
F_1	feedback compensation transfer function
F_d	desired impedance specification filter transfer function
G	amplifier transfer function
H	desired primary / secondary source velocity transfer function
I	inverse desired impedance scale factor
i	electrical current (A)
j	complex operator
k	wavenumber (m^{-1}) (as subscript $\__k$ - digital time operator)
k_n	modal eigenvalue
L	duct length (m), electrical inductance (H), loudspeaker transfer function
M_{MD}	Loudspeaker moving mass (kg)
p	acoustic pressure (Pa)
P_i	complex pole location
$p_{p,r}, p_{s,r}$	pressure at $\boldsymbol{r}$ due to primary, secondary source
Q	source strength (m^3s^{-1}), resonant quality factor
q_p, q_s	primary and secondary source strengths
R	electrical resistance (Ω)

R_E	loudspeaker DC coil resistance (Ω)
R_{MD}	loudspeaker mechanical suspension resistance (Nsm^{-1})
R_r	acoustic radiation resistance
r	distance from source (m)
$\boldsymbol{r}$	receiver location
$\boldsymbol{r_0}$	source location
S	duct cross-sectional area (m^2)
S_D	loudspeaker diaphragm area (m^2)
T_{60}	reverberation time (s)
U	volume velocity (m^3s^{-1})
u	acoustic particle or mechanical velocity (ms^{-1})
V	room volume (m^3)
$v_{in,p}$, $v_{in,s}$	primary and secondary path power amplifier input voltages
W	adaptive control filter transfer function, power absorbed by controller
$w_{0,1,2...}$	filter weight
X_r	radiation reactance
x,y,z	Cartesian room coordinates
x_p, x_c	control filter inputs
y_p, y_c	control filter ouputs
Z	generalised impedance
Z_i	complex zero location
Z_m	mechanical impedance (Nsm^{-1})
Z_{RAD}	loudspeaker radiation impedance (Nsm^{-1})
Z_{source}	mechanical source impedance
Z_a	acoustic impedance (Nsm^{-5})
$Z_{p,r}$, $Z_{s,r}$	primary and secondary path specific transfer impedances
z	z-domain operator
α	decay constant
α_x	complex eigenvalue - imaginary part
β_x	complex eigenvalue - real part
δ	Kronecker delta function
δ_n	modal damping constant

ϵ	axial/tangential/oblique modal energy scale factor
ζ	specific boundary impedance ($Z_a / \rho_0 cS$)
ξ	specific boundary impedance - real part
η	specific boundary impedance - imaginary part
θ	generalised angle
Λ_n	eigenvector normalisation constant
ρ_0	density of air at STP (1.21 kgm^{-3})
χ_n	eigenvector integration constant
ψ_n	modal eigenvector
ω	angular frequency
ω_n	modal natural frequency

Abstract

The normal modes of an enclosed sound field introduce spatial, time and frequency domain artefacts to signals reproduced in such an environment, such that undesirable colouration of these signals may be perceived. Modal density with respect to frequency is minimal at low frequencies, and in small rooms this means that widely spaced discrete modes dominate sound reproduction up to frequencies of the order of one hundred Hertz. The removal of unwanted colouration is not straightforward; conventional passive absorptive treatments offer poor performance at low frequencies, and where their use is attempted costs (in terms of space consumption) may be prohibitive.

This Thesis presents a series of investigations into the active control of low frequency acoustic resonance, using both adaptive digital filters in feedforward and feedback configurations, and fixed feedforward controllers. The adaptive filters are based around the active control of acoustic impedance, using hardware available to the project as the product of previous work at Salford University. The application of the technique to the control of modes in a three dimensional environment is however novel. The fixed feedforward controllers use a novel application of an analytical modal decomposition of an enclosed soundfield as the basis for a digital IIR acoustic model. This model is utilised in order to manipulate the locations of z-plane poles and change the behaviour of the sound field.

These two techniques are applied to a number of control tasks in one- and three-dimensional test environments, using numerical models and practical hardware implementations. The tasks include pressure cancellation, and more usefully the control of frequency domain Q-factor and corresponding modal decay times. It is shown that active impedance methods are superior in the duct; the fixed feedforward controllers suffer from the combined effect of the finite source impedance of practical control loudspeakers with changing and strongly modal radiation loads. In the room, both techniques are shown to be capable of useful reductions in modal Q-factor and decay time. Fixed methods offer control over a defined spatial volume, and adaptive techniques may be further developed by the refinement of the control hardware.

Chapter 1

Introduction

When audio signals are reproduced in an enclosed space, the boundaries of that space cause the soundfield to exhibit resonant behaviour which affects the way in which sound is perceived in that space by a listener. These resonances are known as the normal modes, which form a component of the steady state response of a room and are also responsible for the decay of the soundfield. At low frequencies, each normal mode introduces properties to the space which can be usefully separated into frequency, space and time effects.

The presence of a mode introduces an irregularity into the frequency domain response of a room, such that the pressure at most points in the room is modified by the mode. Although these frequency response irregularities can be removed by equalizing the sources which excite the space, such equalization does not address the spatial component of room modes. Frequency response irregularities change with location, such that two persons listening in the same space may be presented with greatly differing spectral balances. Equally, an individual moving in the room experiences a differing spectral balance as they move.

Modes are related to the impulse response of the room by the inverse Fourier transform, and so are associated with the generation of components of reverberation. Modes with high Q-factor are responsible for the greatest frequency domain irregularities and are associated with long tonal decay artefacts. It is generally recommended that reverberation times are controlled to be below a certain level for rooms used for critical listening [1,2], although undesirable subjective effects are connected with working in an environment which is too anechoic. Likewise in such a space as a studio control room, colouration introduced by frequency domain irregularities in the steady state response is considered problematic. The greatest difficulties occur at low audio frequencies when modes are widely spaced and have long decay times [3].

In a one-dimensional enclosure, natural frequencies form a harmonic series and are equally spaced with respect to frequency. In a room, each of the three dimensions is associated with a harmonic set of modes, and others are created by interactions between the dimensions. Mode spacing is therefore no longer constant and is a function of the aspect ratio of the room; on average, the modal density is directly proportional to frequency. In very large rooms the lowest frequency modes of the space which are widely spaced and exhibit strong spatial pressure dependance fall at sub-audio frequency. Above 20 or 30 Hz the modal density is sufficiently high that individually resolvable modal components are not a problem, and by a few hundred Hertz the modes blend to form the true diffuse field.

At mid and high audio frequencies, the modal density of small listening spaces is likewise so high that individual modes are not perceived. The adjacent modes sum together to give a broadly frequency independent response. However, the fundamental resonances of small rooms fall inside the audio bandwidth, and the modal density is so low that the effects of individual modes are clearly audible. In order to reduce the influence of a discrete mode, it is necessary to add an energy dissipation path to the room, coupled to the mode which is to be controlled. Unfortunately, the absorption of low frequency sound is difficult or impossible using conventional passive acoustic treatments, and can involve high cost and the waste of large volumes of otherwise architecturally useful space.

In this Thesis, a single secondary electroacoustic source is introduced into a space and controlled in such a way as to reduce the frequency, spatial and time domain artefacts associated with discrete low frequency modes. The aim is the production of a controller which may operate on acoustic or electroacoustic signals, although one technique employed sacrifices some of this generality in order to achieve greater simplicity and stability in operation. The work is concerned with the use of acoustic superposition techniques rather than pre-filtering or deconvolution based systems operating on the primary signal path alone.

The performance of alternative control systems is assessed in terms of their ability to reduce the Q-factor of individual modes and generate corresponding reductions in the modal decay time, implying an increase in modal damping. Reductions in the spatial variance of pressure are investigated, with a view to controlling the largest possible volume within the space. However, the control systems investigated are designed to operate as self-contained control

sources, with no reliance on the distributed fields of error sensing microphones incorporated into some Active Noise Reduction systems.

The study is introduced in terms of a review of published literature in Chapter 2, broken down into the areas of low frequency room acoustics, the history of active control, active absorption, inverse filtering and the subjective effects of resonance. The theory of low frequency room acoustics forms the basis of Chapter 3, where the fundamental mathematics [eg. 6,10,11] which underpin the subsequent active control applications are laid out. In Chapter 4, the first of these applications is reviewed.

Two alternative active control techniques are investigated in this Thesis. The first, Active Impedance Control, uses systems available as the product of earlier research at the University of Salford. These systems drive the surface impedance of a controlled electroacoustic radiator towards a user-specified target value, and may be configured as feedforward or feedback devices. They are constructed around single-channel filtered-x LMS adaptive filter algorithms. The application of active impedance control to one-dimensional acoustic systems has already been reported [eg. 37,41,72], but the use of the technique to control a three dimensional environment is novel. Chapter 4 is the final review chapter in the Thesis, and provides some background on the design and use of the systems which are then investigated in the novel context of the three-dimensional environment in Chapter 8.

The second control technique uses fixed filters rather than adaptive technology to determine an appropriate transfer function between the source strengths of primary and secondary radiators. It has been shown that the control laws applicable in this instance are related to those required for active impedance control [51]. This is a feedforward method, which uses a novel exploitation of an analytical modal decomposition of the enclosed soundfield to form a digital model of the room based on second order IIR biquad filter sections, and is introduced in Chapter 5.

It is shown how the models are exploited in order to control the Q-factor and decay time of modes within the space, by the deliberate re-specification of modal pole locations. This technique is also novel. Because the controllers rely on biquad models of the room

acoustics, they are referred to by the shorthand ' Biquad fit controllers'. Problems of modelling systems with small termination impedance using s- and z-plane modal decompositions are considered, in the context of an acoustic waveguide.

A one-dimensional environment is retained in Chapter 6 where models are used to assess the anticipated performance of Biquad fit methods, using Impedance control as a benchmark. A relationship between modal Q-factor and termination impedance facilitates this comparison, which is made for a number of different control targets and system topologies. Practical biquad fit control is then assessed in a duct in Chapter 7, with the aim of developing the technique and facilitating its use in the more challenging three-dimensional environment.

In Chapter 8, Active Impedance control techniques are applied in the novel context of the three dimensional room. Following a short discussion of surface impedance models, two control applications are considered - real surface impedances and complex surface impedances. Control performance is discussed both in terms of modal Q-factor and modal decay time.

These two metrics are also employed in the analysis of Biquad fit control in a three dimensional environment, in Chapter 9. Three control applications are considered - point cancellation, modal cancellation / replacement, and the Q-factor modification filters introduced in the context of the duct in Chapter 5. Controllers are tested which operate on just one mode at a time, and which control more than one mode simultaneously. The incorporation of loudspeaker electromechanical transfer characteristics into the control filters is investigated as a means to increase the accuracy of the biquad room models, and thereby improve the performance of the resulting control filters.

Finally in Chapter 10, the performance of Active Impedance and Biquad fit controllers is summarised, compared and contrasted in one- and three- dimensional acoustic environments. The remaining difficulties and newly identified opportunities highlighted throughout the text are collated and form the basis of several suggested programs of further work.

Chapter 2

Literature review

2.0 Introduction

The field of the Active Control of Sound is well established and extremely wide. Beneath this broad umbrella are contained subject areas as diverse as the study of digital signal processing algorithms, transducer science, room acoustics, numerical optimisation and vibro-acoustical systems, to name but a few. The applications of active control are likewise varied, ranging from the outright minimisation of a particular soundfield, through to manipulations aimed at changing the subjective spatial impression of a space, or as is the case in this thesis, altering the quality of acoustic resonances. This review will therefore aim to give an overview of the history of the field with reference to particularly significant work and review papers, but will thereafter concentrate on those subject areas of particular relevance to the work presented in this thesis. The subject areas are broken down into the following: Low Frequency Room Acoustics; Active Absorption; Equalisation, Inverse Filtering and Deconvolution; and the Subjective Effects of Resonance.

2.1 Low frequency room acoustics - the wave solution

Underpinning any study of the control of low frequency room phenomena, the theory of the normal modes of vibration of air in an enclosed space is fundamental to the derivation of successful control strategies and representative means of the assessment of their performance. Of particular interest is the so-called wave solution, where ideas borrowed from Fourier analysis facilitate the decomposition of pressure into an infinite number of orthogonal components with unique spatial and frequency domain behaviour, and corresponding time domain decay characteristics. It is interesting to note that early work

initiated by a small number of key figures continues to be regularly cited by current researchers, and it has not been necessary to re-visit the basic physics of modal behaviour for perhaps 50 years.

Amongst the first references containing a full and sufficient modern analysis of low-frequency acoustic modal behaviour is that of Morse and Bolt [4] (later of Bolt, Beranek and Newman), in which as early as 1944 the eigensolutions for air in an enclosed space were laid out. The article, entitled 'Sound Waves in Rooms', forms a definitive review of much early acoustic research and in essence is more like a 77 page acoustics text-book than a journal paper. The use of conformal transformations in the absence of numerical solutions to some of the mathematical content makes the material appear dated, but in fact the underlying formulae are those employed by recent research [eg. 5]. The work on non-rigid boundary conditions is especially useful and is more clearly laid out than in more modern texts.

Much of the work in this paper appears in Morse's seminal 1948 text, 'Vibration and Sound' [6]. More wide-ranging in scope, some of the work on room acoustics is rather dense and the wide use of unorthodox symbols (for example: ν is used for frequency) can leave the reader struggling for familiar ground. The mathematics are however extremely thorough and give so much detail that it is sometimes difficult to see how a model may be best approximated.

Morse's work is incorporated into other texts [7,8], which expand the scope of the theoretical models in some circumstances, but which remain densely mathematical and perhaps not easily approached by those with a more practical interest in room acoustics. Independently the work of Doak [9] also presents a mathematicians view of the enclosed soundfield, but with the practical application of determining metrics for the ratio of peak to average and peak to minimum spatial pressures.

Doak introduces the idea of analysing an enclosed soundfield in terms of the addition of travelling and standing wave components - a concept utilised by Maa [24,25] and discussed in Chapter 7 of this Thesis. In addition to an Eigenfunction analysis of the enclosed soundfield and an unusual derivation of shape functions for a rectangular enclosure, a

number of interesting observations regarding the spatial- and frequency- domain variance of pressure are presented as related to the shape of the enclosure. In particular, Doak asserts that

> *'...it is impossible to alter the oscillatory nature of the soundfield by changing the wall shape, and there is a strong inference that changes of any practical utility in the distribution and spacing of the null surfaces cannot be produced by changes in wall shape...the shape of a typical standing wave peak cannot be "squared up" by making the wall surfaces "diffuse"'.*

The work of Schroeder is referred to in relation to the latter point, since there it is suggested that a small amount of irregularity in wall shape is sufficient to randomise the distribution of peak heights. However the utility of surface diffusion is shown to be minimal, and it is apparent that at low frequencies, alterations in room dimensions cannot be employed to break up modal behaviour, leaving passive absorption and active methods as the only candidates for control.

Standard undergraduate acoustic texts also contain material of interest. The second edition of the widely read 'Fundamentals of Acoustics' by Kinsler and Frey [10] is perhaps more useful than the third edition, rewritten by Coppens and Sanders. In particular, useful material on standing waves in enclosures is greatly attenuated in the later text, and a discussion of the damping of standing waves is omitted altogether. These sections are helpful in that they contain much explanatory text, although the mathematical analysis is not as comprehensive as that presented by authors such as Morse.

Lying somewhere between these two approaches is Kuttruff's excellent 'Room Acoustics' [11]. This book presents a full treatment of the hard-walled rectangular enclosure, in terms of a modal decomposition and an analysis of the corresponding reverberant decay. The section on damped oscillations is curtailed in the third edition, although material in the earlier works is incomplete and graphical data concerning the shape functions applicable to non-rigid boundary conditions is potentially misleading. Whereas Kuttruff, and Kinsler and Frey, both give a good introduction to the technique of modal decomposition and derive workable formulae for the frequency and spatial characteristics of the enclosed soundfield, the work of Morse is more helpful in investigating more complex problems with soft walls and non-rectangular geometries.

One relatively recent text combines an analysis of low frequency room acoustics with a thorough investigation of active noise control. Nelson and Elliot's 'Active control of sound' [12] provides a useful resource, and makes use of the approaches of Morse and Kuttruff in establishing a model for the active control of low frequency enclosed soundfields. Because the work forms a small part of a text whose main object is a discussion of active control, the material is a little dense and is perhaps best approached using another of the source texts. The matrix approach to a solution of linear systems of equations used by the book is taken from earlier published research [eg.18], and is more clearly laid out in these papers.

The integration of the analysis of the enclosed soundfield with material concerning its active control enables the rapid development of control laws and desired responses in a number of different environments. Starting with the one dimensional enclosure, the authors go on to look at a two-dimensional 'room' (using the work of Bullmore [5,21]) as a simplification of the more commonly encountered three-dimensional case. Throughout the book, the text draws heavily on the journal publications of the authors and their collaborators. This material encompasses active absorption (eg. [36,39]) and a number of papers concerned with the active minimisation of noise in a room, which are reviewed in the following short history of the field.

2.2 A short history of active control

The origin of the active control of acoustic signals is found in a German patent *DRP 655508* filed in 1933 by one Paul Leug [13]. The patent and its US counterpart form the subject of an interesting historical paper by Guiking [14], himself an investigator of active control at the University of Göttingen. In a review of his professional life, Guiking highlights the difficult political circumstances which eventually drove Leug to abandon physics and train as a medical doctor. Although the Nazi administration originally considered active control to be of military significance, problems of generating sufficient volume velocity with loudspeakers to silence aircraft and artillery (quite apart from solving the acoustics of these problems and obtaining a suitable reference signal) meant that a working system did not appear in the literature until many years later. De Heering [15] comments that a Frenchman, H. Coanda, may have preceded Leug's patent application by a number of months, but

nevertheless it is the German physicist who is widely credited with the invention of active noise control.

The next mention of active techniques in a paper concerned with acoustics is by Olson [32], but since this paper specifically considers the active *absorption* of sound it is considered in section 2.3. The technology is based around simple analogue circuits employing feedback, and it was not until the revolution in the availability and cost of digital computers in the late 1970s and early 1980s, and corresponding advances in the field of digital signal processing, that the complex filtering requirements inherent in many active control applications became realisable. At this point in time the field expanded extremely rapidly. The following papers are a subset of those concerned with the attenuation of acoustic signals within enclosed environments, since these are most relevant to this Thesis.

Amongst the first of this new wave of published work, Warnaka *et al.* [16] consider the *cancellation* of unwanted noise within an interior space. The maximum possible attenuation is required of sinusoidal and broad-band soundfields, using in the first case manual adjustments of a control signal magnitude and phase, and in the second an 'automatic adaptive noise canceller'. Results are presented which suggest that 20-35 dB global pressure reductions may be achieved throughout a model fuselage and within a reverberation room, in the latter case across a broad bandwidth of 50-350 Hz.

Unfortunately these measurements are presented in the context of an extremely brief conference paper, where a full experimental method is not given. No details of measurement locations, control system design, control law or reference signal derivation appear, and comparison with later authors suggests that the results are misleading. The broadband reverberant reductions especially are so large as to suggest that the measurement must have been made at the (assumed) error sensing microphone, and would not be anticipated over significant spatial volumes. The large pressure reductions in the model fuselage are only obtained using sine-tone excitation where the sources are large compared to the model dimensions. The reduction of the fuselage to a one-dimensional waveguide where the velocity of the entire terminations may be controlled appears to be an over-simplification, and the degree of attenuation is perhaps not as remarkable as might at first be thought.

More thorough presentations are made by investigators at the ISVR, Southampton, under the leadership of the aforementioned Nelson and Elliot. An article in the Journal of the Acoustical Society of America [17] is concerned with the active suppression of acoustic resonance. The control laws associated with the acoustic virtual earth (pressure release), characteristically absorbing termination and the minimization of acoustic potential (or total) energy are compared in a one-dimensional waveguide. The object of control is the minimisation of the total energy in the duct, broken down into potential and kinetic components - in practice this corresponds to the cancellation of the resonant soundfield. The article is very clearly written; especially helpful are the inverse Fourier transforms of the frequency domain transfer functions relating primary and secondary source strengths in each case.

A time-domain interpretation of the action of the secondary source in response to an incident pulse differentiates between each control action, and clearly illustrates why the minimisation of acoustic energy implies an acausal filter function. The best reduction of the enclosed soundfield obtained using a causal system is shown to be given by the absorbing termination. It is suggested that in the duct this corresponds to maximum power absorption, although reference to Mazzola [42] indicates that this condition is achieved by controlling the surface impedance to equal the negative conjugate of the (modal) in-duct radiation load, meaning that 'maximum absorption' and the absorbing termination represent different control applications. Pressure release is shown to be an inappropriate target function since the halfwave duct resonances are replaced by a quarter wave set, although other authors have subsequently experimented with the acoustic virtual earth in conjunction with passive absorptive treatments [55].

Source locations are recommended on the basis of coupling a velocity source into high modal input impedances, and the problems of uniquely specifying an optimal set of transfer functions between multiple secondary sources are outlined. As a practical strategy towards the minimisation of acoustic potential energy, it is suggested that multiple error sensors are distributed throughout the enclosed volume and the sum of the squared pressure is minimised - this is shown to approximate to an optimal reduction in acoustic potential energy irrespective of source location. Results are encouraging, but rely on fields of distributed pressure sensors which may limit the utility of the method in practice.

A trio of papers presented in the Journal of Sound and Vibration by Nelson, Elliot, Bullmore and Curtis are concerned with the active minimisation of harmonic enclosed soundfields, broken down into theory, simulation and experimental measurement [18,20,21]. It is important to note that the aim is specifically pressure cancellation, rather than the explicit control of the quality of low frequency resonance, and that only steady-state signals are considered - the control of a time-varying primary source and the resulting dynamic issues are not covered.

In the first paper [18], a straightforward modal decomposition is used to model the enclosed soundfield. Upon the introduction of secondary sources, vector / matrix notation complicates things for readers unfamiliar with such conventions, but permits the elegant exposition of the control problem. A useful introduction to matrix algebra and the solution of systems of linear equations is provided by Aitken [19].

It is shown that if the number of secondary sources is equal to the number of modes, total cancellation can occur regardless of the primary source distribution - unfortunately a modal decomposition remains approximate unless an infinite summation is adopted, which in practice limits the degree of attenuation possible. As in the previous paper, the minimisation of acoustic potential energy (in practice the sum of squared pressures from a large microphone array) is proposed as a practical control task, and this task is cast in terms of vectors of secondary source strengths and the respective coupling terms into the modal amplitudes. It is further shown that a unique minimum value of the enclosed acoustic potential energy exists, specified by one value of the vector of secondary source strengths which turns out to be real compared to the primary source strengths.

A matrix form of the soundfield due to a point source in a lightly damped enclosure (after Morse [6]) is developed, which illustrates the use of the matrix algebra very clearly and forms the basis for the work presented in the authors later book 'Active control of sound' [12]. The model is then applied to the solution of the minimisation problem at high modal densities, where the excitation lies above the 'Schroeder cut off frequency' [20]. It is shown that appreciable reductions in the total time-averaged acoustic potential energy can only be obtained if the primary and secondary sources lie within one half-wavelength of each other. Models at lower modal densities more relevant to this Thesis are presented by Bullmore *et*

al. in the second paper [21] - a computer simulation of the two dimensional enclosure referred to by Curtis [17] in the earlier work.

Of all the published work referred to in this review, Bullmore's paper probably contains the most useful collection of material which informs the control applications attempted in this Thesis. A precis of the matrix mathematics outlining the modal control problem is given from Part I [18], but rather than employing a point source, a rectangular piston is chosen which alters the form in which the source shape function appears in the modal decomposition. Elemental monopole contributions to the shape function excitation are summed over its surface; in practice a two-dimensional integration is performed of cosine eigenvectors over the surface of the piston source, and the resulting modal input impedance differs markedly from the point source case.

It is clearly shown that for a point source, a modal decomposition of *radiation impedance* requires an infinite number of modes. Because the piston source extends over a finite area, residues of high frequency modes may be excited over a considerable proportion of their wavelength. Therefore a lower number of coherent residues add at the source, and a smaller number of modes may be used in the decomposition. These ideas present an interesting alternative to the method of Maa [24] in modelling the direct component of pressure radiated close to a source.

Although the control task in Bullmore's paper is the minimisation of harmonic enclosed soundfields, the discussion of the spatial variance in sound pressure and the influence of secondary source location form useful background reading. The futility of control source locations on modal pressure nodes is perhaps obvious, but their location near to such points is also shown to be unwise. The increased velocity required to couple into low modal input impedances may strongly excite residues of neighbouring resonances with antinodal pressure distribution at these positions. The two-dimensional enclosure enables useful three-dimensional pressure plots (two spatial axes and one for magnitude pressure) which illustrate these points very clearly, especially in the more complex scenario of multiple secondary sources.

Of less direct relevance is work concerned with the minimisation of pressure at a number of discrete sensor locations, as a practical approximation of the energy minimisation task. It can briefly be summarised that corner sensor locations offer the most economic route to such an approximation, and that these locations offer reasonable performance even where modal degeneracy means that the pressure response is made up of two or three dominant contributions. It is also shown that even where modes are degenerate, they may be controlled using a single secondary source so long as the primary modal contributions at the source have the same relative phase and roughly equal amplitudes - this is an important result and is relevant to practical results presented in Chapter 7.

The utility of the models upon which these simulations are based is tested in the last of the three papers [22], where measured results are compared to those predicted by theory and with computer simulation. The primary field is set up using a sine tone oscillator, and a real-time control system used to minimise the sum of the squared pressure at a number of microphone locations using up to three secondary sources. It is noted that the source loudspeakers have finite internal impedance, with the result that the operation of one is likely to influence the dynamics of the others. Coupling between sources is built into the mathematics upon which the controller is based; whilst the linear behaviour of sources is not called into question and control may be still be possible it can form a substantial obstacle to plant characterisation and is discussed further in Chapters 6 and 8.

Because the acoustic stimulus is a steady pure-tone signal, the derivation of control signals can be elegantly arranged. Sin and Cos quadrature components are fed to a digitally controlled step attenuator, which alters the relative magnitude of each signal fed to each loudspeaker and so defines their relative magnitude and phase. These are controlled in a multi-dimensional optimisation problem, where the cost function is a DC signal proportional to rms pressure summed over the error microphones. Each secondary source occupies two dimensions (effectively a_1 and b_1 of a Fourier synthesis), and a 'pattern search' algorithm performs the minimisation, although it is noted that gradient descent methods may also be used.

A small two dimensional scale model enclosure is used for the experiments, and it is relatively easy to compare measured results with theoretical predictions - even the spatial

variability of the soundfield is quickly observed using a mobile 5 microphone array. Agreement is very good - it is clearly demonstrated that source and error microphone must couple well into the mode under control, and that control of pressure at a 'dip' in the measured transfer impedance where two modal contributions are in antiphase, cannot be realised. Although the minimisation of pressure over 'a range of frequencies' is reported, this is actually accomplished by repeated convergence on a sine tone which is sequentially incremented in frequency. It is not clear whether causal control filters may be specified with the correct transfer functions to control broad-band signals.

This question is addressed in a paper by Nelson *et al.* from 1988 [23], which investigates the control of stationary random, rather than harmonic, enclosed sound fields. A time-domain analysis is employed throughout which necessitates the use of convolution-integral equations and in such a short paper makes the presentation rather dense. It is claimed that the earlier sine-tone work is '*entirely adequate for the analysis of problems involving the control of deterministic sound fields*' which cannot be true - a deterministic sound field may contain many frequency components, and a control system which can only be optimised on a pure tone will have arbitrary response at other frequencies which may well enhance rather than attenuate the chosen cost function. Nevertheless, it is shown that in a one-dimensional system the best causal control results from the adoption of an absorbing termination. This echoes the earlier result of Curtis *et al.* [17] who derive the same result with considerably clearer presentation in a frequency domain analysis.

A frequency domain approach is taken by Maa [24] in an interesting paper where a conventional modal decomposition after Morse [6] is augmented by a term explicitly designed to account for the direct field radiated by a source. It is claimed that this step '*completes the solution of the wave equation*' although this is not correct - each orthogonal mode satisfies the wave equation individually and a spherically divergent term is unable to meet the requirements of the boundary conditions of an enclosure. However, the technique does enable the pressure adjacent to a source in a modal environment to be rapidly approximated without recourse to large and time consuming modal summations. This technique is investigated further in Chapter 7.

Maa presents further work in this area in a later paper [25], where incorrect assumptions concerning the formation of a modal decomposition in relation to a direct / reverberant division of sound energy are more clearly revealed. A rather simplistic control system is also proposed where a microphone and control source are collocated in a room corner, and an analogue negative feedback controller is used in attempts to minimise the global primary sound field. Pressure reductions at the reference microphone location of the order of 10dB are shown, but these results are no more significant than the much earlier work of Warnaka *et al.*[16]. Maa notes that his feedback design suffers from loop instability problems, and suggests that improvement is possible '*...by eliminating the direct wave feedback completely...e.g. with the help of a recognizer* [sic] *circuit to sigle* [sic] *out the direct wave...noise reduction is then unlimited...*' No indication is given of the design of such a circuit, and no consistent scientific basis is shown for its necessity, or indeed for its predicted outcome.

More rigorous investigations are reported by Johnson and Elliot [26] in an application which approaches the problem of global pressure cancellation by minimising the primary and secondary source power outputs. It is shown that minimisation of acoustic potential energy, and minimisation of total source power output, in practice produce very similar results. In the single channel case, it is only necessary to consider secondary source power output in order to uniquely specify the transfer function between primary and secondary source strengths, which results in an overall minimisation in radiated power - surprisingly this occurs when the secondary source power output is equal to zero. The added constraint that the source strengths must have a real relationship enables a control signal to be optimised where only one dimension - amplitude - must be considered.

The practical supporting experiments in this paper require the transduction of radiated power, which necessitates pressure *and velocity* measurements. This is true of the impedance-sensing systems investigated in this Thesis, and Johnson's suggested velocity transduction methods [67,68] are considered in Chapter 6. The practical system was set up in a large enclosure instrumented with a 32-microphone array, which enabled an assessment of the declared aim of a minimisation of global mean-square pressure. The system was tested using a sinusoidal steady-state tone and manual adjustments of secondary source strength, leading to the same limitations in generality as noted for earlier work [18,21,22] -

some suggestions are made for adaptive filter optimisations in order to automate filter convergence.

Results are only reported at one frequency, which lies between the normal modes of the enclosure. When the secondary source is located remote from the primary, small reductions are reported in global acoustic potential. No thorough discussion of modeshapes and coupling is attempted, but following Bullmore [21] it is perhaps not surprising that where individual modal residues have varying magnitude and phase, control performance is poor. Where the sources are located close together, much larger global pressure reductions are reported.

The mechanism of control is not discussed, but it appears that forcing total pressure and velocity at the secondary source to be in quadrature will by reciprocity result in a purely imaginary radiation impedance at the neighbouring primary source, and so no total power will be radiated. This is equivalent to an early result noted by Ford [33]; later researchers have also reported similar conclusions while investigating active absorption in the context of enclosed pressure minimisation [36,43]. The technique has the major limitation that the secondary source acts like a purely reactive passive element and so cannot influence the Q-factor or decay rate of the resonant modes

Much of the work in their preceding papers is summarised in Nelson and Elliot's book 'Active control of sound'[12]. Having published papers on such a broad range of active control problems it is not surprising that they should be collected into what forms a thorough treatment of a variety of control tasks in different acoustic environments. These are not constrained to low-frequency modal enclosed soundfields, and the book includes interesting sections on control in diffuse environments - whilst not strictly relevant to this Thesis, the interested reader is referred to this book and subsequent work [eg. 27,28]. The former paper contains a thorough treatment of the on- and off- axis behaviour of radiating pistons which is of general interest, and the latter deals with the total sound field in an enclosed space as the sum of direct and reverberant components, which is a technique considered in Chapter 7.

The active control of sound in enclosed spaces is compared to more conventional passive techniques in a conference paper by Herzog *et al.*[29]. These authors have a background in theoretical room acoustics and this is evident in the paper - the damping offered by active and passive sources is considered in terms of coupled modal behaviour in a sparse mathematical treatment which does not easily translate into the results which are presented alongside. Passive resonant sound absorbers are shown to have a response very similar to the 'dynamic absorbers' familiar from passive vibration control. The addition of a system with its own resonance very close to that of the original system adds a degree of freedom and where suitable loss mechanisms are incorporated results in the creation of two new modes above and below the original resonance. Broadband control is shown to require banks of resonators, each tuned to a series of frequencies spanning the range of interest.

Full details of the active system with which passive control results are compared are not given, although it appears to have feedback configuration and to drive a dipole secondary source. Some attenuation of individual modes is in evidence, although others are enhanced. The choice of a dipole control source is interesting - a baffled loudspeaker with no enclosure is used which simultaneously excites each modeshape with out-of-phase velocity components and can be considered to be uncoupled from low order modes whose wavelength is far greater than the dimensions of the source. Such devices have been proposed as primary low-frequency radiators in enclosed spaces as they incorporate an inherent reticence towards modal excitation [30], and so their choice as a control source in this environment seems inappropriate.

Of the more recent papers concerned with active control, this review concentrates on those pertaining to active absorption (discussed in section 2.3) and those concerned with equalisation and inverse filtering (discussed in section 2.4). Readers looking for a more general review of active control techniques might refer to Kuo and Morgan's 'Tutorial review of active noise control' [31], which contains a good introduction to the nomenclature of active control and a substantial list of 156 references dating from Leug's original patent through to the present day.

The review is broken up into sections, the first of which contains a review of feedforward broadband active control techniques, with useful discussions of the filtered-x LMS algorithm

and feedback compensation which are introduced in Chapter 4. Feedback active control is then introduced, after which the possibilities offered by multi-channel controllers are explored with reference to the excellent trio of papers by Nelson *et al.* [18,21,22] referred to earlier in this Chapter. As might be expected from a paper published in the proceedings of the IEEE, the review is weighted heavily towards comparison between a variety of fixed and adaptive signal processing algorithms, rather than any treatment of the acoustics of the control of sound. At the end of the paper however, a number of potential noise control applications of active techniques are identified, and after brief qualitative discussion a number of references are provided to recent work in the respective fields.

2.3 Active absorption

The patent of Leug was at first questioned by German authorities who considered the idea to be an extension of the well-understood principle of wave interference[14]. Whilst it is possible to conceptualise active control in these terms, a number of researchers have investigated manipulations of the boundary impedance of a space in order to modify the interior soundfield. When the surface impedance at a controlled boundary element is such that power is absorbed rather than radiated, the control approach can be classed as active absorption.

The novelty of active control techniques in 1953 is illustrated by Olson and May's paper [32], which contains no references to earlier work. Passive resonant sound absorbers are reviewed and contrasted with active absorbers, and it is shown that the latter offer absorption performance over a much wider bandwidth, whilst occupying vastly reduced spatial volumes. Although the hardware employed is anachronistic by current standards, concepts of operation are introduced which have defined active acoustic control applications right up to the present day. Two particular control tasks are of especial interest - the 'acoustic short circuit', where a pressure zero is forced in the vicinity of a radiating object, removing the potential to radiate acoustic power - and the acoustic absorber proper.

Most of the discussion in the paper revolves around the former scheme, but a design for a true absorber (where a thin passive absorbent layer is backed by an actively controlled low

impedance) is outlined. Exploitation of this design has only occurred in the recent past, with hybrid absorber designs such as that due to Furstoss *et al.* [55]. Olson and May's paper is of interest to this thesis in that they introduce the idea of controlling the resonant behaviour of enclosed spaces by the incorporation of active control sources, and recommend corner source locations where coupling is maximised into the largest number of modes.

A naive reading of the work of Olson and May throws up a worrying question - if two sources radiating into a space can produce a sound field of lower magnitude than one operating alone, what happens to the power radiated by those sources? Ford [33] looks at this issue in an early paper forming part of a discussion on the possibilities of active absorption at the 11th International Congress on Acoustics. Whilst primary and secondary sources both exhibit finite velocities, radiated power is a function of the in-phase component of pressure with these velocities. It is shown for a one-dimensional control application that theoretically no power should be radiated either by a secondary source (controlled as a pressure release), or by the primary source since under control its radiation load is purely reactive. Practical measurements support these conclusions with the qualification that some power is lost to the real part of the non-rigid wall impedance of the experimental duct. No details of a control system are given, although since the aim is local pressure release it seems likely that a negative feedback analogue controller is used.

Guiking, Karcher and Rollwage [34] report further early attempts to realise an absorber system operating on a one-dimensional system using analogue feedback control, with manual adjustments of the magnitude and phase of loop gain designed to implement a desired surface impedance. They report excellent results in a duct, but in the three dimensional free field, complications introduced by predicting the directivity of arrays of control loudspeakers limit the utility of the technique. It is interesting to note that an incident pressure signal is derived from the total pressure in the duct using a two-microphone technique, and improved stability of operation results when this signal is used as the feedback reference.

The same authors report advances in their techniques in a later paper [35], where the possibility of an absorbing boundary in three dimensional space is considered. Arrays of loudspeakers are employed ranging from 3x3 (where measurements support modelled results) to theoretical investigations of large13x3 distributions. A reflection coefficient is

modelled using an image source method from a single reflecting boundary, and the phase and magnitude of array elements is manipulated in order to send an appropriate wave back in the direction of the incident energy, such that 'absorption' (=cancellation of the reflected wave) takes place.

The work concentrates on the spatial waveform produced by an array, since the object appears to be free-field absorption with the only boundary being that into which the active elements are incorporated. The transfer functions between array elements are adjusted manually, and no control system is proposed. Useful findings include the necessity for amplitude weighting (eg. Hamming) between array elements to attenuate side lobes, and investigations are initiated into the relationship between dynamic (cone) and static (baffle) elements of the driver arrays. The optimal spacing of array elements is unsurprisingly linked to the wavelength of the acoustic stimulus, and in the limited case of absorption from a single boundary, results demonstrate an impressive reduction in comb filtering effects. The work is not however extended to the general case of the enclosed soundfield - this forms a major part of later work by Elliot, Nelson *et al.*

Although these researchers frequently concentrate on the active minimisation of sound pressure, their interest encompasses active absorption. A 1991 paper [36] refers to earlier noise control work covered in section 2.2 [26], and deals explicitly with enclosed soundfields of low modal density in terms of power absorption using a feedforward control topology. A general mathematical framework is established in which two principal control tasks are compared: minimising the total power output of primary and secondary sources, and maximising the power absorbed by an array of secondary sources. These tasks are considered in enclosed volumes at high and low modal densities (frequencies), as well as in the free field case.

The two tasks turn out to have a surprisingly simple relationship, although their control action differs markedly. In the enclosed low frequency case most relevant to this thesis, minimising total power output is very nearly equivalent to minimising acoustic potential, with the result that acoustic resonances are suppressed. Minimising total power output is shown to result in an orthogonal relationship between pressure and velocity at the secondary source locations. The secondary source power output is therefore zero - a result which

is true in the general acoustic environment where reciprocity holds, and which is demonstrated for a single control source in the presence of one dominant mode. By contrast, maximising the power absorbed by a secondary source can actually increase the power radiated by a primary source (and hence the pressure inside the enclosure) by increasing the magnitude of the real part of the primary radiation impedance. This result is supported by the findings of this thesis in the deployment of a source with actively controlled impedance, and rules out this perhaps most obvious control task as suitable for controlling modes in a three dimensional space.

This paper is broad in scope and comprehensively defines the mathematics for two control tasks in a number of environments. The work forms a substantial basis for the relevant parts of Nelson and Elliot's book 'The active control of sound' [12], which is reviewed in section 2.2. The contents are a purely theoretical analysis, and no systems are proposed with which to implement active absorption. One such system is proposed by Nicholson and Darlington [37], who approach the active control of enclosed soundfields with an explicit active absorber design.

In this paper, active absorption is implemented by the direct transduction of the surface impedance at a control source using a pressure microphone and accelerometer. These signals are used as inputs to a recursive filtered-U LMS algorithm, which updates the weights of an adaptive filter to derive a signal to drive the cone surface impedance to a user specified target value. It is demonstrated that in a duct, a real and characteristic termination impedance may be imposed which could be expected to act as an anechoic termination. Performance limits are identified in terms of maximum cone displacement and maximum power criteria, although it is noted that at these extremes the driver is likely to exhibit non-linear behaviour which is not anticipated in the filter design.

It is stated that the adaptive control filter is employed to cater for '*quasi-periodic or random*' excitation, but the test results concern sine tones. It is not clear whether the authors expect adaptation to take place in run time, or whether a noise signal will be employed, when following convergence the filter will have appropriate response regardless of the frequency content of excitation. In the former case the speed of adaptation might be expected to limit the usefulness of the technique, since high convergence speeds can often

lead to instability in adaptive filters. In the latter case, the length of filter would be one factor determining the degree of convergence, since it might be expected to be poorer than that obtained using deterministic signals.

The operating constraints on a controlled electrodynamic loudspeaker operating as an absorber of acoustic energy are reiterated in a later paper by the same authors [38], together with new material concerning the loop stability of a filter with feedback topology. The existence of a feedback cancellation network is stated which enables the system to operate outside of derived stability limits given in the paper, but the structure of this network is not revealed. Also commented upon are propagation delays in the system which limit the ability of the control filter to behave causally and hence achieve the desired termination impedance. It is suggested that obtaining a suitably time-advanced reference signal will circumvent these problems, although the existence of such a signal is dependant on the particular control task in hand.

A different approach to adaptive acoustic impedance controllers is presented by Orduna-Bustamante and Nelson [39], who employ the two-microphone impedance transduction method of Chung and Blaser [40] rather than using pressure and velocity signals. A framework for impedance control using a feedforward LMS control system is established, and an optimally absorbing characteristic termination impedance arrived at using a knowledge of system transfer functions. Experimental results on a practical duct using sinusoidal, random and transient signals are impressive, demonstrating the removal of steady-state frequency domain modal peaks and time domain reflections. The two microphone method is widely acknowledged as providing rapid results (compared to standing wave ratio methods) at the expense of limitations concerning the frequency bandwidth over which a given setup is valid - here, no mention is made of these limitations which are discussed in a later paper by Darlington, Nicholson and Mercy [45].

A generalised discussion of control tasks and results for the Salford pressure-velocity absorber system is presented by Nicholson and Darlington [41], which is particularly interesting in that it contains time-domain as well as frequency domain results of active impedance control. In this paper it is explicitly stated that the adaptive filter is trained on band-limited noise for a fixed period, after which adaptation is turned off and the

performance of the system is measured. A controller is configured to implement a characteristic duct termination in a feedforward topology, and is shown to be able to reduce the measured reflection coefficient substantially (although perfect absorption is not achieved). In the time domain, an uncontrolled impulse response is compared to that measured with the controlled characteristic termination - the result of control is a clear removal of pulse reflections inside the duct.

These results are similar to those of Orduna-Bustamante and Nelson, but whereas those investigators used a two microphone impedance transduction method exclusively, Nicholson and Darlington report results based on the direct transduction of surface impedance. This method is also used extensively by Mazzola, in a small 1993 book 'Active Sound Absorption'[42]. A purely theoretical analysis of feedback controllers using pressure and velocity signals is attempted, and in much of the work it is assumed that a ρc control law is required. This limits the applicability to one-dimensional acoustic environments and the control of normally-incident plane waves.

Useful material includes the presentation of problems in terms of a 'blocked' and 'dynamic' impedance scheme; the pressure radiated by an oscillating control source is modelled as being that reflected from the source whose velocity is constrained to be zero, added to that pressure determined from the velocity of the source and the impedance into which it radiates. A clear appreciation of the principle of superposition is helpful in formulating solutions to many active control problems, although the linearity of the systems under control must be without question - a concern not raised by this book. Additionally, much of the later material concentrates on maximising power absorbed by a control source. In the light of earlier work by Elliot, Joseph *et al.* [36] the utility of this control law is questionable.

Snyder and Tanaka [43] examine the issue of control source power absorption further in a paper entitled 'To absorb or not to absorb: Control source power output in active noise control systems.' In this paper a mathematical proof is laid out showing that for optimal control conditions and where reciprocity between control and primary sources exists, the control source power output will equal zero. This reiterates the earlier conclusions of Elliot and Joseph *et al.*[36] with regard to minimising acoustic potential and total power output.

The result appears to contradict the aims of active absorption which by definition is concerned with forcing a control source to radiate negative power. However, by 'optimal conditions' the authors imply the total cancellation of acoustic pressure, which is not necessarily the aim of an absorber system. They also go on to note that in conditions other than free space, reciprocity may not exist between the two sources, and in such instances a control source may well be observed to be absorbing power.

An architectural application of an absorber system is investigated in Darlington's 1994 paper [44], which focusses on the suppression of room modes. Simplified room geometry is adopted in order to derive optimal (complex) and sub-optimal (real) control laws aimed at maximising the acoustic power absorbed by the control system. The absolute maximisation of absorbed power has been shown by a number of authors [36,43] to be a bad idea in the context of a modal soundfield, but using Darlington's simplified geometry useful targets for control are derived which are seen to be of genuine benefit in reducing the Q-factor of a low frequency mode. Further work following this paper forms the basis for Chapter 7 of this thesis, where the practical utility of real and complex control laws in a three dimensional environment is considered in greater depth.

The effect of errors in the specified surface impedance of a controller implementing a characteristic duct termination (due mainly to transduction errors in the microphone, accelerometer and associated signal conditioning) are considered in a 1995 paper by Darlington, Nicholson and Mercy [45]. The result of gain and phase errors in impedance observation are considered independently, and both the direct transduction of surface impedance and the two microphone method of Chung and Blaser are investigated.

It is demonstrated that accuracies of the order of 1dB magnitude and 5 degrees of phase must be achieved if the reflection coefficient of the controlled boundary is to be below 5%. With the two microphone technique the optimum error case approaches these figures, but errors are also dependant on the relationship between microphone spacing and wavelength - when the microphones are separated by one whole wavelength then the effect of any gain or phase error is greatly amplified. In conclusion, the direct transduction of surface impedance appears more reliable that the use of the two-microphone method.

Clark and Cole [46] present an interesting alternative to the largely feedforward approaches to active absorption introduced so far. Their method is not described as active absorption, but it has the effect of increasing the damping offered to the normal modes of an enclosed space. This is achieved by making the control source strength proportional to the adjacently measured pressure. Analysis is produced showing the effect of feedback to be an increase in the physical damping offered to the normal modes, and stability criteria for the system are identified. Modelled results show remarkable reductions in steady state pressure (broadband and harmonic excitation) and corresponding reductions in modal decay time; replication of these results in a practical system would represent a significant advance in technologies for controlling low frequency resonance.

Some attempt at such a practical realisation is reported in a recent paper by Clark and Gibbs [47] concerning control of the reverberant soundfield inside a small aircraft. Single channel devices are compared to multi-transducer systems where a number of distributed sources are driven with signals weighted in order to provide coupling into specific pre-determined modeshapes. Controllers follow the feedback design of Clark and Cole's earlier paper, where a microphone is placed adjacent to a control source and filters are introduced to maintain closed loop stability and to attenuate modal artefacts of the enclosed soundfield.

In a section on modal theory, the authors correctly identify the contribution of a large number of higher modal residues on the transfer function between a collocated source and receiver. However, they propose the adoption of a scalar constant to be added to a limited modal summation in order to model the '*stiffness contribution*' of the summation of a (potentially infinite) number of in-phase residues. It is shown in Chapter 7 of this thesis that such a function should actually be directly proportional to frequency, and that an approximation for the direct field radiated by the source is appropriate in practice.

Clark and Gibbs approximate the acoustics of the aircraft cabin with the familiar modal decomposition of a rectangular enclosure with rigid walls - this is arguably less accurate than the cylindrical models adopted by other authors for this application (eg. Bullmore [5]). It is claimed that the modal density is 'high', although the fundamental axial modes of the space are under discussion and compared to Schroeder's diffuse field limit [20,48,49] the modal density is actually rather low. The analysis is useful however - it is stated that

> *"...To exercize global control, the loop transfer function must be modified such that the closed loop poles can be move* [sic] *further into the left-half s-plane...".*

This re-specification of 'desired poles' forms the explicit goal of the biquad-fit controllers introduced in Chapter 4, although here the implementation is feedforward rather than feedback.

The measured performance of Clark and Gibb's system is disappointing compared to the theoretical results presented by Clark and Cole. No decay modification data is reported, and the steady state reductions obtained, whilst measurable, are not subjectively audible. The largest pressure reductions are made in the vicinity of the control microphones; their local nature is similar to results of modal control in an aircraft cabin reported by Avis and Darlington [50], in one of a pair of papers concerned with the theory and application of active impedance control.

In Darlington's accompanying theoretical presentation [51], it is established that active absorption offers an alternative conceptual framework to the fixed feedforward superposition of a number of source contributions in order to modify a given soundfield. The relationship between the surface impedance of an active absorber and the fixed transfer function between corresponding primary and secondary source strengths is expanded on using blocked impedance concepts introduced by Mazzola [42]. The relationship is made explicit for a number of control cases, including the Canceller, Dereverberation filter [52] and Practical Absorber [53,54] solutions investigated in collaboration with Avis. These relationships form a link between the fixed, feedforward Biquad Fit controllers, and the Active Impedance controllers, investigated in this Thesis.

Much of the work reported by Furstoss *et al.* [55] is not original, but repeats Darlington and Nicholson's application of direct pressure/velocity transduction of surface impedance combined with a filtered-x implementation of an absorber-controller. Rather than testing the system on a duct, an anechoic room is used, but the same conclusions (particularly those concerning the difficulties of a feedback configuration when using a broad-band training signal) are reached as those of the earlier investigators. Furstoss and his collaborators take the work further by considering the combined action of an absorbing or cancelling actively

controlled surface placed behind a piece of porous material, which is termed a hybrid passive / active strategy. This follows an original approach of Olson and May [32], who were concerned with the absorption of porous layers and its dependance on the surface impedance of the backing layer or plate.

Since a system exists whose surface impedance may be specified by the user, the appropriate value for that impedance at the rear of a porous layer is investigated in order to maximise the combined absorption. This impedance is seen to depend on the thickness of the porous layer, and the frequency at which the hybrid system is excited. A pressure release (zero impedance) condition is found to be a good approximation of the optimal, complex impedance required to maximise absorption, and broadband coefficients very close to unity are obtained for fibreglass samples only a few centimetres thick. The adaptive filters used in the research are feedforward designs - a simple fixed second-order feedback system is investigated which can implement the pressure release, and this too is found to markedly increase the absorption performance of the porous layer. It would be extremely useful to compare the performance of designs of this type with the use of direct-radiating impedance controlled sources, with a view to reducing Q-factors of low frequency room modes.

Gentry *et al.* [56] take the hybrid passive / active concept a stage further, in a design for 'smart foam' which encapsulates an active PVDF element inside a foam layer. This device is attached to a vibrating piston of presumably high mechanical source impedance. Rather than affecting changes in an enclosed soundfield, investigations are reported whose aim is to change the radiation behaviour of the piston and reduce the radiated sound pressure in an anechoic environment. Since the piston motion is not resonant, the attached foam does not act as a damping layer, but rather changes the radiation impedance driven by the piston and in this way reduces the overall radiated pressure.

The unconventional use of foam as a noise control element in a non-resonant environment is shown to produce significant broadband reduction in radiated pressure. Considerable effort is expended in the description of the PVDF actuator; when this is driven by a feedforward LMS adaptive control system, increased pressure reductions result, especially at low frequency. It is claimed that the smart foam modifies the resistive radiation impedance of the source resulting in global noise 'cancellation', and if this is the case then

it is possible that such devices might be useful in modifying the boundary impedance of enclosed spaces in such a way as to alter modal behaviour.

2.4 Equalisation, inverse filtering and the deconvolution of room responses

Conventional approaches to the active control of sound have frequently concentrated on the minimisation of acoustic pressure or some other cost function to achieve a desired target state. Active absorption is one variation on this approach, which may be used to reduce the influence of an enclosure upon the soundfield within by modifying the impedance of the boundary. Alternatively, the formal deconvolution of the transfer impedance from a source out to some listening location may be attempted in order to remove the influence of the room boundaries, if only at that one location.

Neely and Allen [57] were among the first to report attempts to build inverse filters of room transfer functions, in order to remove the 'distortion' applied to speech signals by the reverberation added during propagation through an enclosed space. An image source model was used to generate synthetic room impulse responses which were then Fourier transformed in order to obtain transfer impedances. The existence of a stable inverse filter was found to depend on whether the transfer function was substantially minimum-phase; the presence of a non-minium phase component which was not a simple delay ensured that the inverse filter contained poles in the right-half s-plane. The existence of such poles was found to be a function of source / receiver location, and the reflection coefficient of the room boundary. For practical rooms it is suggested that source and receiver must lie extremely close to each other for a stable inverse to exist and that other methods other than the formal deconvolution of the room transfer function must be sought.

Mourjopoulos [58] comments further on variations in impulse response functions measured throughout an enclosure, and the invertibility of these functions. Since his main interest was in removing reverberant energy from a speech signal rather than addressing discrete low frequency modes, the frequency range 100-4kHz is used, which limits the application of the work to the present study. Room responses were analysed in terms of direct/reverberant, and early/late (50mS criterion) energy ratios, and the performance of inverse filters was

assessed in terms of those parameters. The performance of inexact inverse filters calculated for receiver locations other than that used in the evaluation was also investigated.

It is suggested that whereas exact response inversion, where possible, can be shown to improve speech intelligibility measures in the room, any approximation of the inverse filter causes further degradation of the original signal. Image source models of real rooms likewise do not result in satisfactory deconvolution filters for application in a real test environment, and it is concluded that the formal deconvolution of the room response therefore has limited application for reverberant signal enhancement. Mourjopoulos has considered alternative methods which may facilitate the removal of unwanted room effects from a signal.

Two such methods form the subject of work by Mourjopoulos and Paraskevas [59], where all pole (IIR) and all zero (FIR) models of room responses are formulated in an attempt to reduce the model complexity and increase the spatial generality of the result. A least-squares technique is described by which pole locations may be obtained, and the optimum filter order is investigated using the power in the error spectrum between a model and practical measurements as a cost function. The techniques are evaluated using measurements in two test rooms, and by using image-source models of one of those enclosures.

Mourjopoulos shows that all pole models are shown to be far more computationally efficient than all zero equivalents, although the all zero FIR models are more accurate. The all pole models are less sensitive to movement of the receiver position in terms of time- and frequency- domain performance, and both techniques work best at frequencies below 500 Hz in terms of defined performance metrics. It is noted that the higher spatial dependance of the zero solution probably results from the fact that notches in the response functions are caused by interference between adjacent modes, and are easily disturbed by slight changes in source / receiver locations; by implication the maxima created by the poles do not vary as rapidly with distance. Since the maxima are scaled by cosine functions which vary slowly at low frequency, this appears to be true. Inverse filters based on the all-pole technique are shown to reduce components of reverberation in both time and frequency domains, although the results presented range over the 0-5kHz bandwidth. It would be interesting to view

results of the all-pole filter within the 500Hz bandwidth over which, it is claimed, superior control is achieved.

Mourjopoulos and Paraskevas cite a different approach taken by Elliot and Nelson [60], in an attempt to find a solution to the room deconvolution problem and in particular increase the spatial generality of control filters. In this paper, FIR filters are constructed to model transfer functions associated with a model of a small rectangular enclosure representing a 'car interior'. The geometry appears to facilitate a modal decomposition rather than representing any realistic vehicle, and modal models of the enclosed soundfield are constructed.

Low frequency equalisation is shown to flatten the response at the equalisation point whilst creating problems at other locations, as was suggested by previous authors in their results at higher frequencies. In response to this, Elliot and Nelson investigate an approach which aims to minimise the sum of squared errors between the equalised pressure and a flat target response at four locations simultaneously, using a multiple input adaptive filter algorithm. Better averaged performance than that obtained for the single channel filter is achieved, but the modal nature of the soundfield means that a flat response cannot be obtained at all measurement locations. This result highlights a central limitation of equalisation, where the unmodified normal modes dictate the behaviour of sound inside an enclosure and can be at best only accommodated in order to produce the 'least bad' averaged result.

The practical implementation of the ideas in this paper is left to Elliot *et al.* in a 1994 report [61]. Single channel and multi-channel LMS adaptive equalisation is performed in small car using an FIR controller of various lengths. As expected, equalisation at one point causes signal degradation at other points consistent with the modal transfer impedances from the source out to the respective measurement locations. A multi-channel optimisation of a single filter gives only small benefits at each location owing to the conflicting requirements of control at each microphone, and it is suggested that a more satisfactory global solution may be arrived at using multiple filters connected to independent loudspeakers.

The controller does not address individual modes *per se* but instead attempts to minimise the total mean-square error between each pressure response and their respective target

signals. It is found that some compromise can be reached between the conflicting equalisation requirements by using a single-point technique with limited numbers of filter coefficients, limiting the resolution of the control filter. This means that the fine detail in the measured response (and specifically the sharp notches with high spatial variability noted by Mourjopoulos) are not built into the equaliser, and so do not perturb the field at the distant measurement locations.

Mourjopoulos summarises much of the preceding work in his excellent review paper 'Digital Equalisation of Room Acoustics' [62]. The work of Neely and Allen is revisited, and a useful Appendix is included showing a z domain analysis of the inversion of mixed phase functions, with some examples. Problems of filter length and the spatial variability of an equalisation filter are examined together; filter length is first reduced using an all-pole approximation, and then the method of Vector Quantisation is employed in an attempt to produce a set of inverse filters which are able to act on transfer functions to any receiver position with minimum error.

Measured or modelled all-pole room transfer functions are numerically classified using vector quantisation into a number of groups, where the intra-group variation is minimised. These groups are used to design a 'codebook' of groups of similar transfer functions, whose inverse filters may all be pre-designed based on the centroid of each group. In run-time, the transfer function out to a particular receiver position is matched to the most suitable centroid, and the associated inverse filter is selected. The technique generates optimal room transfer function averages, whose accuracy is inversely proportional to the number of groups chosen. However, the detection of a receiver location which may vary during equaliser operation is not discussed; if a transfer function must be continually monitored to judge location by acoustic means, it is not clear why this measurement could not be used to design a continuously updated all-pole inverse approximation.

The fact that vector quantisation still equates to essentially single-point equalisation is observed by Haneda *et al.* [63], who combine the approaches of Elliot and Mourjopoulos in using an all-pole model which explicitly aims to optimise the equalisation of room transfer functions at multiple receiver locations. The model is conceived as representing the resonances of the soundfield inside an enclosure with an all-pole approximation - the

polynomials used in the model suggest that these poles form cascaded filter sections, rather than the parallel topology suggested by a modal decomposition of pressure. The pole locations are manipulated in a least-squares optimisation which aims to minimise the error between a number of inverse filtered room transfer functions corresponding to a number of receiver locations, and the input signal to the filters.

Results from the multiple-point all pole filter are compared to approaches suggested by Elliot and Mourjopoulos, and although the soundfield is not completely flattened at any one receiver point, neither is the response made more irregular as with earlier techniques. The most noticeable equalisation occurs at those frequencies where the all-pole equaliser has the best fit - those resonances with high Q-factor which are emphasised in the original response, and whose minimisation has most bearing on the cost function used to select pole locations. Results are optimised over a bandwidth of 200Hz to 3.4kHz - a broad bandwidth and higher in frequency than that investigated in this Thesis - and support the authors claims that equalisation is possible over a broad spatial area if notches in the filter responses are ignored.

2.5 Subjective effects of resonance

An attempt to control low frequency room modes presupposes that this task is worthwhile - that the steady state and decay distortions introduced by the modes represent an audible and deleterious modification of program material reproduced within that environment. Although this understanding certainly forms part of the received wisdom of room acoustics and studio design, it is not necessary to rely on hearsay for motivation in attempts at modal control. Published research exists whose aim is to quantify the audibility of resonances, in an attempt to define the performance requirements of technologies used to correct them [3].

Amongst the earliest reported work is that due to Bücklein [64], who examined the audibility of spectral irregularities using speech, music and broadband noise signals. Peaks in responses were found to be more audible than dips, and the width of a resonance was found to be directly proportional to its detectability. At least with steady state signals and most particularly with noise sources, the Q of a resonance was found to be inversely related

to its effect on the perception of the source - a result which appears counterintuitive but which is supported by later research.

The work of Bücklein is referenced by Toole and Olive [65] as part of a review of work on the modification of timbre by resonances. This paper is focussed towards an understanding of the factors which influence the perception of timbral changes introduced into steady-state noise signals by resonant phenomena, but also includes some analysis of the perception of resonances excited by impulsive events, and by a variety of speech and music sources. Practical subjective tests rely on extremely small sets of data (between two and six listeners), to the point where the results must be considered preliminary and indicative rather than definitive.

The audibility of timbral modifications is found to depend on the Q, frequency and amplitude of the resonance, but the type of program material also is a factor. This may be because whereas continuous signals with dense broadband spectra produce results which agree with Bücklein, impulsive sources may excite resonances in such a way as to make high-Q phenomena more easily detectable than their low-Q counterpart. There is some discussion of possible mechanisms for the detection of impulsively excited resonances, and it is reported that whilst the initial amplitude of a decay may be important, the duration of ringing is itself an unreliable indicator of resonance audibility.

Olive took this work further with new collaborators in an investigation of the effect of loudspeaker placement on listener preference ratings [66]. It was found that the placement of a loudspeaker within a room has a significant effect on its perceived sound quality, and in the particular subjective tests reported the variation in results due to location were more significant than the variation due to the differences between the loudspeakers themselves. Room modes and in particular the low modal density of typical listening rooms at low audio frequencies are suggested as a mechanism for the generation of such differences, since the degree of coupling into discrete low frequency modeshapes will be strongly dependant on source location.

The same team of researchers have published a more recent paper looking at detection thresholds of resonances specifically at low frequencies[3], and it is this work which has

most relevance to this Thesis. The thresholds of audibility of added resonances and 'antiresonances' (notches) were investigated at octave band centre frequencies between 63 and 500 Hz, with values of Q of 1, 10 and 30. Once again, the extremely small sample size (four listeners) renders the results indicative rather than conclusive. It should also be borne in mind that some of the results contrast Q factors of 1 and 30, whereas practical controllers introduce changes in Q from an uncontrolled value of approximately 50 to perhaps a value of 10. Extremely low Q resonances are not encountered in practice and if these tests are neglected the results of Olive and Schuck are less conclusive still.

Notwithstanding these criticisms, when listening to steady state pink noise, subjects required more magnitude amplification of a resonance to detect those with high *Q*. *Such resonances* centred on the lowest octave bands were the hardest to detect. This result suggests that building control systems to lower the Q of room modes *might increase* the colouration *they* introduce to reproduced sound, at least in terms of timbral modification. However, in contrast to the thresholds measured with pink noise, thresholds measured using an impulsive signal decrease as the Q of the resonance increases, suggesting that temporal effects are the most important cues for detecting low frequency resonance. If this is the case, there are important ramifications for control systems, which must be able to control low frequency modal decay artefacts set up by a reproduced music signal containing both impulsive and band-limited noise characteristics, rather than simply aiming for a flatter frequency response measurement.

Chapter 3

Modal treatment of sound fields in one- and three-dimensional spaces

3.0 Introduction

The work presented in this Thesis is concerned with the active attenuation of acoustic standing wave phenomena, discussed largely in terms of modal decompositions of enclosed sound fields. The assumptions underlying this approach fail under some circumstances, and a thorough appreciation of the validity of the model becomes important when formulating strategies for active control.

A simple plane-wave model is discussed which allows the calculation of pressures in a duct for any known termination impedance. This is compared to modal solutions with no damping, light but finite damping and finally significant damping. The solution is applied to the duct, and a three dimensional modal decomposition for a room is investigated under various damping conditions.

No novel material is presented in this chapter, but the material is central since the models used in Chapters 5 to 9 rely on these mathematical approaches. A summary is given here with reference to more detailed presentation in published literature.

3.1 Standing waves in pipes

Kinsler and Frey [10] develop a plane wave model of a fluid-filled duct of cross section S with known mechanical termination impedance Z_{mL}. driven harmonically by a piston. It is shown that if the walls of the duct are assumed to be rigid and there are no absorptive losses to the wave as it propagates along the duct, the wave velocity (and hence wavenumber k)

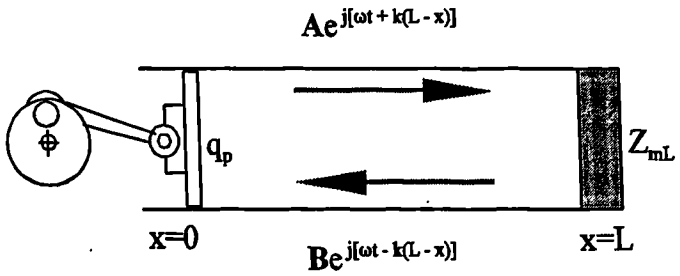

Figure 3.1 - Duct excited by harmonically driven piston

are real and the input impedance to the duct can be written as

$$Z_{m0} = \frac{Z_{mL} + j\rho_0 c S \tan kL}{1 + j\frac{Z_{mL}}{\rho_0 c S}\tan kL} \qquad 3.1$$

The relationship between the pressure and volume velocity at the input and output of the pipe can be expressed as a pair of simultaneous equations in the form of an acoustic two-port - using acoustic rather than mechanical impedances:

$$\begin{bmatrix} p_0 \\ U_0 \end{bmatrix} = \begin{bmatrix} \cos kL & \frac{j\rho_0 c}{S}\sin kL \\ \frac{j}{\rho_0 c}\sin kL & \cos kL \end{bmatrix} \cdot \begin{bmatrix} p_L \\ U_L \end{bmatrix} \qquad 3.2$$

The input impedance of the pipe is therefore a function of frequency, pipe length and termination impedance. Figure 3.2 shows the pressure at the piston for a unit velocity input into a duct of length 4m where $Z_{aL} \to \infty$. Losses along the length of the duct (due to radiation through the duct walls and absorption in the fluid medium inside the duct) have been neglected.

The duct resonances at $kL = n\pi$ are clearly visible - pressure is only prevented from approaching infinitely positive and negative values by the finite frequency resolution of the simulation. Each resonance may be treated individually as a natural mode of the system, whose total response is equal to the sum of an infinite number of such modes. This approach requires that the soundfield is broken down into a modal decomposition; a technique which is described in section 3.2.

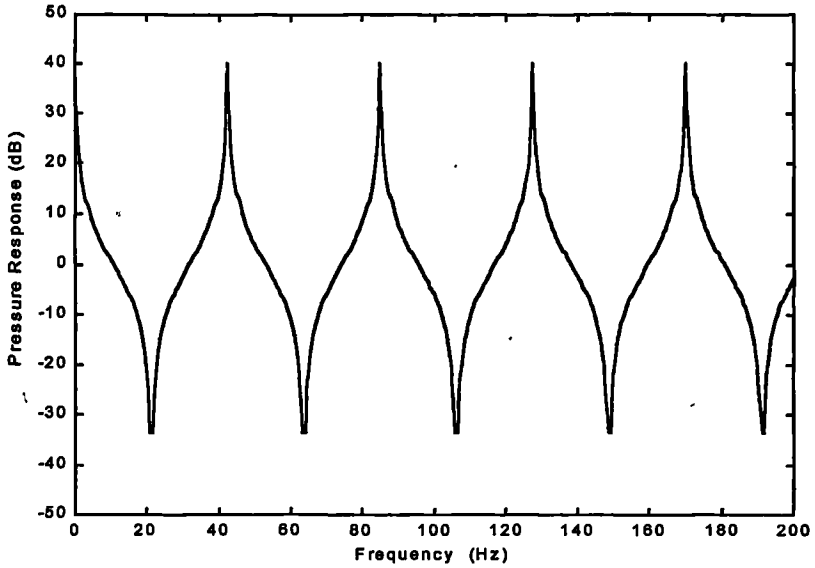

Figure 3.2 - Magnitude input impedance of a rigidly terminated 4m duct

3.2 A modal solution for the soundfield in a duct

The solution of the one-dimensional acoustic waveguide terminated by a known impedance may be thought of as analogous to a rectangular enclosure where only one dimension is considered. A modal decomposition of the resonant acoustic behaviour of a rectangular enclosure is presented in a number of references [eg 6,8,11,12].

Perhaps the best compromise between clarity and comprehensiveness is found in Kuttruff. Starting from a solution of the time independent one-dimensional wave equation, the Green's function is obtained for point excitation such that:

$$p(r) = j\omega\rho_0 Q \sum_n \frac{\psi_n(r)\psi_n(r_0)}{\chi_n(k^2 - k_n^2)} \qquad 3.3$$

The shape functions or eigenvectors $\psi_n(r)$ and $\psi_n(r_0)$ take the conventional cosine form, the resonant frequencies or eigenvalues being found from the roots of

$$e^{jk_{n,x}L} = \pm 1$$

and so 3.4

$$\cos k_{n,x}L + j\sin k_{n,x}L = \pm 1$$

This equation is satisfied when $k_{n,x} = n_x \pi / L$ - the same result as for the impedance peaks which defined the set of natural frequencies found from **(3.2)**.

Where damping is included in the system, **(3.3)** must be modified to take account of the fact that when the system is forced on-resonance, pressure will not become infinite. Kuttruff shows that for light damping

$$p(r) = j\omega\rho Q c^2 \sum_n \frac{\psi_n(r)\psi_n(r_0)}{\chi_n(\omega^2 - \omega_n{}^2 - 2j\delta_n\omega)} \qquad \textbf{3.5}$$

The pressure response therefore follows the conventional form of a second-order bandpass function, where the damping ratio δ_n refers to the ratio of actual to critical damping, and defines the decay rate of an underdamped system in the form $e^{-\delta t}$ [69]. It is shown that δ_n may be related to the specific boundary impedance by

$$\delta_n = \frac{2c}{\xi_x L_x} \qquad \textbf{3.6}$$

A modal decomposition in a duct with large, real termination impedance **(3.5)** can be compared with the 2-port solution given in **(3.2)**. Figure 3.3 shows this comparison in terms of the input impedance to a 4m long duct with termination impedance $Z_a = 10.\rho c/S$. Four hundred modes were used in the summation.

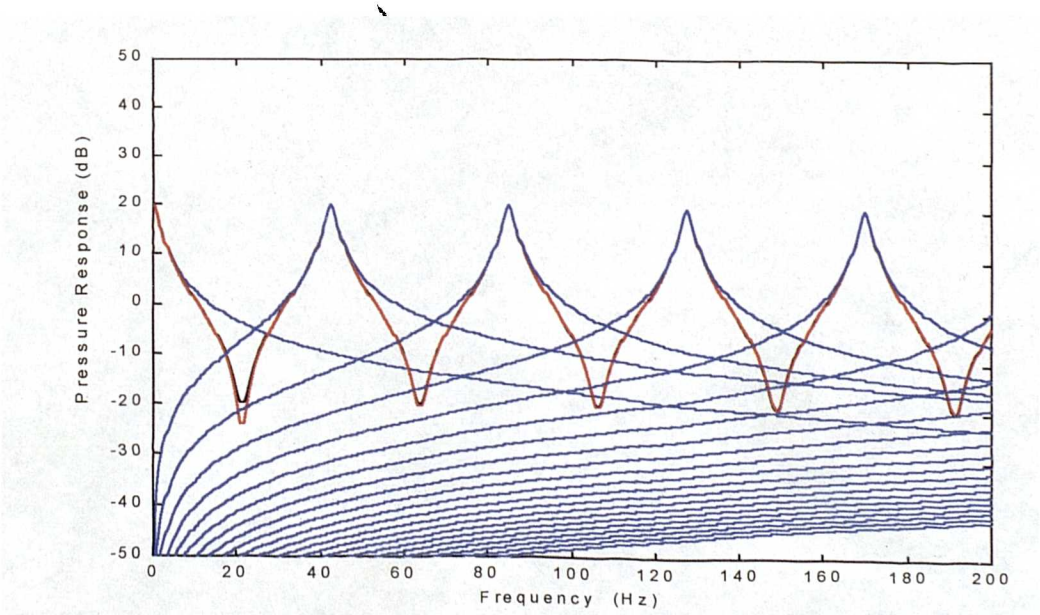

Figure 3.3 - Input impedance of duct with large real Z_L
a) Model sum b) 2 port c)Individual modes

For a damped system the eigenvalues have real and imaginary parts, and the cosine eigenvectors introduced in (**3.3**) are found to have complex argument. Many practitioners of room acoustics [eg 24,6] assume that the imaginary part is negligible. In this case, a damping coefficient is incorporated into the modal summation whilst at the same time retaining the simple cosine modeshapes which strictly speaking no longer apply.

Kuttruff argues that a phase angle may be added to the argument of the cosine modeshape to take into account the absorption of the wave at the boundary. However, the graphical results published are confusing and perhaps contradictory, and the analysis is absent from the third edition. A thorough treatment of modes in the presence of damping is given by Morse and Bolt (4) - the notation is a little difficult to follow and the working is expanded more clearly in Appendix G.

3.3 Solution for lightly damped modes according to Morse and Bolt

Morse and Bolt adopt a hyperbolic trial solution of the form:

$$\psi_n(x) = \cosh(jk_n x - \phi_n) \qquad \textbf{3.7}$$

This is solved in the presence of a locally reacting boundary condition of known impedance to show that the resonant frequencies or eigenvalues of the system become

$$k_n = (jk/L)^{1/2}(1/\zeta_{x_0} + 1/\zeta_{x_L})^{1/2}\left[1 - \frac{jkL}{6}\cdot\frac{(1/\zeta_{x_0}{}^3 + 1/\zeta_{x_L}{}^3)}{(1/\zeta_{x_0} + 1/\zeta_{x_L})^2} + \ldots\right] \qquad \textbf{3.8}$$

$n=0$

$$k_n = \frac{n\pi}{L} + \frac{jk}{n\pi}(1/\zeta_{x_0} + 1/\zeta_{x_L}) + \frac{k^2 L}{\pi^3 n^3}(1/\zeta_{x_0} + 1/\zeta_{x_L})^2 + \ldots \qquad \textbf{3.9}$$

$n>0$

These eigenvalues are substituted into (**3.7**) to find the modeshapes. As long as the walls are fairly hard, terms in powers of $1/\zeta$ higher than 2 can be neglected [4]. It is then found that the cosine shape functions are superceded, so that

$$\psi_n(x) = \cosh\left(\left[\frac{kl}{j(1/\zeta_{x_0} + 1/\zeta_{x_L})}\right]^{1/2} \frac{1}{L}(L/\zeta_{x_0} - x/\zeta_{x_0} - x/\zeta_{x_L})\right) \qquad n=0$$

$$\psi_n(x) = \cosh\left(\left[\frac{jn\pi x}{L}\right] - \frac{k}{n\pi}\left[(x/\zeta_{x_0} + x/\zeta_{x_L}) - \frac{L/\zeta_{x_0}}{1 + \frac{jkL(1/\zeta_{x_0} + 1/\zeta_{x_L})}{n^2\pi^2}}\right]\right) \qquad n>0 \qquad \textbf{3.10}$$

Examples of this expression for the eigenvector are shown in Figure 3.4 where the impedance is taken as equal on opposing walls and where *a)* $\zeta \to \infty$, *b)* $\zeta=5$ and *c)* $\zeta=2$. The modeshape is shown for mode order $n=4$, and driving frequency $k=k_4$. Case *c)* ties up well with the aforementioned plate by Kuttruff [11], although the validity of the series truncations used to derive (**3.10**) must be in some doubt as the specific boundary impedance lies so close to unity. These truncations are explored further in Appendix G, and the significance of modeshape error as a system approaches characteristic termination are discussed in the context of control filter models in Chapter 6.

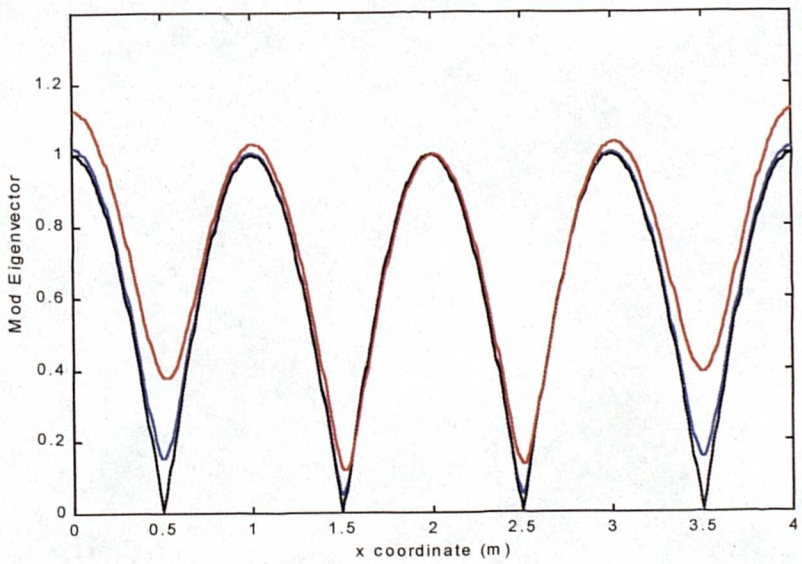

Figure 3.4 - Modeshapes where n=4, k=k4
a) $\zeta \to \infty$ *b)* $\zeta=5$ *c)* $\zeta=2$

3.4 Moving into three dimensions

Up to this point in the chapter, the solution to a one-dimensional system has been formed from arguments derived from references dealing with modes in rectangular rooms. A solution explicitly for the three dimensional case follows readily. The one-dimensional wave equation is split into three orthogonal coordinate axes, and the eigenvectors now must satisfy the homogenous Helmholtz equation

$$\left(\frac{\delta^2}{\delta x^2} + \frac{\delta^2}{\delta y^2} + \frac{\delta^2}{\delta z^2} \right) \psi_n(x) + k_n^2 \psi_n(x) = 0 \qquad \textbf{3.11}$$

Each coordinate axis assumes its own set of boundary conditions at $x=0$ *and* L_x, $y=0$ *and* L_y and $z=0$ *and* L_z. When the walls are rigid and $\zeta \to \infty$, cosine shape functions prevail, but this time exist in three dimensions. Therefore

$$\psi_{n_x,n_y,n_z} = \sqrt{\epsilon_{n_x}\epsilon_{n_y}\epsilon_{n_z}} \cos\left(\frac{n_x \pi x}{L_x} \right) \cos\left(\frac{n_y \pi y}{L_y} \right) \cos\left(\frac{n_z \pi z}{L_z} \right) \qquad \textbf{3.12}$$

and the eigenvalues are found from

$$k_{n_x,n_y,n_z} = \sqrt{\left(\frac{n_x \pi}{L_x} \right)^2 \left(\frac{n_y \pi}{L_y} \right)^2 \left(\frac{n_z \pi}{L_z} \right)^2} \qquad \textbf{3.13}$$

The scaling factors ϵ_n are present to ensure that the volume integral of each shape function is normalised to the room volume. In the one-dimensional case, the normalisation factor required a comparison between the 'zeroth' and higher order modes, but in three dimensions the latter group subdivides into the three distinct categories of axial, tangential and oblique modes. Then,

$$\Lambda_n = \frac{1}{\epsilon_{n_x}\epsilon_{n_y}\epsilon_{n_z}}$$

$$\textit{where } \epsilon_{n_x},\epsilon_{n_y},\epsilon_{n_z} = 1 \quad n=0 \qquad \textbf{3.14}$$

$$= 2 \quad n>0$$

The normalisation factor is not the only term to require modification. In a three-dimensional system, the relationship between termination impedance and modal damping factor δ_n (**3.6**) is no longer straightforward. Three sets of boundaries are now potentially involved, and it is possible that the particle velocity of the modal soundfield may not be aligned normal to any boundary. The three-dimensional damping coefficients δ_n are approximated by Morse [6] as 'average wall coefficients' which are a measure of the power loss from each mode at the walls. It is shown to a first order approximation that where boundary impedances are large and real, the quantity $8/\xi$ corresponds to the random incidence absorption coefficient α and the damping coefficient is found from

$$\delta_n = \frac{c}{8V}\left[4\epsilon_{n_x}(1/\xi_{x_0} + 1/\xi_{x_L})S_x + 4\epsilon_{n_y}(1/\xi_{y_0} + 1/\xi_{y_L})S_y + 4\epsilon_{n_z}(1/\xi_{z_0} + 1/\xi_{z_L})S_z\right] \qquad \textbf{3.15}$$

These coefficients apply when the surface impedance is large, and the surfaces involved have impedance which is broadly similar. In cases where the modes are more highly damped, it is helpful to consider the work of Morse and Bolt applied to a three dimensional environment.

3.4.1 Morse and Bolt solution in three dimensions

The shape functions defined in (**3.10**) may likewise be expanded into three dimensions by taking the product of three eigenvectors in mutually orthogonal directions. Thus

$$\psi_n(x) = \psi_{n_x}(x)\psi_{n_y}(y)\psi_{n_z}(z)$$

and **3.16**

$$k_n^2 = k_{n_x}^{\ 2} + k_{n_y}^{\ 2} + k_{n_z}^{\ 2}$$

Because the shape functions are now cosh functions with complex argument, calculation of the normalisation factor Λ_n is somewhat more complicated. Morse and Bolt give the result shown in (**3.17**).

Graphical comparisons of the solutions of Morse and Bolt with those applicable for enclosures bounded by more rigid terminations are given in Chapter 6. These comparisons are made in the context of a discussion of novel IIR feedforward controllers which form one of the two classes of active controllers investigated in this Thesis.

$$\Lambda_n = \frac{1}{\epsilon_{n_x}\epsilon_{n_y}\epsilon_{n_z}}$$

$$\epsilon_n = L\left[1 - \left(\frac{jkL}{3}\right)\frac{(1/\zeta_0^3 + 1/\zeta_L^3)}{(1/\zeta_0 + 1/\zeta_L)^2}\right]$$

$$n=0\,;\,\frac{kL}{\zeta_0\pi}, \frac{kL}{\zeta_L\pi} < 1 \qquad \textbf{3.17}$$

$$\epsilon_n = \frac{L}{2}\left[1 + \left(\frac{jkL}{\pi^2 n^2}\right)(1/\zeta_0 + 1/\zeta_L)\right]$$

$$n>0\,;\,\frac{kL}{\zeta_0\pi}, \frac{kL}{\zeta_L\pi} < n$$

3.5 Summary of modal treatment of sound fields

Theory has been presented which is central to the understanding of the behaviour of enclosed sound fields in one and three dimensions. This material is used to model the behaviour of the two active control strategies which form the subject of this Thesis. The first of these strategies - active impedance control - is reviewed in the next chapter. This technique is applied to control in a three-dimensional environment in Chapter 8, where modal theory enables the original specification of appropriate target impedances.

The second control strategy - fixed feedforward IIR controllers - exploit the modal decomposition analysis introduced in this chapter specifically in the derivation of a novel filter structure whose aim is the re-specification of acoustic pole locations and the reduction of modal quality factor. These systems are introduced in Chapter 5, and are investigated in Chapters 6 and 7 in a duct and Chapter 9 in a room.

Chapter 4

Review of Active Impedance Control

4.0 Introduction

This Thesis details attempts to modify the low frequency acoustics of an enclosed space using two active control techniques, the central aim being the construction of a self-contained control source without a requirement for distributed fields of error-sensing microphones. Ideally, such a system might be required to control the soundfield resulting from any acoustic or electroacoustic source, and as such might be expected to operate without a requirement for an electrical reference signal correlated to the primary sound source. Here we review the first of these control techniques, active impedance control.

A single-channel filtered-x LMS adaptive system is used to control the surface impedance of an electrodynamic loudspeaker which is placed in the environment over which control is required. The signal processing necessary for this approach uses a conventional filtered-x LMS topology, and was available to this project as a product of a previous piece of research [72]. The application of active impedance control to one dimensional acoustic systems has already been reported [eg 41,45]; however investigations into the active control of surface impedance in the context of a three-dimensional acoustic environment are novel.

This Chapter comprises a short review of the Salford impedance control system . No novel material is included - the aim is to present background material concerning the system design and implementation. The operation of the controller is first discussed, followed by an examination of the factors influencing accurate impedance transduction. The performance of an impedance controller is then assessed in operation on an acoustic waveguide.

Subsequently, control applications using the system in a three dimensional environment are reported in Chapter 8. An impedance controller also gives a useful point of reference for the development of novel one-dimensional control techniques in Chapters 6 and 7.

4.1 Active Impedance control

A series of adaptive active control systems have been constructed at the University of Salford and applied to the problem of resonant modes in the built environment [eg 37,38,41,44,72]. The method has been termed 'active absorption' and relies on a specification of the surface impedance at a control or secondary source - a conventional electrodynamic loudspeaker driver. A schematic diagram of the absorber system used in this project is presented in Figure 4.1.

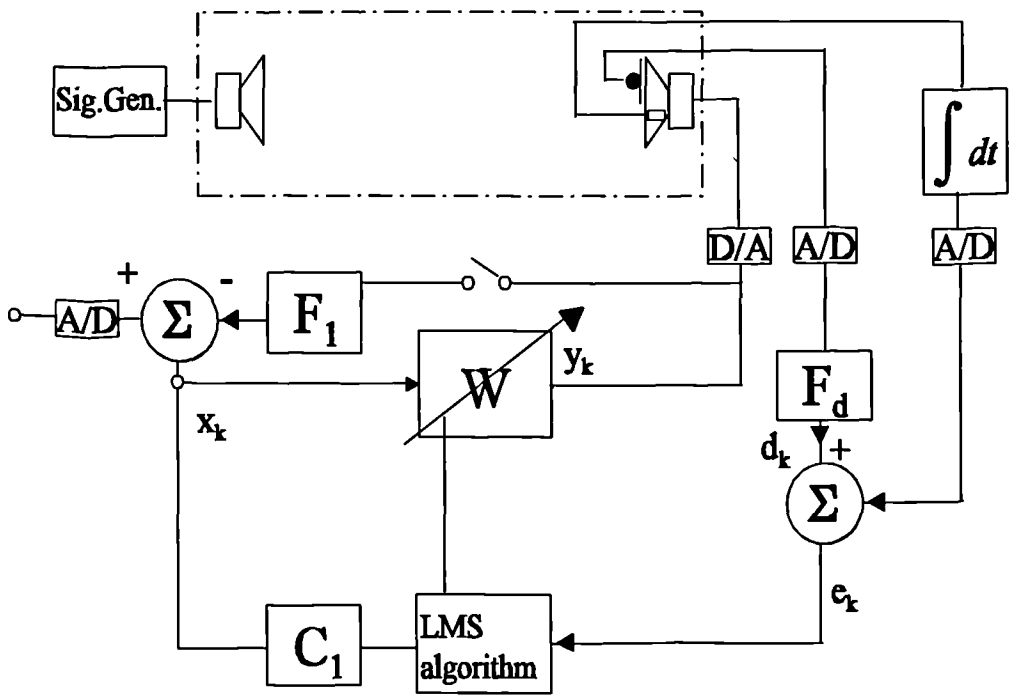

Figure 4.1 - Active impedance control system

The difference between the active acoustic absorber and the archetypal filtered-x LMS control system [71] resides in the derivation of the desired signal d_k. The control loudspeaker is instrumented with a microphone and accelerometer; the accelerometer output is then integrated with respect to time giving a signal proportional to cone velocity. Therefore it is possible to directly measure the specific acoustic impedance at the cone

surface. The measurement of specific acoustic impedance is the subject of further discussion in section 4.2 (one dimension) and Chapter 8 (three dimensions).

Filter F_d acts on the microphone output with coefficients specified by the user, and has response equal to the inverse of the desired impedance at the cone (**4.1**). The output from F_d is therefore a desired velocity u_d, which is compared with the actual velocity in order to derive the error signal e_k.

$$F_d = \frac{1}{z_d}$$
$$\Rightarrow u_d = p.F_d \qquad \textbf{4.1}$$

The user may also manipulate the LMS update gain, which determines the speed at which the specific acoustic impedance at the cone converges to the value chosen by the specification of F_d. High update gains often cause instability in operation [72].

The system may be configured in either a feedforward or feedback topology, depending on the source of reference input x_k. If driven from the signal generator which feeds the primary source, the system will be feedforward. Alternatively the reference input may be connected to an external measurement microphone, or one of the transducers which instrument control source velocity and cone pressure. In this feedback case compensation filter F_1 is required to ensure stable operation over the widest possible operating bandwidth. Feedback systems investigated in this report use the pressure signal from the control source cone microphone as the reference input.

Any realisation of the active impedance controller means that appropriate arrangement must be made for the transduction of the impedance at the surface of the control source. In published investigations in a one-dimensional test environment [37,41], a termination consisting of one KEF B200 driver instrumented with a Knowles BU1771 accelerometer and an omnidirectional electret microphone capsule was employed. The output from the accelerometer was integrated and the pressure and velocity signals used as control inputs to derive a control signal which aimed to force the ratio of cone pressure to velocity to a real and user-defined value.

These arrangements have been maintained for measurements in the one-dimensional waveguide reviewed in section 4.4, and form the basis for the novel investigations into three-dimensional active impedance control in Chapter 8. Calibration data and circuit diagrams for pressure and velocity transducers and associated signal conditioning is available in Appendix C. It is important to appreciate that the success or failure of active impedance control rests in part on the accuracy with which controller surface impedance may be transduced, and the measurements required for this transduction are now reviewed.

4.2 Impedance measurement for practical controllers

Practical impedance measurements are used in the derivation of a signal which is applied to the voice coil of the control loudspeaker in order to make the surface impedance converge to a user-specified target value. In order that the impedance converges to the correct value, the measurements on which the control signal derivation is based must provide a true and accurate measurement of the actual ratio of pressure and particle velocity. Any error in these measurements will result in convergence to a value other than that desired by the user.

A theoretical analysis of the significance of transduction errors for active impedance control in a one dimensional waveguide is presented by Darlington *et al* [45], along with measured results derived from the intentional perturbation of pressure and velocity control signals. It is concluded that

> *'...the transducers and associated signal conditioning circuits should be calibrated to within 1dB magnitude error and 5 degrees phase error in order to achieve better than 95% acoustic absorption'.*

This analysis is helpful in that it identifies the significance of transduction errors, but a discussion of the measurement method itself and its relation to a theoretically modelled ratio of pressure and velocity at the surface of a loudspeaker cone is not attempted. This relationship is important in two ways.

Firstly, the accuracy of the model chosen for the pressure radiated by the source (compared to the true relationship between source velocity and pressure) is influential in determining the authenticity of any theoretical attempt to find the optimal surface impedance which the controller should exhibit. If the model of the radiation load seen by the source *is* accurate

and an optimum controlled surface impedance can be calculated, the ability to *measure* this impedance determines the accuracy with which the practical controller approximates the theoretical optimal control outcome. The aforementioned paper deals with the second point in terms of transduction errors, but does not consider whether theoretical models are representative of the *true* surface impedance at the device. The question emerges: can a model of the impedance at the surface of a loudspeaker be corroborated by practical measurement, in such a way that models of active control may be realised in practice?

Physical measurements of the impedance at the loudspeaker cone depend on two factors - the correct transduction of cone velocity, and a suitable measurement of the pressure at the cone surface. Of these two tasks, an adequate measurement of the velocity of the loudspeaker cone is perhaps the easier to arrange.

4.2.1 Measuring velocity

Non-contact laser interferometry provides a definitive method for the measurement of loudspeaker cone velocity [78]. No change in mechanical impedance results, as is the case for velocity transducers which are physically attached to the surface of a loudspeaker and whose added mass changes the dynamics of the system. The effects of non-pistonic motion can also be determined, to great effect in the diagnosis and correction of cone break up and associated colouration. As a strategy for impedance measurements the principal drawbacks are in terms of cost, complexity and physical space penalties.

Laser interferometry is the first of several methods for measuring source volume velocity considered by Elliot and Anthony [79]. They note that a velocity gradient exists across the surface of a driver cone; ideally this gradient would only exist across the roll surround itself, but even within the 'pistonic' region a gradient is measured across the entire cone surface. The result is that the effective radiating area of the diaphragm is reduced, and in as much as it relates a point velocity measurement to the total effective source strength, it is found to be complex and frequency dependant. However, if the effective radiating area is known then it is noted that a single point measurement of particle velocity is sufficient to enable the correct specification of source strength. It is also noted that the 110mm diameter driver used in the test moved broadly in-phase (to 20° tolerance) up to a limit in frequency of about 500Hz. The 200mm drivers used in this project would be expected to exhibit break-up at

a lower frequency; no interferometry system has been available to this project, and so no measurement of the frequency limit of pistonic motion has been possible.

The second method reviewed by Elliot and Anthony is due to Salava [68]. The rather cumbersome device consists of two similar drivers positioned face-to-face where one is mounted within a sealed enclosure. This loudspeaker is driven electrically and the motion of the second is transduced using the electrical signal appearing at the voice coil terminals in the knowledge that

$$e = Blu \qquad \textbf{4.2}$$

Salava comments that as long as the compliant volume enclosed between the two loudspeaker cones is minimised, 180mm drivers may be used up to a limiting frequency of about 500Hz. It is also noted that determining the exact acoustic centre of the device may be difficult - this is likely to cause problems when modelling the radiated pressure in a room, although in the one-dimensional duct the issue is less significant.

A similar dynamic velocity transduction technique is reported by Salava [67] in an application where a driver is fitted with an additional voice coil which is used to transduce the coil velocity. The mechanical stiffness of the elements joining the two coils may limit the bandwidth of accurate coil velocity transduction, and electromagnetic coupling between the coils must be considered. However, the acoustic centre of this device is easier to determine which makes its performance in a three dimensional environment easier to predict.

Salava [68] also approves the use of drivers with a built-in accelerometer. It is noted that calibration and tests for linearity are important, and in applications where the phase of radiated pressure is important (eg active control) the microphone used for pressure detection should be likewise calibrated. The effect of the additional mass of the measurement accelerometer is not considered - however Nicholson [72] discusses this problem in some detail, along with other factors connected with the use of direct transduction of velocity using the Knowles accelerometer.

Nicholson considers the mass load applied by the addition of a measurement accelerometer both in terms of a change in the overall mass part of the lumped mechanical impedance of the source, and in terms of the local changes in surface mass introduced by a device. The

added mass of the BU-1771 at 0.28g is small compared to the quoted mass of the KEF B200 cone at 24g, and no significant change in the fundamental lumped mass-spring resonance of the device is introduced. However, the position of the measurement accelerometer is shown to be crucial. At frequencies as low as 150Hz significant differences appear in the magnitude and phase of velocity between accelerometers mounted at different points on the cone, as the local mass load encourages the onset of non-pistonic motion. Accelerometer locations where the dust cap meets the cone are shown to be most suitable - at these points the cone is maximally stiff, and differences between measurements taken around the edge of the dust cap are insignificant below 200Hz. Such an accelerometer mounting location was retained for measurements presented in this Thesis.

Nicholson also examines the calibration of the BU-1771 accelerometer, and notes that different wiring arrangements (allowing various gain settings from the internal FET amplifier built into the accelerometer package) result in changes in the phase difference between the Knowles output, and a reference output from a B&K type 4374 device. The chosen response for the velocity measurement is optimised by observing the performance of the controller in achieving an optimal characteristic termination. The accelerometer connection selected by Nicholson has been retained for this project. Schematics of the accelerometer and associated signal conditioning are presented in Appendix C along with calibration data comparing the output of the BU - 1771 unit with a D.J.Birchall type A/23/E unit.

4.2.2 Measuring pressure

A measurement of pressure is required which is representative of the total pressure at the surface of the loudspeaker, and which can be used to determine the surface impedance of the control source. In three dimensions pressure varies considerably over the surface of the cone, and some care is required in selecting an appropriate measurement location which is representative of the actual surface impedance. The three-dimensional case is the subject of further comment in Chapter 8. Below the 'plane wave cut-off frequency' [8] the pressure in the one-dimensional duct consists solely of plane waves which propagate along the duct axis. The location of the microphone used for impedance sensing is therefore less critical. At low frequencies standing wave patterns form which vary slowly with location along the duct, and it is unlikely that the termination impedance will be such that a microphone located close to the cone of the control source is placed at a pressure node.

Nicholson [72] investigates microphone locations immediately adjacent to the control source cone, and on a frame 5mm from the dust cap facing the source. It was found that mounting on the cone produced a slightly flatter measured pressure response in a duct, and no problems due to vibration pick-up were reported. The final choice of microphone location was made on the basis of the observation of performance of active control. The frame mounting 5mm from the dustcap was selected, and has been retained for measurements presented in this Thesis.

During preliminary investigations associated with measurements presented in Chapter 7, it was found that the system becomes unstable and performs unpredictably if the microphones have any sensitivity to either the mechanical velocity of an adjacent loudspeaker cone, or to the acoustic particle velocity of the sound field at the microphone location. A signal is required which is only proportional to pressure, and any directional component in the microphone response has the result that the true surface impedance can no longer be detected. Some care was taken to select sealed omnidirectional electret pressure capsules, and tests were carried out to ensure that the performance of the devices did not deviate from that of a calibrated omnidirectional condenser measurement microphone within the strongly reactive standing wave sound field inside the duct. Microphone calibration data is included in Appendix C along with schematic diagrams of signal conditioning apparatus.

4.3 Relating measured pressures and velocities to surface impedance

Standing wave ratio measurements were carried out in a duct in order to test the function of the control system in detecting the control source surface impedance and forcing it to a user specified value. Descriptions of the standing wave ratio method for the measurement of specific acoustic impedance are widely available [eg 80,81,82], and a method is included in Appendix B. Figures 4.2 and 4.3 show the magnitude and phase of the termination impedance provided by a KEF B200 driver driven acoustically at the end of a 4m long duct, as a function of frequency. The electrical connections to the driver were shorted to simulate connection to a low output-impedance 'constant voltage' amplifier. Calibrated pressure and velocity measurements are compared to results obtained using the standing wave ratio method.

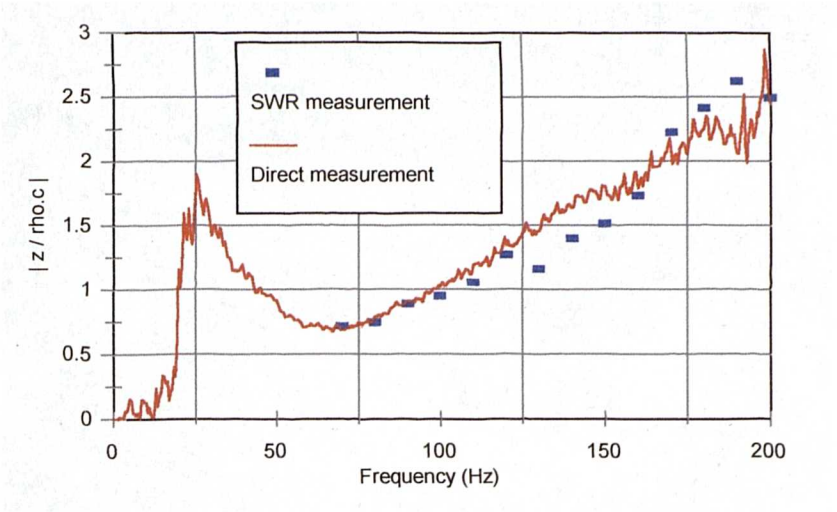

Figure 4.2 - Magnitude duct termination impedance due to acoustically driven KEF B200 loudspeaker

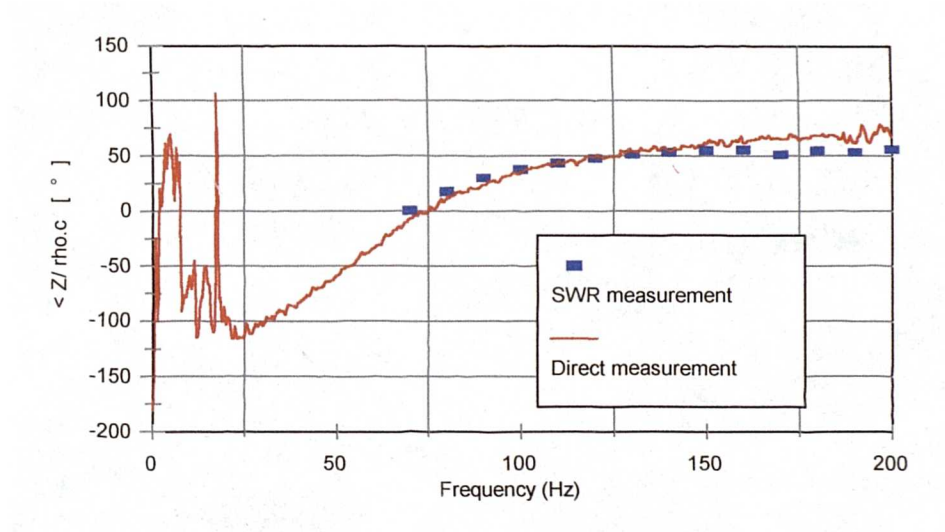

Figure 4.3 - Phase of duct termination impedance due to acoustically driven KEF B200 loudspeaker

It should be noted that for frequencies below 25Hz, low-frequency pressure 'leaks' in the test duct conspire with the frequency response of the transducers and associated signal conditioning, such that very low frequency impedance results by direct measurement are in error. Reasonable agreement is however seen between standing wave ratio measurements and impedances derived from the direct measurement of pressure and velocity. The acoustically driven loudspeaker presents a near characteristic load to the duct between approximately 75Hz and 100Hz - in the vicinity of its own mechanical resonance. Further

discussion of these measurements is undertaken in Chapter 7, in the context of active control using the biquad fit method.

The input impedance to the duct and the termination impedance were also measured during the operation of the active impedance control system. The system was configured to drive the ratio of pressure to velocity to a real value, given by system variable I. This constant sets the gain of filter F_d in the pressure measurement signal path (Figure 4.1), and is inversely proportional to the impedance magnitude at the surface of the controlled source.

The calibration of I in terms of the true specific acoustic impedance at the control source is a function of the sensitivity of the transducers and the gain inherent in the signal conditioning used in each signal path. Comments by Darlington [45] on the effect of gain and phase errors due to the transducers and associated electronics have already been noted. Figures 4.4 and 4.5 show the magnitude and phase of impedance measured directly; the termination impedance measurement may be compared to data derived using the standing wave ratio method . The measurement was made at a frequency of 45Hz - the lowest axial modal frequency in a small test room used for active impedance control.

Magnitude standing wave data follows similar trends to direct measurement impedance results. Smaller values of I result in a termination impedance which appears slightly larger

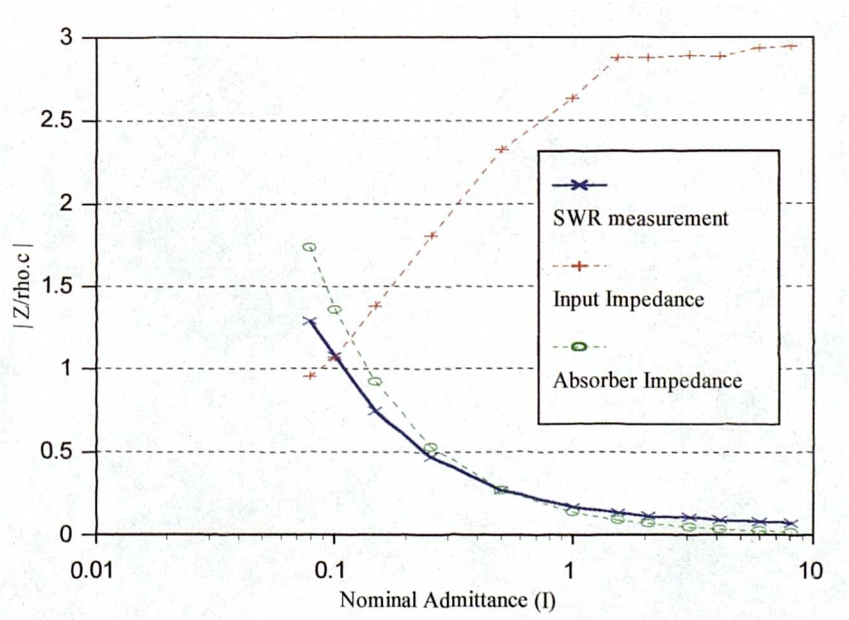

Figure 4.4 - Magnitude of controlled duct termination impedance

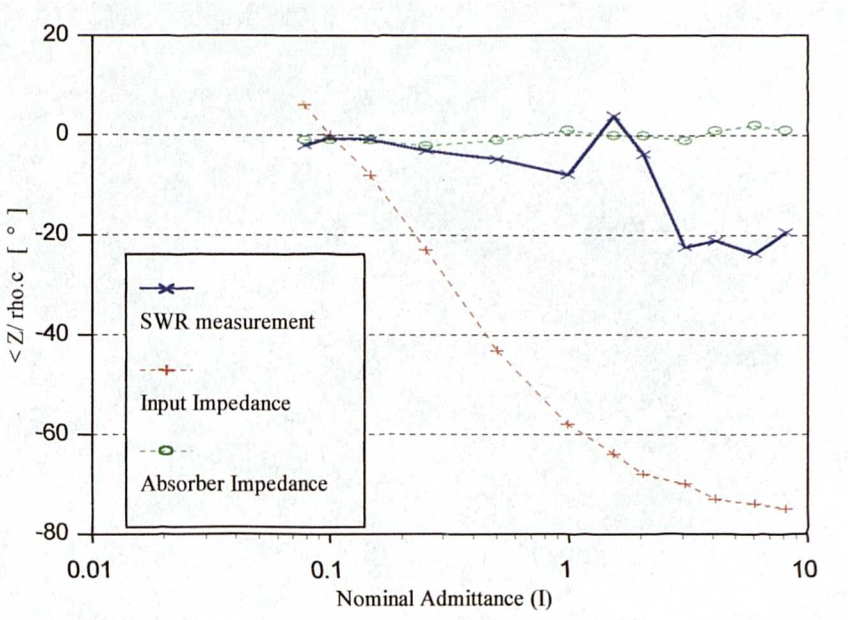

Figure 4.5 - Phase of controlled duct termination impedance

in magnitude using SWR measurement than by direct transduction. However in this region the phase between the two methods agrees more closely. Direct measurements suggest that the controller is able to maintain a purely real termination impedance of varying magnitude. Standing wave ratio measurements suggest that the impedance may have a small imaginary part which is inversely proportional to the magnitude of the controlled surface impedance.

4.4 Active impedance controllers and modal control of a one-dimensional duct

The system described in sections 4.1 to 4.3 has been used to modify the acoustics of one-dimensional environments, and the results of such investigations are available in the literature [eg. 37,38,41,45,54,72]. These results are important in terms of providing a point of reference for the development of novel IIR feedforward control systems in Chapters 6 and 7, as well as providing a foundation on which the novel investigation of impedance control in a room takes place in Chapter 8. A summary is therefore provided in sections 4.4.1 and 4.4.2, in terms of the derivation of appropriate target impedances for one-dimensional control and the performance of practical implementations of these impedances.

4.4.1 Target impedances for one-dimensional control

In Chapter 3 it was shown that large termination impedances produce clearly identifiable natural modes in a duct, which are scaled by shape functions or eigenvectors which describe the spatial distribution of these modes. Further it was shown that the termination impedance determines the amount of damping in the system, which sets the Q factor for each mode. Using the two-port formulation of the pressure in the duct derived in section 3.1, the effect of changing termination impedance can be clearly demonstrated.

Figure 4.6 shows that if the specific termination impedance of the duct is set to equal ρc, the frequency characteristic of the input impedance (and hence pressure) is found to be flat, and this finding is true at all locations along the duct.

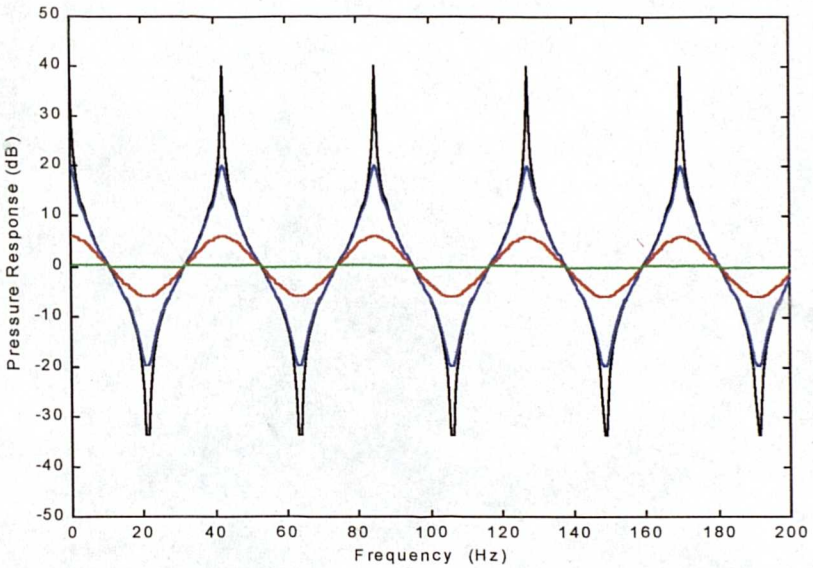

Figure 4.6 - Input impedance of a 4m waveguide. Z_L= : a) 100.ρc, b) 10.ρc c) 2.ρc d) 1.ρc

Figure 4.7 further demonstrates that at a point 1.8m along the 4m duct, the frequency characteristic of pressure for unity velocity input is still flat when $Z_L = \rho c$. When $Z_L = 10.\rho c$, a modal response prevails and the pressure is scaled by the values taken by the eigenvectors at the specific receiver location. It is therefore clear that a characteristic termination defines the optimal target impedance in terms of a reduction in the variance of pressure with respect to frequency and space. Such a termination also provides optimal control of the time domain decay of the acoustic modes of the duct, as shown by the practical measurements reported in section 4.4.2.

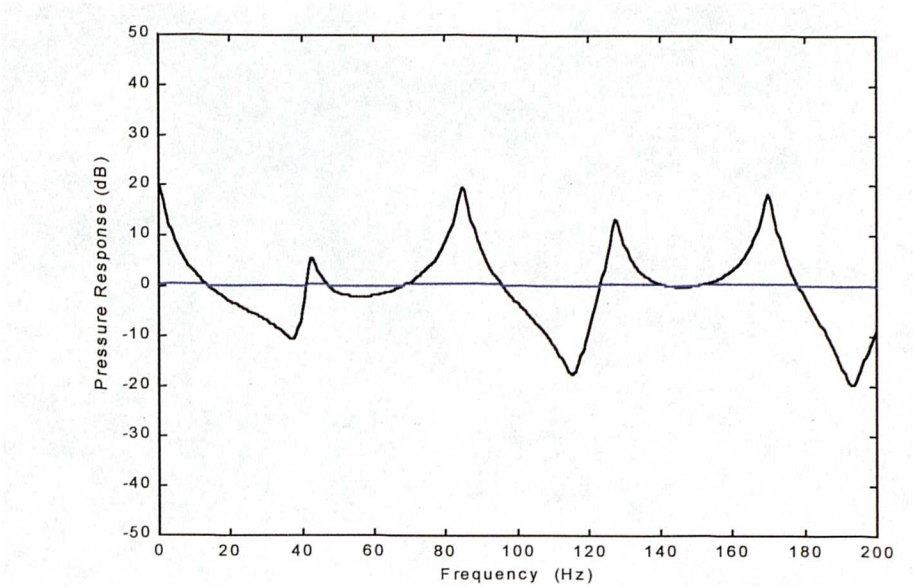

Figure 4.7 - Pressure at x=1.8m a) $Z_L = \rho c$ b) $Z_L = 10.\rho c$

4.4.2 Practical performance of one-dimensional impedance control systems

Practical demonstrations of active impedance control in the one-dimensional waveguide are detailed by Nicholson [41]. The following results were obtained by Darlington and Avis [54] in a comparison of the time/frequency response of a 4m duct and a small room with active impedance control. Decay Spectra are presented which describe the control of normal modes of an enclosed soundfield using an impedance controller. The visualisation techniques are introduced in the context of a resonant waveguide and are extended in Chapter 8 to investigate the acoustics of a small reverberant room.

Figure 4.8 shows the raw time/frequency response of the 4 metre circular duct to excitation from a KEF B200 loudspeaker at x=0, terminated with a similar loudspeaker at x=4m. The terminating loudspeaker was not electrically driven, but had a velocity governed by the pressure at its cone, and its own mechanical impedance. The low value of this impedance near the resonance of the terminating loudspeaker (Figure 4.2) gave the lowest frequency modes a rather poor quality factor and so the response at higher frequency is shown. The dependance of the eigenvalues and modal Q factor on the complex impedance provided by the terminating driver are discussed further in section 7.1.

The measurement was made by exciting the system with pink noise, which was truncated at time $t=0$. The time history of the energy decay in the duct was then captured, and by

division into successive windows the measurement was transformed into the frequency domain. This technique requires that the decay of the system is relatively long compared to the length of window used in the FFT analysis, and the bandwidth and order of that analysis was chosen accordingly.

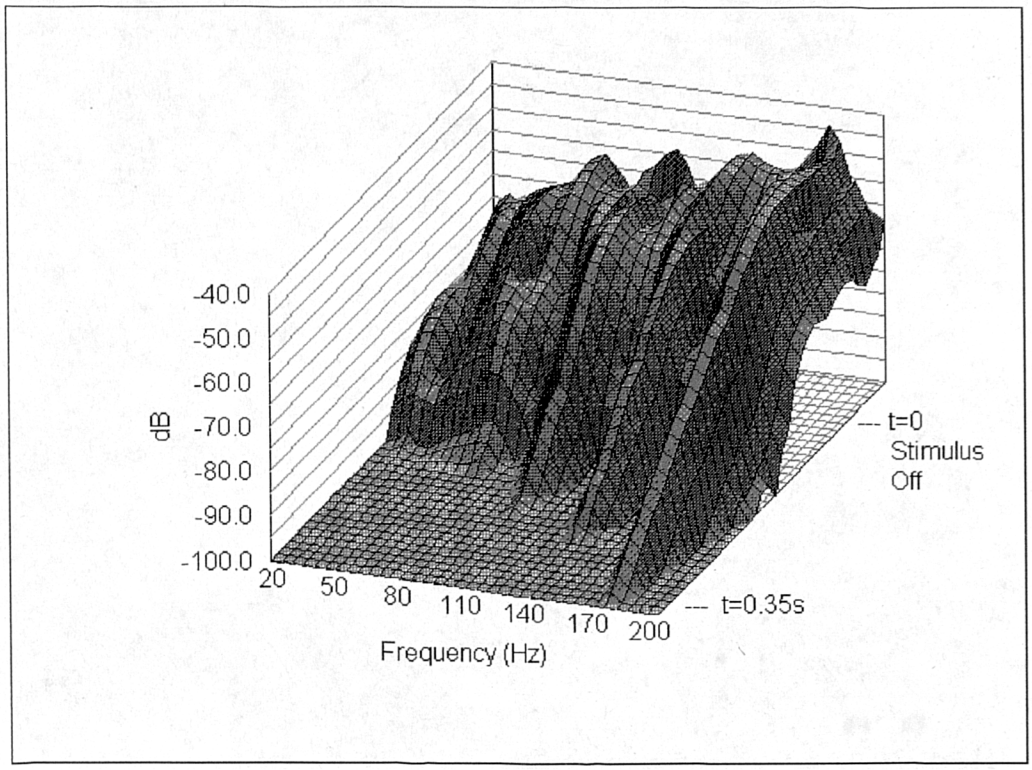

Figure 4.8 - Measured raw time / frequency response of a 4 metre duct terminated with a loudspeaker.

When the terminating loudspeaker is controlled to act as a characteristic termination (Figure 4.9), two effects are immediately visible. Firstly, the steady state response of the actively terminated duct is smoother, as the absorption has reduced the quality factor of the modes. Secondly, the decay rate of the modes is dramatically increased. This relationship is anticipated by the mathematics of Chapter 3, and as a result the decaying sound pressure possesses a far less tonal characteristic.

4.5 Summary of active impedance control

A control system has been developed which enables the specification of the complex surface impedance of a moving coil loudspeaker. This system relies on the accurate transduction of pressure and velocity, in order to implement useful control target impedances. The issues

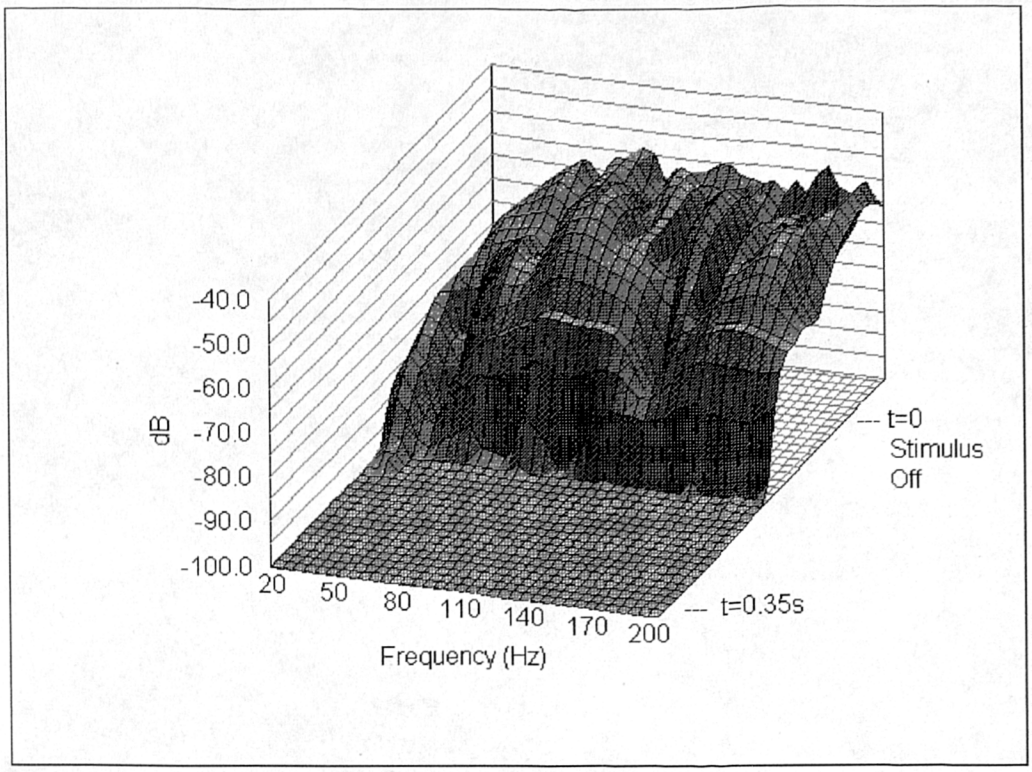

Figure 4.9 - Measured raw time / frequency response of a 4 metre duct actively terminated with a loudspeaker controlled to approximate a characteristic load.

of pressure and velocity measurement in a one-dimensional waveguide are considered in the literature, and have been summarised in sections 4.2 and 4.3.

It has been shown that a characteristic termination defines the optimal target impedance for a control system operating in a one-dimensional environment, and that a practical implementation of an active impedance control is able to converge to this target. Frequency and time -domain artefacts associated with the modal nature of the enclosed soundfield are shown to have been substantially attenuated, in line with behaviour anticipated in theory. Although these results are replicated elsewhere in literature, they are important in providing a starting point for the investigations of Chapters 6 to 8 in this Thesis.

The impedance controller is used as a point of reference in the development of novel one-dimensional control strategies in Chapters 6 and 7. However, the novelty associated with active impedance control itself resides in Chapter 8 where the technique is applied in a three-dimensional room. In this situation, issues surrounding accurate pressure transduction are revisited, building on the basis provided by the one-dimensional investigation.

Chapter 5

Novel feedforward active controllers

5.0 Introduction

The active control of acoustic impedance has been introduced as one potential strategy for the modification of modal sound fields. The second approach taken in this Thesis looks at fixed rather than adaptive control filters, where the transfer function between the source strengths of primary and secondary sources, rather than the surface impedance of the secondary source, are controlled. The control laws applicable in these two cases are related, as shown by Darlington [51].

The motivation behind an investigation into fixed filters resides in the desire of the industrial sponsor to avoid the hardware and potential instability costs of an adaptive system, and as a result a number of interesting alternatives have been explored. These solutions sacrifice some of the generality offered by impedance control systems, since the explicit specification of the transfer function between source strengths limits control applications to electroacoustic sources. The requirement for an electrical reference opens up the possibility of operating on the primary signal alone (ie. dispensing with the secondary sound source altogether) - however the work presented in this Thesis retains a primary / secondary source acoustic superposition and in this way the results obtained using each technique are directly comparable.

The transfer function between source strengths has been determined using digital filter models of the acoustics of the enclosure in which the sources are placed. FIR deconvolution based methods for removing room responses have been shown to be computationally expensive and slow to implement due to the length of filter required, particularly at low frequency where the decay time associated with uncontrolled natural

modes can be of the order of several seconds [58]. As an alternative, the use of IIR biquad models is investigated here as a basis for efficient active attenuation of low frequency room modes.

All-pole (ie recursive) inverse filters have been reported by Mourjopoulos *et al.* [59,62], where measured room responses are fitted with a filter approximation whose poles are located using numerical optimisation techniques. In contrast, the models in this work exploit an analytical description of the enclosed soundfield in terms of a modal decomposition, and in this sense are novel. This chapter is concerned with the development of these filters and contains a theoretical evaluation of some of the potential objections to the use of the technique. Numerical evaluations are carried out in Chapter 6 in a one-dimensional waveguide, and practical evaluations are reported in Chapter 7 for the duct and Chapter 9 for a three-dimensional room.

5.1 Non-adaptive IIR filter active control techniques

Where a medium in which control takes place does not change significantly during a time period when control is required (and is therefore 'time invariant'), a control filter may be designed for all time on the basis of one set of measurements which characterise that medium. If such a scheme is adopted then W is said to be non-adaptive or fixed. For control in an enclosed soundfield, a theoretical analysis suggests that the filter may be designed using a room model where the normal modes themselves form the building blocks from which the model is constructed. Not only is this approach intuitive in the formation of the room model; a modal description of room behaviour also offers possibilities for efficient control structures which simultaneously address frequency-domain Q-factor and time domain decay duration issues.

The normal modes of an enclosed space have been described in Chapter 3 and are essentially second-order functions. When the reverberant (at low frequency *modal*) soundfield in a room dominates the total pressure measured at some point, it seems reasonable to suggest that the measured soundfield might be well approximated in the frequency domain by the summation of a number of parallel second order bandpass filter sections. In terms of a digital implementation, these filter sections are available as biquadratic IIR filters [77]. A

description of the process of modelling measured transfer impedances with biquad sections is given below, and subsequently control options using biquad room models are discussed.

5.2 Room modelling using IIR filter sections

The wave solution for the sound field in one- and three- dimensional enclosures has been described in Chapter 3. An expression for the modal soundfield in a rectangular enclosure is reproduced below.

$$p(\boldsymbol{r}) = j\omega\rho Q c^2 \sum_n \frac{\psi_n(\boldsymbol{r})\psi_n(\boldsymbol{r}_0)}{\chi_n(\omega^2 - \omega_n^2 - 2j\omega\delta_n)} \qquad \textbf{5.1}$$

If source and receiver are located with respect to a modeshape such that the particular mode is excited and can be observed in the frequency response, (**5.1**) shows that in the frequency domain the mode appears as a second-order bandpass function whose magnitude is scaled by source and receiver shape functions. The phase of pressure is a function of damping and the proximity of the forcing frequency to the natural resonant frequency; and may additionally be flipped through 180° by a polarity change in one or other of the modeshapes.

Each individual mode may be modelled using a biquad filter section. Biquad filters are used here as second order bandpass networks, with zeros at DC and half-sample frequency, and a conjugate pole pair whose location in the Z-plane determines the centre frequency and Q factor of the transfer function. The Q-factor of the filter models damping and a scale factor is applied whose magnitude and sign reflects the magnitude and sign of the respective modal shape function due to source and receiver locations.

The success of a modal approach to designing a fixed control filter is partially dependant on non-modelled components (such as the residues of high-order modes) not introducing significant error when the system tries to reconstruct a desired soundfield in the space. The accuracy of the IIR room model (or 'Biquad fit') will be a function of frequency, source location, receiver location and damping. It might be expected that on-resonance, the fit (and so degree of control) might be superior to that off-resonance, when residues have significant magnitude in comparison to the dominant mode.

Following (**5.1**), a number of modes are modelled simultaneously by the summation of a similar number of bandpass biquad sections in parallel. Each modal peak in a measured transfer impedance is fitted with a modelled biquad response, where pole locations are manually adjusted to achieve the correct resonant frequency and Q-factor. The magnitude of the peak determines the size of the scale factor, whose polarity is found from phase data which reflects the sign of the modeshape.

Since (**5.1**) describes the pressure field resulting from a known source strength Q :

$$Q = \textit{surface velocity} \;.\; \textit{radiating surface area}$$

$$= u_0 \;.\; \textit{area}$$

it would seem appropriate to use the biquad analogy to fit transfer impedance measurements of

$$\frac{p(\boldsymbol{r}|\boldsymbol{r}_0)}{u_0} \qquad \textbf{5.2}$$

The transfer impedance is used since it conveniently relates the measured pressure at any location $\boldsymbol{r}$ within the room, to a source with velocity u_o located at $\boldsymbol{r}_0$. However, it is not always convenient to instrument a driver with an accelerometer and associated integrator to derive a velocity signal, and so transfer function fits are also investigated based on a measurement of

$$\frac{p(\boldsymbol{r}|\boldsymbol{r}_0)}{V_{in}} \qquad \textbf{5.3}$$

V_{in} = *input signal to amplifier driving control source*

It might be expected that this would introduce errors due to the transfer functions through the amplifier, and the voltage-velocity transfer function of the loudspeaker. These errors are discussed further in Chapter 9, where examples of each type of model are given; in either case, the biquad filter follows the z-domain form

$$Z_{r_0,r} = \frac{a_0 z^2 + a_1 z + a_2}{z^2 + b_1 z + b_2} \qquad \textbf{5.4}$$

where

a_0, a_1 and a_2 define the zero locations, b_0, b_1 and b_2 define the pole locations and $Z_{r0,r}$ describes the transfer function between source and receiver locations r_0 and r.

If the zeros are placed at DC and half sample frequency and the poles are conjugate (implying a causal filter which is realisable using real filter coefficients) then (**5.4**) reduces to

$$Z_{r_0 r} = \frac{z^2 - 1}{z^2 - 2Re(p)z + |p|^2} \qquad \textbf{5.5}$$

Examples of measured transfer impedances modelled using parallel banks of biquad filters of the above form are shown in Chapters 7 and 9 for one- and three- dimensional control environments respectively.

5.2.1 Modelled transfer functions within a one-dimensional waveguide

The preceding concepts are well illustrated by the formation of biquad models of a one-dimensional waveguide, using the modal solution for duct resonance introduced in section 3.2. It has been shown in Figure 3.3 that when the termination impedance is large, a good correlation between the pressure found using the sum of a number of modes and that found using the acoustic two-port (**3.2**) is achieved. The modal 'fit' may be thought of as an s-plane model of the sound field in the duct.

The IIR controllers investigated in this chapter require that the two port result can be modelled in the z-plane using a parallel bank of biquad filter sections. Because a z-plane modal 'fit' is carried out, the control method is referred to as the 'Biquad fit' method. The modal decomposition translates into the digital domain using (**5.5**), with biquad filter sections in the form

$$\frac{p(\boldsymbol{r})}{u} \propto Z_r(z) = \sum_i \frac{(z^2 - 1)}{z^2 - 2re(P_i)z + |P_i|^2} \qquad \textbf{5.6}$$

In the specific case of control of modes in a one-dimensional duct, a relationship is required between the s-plane mode fit shown in Figure 3.3 and a z-plane mode fit. Zero locations are chosen at DC and half-sample frequency, resulting in the $(z^2\text{-}1)$ numerator of (**5.6**). Pole locations are determined by equating the Q-factor and resonant frequency of modes modelled in the s-plane with the z-plane model.

The termination impedance of the system determines the damping applied to each mode, as described in (**3.6**). Damping coefficient δ_n is shown to equal $2c/\xi L$, where ξ is the large real

part of the specific normalised termination impedance. For a second order system, $Q=\omega_n / 2\delta_n$.. Therefore Q can be expressed as a function of termination impedance:

$$Q = \frac{\omega_n L \xi}{4c} \qquad \textbf{5.7}$$

The Q-factor can be derived from a ratio of resonant frequency to -3dB resonance bandwidth, and it can be shown that if

$$Q = \frac{\omega_{res}}{\omega_{upper\_3dB} - \omega_{lower\_3db}}$$

then **5.8**

$$\omega_{upper\_3dB} = \omega_{res} \cdot \left[1 + \frac{1}{2Q}\right]$$

For a given sample rate f_s,

$$\frac{(z_{res}^2 - 1)}{z_{res}^2 - 2re(P_i)z_{res} + |P_i|^2} \div \frac{(z_{-3}^2 - 1)}{z_{-3}^2 - 2re(P_i)z_{-3} + |P_i|^2} = \sqrt{2}$$

where **5.9**

$$z_{res} = e^{j\omega_{res}T}, z_{-3} = e^{j\omega_{-3}T}, T = \frac{1}{f_s}$$

The real and imaginary parts of the pole locations $P_i = a + jb$ may be found as functions of normalised specific termination impedance using (**5.7**) and (**5.8**) given that

$$\omega_n = \tan^{-1}\left(\frac{b}{a}\right) \cdot \frac{f_s}{2\pi} \qquad \textbf{5.10}$$

Analytically this solution is not straightforward. However, the problem may be solved numerically by selecting a value for resonant frequency (from the set of eigenvalues applicable to the boundary conditions in place) and using the relationship between Q and termination impedance to find the respective upper -3dB frequency. The z-plane angle for pole locations $\phi = \omega_{res} / f_s$, and the poles themselves may be incrementally moved along radii at $\pm\phi$ until (**5.9**) is satisfied.

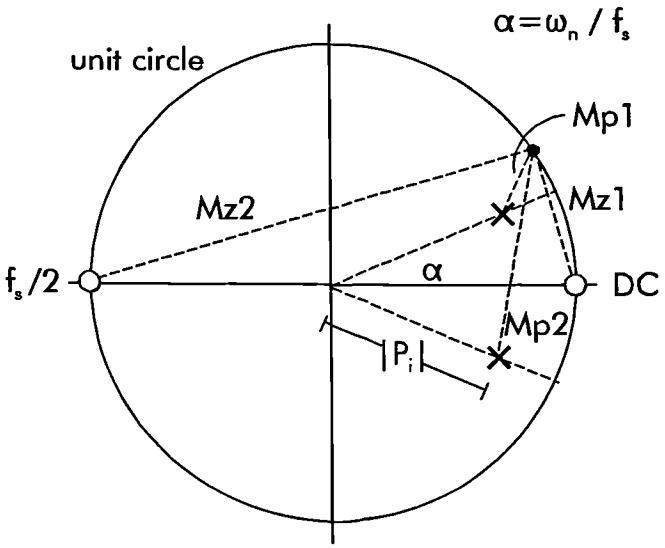

Figure 5.1 - Z-plane response of second-order bandpass filter

This process may be visualised using Figure 5.1. Graphically, the magnitude response of the biquad filter is found from [77]

$$|H(z)| = \frac{Mz1 . Mz2}{Mp1 . Mp2} \qquad \textbf{5.11}$$

Therefore as the pole radius $|P_i|$ is reduced, the Q of the filter will also reduce.

In order to complete the z-plane model, it is necessary to build a 'zeroth mode' component to represent the lumped compliance of air inside the duct. In an s-plane model this is accomplished using a single-pole first order filter having frequency response:

$$H(j\omega) = \frac{1}{j\omega - P_0} \qquad \textbf{5.12}$$

P_0 is a left-half plane pole which is real in s, and has magnitude α. Therefore when $\omega=\alpha$ the magnitude frequency response will have fallen by 3dB. The s-plane pole location is given by the damping coefficient such that $\alpha = -\delta_n = \omega_{-3dB}$. With this knowledge of the 3dB-down frequency, the pole location for the z-plane zeroth mode model is found using the one-dimensional optimisation method (Figure 5.1) employed to locate the higher mode poles.

The response of a biquad filter model of the 4m duct is compared to the s-plane modal decomposition and two-port models in Figure 5.2. A sampling frequency of 5kHz was used in conjunction with a specific termination impedance equal to $50\rho c$. The response to a unit velocity input is plotted, for a receiver adjacent to a source at one end of the duct.

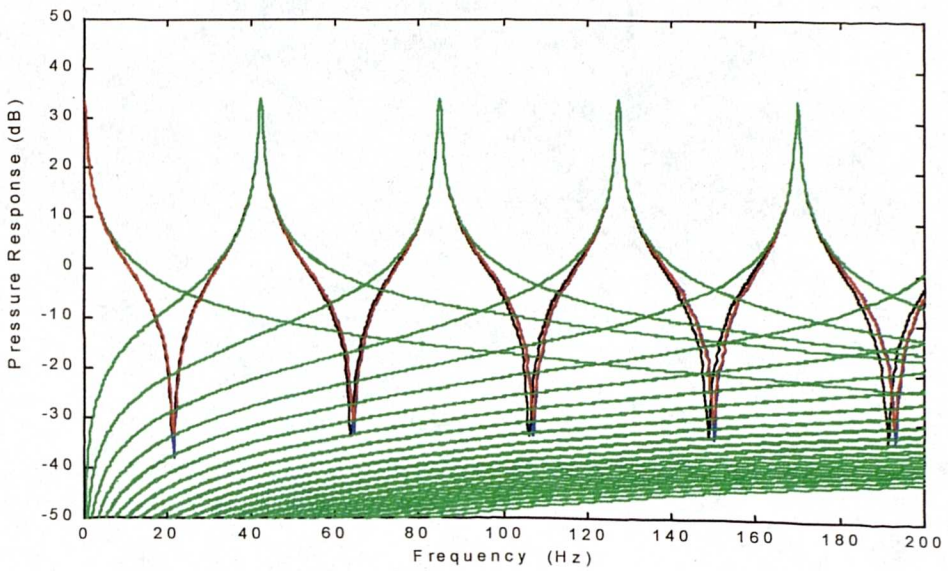

Figure 5.2 - Modal decomposition of pressure in 4m duct a) s plane modal sum b) z plane sum c)Two-port formulation d) individual modes in s and z

Respective individual s-plane and z-plane modes (shown in green) overlay to the point where they are not distinguishable. A summation of either modal decomposition fits a two-port duct model well, but off resonance the fit is poorer, especially at higher frequency. This is due to the small number of modes used in the summation (in this example $n=20$); the absence of many (largely coherent) modal residues ensures that when no one mode is dominant, the summation is in error. The significance of this error is therefore a function of the ratio of dominant modal amplitude to the amplitude of the sum of residuals.

This result is also noted by Bullmore *et al.* [21] - the rate of convergence of a modal summation is described as decreasing with increasing frequency, meaning that more modes are required to model the true pressure as the forcing frequency is raised. This result is observed in Figure 5.2, and is even more pertinent to the point source models used in this work, than to the rectangular pistons adopted by Bullmore.

5.3 Implementing control using a biquad model

Before the model can be used to implement active control, the task must be specified. In more complex acoustic environments this can itself present a challenge, but in the one dimensional waveguide the desired target for control is more self evident. An analogy with active acoustic impedance control suggests that what is required is a reduction in modal Q factor, corresponding to a real specific termination impedance which takes value somewhere between infinity and ρc.

Considering one individual mode in the summation, a re-specification of the pole locations is needed in order to reduce the Q factor. Such a reduction could be expected to reduce the scaling of the modeshape and hence the spatial variation of pressure due to the one mode. Considering the relationship between Q factor, damping and modal decay constant discussed in section 3.4 the decay time of each mode should also decrease - a significant objective in the light of the findings of Olive *et al.* [3] in respect of subjective modal audibility. The relocation of system poles by the introduction of a control source and associated filters forms the object of the following mathematics.

The pressure at a particular location in a duct is given by the sum of contributions from primary and secondary sources. If the input to the secondary source is passed through a control filter with z domain response *C(z)*, a model of the total pressure due to one mode is given by

$$y(z) = \frac{scale_p(z^2-1)}{z^2-2Re(p_i)z+|p_i|^2} + C(z).\frac{scale_s(z^2-1)}{z^2-2Re(p_i)z+|p_i|^2} \qquad \textbf{5.13}$$

where

C(z) is the z-domain response of the control filter

The scale factors associated with each section describe a combination of the respective source strengths and the product of the respective values of modal shape functions at source and receiver locations. They may be specified by a set of values determined from an iterative 'biquad fit' process, where scale factors along with resonant frequencies and Q factors are assigned to each z-plane mode by comparison with measured data. In this way, the pole locations p_i reflect the biquad fit of practical measurements.

If the mode is to be controlled and the Q-factor reduced, the poles must be moved to new locations $p_{i,n}$ by the action of the control filter. The RHS of (**5.13**) is equated with a new mode model representing the desired room response component provided by the mode in question:

$$\frac{scale_p(z^2-1)}{z^2-2Re(p_{i,n})z+|p_{i,n}|^2} = \frac{scale_p(z^2-1)}{z^2-2Re(p_i)z+|p_i|^2} + C(z).\frac{scale_s(z^2-1)}{z^2-2Re(p_i)z+|p_i|^2} \qquad \textbf{5.14}$$

$p_{i,n}$ represent desired z-plane pole locations for the i^{th} mode: p_i represent existing locations

Making the controller *C(z)* the subject,

$$C(z) = \frac{scale_p}{scale_s}.\frac{-2[Re(p_i)z-Re(p_{i,n})z] + [|p_i|^2 - |p_{i,n}|^2]}{z^2-2Re(p_{i,n})z+|p_{i,n}|^2} \qquad \textbf{5.15}$$

Inspection of (**5.15**) reveals the important result, that the controller is comprised of a single biquad. The poles of this filter are defined by the poles of the new desired mode specified on the LHS of (**5.14**), and the controller zeros are found from the subtraction of the poles of the desired mode from the poles of the existing mode.

If more than one mode is considered simultaneously, then the filter structure becomes more complex. For instance, with two modes

$$y(z) = \frac{scale_{pi}(z^2-1)}{z^2-2Re(p_i)z+|p_i|^2} + \frac{scale_{pj}(z^2-1)}{z^2-2Re(p_j)z+|p_j|^2} + C(z).\left[\frac{scale_{si}(z^2-1)}{z^2-2Re(p_i)z+|p_i|^2} + \frac{scale_{sj}(z^2-1)}{z^2-2Re(p_j)z+|p_j|^2}\right] \qquad \textbf{5.16}$$

so let

$$y(z) = \frac{scale_{pi}(z^2-1)}{z^2-2Re(p_{i,n})z+|p_{i,n}|^2} + \frac{scale_{pj}(z^2-1)}{z^2-2Re(p_{j,n})z+|p_{j,n}|^2} \qquad \textbf{5.17}$$

The maths is simplified by writing

$$\frac{(z^2-1)}{z^2-2Re(p_i)z+|p_i|^2} = F_i(z) \qquad \textbf{5.18}$$

and (**5.15**) is solved for *C(z)* such that for *N* modes

$$C(z) = \frac{\sum_{i=1}^{N} scale_{pi}.(F_{i,n} - F_i)}{\sum_{i=1}^{N} scale_{si}.(F_i)} \qquad \textbf{5.19}$$

The denominator of (**5.19**) involves the formation of the inverse secondary path transfer function.

Where more than one mode is considered simultaneously, this inverse requires careful design. Considering initially two modes in the secondary path:

If

$$Z_{s,r} = \frac{scale_1(z^2-1)}{z^2-2Re(p_1)z+|p_1|^2} + \frac{scale_2(z^2-1)}{z^2-2Re(p_2)z+|p_2|^2}\,[+...]$$

then

$$Z_{s,r} = \frac{scale_1(z^2-1).(z^2-2Re(p_2)z+|p_2|^2) + scale_2(z^2-1).(z^2-2Re(p_1)z+|p_1|^2)}{(z^2-2Re(p_1)z+|p_1|^2).(z^2-2Re(p_2)z+|p_2|^2)} \qquad \textbf{5.20}$$

and

$$\frac{1}{Z_{s,r}} = \frac{(z^2-2Re(p_1)z+|p_1|^2).(z^2-2Re(p_2)z+|p_2|^2)}{(z^2-1).\left[scale_1.(z^2-2Re(p_2)z+|p_2|^2) + scale_2.(z^2-2Re(p_1)z+|p_1|^2)\right]}$$

More generally, for more than two modes

$$\frac{1}{Z_{s,r}} = \frac{(z^2-2Re(p_1)z+|p_1|^2).(z^2-2Re(p_2)z+|p_2|^2).(...).(z^2-2Re(p_N)z+|p_N|^2)}{(z^2-1).\sum_{n=1}^{N} scale_n.\left[\prod_{k=1}^{N}(z^2-2Re(p_k)z+|p_k|^2)\right]} \qquad \textbf{5.21}$$

where k cannot assume the value taken by n - eg. n=2, *N*=5, *k*=1,3,4,5

The term inside the sum in the denominator of (**5.21**) is a 2(*N*-1) order polynomial, which can be solved numerically to determine its roots (an algorithm implemented in the package 'MATLAB' has been used in this work). These roots are found to occur in conjugate pairs, with the result that the *N* parallel sections of $Z_{s,r}$ are transposed for $1/Z_{s,r}$ into a cascade of *N* sections, one of which has poles described by $(z^2 - 1)$.

This holds true whilst all modes have a common numerator (ie zeros at DC and half-sample frequency.) The 'zeroth' mode of a space (the mode centred on DC representing the lumped acoustic compliance of the air volume, with losses provided by leakage) has been shown to be correctly modelled by a first order transfer function with one real z-plane pole. Therefore, when attempting to incorporate a model of the zeroth mode of a space, an approximation must be made to enable the filter section to follow the same general form as the higher modes. Where an approximation has been used in this work, it takes the form of a second order bandpass function centred on a very low frequency with Q-factor adjusted to approximate practically measured data.

Having dealt with the denominator, the numerator of (**5.19**) is solved as follows;

$$scale_{pi}.(F_{i,n}-F_i) = scale_{pi}.\left[\frac{(z^2-1)}{z^2-2Re(p_{i,n})z+|p_{i,n}|^2} - \frac{(z^2-1)}{z^2-2Re(p_i)z+|p_i|^2}\right]$$

$$= \frac{scale_{pi}.(z^2-1).\left[-2[Re(p_i)z-Re(p_{i,n})]z + |p_i|^2 - |p_{i,n}|^2\right]}{(z^2-2Re(p_{i,n})z+|p_{i,n}|^2).(z^2-2Re(p_i)z+|p_i|^2)} \qquad \textbf{5.22}$$

On closer inspection, (**5.22**) turns out to be formed by two biquad sections in series. Poles are provided by existing and desired modes respectively. The zeros of one biquad are at DC and half sample frequency, and the zero of the other biquad is provided by the term in square brackets. One section must include the scale factor. The complete control filter therefore has *N* parallel branches with two series modes in each (**5.22**) representing the numerator of (**5.19**), which are summed and fed into a cascade of *N* sections which form the denominator. The filter is illustrated overleaf in schematic form as Figure 5.3.

The preceding mathematics illustrates that in order to use z-plane biquad fit models for modal control, a z-plane expression for the *desired* modal behaviour (ie a reduction in Q factor) must be specified. Whilst the construction of a z-plane model of one dimensional system with large termination impedance has been demonstrated in section 5.2.1 (and specifically in Figure 5.2), the same process is not so straightforward if the termination impedance tends towards a characteristic value. This is of great importance when building a model for the *desired* pole locations, since in the limit it appears that a requirement exists for a modal model of a characteristically terminated system.

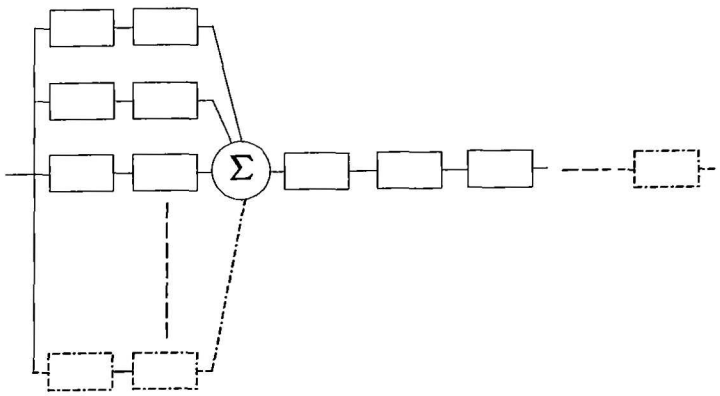

Figure 5.3 - Schematic layout of Q-factor modification filter

5.4 Modelling desired responses with a modal decomposition

Before a digital model of a system with limited boundary impedance is attempted, it is instructive to consider the s-plane modal deconstruction built up through Chapter 3. As termination impedance tends towards ρc, the modal solution starts to become inaccurate. Figures 5.4 and 5.5 below may be compared with Figure 5.2; the equivalence of the two-port duct model (black trace) and an s-plane modal summation (blue trace) starts to break down as termination impedance decreases from $10\rho c$ to $2\rho c$ and finally to ρc.

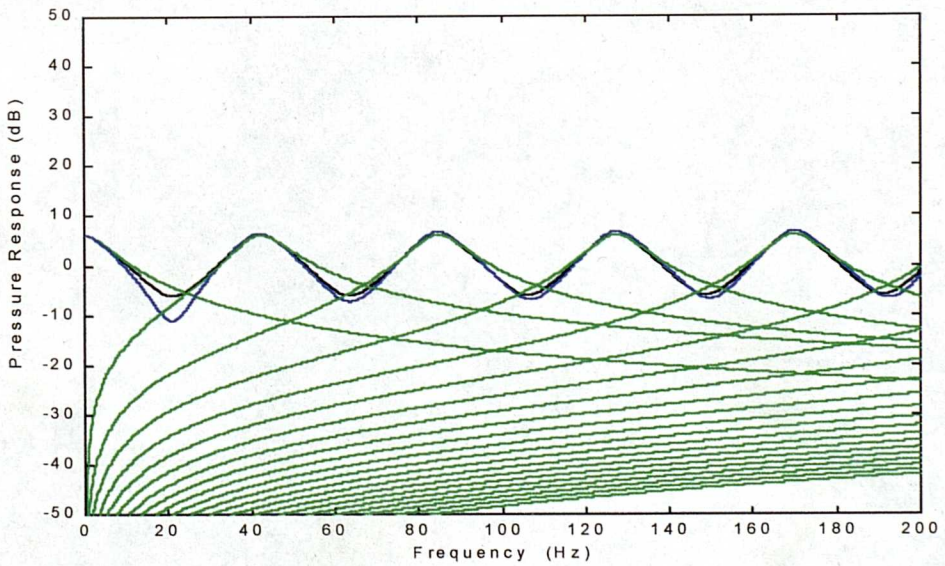

Figure 5.4 - Modal decomposition where $Z_L = 2\ \rho c$
a) s plane modal sum b)Two-port formulation
c) individual s -plane modes

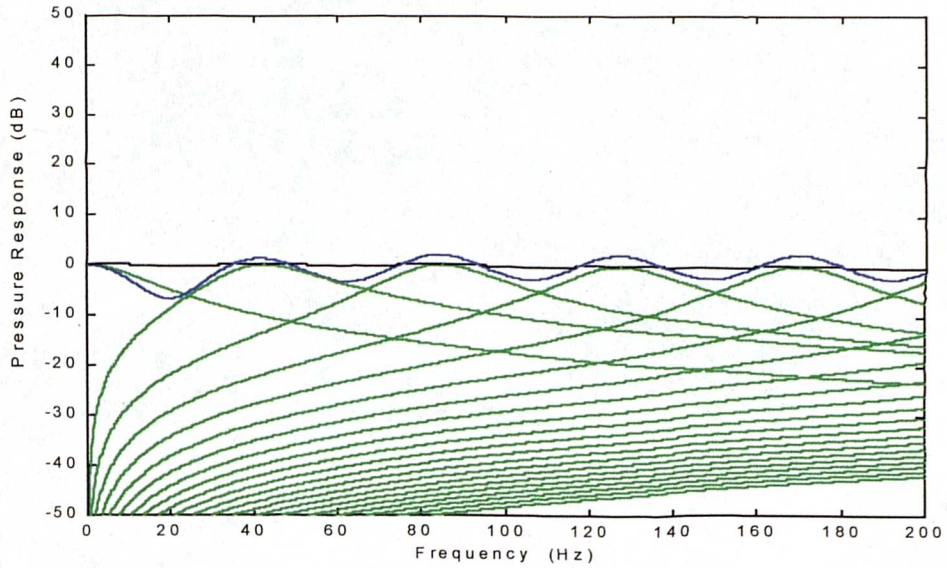

Figure 5.5 - Modal decomposition where $Z_L = \rho c$
a) s plane modal sum *b)Two-port formulation*
c) individual s -plane modes

As the termination impedance approaches a characteristic value, the sum of the conventional set of second-order modes no longer agrees with an acoustic two port solution. In the ρc limit, the two port solution correctly predicts a flat pressure response with respect to frequency, but the modal decomposition deviates from this result. Two explanations are possible for this deviation:-

- The relationship between damping coefficient δ_n and termination impedance of **(3.6)** may become increasingly inaccurate as the boundary condition becomes less rigid. Therefore the modal decomposition may still be valid, but the Q of individual modal contributions may require modification in order that the sum of the modes produces the expected result.

- It may be true that the sum of a number of conventional second order bandpass functions no longer forms a solution to the wave equation in the duct, when the boundary condition tends towards a characteristic value.

Since the derivation of the modal decomposition of pressure in an enclosed soundfield takes place for systems with rigid or near-rigid boundaries [6,11], it appears that the second explanation is the more likely. This appears to limit the possible control benefit which may

be gained by specifying pole locations for desired modes with very low quality factor. However, within the constraints imposed by the limitation of the applicability of modal theory it is still possible that useful control outcomes may be achieved.

Figures 5.4 and 5.5 describe the input impedance to the duct, where all modeshapes have unit value. At locations *along* the duct, the picture is further complicated by the invalidity of the use of simple cosine modeshapes when termination impedance is small. In Figure 5.6, cosine modeshapes are compared to a solution using the Morse and Bolt cosh modeshapes introduced in section 3.3. The duct length is 4m, mode order $n=4$, the termination impedance is $2\rho c$ and the forcing frequency corresponds to the eigenvalue k_4. The source driver impedance is effectively infinite since the velocity of the source is specified explicitly.

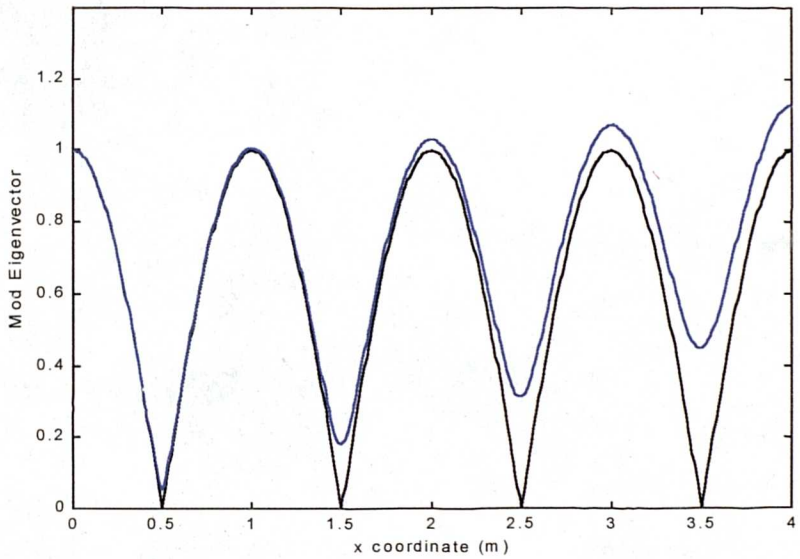

Figure 5.6 - Comparison of a) Cosine modeshapes to b)Morse and Bolt formulae

The difference in application of these alternative modeshape formulae can be clearly seen in Figure 5.7, where the pressure response at a point 1.8m along the duct is calculated using the acoustic two-port and compared to results derived using Morse and Bolt, and cosine, modeshapes.

These differences are exacerbated if the termination impedance decreases further to ρc. Even though the Morse formula is not strictly valid as the boundary condition becomes characteristic, the result in Figure 5.8 suggests a model using this result can track the two-

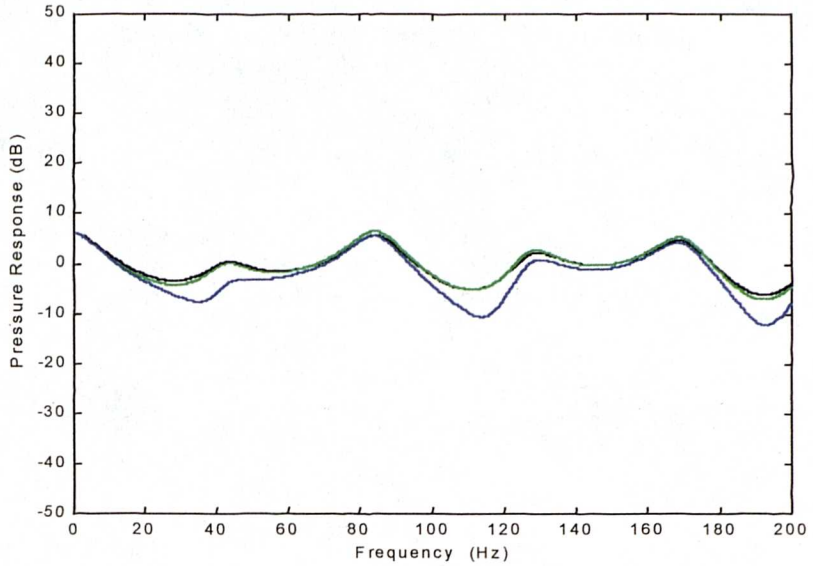

Figure 5.7 - $Z_L = 2\rho c$, x=1.8m. Comparison of
a) Cosine modeshapes b)Morse and Bolt formulae
c) Two-port formulation

port model (with *no* visible modal features) much more accurately than when cosine modeshapes are employed.

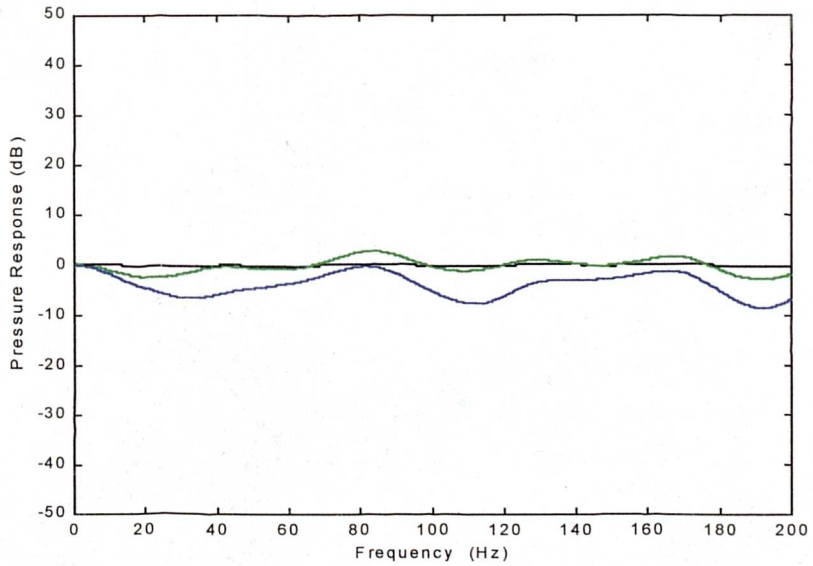

Figure 5.8 *$Z_L = \rho c$, x=1.8m. Comparison of*
a) Cosine modeshapes b)Morse and Bolt formulae
c) Two-port formulation (y=0)

The result echoes that developed in Appendix G, where it is shown that as the termination impedance starts to approach characteristic value, the truncation of the series expansions used in the derivation of the modeshape formulae become significant. It is possible that the

error between series *b)* and *c)* of Figure 5.8 would be further reduced by the inclusion of higher powers of boundary impedance ζ, but Figure G2 suggests that this is of marginal benefit when the boundary is significantly non-rigid.

Feedforward control processes utilising biquad system models require the specification of a desired mode in terms of a *z-plane* filter section with low Q-factor. In the following section 5.4.1, z-plane filter responses are related to the s-plane work in Figures 5.6 to 5.8, and additional sources of error are identified.

5.4.1 Using z-plane filters to model a desired response when termination impedance tends to characteristic value

Rather than incorporating shape functions into the model from the outset, this analysis commences with an investigation of a duct input impedance modelled using z-plane biquad filters. Z-plane modal decompositions are compared with s-plane counterparts in Figure 5.9. To facilitate comparison with the s-plane decomposition, the same desired specific termination impedances of *a) 10.ρc, b) 2.ρc* and *c) ρc* are considered.

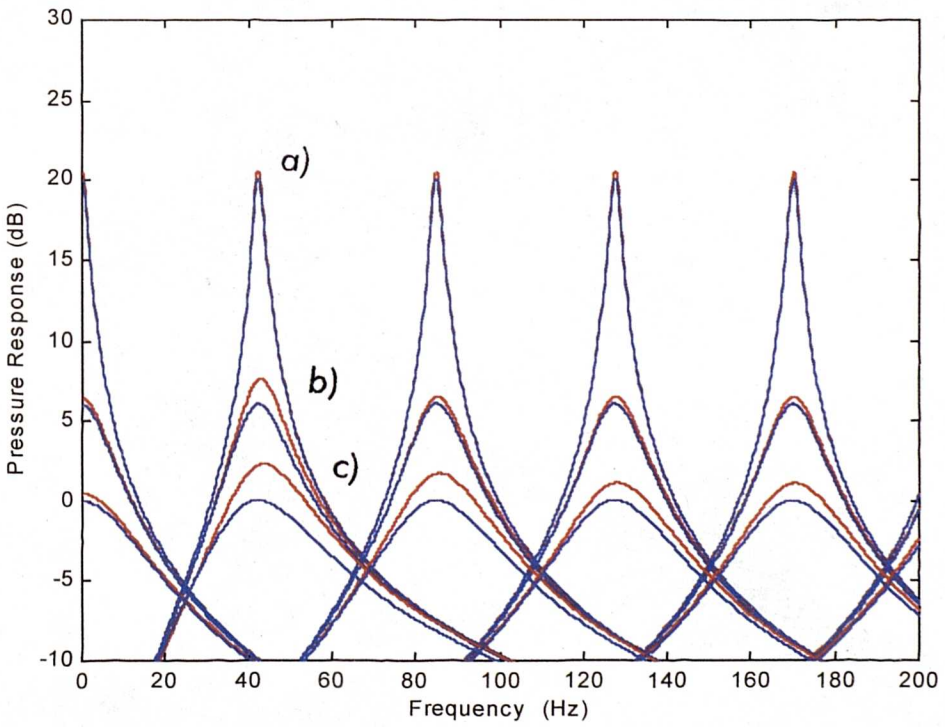

Figure 5.9 - Comparison of modal decompositions using i) s-plane ii) z-plane polynomials

S- and z- plane zeroth mode models are very nearly equivalent regardless of termination impedance. However, as the termination impedance tends to characteristic value the other modal responses show respective s- and z- plane responses which increasingly diverge. This divergence is greatest for lower Q-factor, coinciding with decreased z-plane pole radius $|P_i|$.

Comparison of z-plane and s-plane bandpass pole-zero plots suggests a basis for this divergence (Figure 5.10). For hi-Q filters, poles lie close to the unit circle and close to the real frequency axis. The dominant pole determines the shape of the resonance, and the second pole has little influence on frequency response. With lower Q z-plane filters

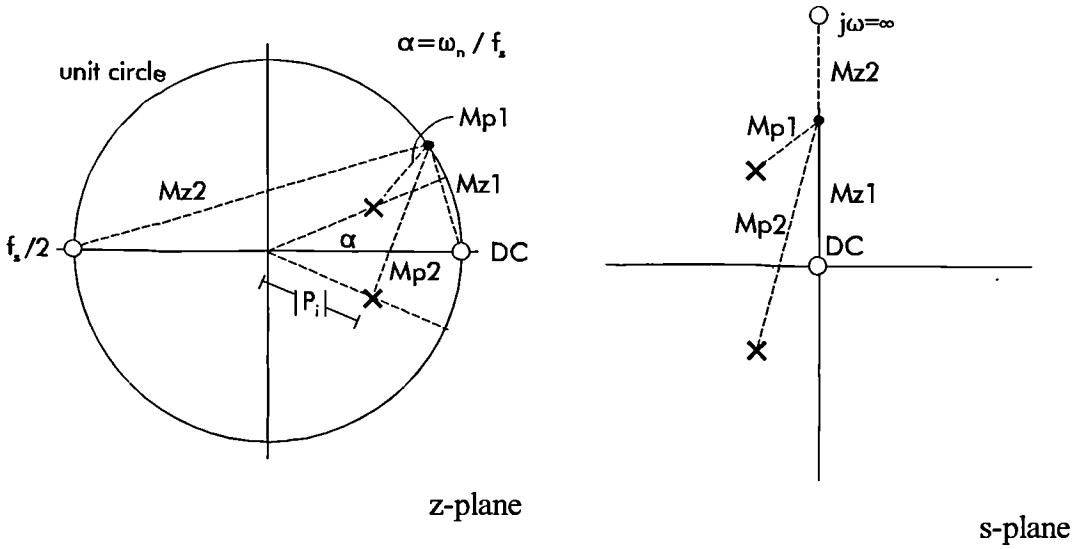

Figure 5.10 - Pole-zero diagrams of z-plane and s-plane second order bandpass filters

the distortions introduced by the 'wrapping' of the real frequency axis around the unit circle become more apparent. This is especially true for low-order modes where angle α is small; distortions of the shape of the mode in frequency are most noticeable. Small reductions in this distortion can be achieved by raising the sample frequency, which decreases angle α for all modes and slightly reduces the effect of the asymmetry inherent in the z-plane modal implementation. Above a sample frequency of 5kHz these reductions are negligible in the case of the 4m duct under investigation.

It is therefore clear that a modal summation based on a z-plane decomposition is subject to further inaccuracies when compared to an s-plane alternative. The summation of a number

of biquad modes as a model of a system with termination impedance approaching ρc is subject to errors when compared to the s-plane decomposition, which itself is unable to track the true pressure response as illustrated by comparison to the two-port result. A comparison of the three approaches in terms of a model of the input impedance of the 4m duct is made in Figure 5.11. The termination impedance is *a)* $2\rho c$ and *b)* ρc, and one hundred modes are used in the summation. The errors in the z-plane approach are likely to be significant when forming a model of a desired transfer impedance (with low Q-factor) in order to execute feedforward control. The significance of these errors for a feedforward controller is discussed further in Chapter 6.

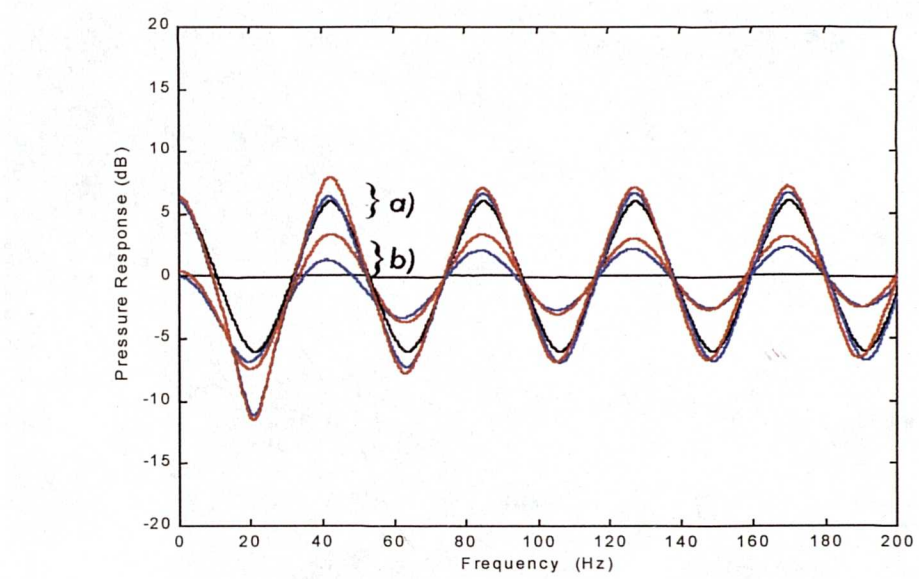

Figure 5.11 - Modal decomposition of duct input impedance
Two port formulation, s-plane modal sum and z-plane modal sum

Z-plane models of transfer impedance to a point *along* the duct are subject to the same constraints in terms of the validity of cosine modeshapes as their s-plane counterparts. When building a practical control system however, a strong incentive appears for the retention of simplified cosine modeshapes rather than the adoption of modeshapes based on the work of Morse and Bolt. The scale factors in Equations **(5.18)**, **(5.20)** and **(5.21)** are included to facilitate the design of a controller at some location where the modeshapes do not have unit value. At these locations, each different mode is subject to a corresponding scaling due to the location of source and receiver relative to the modeshape. Cosine modeshapes yield real-value scale factors which can be easily implemented in a practical system to derive the control filter *C(z)*. Cosinh function modeshapes such as those employed by Morse and Bolt yield scale factors which are complex, and which imply the

introduction of extra phase or time delays between biquad sections comprising the control filter. The structure of such a filter has not been investigated in this work, but provides one suggested area for further investigation.

5.5 Summary of Biquad fit control

The strength of the Biquad fit technique has been identified as residing in a novel exploitation of a modal analysis of the enclosed soundfield, in order to derive feedforward controllers whose aim is the re-specification of system poles. Threats to the successful fulfilment of this aim have also been identified, in terms of errors in the accuracy of biquad models of systems terminated with small boundary impedances. The significance of errors in the biquad fit is determined by the particular application of the modelling technique to a specific control task. The mathematics of one such application - the re-specification of the poles of a duct terminated by a control source - have been described in Equations (**5.12**) to (**5.21**), and a model of the application of this technique in a duct is presented along with a discussion of the significance of the fit errors, in Chapter 6.

Chapter 6

Feedforward IIR controllers in a one-dimensional waveguide - mathematical models

6.0 Introduction

The one dimensional acoustic waveguide provides a useful starting point in assessing strategies for control of resonant behaviour. The relationship between duct termination impedance, spatial pressure distribution and modal decay times and quality factor is simple and well defined. There can be no doubt that a characteristic termination impedance will result in the flattest possible pressure response in space and frequency in the duct, corresponding to an absence of modal behaviour and thus infinitely short modal decay times.

It can also be shown that in the one dimensional environment, a carefully placed single control source might be expected to assert a degree of control over all acoustic modes within the space [eg.12,37,41]. This is a situation which does not persist into three-dimensions, and which forms the subject for further comment in Chapters 8 and 9. However, taken together all these characteristics of the duct suggest that it forms a test environment where novel feedforward IIR control methodologies may be usefully developed using proven impedance control systems as a benchmark, and this is the aim of this chapter.

This development takes place in terms of a numerical simulation of control over the acoustic modes of a duct, following which the practical performance of IIR biquad controllers in one dimension is discussed in Chapter 7. Where comparisons are made between the modelled performance of feedforward IIR controllers and active impedance control systems, the reader is referred to Chapter 4 which provides some background to published work on the active control of duct termination impedance.

6.1 Motivation for biquad fit controller investigation in a waveguide

When a comparison of the two control systems takes place in a duct, the propriety of the control target has no bearing on the relative and absolute performance of the systems themselves, since the specification of an appropriate control target is greatly simplified by the straightforward low-frequency acoustics of the one-dimensional enclosure. Figure 6.1 illustrates the two control scenarios:

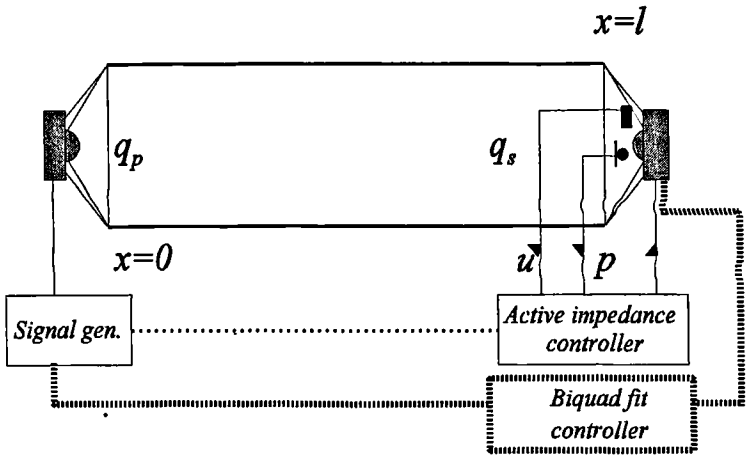

Figure 6.1 - One dimensional enclosure

Achieving an appropriate impedance at $x=l$ defines the control task for both controllers, and the impedance solution has been reviewed in section 4.4. This task may alternatively be conceived as achieving an appropriate transfer function between primary and secondary source strengths q_p and q_s. Nelson and Elliot [12] suggest that in one dimension, this relationship is optimally defined by

$$q_s = -q_p e^{-jkL} \qquad \textbf{6.1}$$

Figure 6.2 shows this result graphically, for two sources are positioned at opposite ends of a 4m long duct. The secondary source at the RH duct termination only operates between frequencies 75.0 and 96.0 Hz - at all other frequencies it is modelled as having zero velocity. A response equivalent to characteristic termination is achieved over the operating bandwidth, and it appears that **(6.1)** defines the optimal feedforward transfer function.

Unfortunately, this result only holds in the one-dimensional case. The biquad-fit approach on which fixed feedforward control is based in this Thesis is designed ultimately for use in

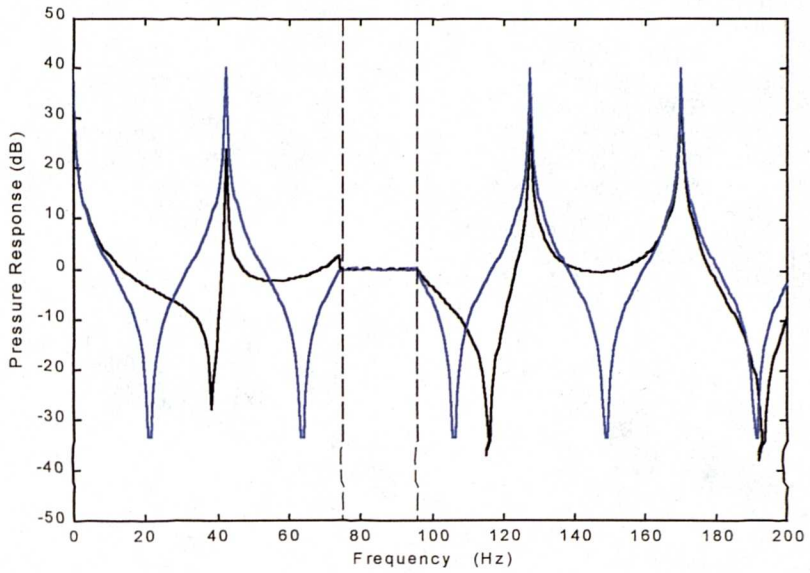

*Figure 6.2 - Implementing (**6.1**) over bandwidth 75-96Hz*
a) x=0 b) x= 1.8m

the three-dimensional room. Therefore attempts in this chapter to use biquad fit control in a one-dimensional test environment should be viewed as part of the development of a system for use in a more challenging environment (see Chapter 9) rather than a complicated attempt to re-define the optimal solution found in **(6.1)**.

Control filters of the form of Figure 5.3 are evaluated in the following section in a mathematical model of modal control in a one-dimensional system. This evaluation aims to determine the significance of the fit errors identified in Chapter 5, and to enable a comparison with the performance of active impedance control in an environment where termination impedance and modal Q-factor are simply related.

6.2 Modelled control results comparing biquad fit and active impedance methods

Results of a numerical model of the application of biquad fit control to the 4m duct are presented below. Equations **(5.18)** to **(5.21)** are implemented in a MATLAB model of a duct where the termination impedance, number of included modes and desired modal Q-factor are all user-defined variables. The location of the receiver point at which the 'measured' pressure (here modelled using the two-port formulae of section 3.1) is fitted using biquad filter sections may also be varied. The chosen receiver location is referred to as the 'solution point'.

The desired modal Q-factor has been manipulated by selecting a desired specific termination impedance r_d. The desired-mode filter coefficients are calculated by fitting z-plane biquad sections to modes modelled in a duct terminated with impedance r_d using the numerical method described in section 5.2.1. The uncontrolled duct termination impedance is modelled as practically rigid ($100\rho c$). In all cases the zeroth duct mode is not built into the biquad fit controller, for reasons outlined in section 5.3. The pressure at given locations in the duct is calculated for a controlled termination impedance r_d using the two-port result outlined in Chapter 3. This result is compared to the uncontrolled primary field, and the results of biquad fit control.

Results are analysed in two main groups; firstly when a solution point is adopted lying very close to the primary source, and secondly when an arbitrarily located solution point is chosen. The effects of desired Q-factor, number of modes modelled in the controller and performance at locations away from the solution point are all considered. All graphical data is presented with amplitude normalised to that pressure which would be created in an infinitely long duct with similar primary source velocity.

6.2.1 Solution point at primary source - field reconstructed at solution point

In Figures 6.3 to 6.5 active impedance and biquad fit controllers are compared, with the aim of reducing the Q-factor of the two lowest frequency modes. For an equivalent desired

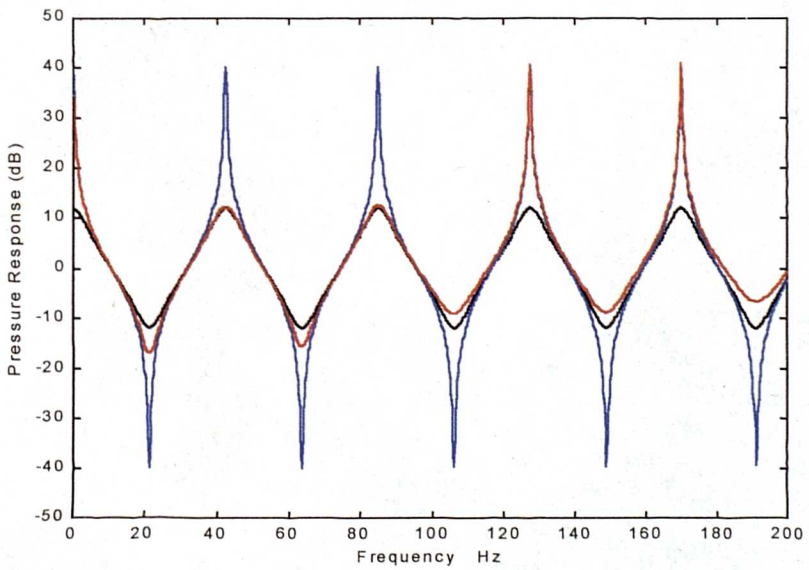

Figure 6.3 - 2 modes in biquad controller $r_d = 4\rho c$
a) Uncontrolled b) Biquad c) Impedance

specific termination impedance $r_d=4.\rho c$ (Figure 6.3), the biquad fit controller performs comparably to impedance control at the duct resonances. The two highest modes and the zeroth mode are not attenuated since they are not modelled in the biquad fit controller. Off-resonance around 20, 65 and 105Hz the performance of the two approaches diverges, due to the poor fit of the modal decomposition. The fit suffers when the number of included modes is small, and is especially poor when the ratio of dominant mode to modal residues is small, as described in section 5.2.1.

When the equivalent desired termination impedance is reduced to $r_d=2.\rho c$ (Figure 6.4), a similar pattern emerges. The performance of the biquad fit controller diverges further from impedance control. When r_d is small, the desired filter sections are not representative of the true soundfield in the duct. The modal decomposition becomes increasingly approximate with decreasing termination impedance, resulting in the divergence of the two control approaches.

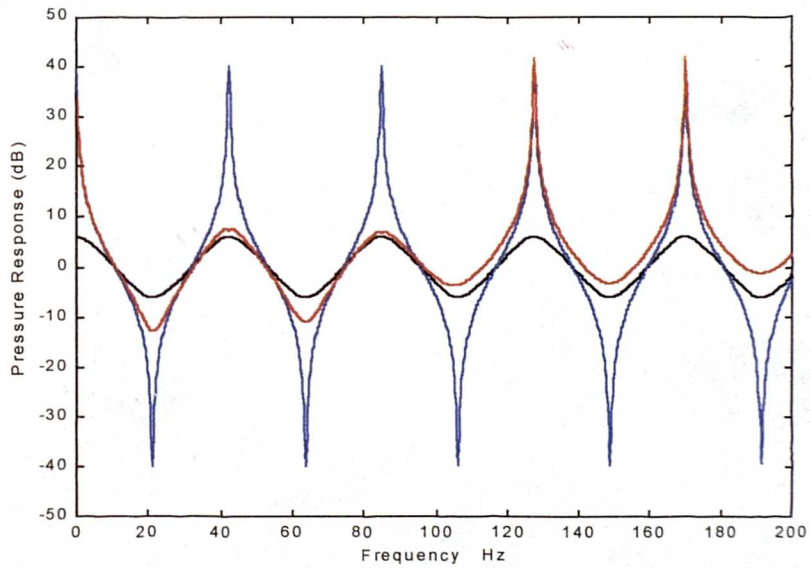

Figure 6.4 - 2 modes in biquad controller $r_d=2\rho c$
a) Uncontrolled b) Biquad c) Impedance

This limitation of the modal decomposition method was noted in section 5.4. The effects are most dramatic when the desired termination impedance is characteristic (Figure 6.5), when the biquad fit method is unable to replicate the active impedance control results and a flat frequency response cannot be achieved. However, modelled pressure reductions of 30 - 40 dB are still shown, and represent a significant degree of control over the resonant sound field.

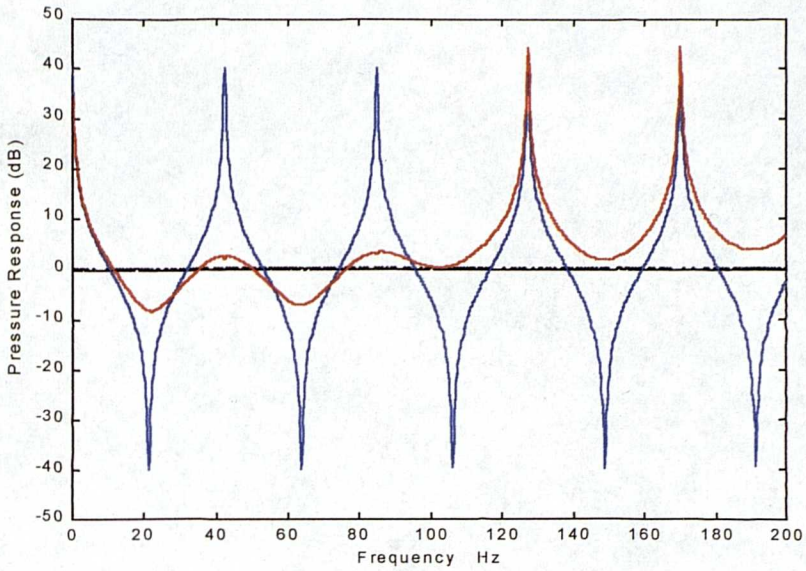

Figure 6.5 - 2 modes in biquad controller $r_d = \rho c$
a) Uncontrolled *b) Biquad* *c) Impedance (y=0)*

It is worth noting that the errors incorporated into the biquad fit controller result from differences between a two-port formulation for pressure (used to model the reconstructed soundfield in the duct) and the z-plane modal decomposition from which the controller is constructed. In the results presented in Figures 6.2 to 6.5 these differences arise partly due to the inclusion of an insufficient number of modes in the summation, and partly due to the increasing approximation with which the decomposition tracks the true pressure in the duct as the termination impedance becomes small. The modeshape function is not yet a factor, since pressure has been calculated at a solution point adjacent to the primary source where all modeshapes have unit value.

To some extent the situation may be remedied by the inclusion of more modes in the biquad fit controller. This measure extends the bandwidth of control and, by the inclusion of a larger number of modal residues, has the required effect of increasing the accuracy of the biquad model. Figure 6.6 shows in more detail the divergence of the two control approaches when the target for control is a characteristically terminated soundfield, as the number of modelled sections is increased from 2 to 3 and then to5. An expanded scale is used on the y-axis to show more clearly the differences resulting from increasing numbers of filter sections.

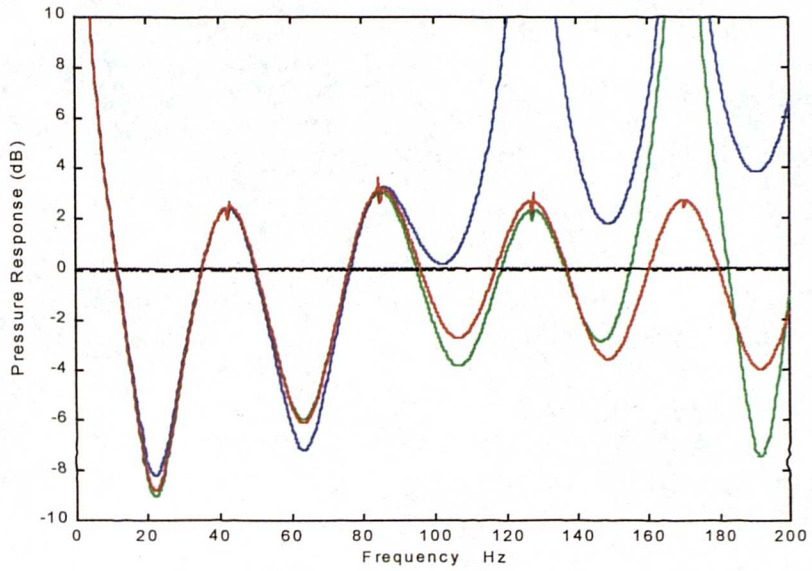

Figure 6.6 - $r_d = \rho c$ No. of modes in Biquad controller = N
a) Biquad - N=2 *b) Biquad - N=3*
c) Biquad - N=5 *d) Impedance (y=0)*

Performance is similar at the resonant frequencies, and as expected large changes in pressure are seen at higher modes once they are included in the control filter. Off resonance the addition of extra modal residues in the summation means that the modal sum more closely approximates the true pressure in the duct, and some improvement is seen in controller performance. Even with five modes modelled in the control filter a soundfield which is flat with respect to frequency cannot be achieved, for reasons described above. When more than five modes are included in this control filter simulation, problems occur which are described below. However, the approximate nature of a modal decomposition in describing a characteristically terminated system means that even if it were possible to incorporate large numbers of modes in the model, a totally flat controlled frequency response would still not be achieved.

6.2.2 Implementation errors in Biquad Fit controller

The mathematics presented in **(5.18)** to **(5.21)** governing biquad fit controllers imply that polynomials of order 2*(no.of included modes) must be formed and solved in order to locate the poles and zeros of the control filter. Specifically, the model of the inverse secondary path transfer function $1/Z_{s,r}$ given in **(5.20)** requires the multiplication of N second order polynomials in z, from which numerator and denominator coefficients may be determined. When N is greater than five, noise is observed in the control filter response which has catastrophic effect on the performance of the biquad fit controller as observed in Figure 6.7.

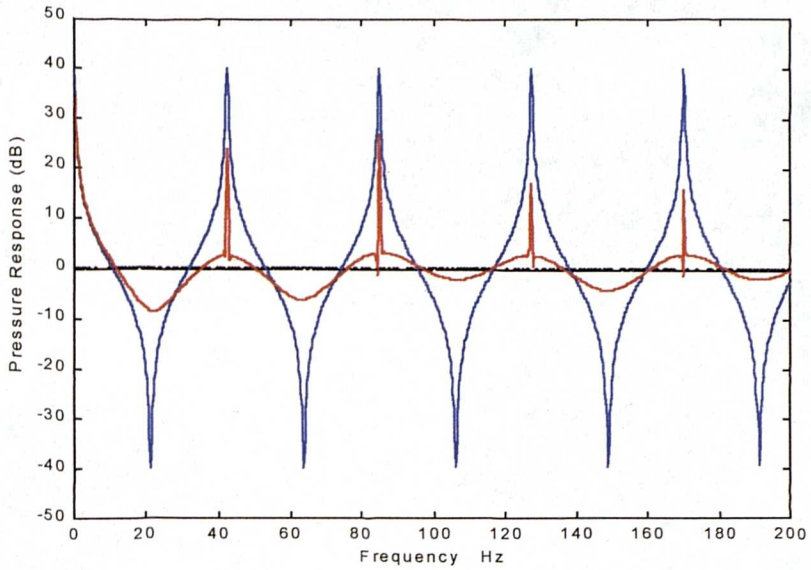

Figure 6.7 - $r_d = \rho c$ 6 modes in Biquad controller
Soln. point at primary source : Pressure at x=0.001m
a) Uncontrolled b) Biquad c) Impedance (y=0)

The noise appears as disturbances in the controller response around the modal frequencies when $N=6$, and corrupts the full bandwidth of the control filter as more modes are included. The performance of the filter is first affected on the resonant modes, and the effect of noise is most pronounced at these frequencies, where the relationship between primary and secondary source strengths is most critical due to the maxima in modal input impedances.

This noise in the control filter can be traced to the polynomial order $2N$ in the numerator of **(5.20)**. As the number of included modes N increases, any error in the pole coefficients of individual modes will compound and disturb the root loci of the control filter. It was originally anticipated that such errors might be responsible for the anomalies of Figure 6.7. Subsequent testing disproved these errors as the source of the problem. All calculations were carried out to double precision accuracy, and the convergence criteria for the numerical derivation of desired and actual pole locations were examined and found to produce stable results regardless of the Q of the mode which was fitted.

The only remaining source of error concerns the functions used to solve for the roots of the polynomial order $2N$ and calculate the response of the control filter. Further investigation into these functions (within the package MATLAB in this simulation) is necessary if more modes are to be incorporated into the controller model. However to reiterate, the

approximate nature of the decomposition for a characteristically terminated system remains the dominant factor in determining controller performance. The results presented up to $N=5$ illustrate the behaviour of the system in sufficient detail, such that further enquiry into the incorporation of large numbers of modes in the model is unlikely to reveal useful information.

It should be noted that all results pertaining to the biquad fit system presented in the remainder of this Thesis incorporate ***less than six modal components*** *and therefore are* ***not*** *subject to these errors in the calculation of control filter coefficients.*

6.2.3 Performance of biquad fit controller at locations remote from solution point

So far the performance of a controller designed for a solution point at the primary source has been investigated by reconstructing the field due to the combined action of primary and secondary sources at that same point. In order to discover the spatial extent within the duct over which control occurs, it is necessary to reconstruct the soundfield at locations distant from the solution point. Figures 6.8 to 6.10 show a model of the pressure generated at locations 1.8m, 2.2m and 3.99m (at the *secondary* source) along a 4m duct for a solution point at the primary source where $x=0$. The desired termination impedance is in all cases characteristic, and desired modes were created accordingly using the numerical fit method.

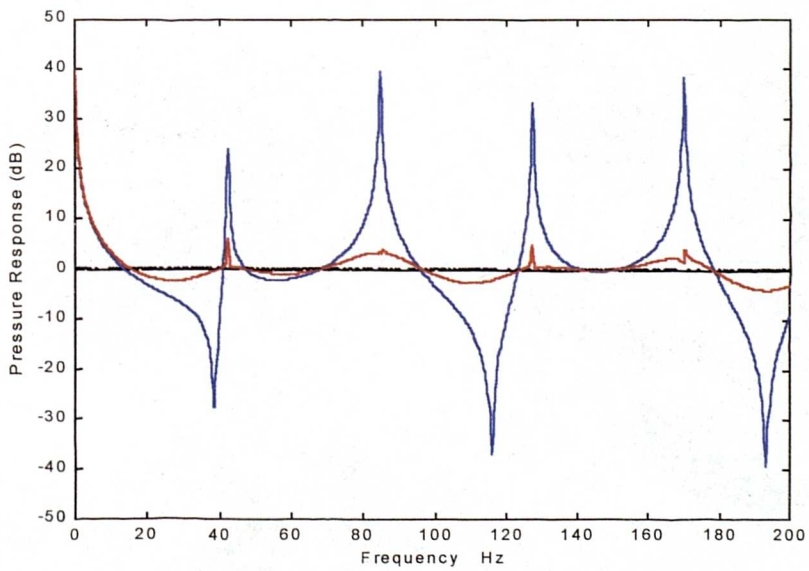

Figure 6.8 - $r_d = \rho c$ 5 modes in Biquad controller
Soln. point at primary source : Pressure at x=1.8m
a) Uncontrolled b) Biquad c) Impedance (y=0)

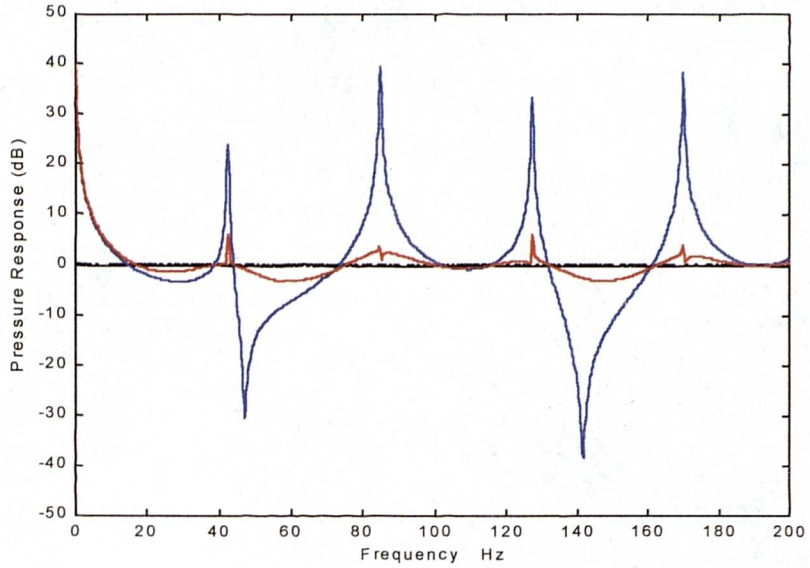

Figure 6.9 - $r_d = \rho c$ 5 modes in Biquad controller
Soln. point at primary source : Pressure at x=2.2m
a) Uncontrolled b) Biquad c) Impedance (y=0)

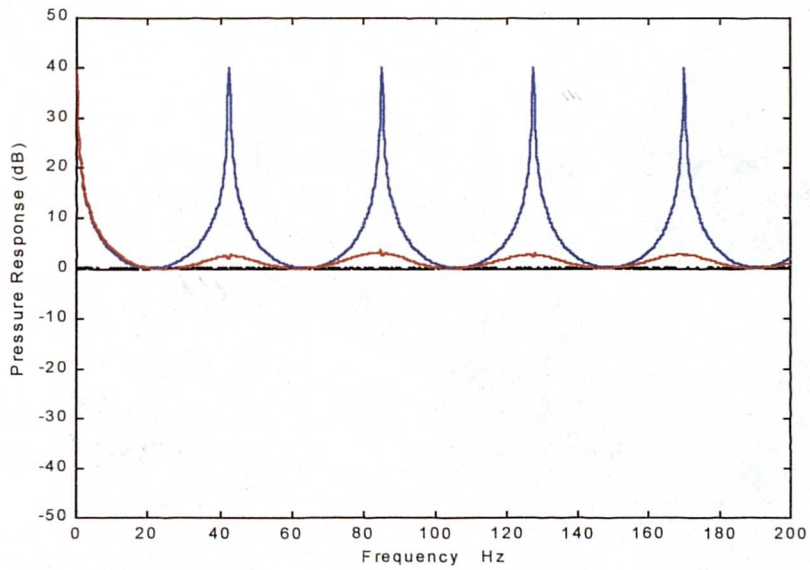

Figure 6.10 - $r_d = \rho c$ 5 modes in Biquad controller
Soln. point at primary source : Pressure at x=3.99m
a) Uncontrolled b) Biquad c) Impedance (y=0)

Although in all cases the pressure resulting from biquad fit control is not flat, large pressure reductions on the modes are predicted. The results lie close to the impedance control result and the differences are accounted for by the error in the modal decomposition for the small termination impedance. On-resonance, small peaks are seen in the pressure generated by the addition of primary and secondary fields where biquad fit control has been

used. These peaks become much more pronounced when a solution point at a location other than the primary source is selected, and are considered along with those results. (It should perhaps be noted that only five modes were used in these control filters, and the peaks here do **not** result from the root-solving errors discussed in section 6.2.2).

6.2.4 Solution point at arbitrary location - field reconstruction at solution point

The mathematics of **(5.18)** to **(5.21)** are not specific concerning which point in a system should be used to form a solution for *c(z)*. The equations suggest that so long as appropriate scale factors are employed which build in the values of primary and secondary field modeshapes, it should be possible to design a solution at any point within the system. One might expect that if locations are chosen which coincide with a pressure node on a particular modeshape, no control may be exerted over that mode. The actual influence of selection of solution point is found to be rather more complex, and is first investigated in Figures 6.11 to 6.14 in terms of the controlled total pressure set up *at* solution points chosen at $x=1.8$ and $x=3.99$. Desired modes for the biquad fit controller are designed with Q-factors corresponding to termination impedances of $2\rho c$ and $4\rho c$, and the result of biquad fit control is compared to a direct implementation of the active control of termination impedance as before.

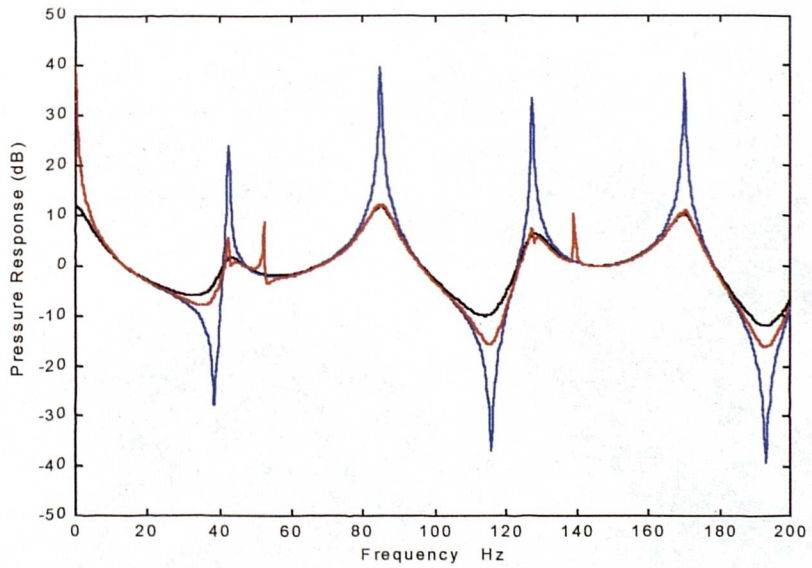

Figure 6.11 - $r_d = 4\rho c$ 5 modes in Biquad controller
Soln. point at x=1.8m : Pressure at x=1.8m
a) Uncontrolled b) Biquad c) Impedance

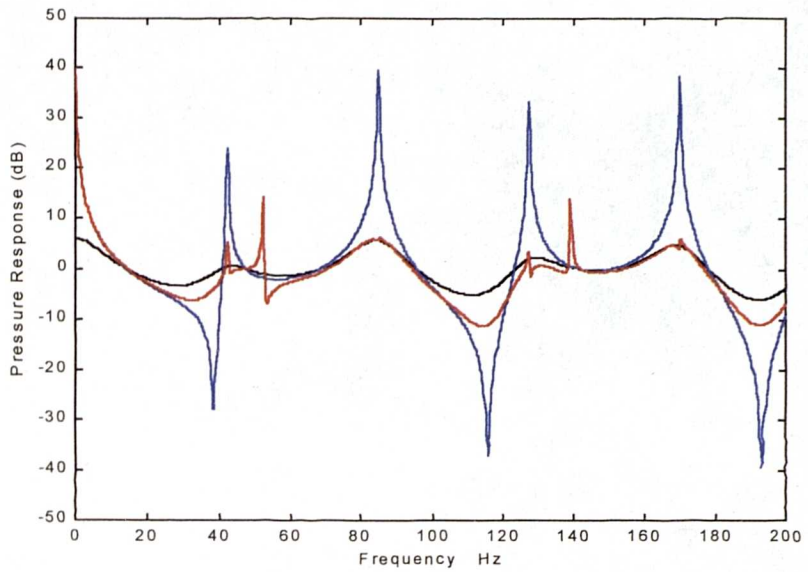

Figure 6.12 - $r_d = 2\rho c$ 5 modes in Biquad controller
Soln. point at x=1.8m : Pressure at x=1.8m
a) Uncontrolled b) Biquad c) Impedance

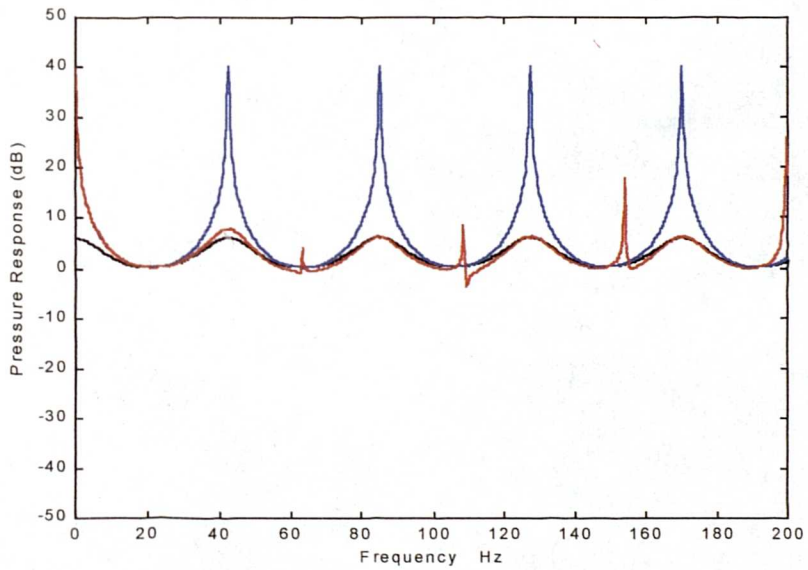

Figure 6.13 - $r_d = 2\rho c$ 5 modes in Biquad controller
Soln. point at x=3.99m : Pressure at x=3.99m
a) Uncontrolled b) Biquad c) Impedance

In all cases the direct implementation of the control of termination impedance is shown to produce a soundfield comprised of modes with lowered Q-factor, scaled appropriately depending on the location of the point at which the controlled pressure is plotted. A change in termination impedance of $2.\rho c$ to $4.\rho c$ simply scales the Q of each resonance as might be anticipated. Biquad fit control on the other hand produces pressure responses which

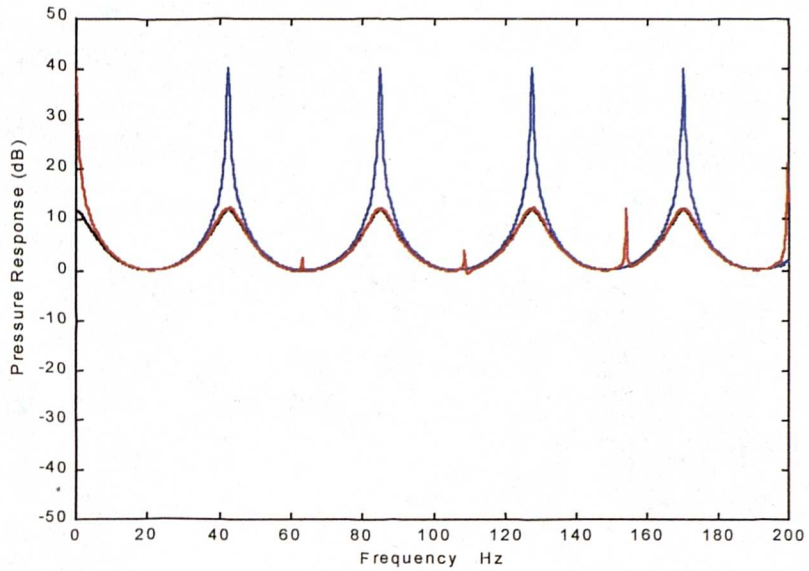

Figure 6.14 - $r_d = 4\rho c$ 5 modes in Biquad controller
Soln. point at x=3.99m : Pressure at x=3.99m
a) Uncontrolled b) Biquad c) Impedance

contain pronounced 'spikes' at particular frequencies. When the solution point lies at $x=1.8$m (Figures 6.11 and 6.12) these spikes lie at 40, 55, 128 and 140Hz, whereas for a solution point at $x=3.99$m (Figures 6.13 and 6.14) the spikes appear at 65, 110, 155 and 200Hz. These irregularities in the controlled pressure are therefore functions of the chosen solution point.

Changing the desired termination impedance from $4.\rho c$ to $2.\rho c$ has an interesting effect on the magnitude of the frequency response irregularities. As the termination becomes less rigid, the amplitude of the spikes is increased. This points to the influence of fit problems resulting from a choice of near-characteristic termination impedance, due to the approximate nature of the modal decomposition. The fact that these irregularities are far more pronounced when a solution point is chosen away from the primary source further suggests that the scale factors derived from cosine modeshapes are influential in their formation. It has been established that the cosine modeshapes become less accurate as the termination impedance tends towards characteristic value, and so the improvement in performance for a controller designed for a more rigid desired termination impedance is not surprising.

The same trends are observed for solution points at $x=1.8$m, and $x=3.99$m. Initially it might be expected that the performance at $x=3.99$m should be similar to that at the primary source

($x=0.01$m) since the duct is a symmetrical system when considered in terms of cosine modeshapes. Examination of Figure 5.6 reveals however that for a non-rigid termination impedance the system is not symmetrical. Cosh modeshapes model the spatial pressure distribution more accurately, and mean that whilst the eigenvectors take unit value near the primary source, they may take an altogether different and potentially complex value at the opposite end of the duct.

Furthermore, even a simple cosine modeshape model exhibits differences in primary and secondary path transfer impedances at opposite ends of the duct. An impedance modelled close to a source will display residues of neighbouring modes which are in antiphase between the pair of eigenvalues. In contrast, an impedance modelled out to a point at the opposite end of the duct will display in-phase residues, since in a one-dimensional system neighbouring modes are of alternately odd- and even order [12]. The phase relationship between neighbouring modes appears to be of great importance in determining the accuracy of the inverse secondary path model or cascade section of $c(z)$. Closer inspection of the response of the parallel and cascade sections of control filter $c(z)$ is instructive in interpreting the irregularities in the controlled soundfield.

Figures 6.15 to 6.17 show the overall response of $c(z)$, the response of the numerator (parallel sections) and the response of the denominator (cascade sections), respectively. Three solution points are compared for contrast - $x=0.001m$ (solution point at primary source - black trace), $x=1.8m$ (blue trace) and $x=3.99m$ (solution point at secondary source - red trace). The following points should be noted:

- All solution points result in the same magnitude response at the duct resonances.
- Glitches in $c(z)$ occur at frequencies concurrent with glitches in the controlled pressure, when the solution is formed away from the primary source. No such glitches occur for a solution formed at the primary source.

Investigation of the constituent sections of $c(z)$ reveals that the glitches occur at peaks in the magnitude of the cascade section which represents the inverse secondary source transfer impedance. No such peaks occur for a solution point adjacent to the primary source, since at this location the residues of adjacent modes in the secondary source transfer impedance

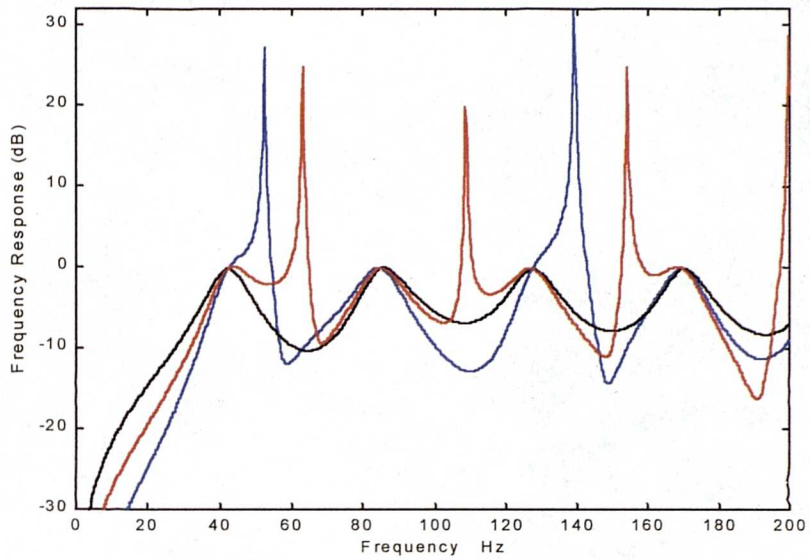

Figure 6.15 - $r_d = 2\rho c$ 5 modes in Biquad controller
Controller magnitude response - Soln. point at
a) x=0.001 b) x=1.8m c) x=3.99m

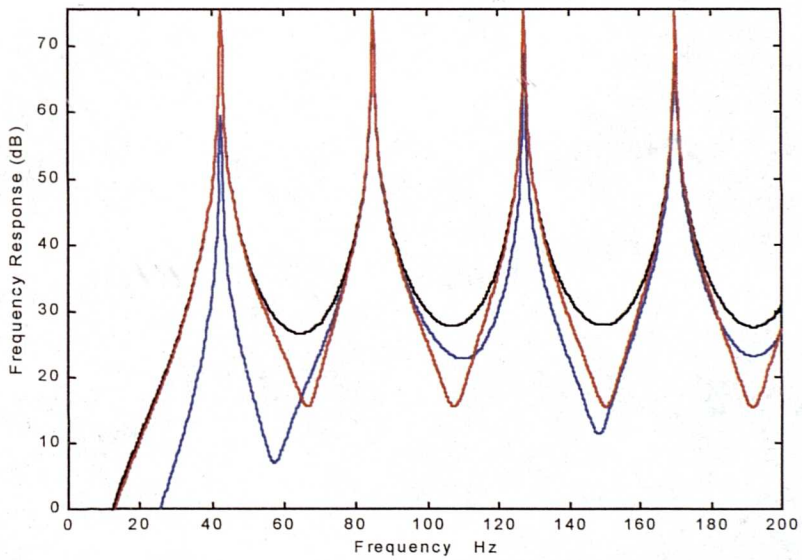

Figure 6.16 - $r_d = 2\rho c$ 5 modes in Biquad controller
Parallel sections (numerator) of controller magnitude response - Soln. point at
a) x=0.001 b) x=1.8m c) x=3.99m

are coherent. No rapid reductions in magnitude take place since the residues are never in antiphase at a frequency where they have comparable magnitude, and so the inverse secondary path model does not contain respective maxima.

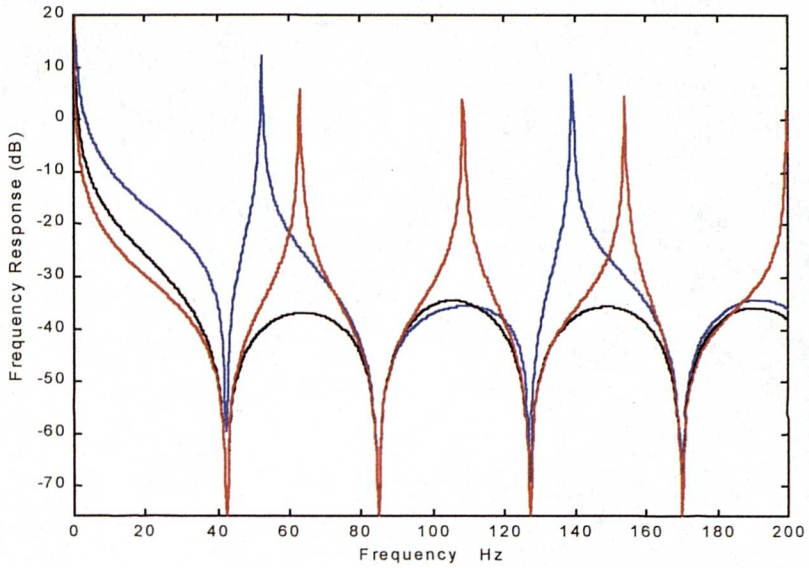

Figure 6.17 - $r_d = 2\rho c$ 5 modes in Biquad controller Cascade sections (denominator) of controller magnitude response - Soln. point at a) x=0.001 b) x=1.8m c) x=3.99m

It therefore appears that the disturbances in controlled pressure result from an insufficiently accurate model of the secondary source transfer impedance. This suggestion is reinforced by Figure 6.18 which compares a two-port model of secondary path transfer impedance with a 5 mode summation at a point 1.8m along a 4m duct. Large discrepancies are shown

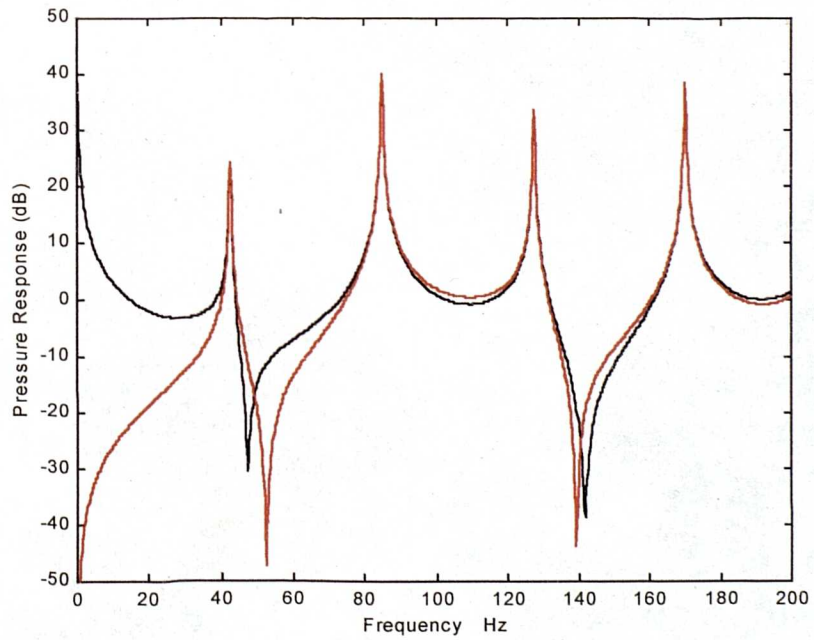

Figure 6.18 - Accuracy of 5 mode decomposition Pressure at x=1.8m a) Two-port formulation b) Modal sum

around 50Hz and 140Hz - the location in frequency of the glitches in the controlled pressure response. In terms of improving the performance of the biquad fit controller at the solution point, it appears that more modes are required in the model of the inverse secondary path transfer impedance. Since in this instance the desired low-Q modes do not appear in this part of the control filter which solely models uncontrolled high-Q secondary path modes, concerns regarding the applicability of a modal decomposition to a system with small termination impedance do not apply.

6.2.5 Performance at locations remote from an arbitrarily located solution point

Whilst an increased number of modes in the biquad fit controller may improve the performance at an arbitrary solution point, the performance at some location away from such a solution point displays large deviations compared to a system based on the active control of termination impedance. Figures 6.19, 6.20 and 6.21 display the controlled total soundfield at locations $x=0.001$*(primary source)*, $x=2.2$ and $x=3.99$*(secondary source)*. The solution point was selected at $x=1.8$ - one of the solution points used to calculate the magnitude controller responses shown in Figures 6.15 to 6.17.

Comparison of these six figures reveals that the peaks in the biquad controller correspond to peaks in the controlled soundfield at the remote locations. The controlled pressure deviates from the active impedance control result at other frequencies, but the deviation is

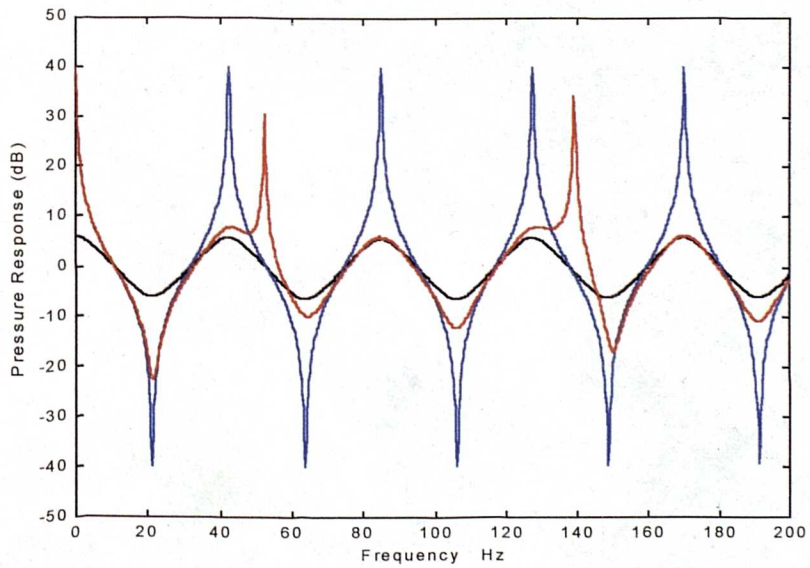

Figure 6.19 - $r_d = 2\rho c$ 5 modes in Biquad controller
Soln. point at x=1.8m : Pressure at x=0.001m
a) Uncontrolled b) Biquad c) Impedance

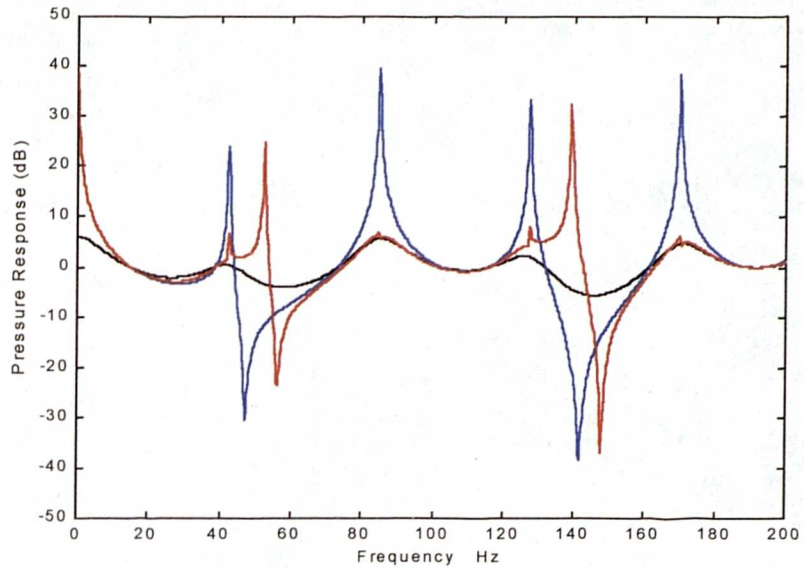

Figure 6.20 - $r_d = 2\rho c$ 5 modes in Biquad controller
Soln. point at x=1.8m : Pressure at x=2.2m
a) Uncontrolled b) Biquad c) Impedance

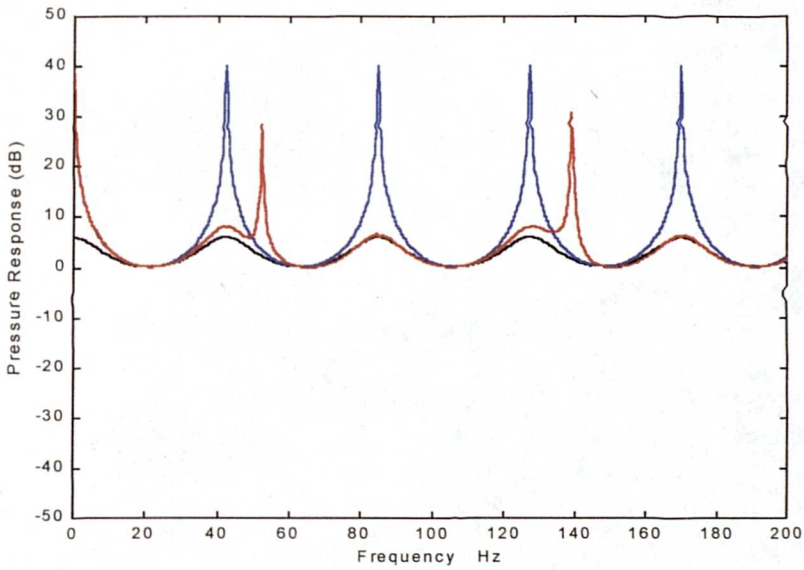

Figure 6.21 - $r_d = 2\rho c$ 5 modes in Biquad controller
Soln. point at x=1.8m : Pressure at x=3.99m
a) Uncontrolled b) Biquad c) Impedance

most marked at those frequencies where $1/Z_{sr}$ contains maxima due to the destructive interaction of neighbouring modes in the secondary path transfer impedance. It is perhaps worth noting that although the control task in Mourjopoulos' work is different (FIR deconvolution), his results concur in that he notes that it is the *zeros* in a particular transfer impedance which prevent the *inverse* of this function from performing satisfactory deconvolution at a remote test point [59]. The only location for a solution point which

ensures that no such maxima exist is at the primary source itself, and it has been noted that when this location is selected as a solution point, biquad fit control works reasonably well throughout the entire system. In other words, the biquad fit controller is never capable of truly global control in the duct when the solution is formed away from the primary source.

6.3 Conclusions on the application of biquad fit control techniques in a one-dimensional environment

Models presented in this chapter suggest that Biquad fit control is effective in decreasing the Q-factor of resonances in the duct, but is increasingly unable to replicate the performance of active impedance control as the desired termination impedance approaches characteristic value. The situation may be partially remedied by including large numbers of modes in the controller, but fundamental limitations in the accuracy of a modal decomposition with non-rigid boundary conditions mean that as the desired impedance approaches ρc the performance of the biquad controller is inferior to the active control of termination impedance.

The spatial extent of control also differs between the two systems. Whereas active impedance control produces results which are predictable along the entire length of the duct for any desired resistive boundary condition, biquad fit control only works in any way globally when the solution is formed at the primary source. Even in this case, glitches in the controlled pressure are seen at turning points in the model of inverse secondary path transfer impedance. For any other solution point, these glitches become more pronounced and cause the control to be local and specific to this point, when not located at the primary source.

From the results of the simulation it appears that the Biquad control formulae derived in Chapter 5 are effective, but that in a one-dimensional environment active impedance control may be more appropriate. This conclusion is investigated in Chapter 7, before Biquad fit control is applied to the three dimensional room in Chapter 9.

Chapter 7

Feedforward IIR controllers in a one-dimensional waveguide - practical measurements

7.0 Introduction

In this chapter, the feedforward IIR Biquad fit controllers introduced in Chapter 5 and simulated in a duct in Chapter 6 are investigated in a practical experiment aimed at controlling the sound field in a 4m duct, terminated at both ends with electrodynamic loudspeaker drive units. As noted in the introduction to the simulations of Chapter 6, one dimensional acoustic waveguides provide a useful starting point in assessing strategies for control of resonant behaviour since the relationship between duct termination impedance, spatial pressure distribution and modal decay times and quality factor is simple and well defined. It is also clear that in the one dimensional environment, a single control source might be expected to assert a degree of control over all acoustic modes within the space.

As in the simulation, the performance of the proven one-dimensional impedance control system is used as a benchmark against which the effectiveness of the Biquad fit system can be judged. In the conclusion to Chapter 6 it is noted that modelling suggests that impedance control is the more suitable strategy in the duct, and this chapter is concerned with verifying this result in practice. The performance of an active impedance control system in a test duct has been reviewed in Chapter 4, and these results are used to make the necessary comparison with the performance of the novel IIR biquad controllers in this chapter.

The chapter starts with a discussion of the difference between measuring transfer impedances relative to velocity, or voltage. There follows a consideration of the influence of source coupling on the control system. A point cancellation filter is then used to illustrate some of the problems of using Biquad fit control in the duct. Finally conclusions are drawn

as to the effectiveness of one-dimensional biquad fit control, which are formative in the discussion of three-dimensional biquad fit control in Chapter 9.

7.1 Practical implementation of biquad fit control

In order to evaluate one-dimensional Biquad fit control, a duct was built from polypropylene piping with wall thickness 3.5mm and internal diameter 153mm. A duct length of 4m was chosen and two KEF B200 drive units attached, one at each end. Drive unit characteristics are listed in Appendix A . A microphone which could be traversed along the length of the duct was added, in order to facilitate pressure measurements at any point within the system. This arrangement also permitted the measurement of duct termination impedance using the standing wave ratio method, which is detailed in Appendix B. This physical system duplicates the numerical model used to predict control performance in Chapter 6 (Figure 6.1). However, several important considerations emerge when investigating the practical biquad fit controller which are not apparent from the initial modelling.

Considering the construction of the biquad fit controller introduced in Chapter 5, a four-stage process emerges:

I. Measure primary and secondary path transfer impedances from each source out to a solution point in the field.

II. Fit each transfer impedance with a biquad model manipulating pole locations to set appropriate modal frequencies, Q factors and scaling.

III. Design a set of desired modes with reduced Q factor, compared to the uncontrolled system.

IV. Solve Equations (**5.18**) to (**5.21**) to find controller *c(z)*.

The mathematical model of controller *c(z)* specifies the relationship between primary and secondary source strengths. For two drive units of similar radiating area, this means that the model of *c(z)* is assumed to directly specify the transfer function between source velocities. In practice, the inputs and outputs relating to this control filter take the form of line-level electrical signals. Therefore additional transfer functions must be introduced into primary and secondary signal paths by the use of power amplification, and by the electro-mechanical transfer characteristics of the drive units themselves (Figure 7.1).

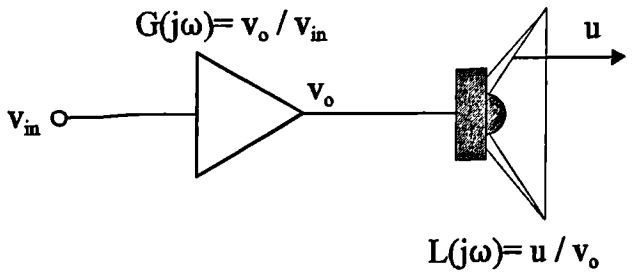

Figure 7.1 - Voltage-velocity characteristic of electrodynamic drive unit

The incorporation of $G(j\omega)$ and $L(j\omega)$ into $c(z)$ can be tackled in a number of ways. Most trivially, if both primary and secondary paths use identical power amplification and loudspeaker drivers, the additional transfer functions can be neglected since they will have similar effect on both primary and secondary fields. Ensuring that both amplifiers have similar performance is relatively straightforward; in these experiments Left and Right channels of a Quad 306 power amplifier were used, and their transfer functions are compared in Appendix D. It will be seen that in magnitude and phase the response of both channels can be considered to be identical.

Ensuring that both loudspeakers have the same voltage-velocity response is rather more difficult. Two KEF B200 units were selected with nominally similar responses. These are compared in Appendix A. Both drivers are mounted in similar cabinets of volume, and both share a similar lumped resonance at around 64Hz. However, the Q factor of this resonance is markedly dissimilar, suggesting that the damping in cabinet or cone suspension is not equal. Both drivers were the subject of MLS based small signal parameter measurement using an added-mass method. The results of this analysis are shown in Appendix A and demonstrate that the two loudspeaker systems do indeed incorporate different amounts of damping. It was subsequently discovered that although the two drivers themselves were not precisely matched, the cabinets were loaded with uneven amounts of wadding, exacerbating differences between the two drivers. In this instance differences could be partially overcome by more careful construction of two equivalent systems, but more problems remain.

Simply neglecting $G(j\omega)$ and $L(j\omega)$ has other disadvantages. If both transfer functions are equal to unity, or are frequency independent scalars, then a control filter $c(z)$ based around

measurements of true *p/u* transfer impedances might be expected to work well, since the filter output to v_{in} (Figure 7.1) would be directly proportional to cone velocity u. Thus far the measurement methodology has assumed that just such impedances are measured, where solution point pressure is divided by source velocity. This approach gives the most chance of an accurate fit using parallel biquad sections, since these filters are then a direct model of the *acoustics* of the system described for example in (**3.5**). However the approach suffers two distinct disadvantages:

- Transfer functions $G(j\omega)$ and $L(j\omega)$ are not incorporated into control filter $c(z)$, which must modify the behaviour of the room using the acoustic model whilst generating a signal to produce an appropriate relationship between source velocities. $G(j\omega)$ and $L(j\omega)$ are in practice neither frequency independent nor scalar, and can greatly modify the performance of an otherwise accurate room model.
- It is not always convenient to use a source which has been instrumented with an accelerometer.

Rather than measuring true transfer impedances, it may be acceptable to measure point pressures divided by the line level electrical input to each path v_{in}. This avoids the use of an accelerometer on the loudspeaker cones, and the design process then fits the function which is driven directly by $c(z)$ (i.e. the electrical inputs to primary and secondary paths). Unfortunately the fit is likely to be less accurate since the measured function is no longer the simple addition of a number of second order modes. The entire acoustic response is now multiplied by the driver electro-mechanical bandpass response detailed in Appendix A, and together with the further low-frequency zeros introduced in the amplifier response (Appendix D) the accuracy of the fit with parallel biquad sections is likely to suffer.

Despite these potential limitations, measurements using input voltage as a reference are attractive and have been used in practice in attempts to design a controller. The Q-factor of the driver electro-mechanical responses is very small compared to that of the modes, and it is possible that the fit errors introduced may be negligible. These errors are the subject of further discussion in the context of Biquad fit control in a room, in Chapter 9. Fit errors and the incorporation of loudspeaker and amplifier transfer functions are not the only difficulties to be overcome in the practical realisation of Biquad fit control. Changes in the

response of the system between the formation of the model in the fit process and the operation of the resulting control filters due to source coupling must also be considered.

7.1.1 Termination impedance, source coupling and fit problems

The loudspeakers which terminate the duct are practical sources which have finite source impedance. This implies that the velocity / voltage transfer function $L(j\omega)$ will not be constant, but will rather be a function of the radiation impedance which the driver sees when radiating energy into the duct. Source velocities are then functions of the modal input impedance seen when radiating into the terminated duct. Sources of finite impedance are considered by Silcox and Elliot [85] for active control applications; it is shown that the pressure in a controlled system remains the linear sum of those pressures radiated by primary and secondary velocities, regardless of the relationship between those velocities which might result from acoustical coupling. This linear relationship facilitates the ready solution of active control problems, but source coupling may still complicate system characterisation, and this is an important consideration for non-adaptive methods such as Biquad fit control.

The influence of finite source impedance is illustrated in Figure 7.2. For a drive unit in a sealed cabinet driving the duct, the mechanical source impedance is given [86] by

$$Z_{source} = \frac{Bl^2}{R_E} + R_{MD} + \frac{1}{j\omega C_{MD}} + j\omega M_{MD} + \frac{S_D^2}{j\omega C_{AB}} \qquad 7.1$$

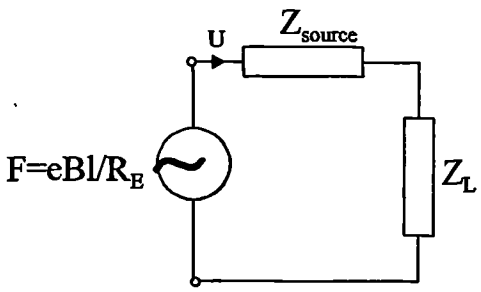

Figure 7.2 Source impedance of loudspeaker driver

The radiation load Z_L when driving the duct is a function of the modal input impedance at the cone, which with a knowledge of the terminating impedance can be found using the two-port approach detailed in (**3.2**). Note that the two-port matrices give the acoustic impedance, which is related to the mechanical load Z_L by a factor of the square of the

radiating area. Where Z_{source} is of comparable size to Z_L, rapid and large changes of the latter with frequency (see for example Figure 4.6) induce changes in the source velocity also.

The source impedance of the terminating loudspeaker must also be considered. It is inversely proportional to the cone velocity excited acoustically by the primary source. This condition is shown in Figure 7.3; the voice coil of the terminating loudspeaker is shorted, simulating connection to a power amplifier having low output impedance.

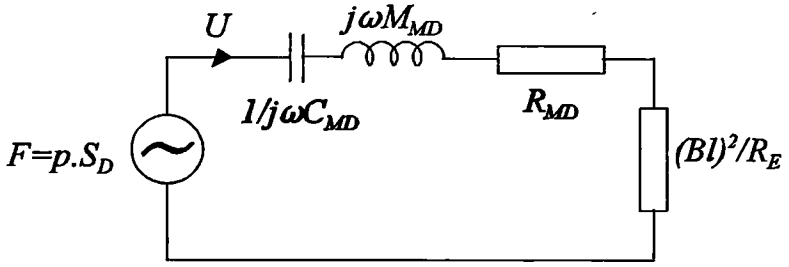

Figure 7.3 - Acoustically driven duct termination

Where the total impedance of the termination is large, the practical realisation of a biquad control system is analogous to the numerical model introduced in Chapter 6. This model assumes that the left hand source sees a duct with a practically rigid termination (supplied by the high-impedance right hand source). A sound field is then calculated due to the left-hand source velocity. Onto this sound field is superimposed the field generated by the right hand source, previously acting as a near-rigid termination, when it in turn is given velocity and radiates into a duct now terminated by the near-rigid left-hand source [42].

In practice, measurements of primary and secondary path transfer impedances are made in the presence of a termination supplied by the 'other' driver driven acoustically, whose specific surface impedance has been shown to be a function of the mechanical and electrical properties of the device. Measurements of this termination impedance were carried out with the voice coil of the terminating device shorted out, simulating connection to the low-impedance output of the power amplifiers used during the control filter operation. Standing wave ratio measurements of the uncontrolled termination impedance were taken and have been presented in Figures 4.2 and 4.3. In brief it can be seen that the termination impedance is not purely real, and near the resonance of the terminating driver it cannot be considered to be large compared to ρc.

Because the source impedance of the loudspeakers is not infinite, the actual process of measuring transfer impedances and fitting with biquad sections in order to derive a control filter is made more complex. Finite source impedance implies that function $L(j\omega)$ is significantly modified when driving the uncontrolled duct when compared to a free-field measurement. The uncontrolled duct presents a strongly modal radiation load which can be seen in Figures 7.4 and 7.5 to change $|L(j\omega)|$ considerably.

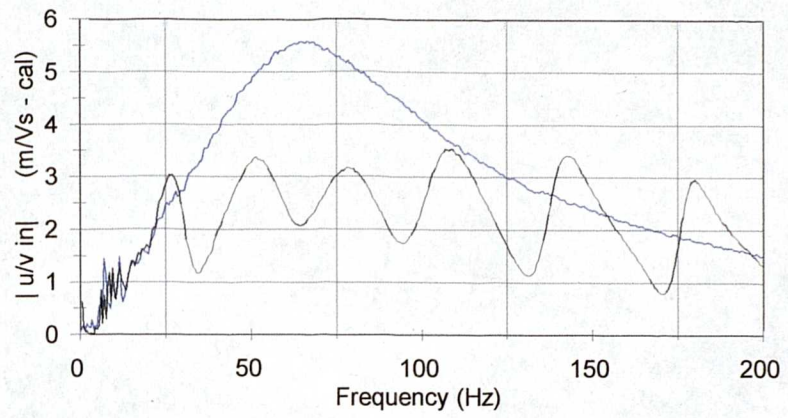

Figure 7.4 - Magnitude velocity-voltage transfer characteristic - B200
a) On duct *b) Free field*

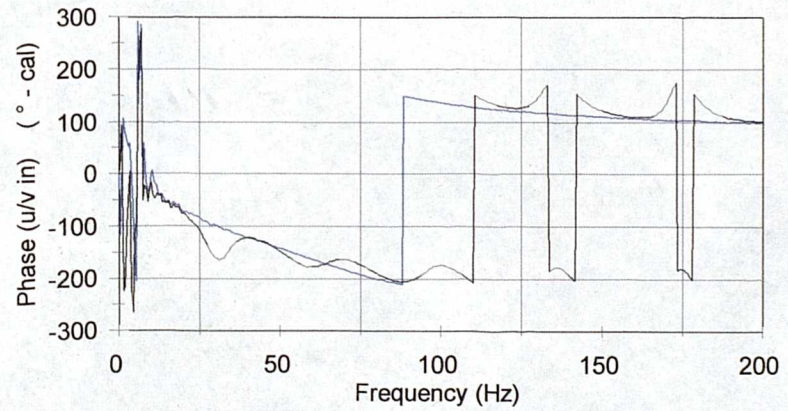

Figure 7.5 - Phase of velocity-voltage transfer characteristic - B200
a) On duct *b) Free field*

During operation of a control filter, it might be expected that the duct behaves as a system terminated with a relatively small impedance, such that the Q-factor of the modes is reduced and the input radiation load tends towards a real and characteristic value. If this is the case,

transfer impedance measurements made off-line in order to characterise the system will no longer represent the dynamics of the run time system, because the radiation load on the drivers will no longer be so strongly modal. These observations suggest that it is necessary to build source coupling into a feedforward control system, so that off-line system characterisation measurements can be used to design a filter which will operate correctly in run-time. The arrangement of appropriate measurements forms the subject of section 7.1.2.

7.1.2 System characterisation measurements including source coupling

For simplicity, a control task of *point cancellation* is used to illustrate the process of system characterisation including source coupling, and results are then applied to a generalised control task. The required ratio of source velocities for point cancellation is given by

$$\frac{u_s}{u_p} = \frac{-Z_{p,r}}{Z_{s,r}} \qquad \textbf{7.2}$$

In the practical design of biquad fit controllers, models of these two transfer impedances are made on the basis of measurements of $p_{p,r}/v_{in,p}$ and $p_{s,r}/v_{in,s}$. If the controller voltage response $c(j\omega)$ is specified on the basis of these two measurements, then for high-impedance sources which do not couple, the optimal run-time controller response is achieved.

$$c(j\omega) = \frac{-p_{p,r}/v_{in,p}}{p_{s,r}/v_{in,s}} \qquad \textbf{7.3}$$

In order to ensure that (**7.3**) accounts for the effect of source coupling, the transfer function measurements *must be made in the presence of the other (acoustically driven) source, connected to whatever amplification will be used in the final run-time control scenario.* The necessity of this measurement arrangement is illustrated in the following short proof:

The pressure at the observation point ***r*** has two components; that due to the primary and that due to the secondary. Each of these pressure components can be written as:

$$\begin{aligned} p_{p,r} &= A.v_{in,p} + B.v_{in,s} \\ p_{s,r} &= C.v_{in,p} + D.v_{in,s} \end{aligned} \qquad \textbf{7.4}$$

or, in matrix form:

$$\boldsymbol{P} = \begin{bmatrix} A & B \\ C & D \end{bmatrix} \boldsymbol{V} \qquad \textbf{7.5}$$

$\boldsymbol{P}$ and $\boldsymbol{V}$ are column vectors of the pressures and voltages respectively. This suggests that the pressure due to the primary input voltage is equal to that part of the pressure driven by the primary source, and that part set up by the acoustically-driven secondary. The same concept applies to the pressure due to the secondary input voltage. If both sources act together, the *total* pressure resulting from the motion of the primary source will equal the linear superposition of that component due to the primary input voltage, and that component due to the primary source moving in response to a voltage input at the secondary source. The same argument applies for the total pressure set up by the secondary source.

The leading diagonal terms of the matrix relating $\boldsymbol{P}$ and $\boldsymbol{V}$ describe the pressure / voltage relationships for each source neglecting coupling; A and D can be measured directly (as pressure / voltage transfer functions) with only one source in the acoustic system at a time:

$$\left.\frac{p_{p,r}}{v_{in,p}}\right|_{secondary\ removed} = A$$
$$\left.\frac{p_{s,r}}{v_{in,s}}\right|_{primary\ removed} = D \qquad \textbf{7.6}$$

On the 4m test duct, this equates to removing each respective source and replacing it with a stiff blanking plate of infinite mechanical impedance in the frequency range of interest. In a room, the unwanted source may simply be removed.

If both sources are present, measurement of the pressure generated when only one source is driven electrically will give the following two results:

$$\left.\frac{p_{p,r}+p_{s,r}}{v_{in,p}}\right|_{v_{in,s}=0} = A + C$$
$$\left.\frac{p_{p,r}+p_{s,r}}{v_{in,s}}\right|_{v_{in,p}=0} = B + D \qquad \textbf{7.7}$$

When the four transfer function measurements described above ((**7.6**) and (**7.7**)) are made, it is possible to identify all the elements of the matrix relating voltages and pressures (**7.5**).

Inverting (**7.5**) to make the input voltages the subject:

$$\boldsymbol{V} = \begin{bmatrix} D/d & -B/d \\ -C/d & A/d \end{bmatrix} \boldsymbol{P} \qquad \textbf{7.8}$$

where d is the determinant AD-BC

In the application of point cancellation, the relationship between pressures required from primary and secondary sources is simple. The desired pressure matrix is

$$\boldsymbol{P} = \begin{bmatrix} 1 \\ -1 \end{bmatrix} \qquad \textbf{7.9}$$

A desired voltage relationship follows once the elements of the matrix in (**7.8**) have been calculated using simple complex algebra from measurements illustrated in (**7.6**) and (**7.7**). Since

$$c(j\omega) = \frac{v_{in,s}}{v_{in,p}} \qquad \textbf{7.10}$$

then in the specific case under consideration (**7.8**) and (**7.9**) can be rearranged to show that:

$$c(j\omega) = \frac{-(A + C)}{(B + D)} \qquad \textbf{7.11}$$

Comparison with (**7.7**) shows that in order to account for coupling in the design of a point cancellation filter, *p/v* transfer functions should be measured in the presence of the acoustically-driven 'other' source. These transfer functions can then be used directly to specify the run-time control filter, in the form

$$c(j\omega) = \frac{\left.\dfrac{-(p_{p,r}+p_{s,r})}{v_{in,p}}\right|_{v_{in,s}=0}}{\left.\dfrac{(p_{p,r}+p_{s,r})}{v_{in,s}}\right|_{v_{in,p}=0}} \qquad \textbf{7.12}$$

7.2 A point cancellation controller for the 4m duct

Figures 7.6 and 7.7 show the required voltage transfer function *c(jω)* for a filter designed to cancel pressure at a point adjacent to the primary source, 0.05m along a 4m duct. Point cancellation has been chosen for the control task since the mathematics defining the coupled

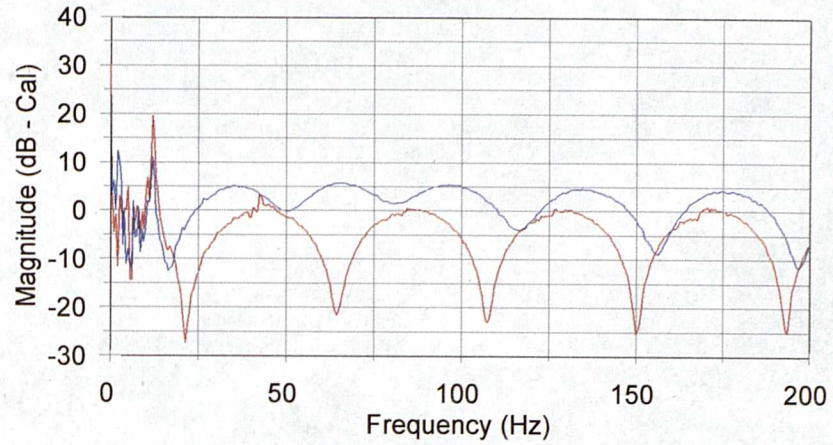

Figure 7.6 - Control filter for point cancellation at x=0.05m - Magnitude
a) Uncoupled controller *b) Coupled controller*

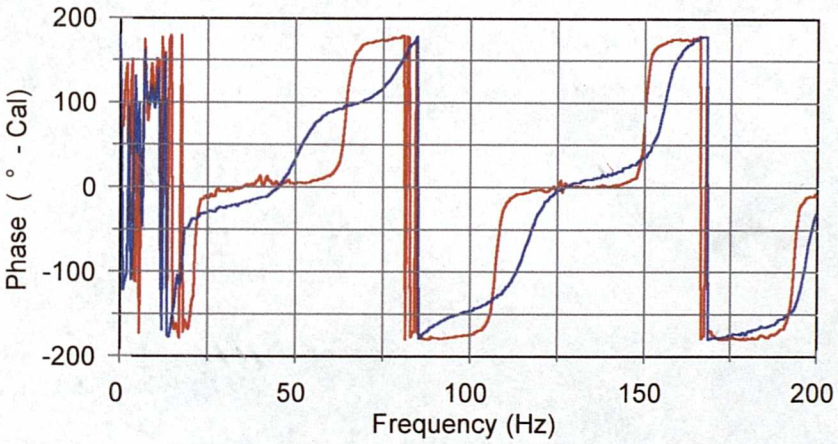

Figure 7.7 - Control filter for point cancellation at x=0.05m - Phase
a) Uncoupled controller *b) Coupled controller*

solution is relatively straightforward, and the problems arising from attempts to realise this solution using IIR filter sections may be clearly demonstrated. Source coupling has been incorporated following section 7.1.2, using actual measurements made on a duct terminated by one KEF B200 drive unit at each end. A control filter designed assuming infinite source impedance is also shown, with design based on measurements of actual driver velocities rather than input voltages using true specific transfer impedances *(p/u)*. The influence of the source impedance of the terminating loudspeaker is removed by measuring in the presence of a rigid end-cap.

It can be seen that the uncoupled solution exhibits a series of maxima at the resonant frequencies of the duct, together with sharp minima and rapid phase transitions at the points in frequency where adjacent modal residues in $Z_{p,r}$ cancel. This filter response is entirely consistent with that expected from (**7.2**), as the constituent transfer impedances are built purely from the parallel addition of a number of second-order bandpass functions.

The controller incorporating source coupling based on (**7.12**) is markedly more complicated in structure. The causes of the change in response from the uncoupled canceller become apparent on inspection of the measurements on which the different controllers are based. Figures 7.8 and 7.9 compare *p/u measurements of primary path magnitude transfer* impedances with *p/v* data. The first graph shows the case where the duct is rigidly terminated, and the second where the termination is provided by a similar loudspeaker driver with shorted voice coil.

In Figure 7.8, whereas the true impedance measurements take the form of a conventional sum of second order bandpass functions, those *p/v* measurements incorporating the driving source impedance are modified substantially. The gross changes in radiation load experienced by the source in the duct resulting from the modal nature of its load impedance mean that a simple second-order model of the pressure / velocity transfer impedances is no longer appropriate. Where measurements are made in the presence of an acoustically-driven terminating loudspeaker (Figure 7.9), the picture is further complicated.

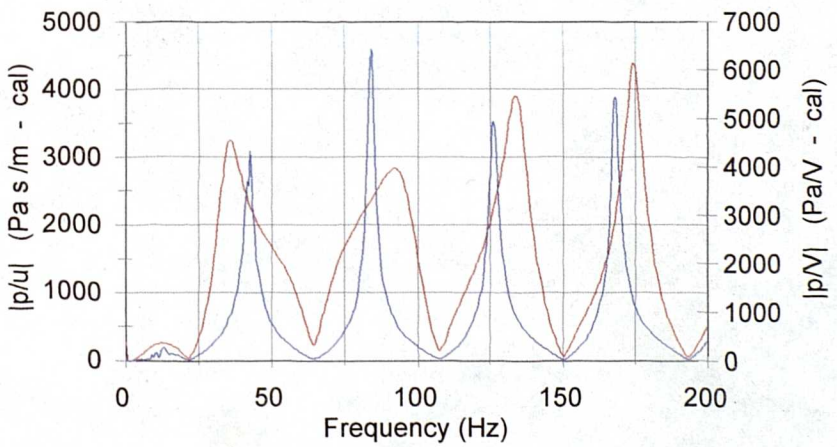

Figure 7.8 - Magnitude transfer functions for rigidly terminated duct
a) pressure/voltage b) pressure/velocity

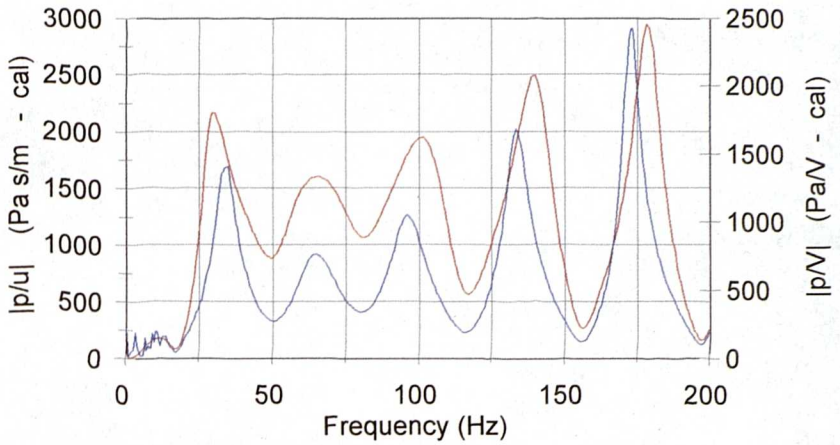

Figure 7.9 - Magnitude transfer functions for duct terminated by driver with shorted coil
a) pressure/voltage b) pressure/velocity

True *p/u* transfer impedance measurements indicate that the field in the duct terminated with the complex and frequency dependant impedance presented by the terminating driver is still described by the sum of a number of resonant modes. However, the terminating driver impedance is small enough near its own mechanical resonance to imply something approaching an *open* termination across a limited range of frequencies around 65Hz. An additional *1/4 wave* resonance appears at this frequency. Over the whole bandwidth of the measurement the termination contains a sufficiently large imaginary component to ensure that remaining duct eigenvalues are shifted substantially [11].

Incorporating the driving source impedance by making a measurement of p/v_{in} yields a transfer function which is further removed from the uncoupled case. Not only are the duct eigenvalues shifted by the complex termination conditions, but the modal radiation load on the driving source means that the p/v_{in} measurement is not simply described by the summation of second-order bandpass sections. The symmetry of the modes with respect to frequency is distorted by the changes in the relationship between the radiation impedance and the driving source impedance. This has important implications regarding the possibility of the construction of a feedforward filter in the duct based on a biquad-fit technique.

Figure 7.10 shows that the phase of *p/u* and *p/v* measurements also differs significantly, suggesting that a biquad fit may be inadequate in terms of phase as well as magnitude. The falling phase characteristic exhibited by the measurement using a voltage reference is

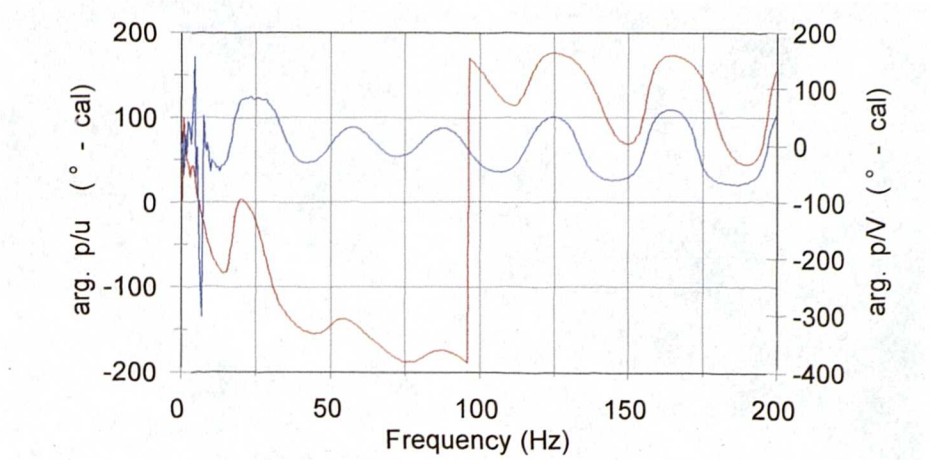

Figure 7.10 - Phase of transfer functions for duct terminated by driver with shorted coil
a) pressure/voltage b) pressure/velocity

dependant on the phase response of the voltage-velocity transfer function of the driving source. In free-field conditions this takes the form of a simple second-order bandpass function, but because the duct presents a strongly modal radiation load the magnitude and phase are both significantly more complex, as illustrated in Figures 7.4 and 7.5.

The modal decomposition of the pressure in a duct presented in Chapter 3 anticipates that the duct has a secondary path impedance having the same Q-factor and eigenvalues as the primary path, with pressure modified by changes in modal shape functions resulting from the adoption of alternative source and receiver locations. Figure 7.11 shows the influence

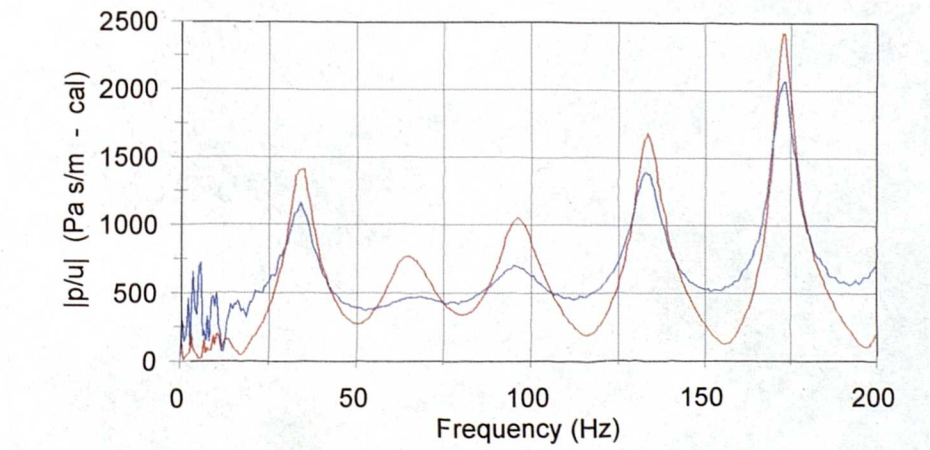

Figure 7.11 - Primary and secondary path transfer impedances for x=0.05m
a) Secondary path b) Primary path

of modeshapes on true measured transfer impedances. Pressures measured close to a source are functions of coherent modeshapes; the phase of all eigenvectors is the same so long as the measurement frequencies are low enough, such that no modal pressure nodes occur between source and receiver location. This means that between two adjacent modes the respective modal residues interfere *destructively* due to the pi phase shift which occurs through resonance. This is the case for primary path transfer function in Figure 7.11, since the measurement location $x=0.05m$ lies adjacent to the primary source..

Pressures measured at the opposite end of the duct are functions of alternately odd- and even- modeshapes, which compensate for the phase inversion through resonance and mean that the residues of adjacent modes add constructively. This effect is observed in the secondary path transfer function of Figure 7.11. Additionally the difference in damping due to each driver acting as a termination is clearly visible, with secondary path modal quality factors being markedly lower than those measured for the primary path. The imaginary part of the impedance presented by both drivers is similar; although eigenvalues are shifted significantly when compared to the result for the rigidly terminated duct, the magnitude of the change is the same for both paths, and eigenvalues occur at similar (shifted) frequencies.

A comparison of measurements of p/v_{in} transfer functions measured on the primary and secondary paths (Figure 7.12) reveals that the combined variation of termination *and source* impedance between the two measurements alters not only the quality of resonance, but also

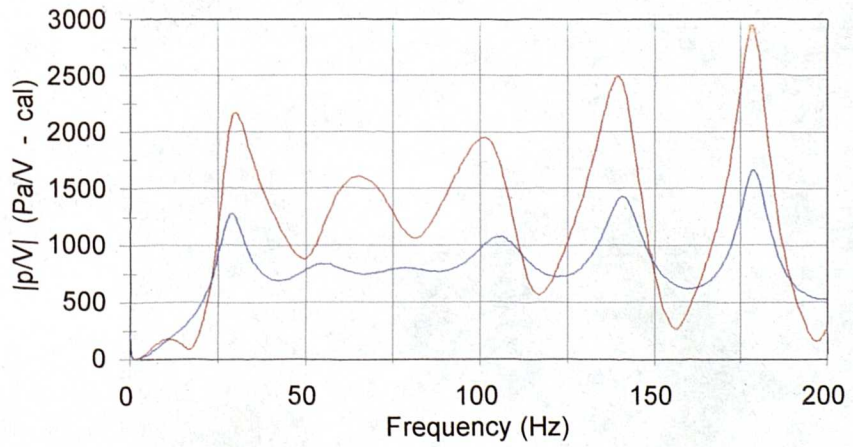

Figure 7.12 - Primary and secondary path p/v transfer functions for x=0.05m
a) Secondary path b) Primary path

the frequency at which resonance occurs. Indeed, the source impedance of the secondary driver is such that an additional resonance (compared to the primary path coupled measurement) of very low Q-factor appears between 50 and 100Hz. This result is not anticipated by the mathematical model, and adds a further complication to the use of biquad fit models for active control. Not only are the functions which must be fit no longer simple second-order bandpass sections, but the eigenvalues in both paths are different. Together these factors are responsible for the increased complexity of the coupled canceller response shown in Figures 7.6 and 7.7.

The significance of the errors introduced by fitting these functions with second-order biquad filter sections is commented upon in the context of practical control filters designed using the biquad fit technique, in section 7.3.

7.3 Design and performance of point cancellation filters incorporating practical source impedance

Firstly let us consider the implementation of the coupled point cancellation controller, the magnitude and phase response of which are shown in Figures 7.6 and 7.7. Initially the performance of the coupled solution is investigated by a frequency domain simulation of the action of a controller having this response.

The pressure at $\boldsymbol{r}$ resulting from a voltage input at the primary source will incorporate a contribution due to the primary source, and a contribution resulting from the resulting coupled motion of the secondary source. The same applies for a voltage input at the secondary source. The pressure set up due to the action of both sources will therefore involve the multiplication of controller $c(j\omega)$ with the transfer function found from (7.7) describing the total pressure contribution to a voltage $v_{in,s}$, onto which must be added that pressure contribution due to the primary input voltage (also from (7.7)). Therefore:

$$\frac{p_r}{v_{in,p}} = c(j\omega).(B+D) + (A+C) \qquad \textbf{7.13}$$

Not surprisingly when $c(j\omega)$ is derived in order to incorporate coupling as described in (7.12), the summation of primary and secondary path pressures leads to total cancellation

of the field at the solution point ***r***. However, the feedforward filters used in this project are based on the biquad fit concept, and so the possibilities of forming $c(j\omega)$ from parallel IIR filter sections must be investigated. This process demonstrates the problems inherent in fitting *p/v* transfer functions measured in the duct with biquad sections.

The filter structure required for point cancellation using IIR filter sections results from consideration of (**7.2**) and (**7.3**). The ratio of source velocities will be defined by

$$\frac{-Z_{p,r}}{Z_{s,r}} \qquad \textbf{7.14}$$

Where only one mode is considered at a time and the transfer functions are fitted with second order biquad sections, the canceller appears as

$$\frac{-Z_{p,r}}{Z_{s,r}} = \frac{-(z^2 - 2Re(p_s)z + |p_s|^2)}{z^2 - 2Re(p_p)z + |p_p|^2} \qquad \textbf{7.15}$$

- the zeros are provided by the poles of the secondary path fit, and the poles are those from the primary path fit. This is the uncoupled solution in the duct and is only valid with sources of infinite source impedance.

Where more than one mode is considered simultaneously, the design of the canceller becomes significantly more complex. $Z_{p,r}$ and $Z_{s,r}$ are then formed by the addition of a number of filter sections representing each mode of the summation in (**5.1**). As $Z_{p,r}$ appears in the numerator of (**7.15**) it can be modelled as the parallel combination of its constituent filter sections. The inverse of a parallel bank of second order filter sections required for $1/Z_{s,r}$ has been described in (**5.20**) and (**5.21**). The N parallel sections of $Z_{s,r}$ are transposed for $1/Z_{s,r}$ into a cascade of N sections (one of which has poles described by $[z^2 - 1]$), and the whole canceller is then formed from a parallel arrangement of N sections for $-Z_{p,r}$ which drive the cascade of N sections representing $1/Z_{s,r}$ (Figure 7.13).

It has been established that a coupled source point cancellation controller is formed from a ratio of transfer functions measured in the presence of a coupled source (**7.12**). Therefore for sources of finite impedance, it is not true transfer impedances which must be used in the biquad fit process, but the *p/v* transfer functions measured in the presence of a coupled source. The magnitude of these functions are illustrated in Figure 6.23. Magnitude and

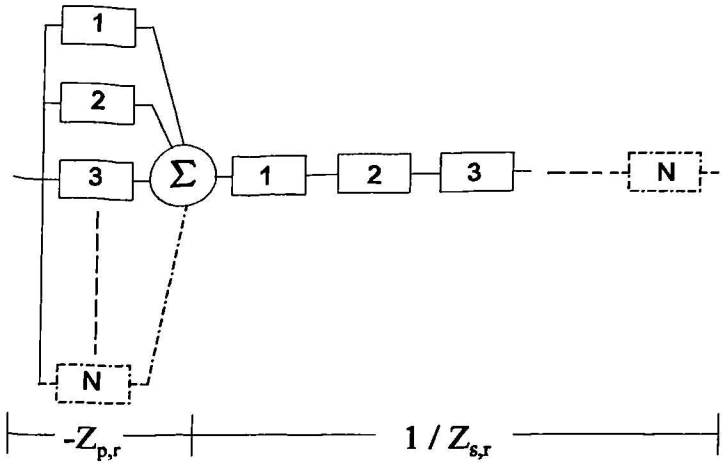

Figure 7.13 - Point canceller schematic

phase fits of primary and secondary path transfer functions out to a solution point 0.05m from the primary source are illustrated in Figures 7.14 to 7.17, where four filter sections have been used to model the highest four modes in frequency, in each measurement.

Primary				
Modal f (Hz)	67.000	99.000	137.000	176.000
Scale	5.500	6.500	6.000	5.500
-2Re(p)	1.949	1.941	1.929	1.905
$\|p\|^2$	0.960	0.965	0.975	0.980

Primary path filter coefficients

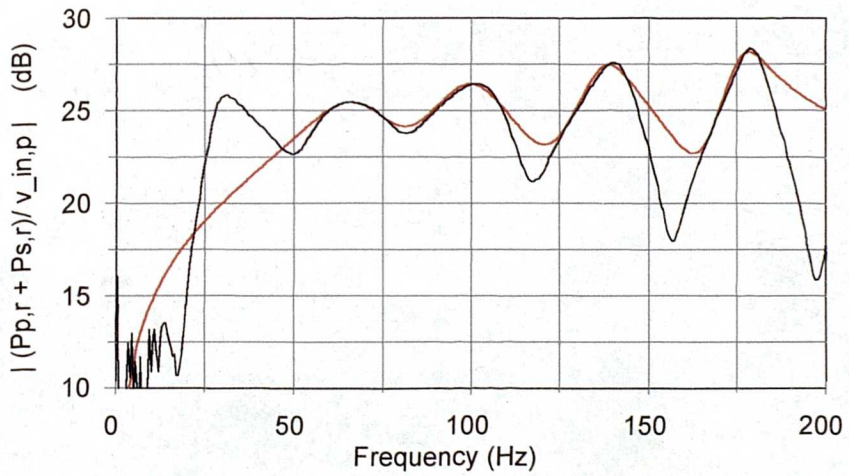

Figure 7.14 - Primary path mode fit - solution point x=0.05 - magnitude
a) Measured data b) 4 mode sum

The changes in resonant frequency between primary and secondary path measurements are illustrated in the tables of biquad fit parameters. Magnitude fit accuracy is better on the modes than off-resonance; the low Q-factor of the transfer functions implies that many more

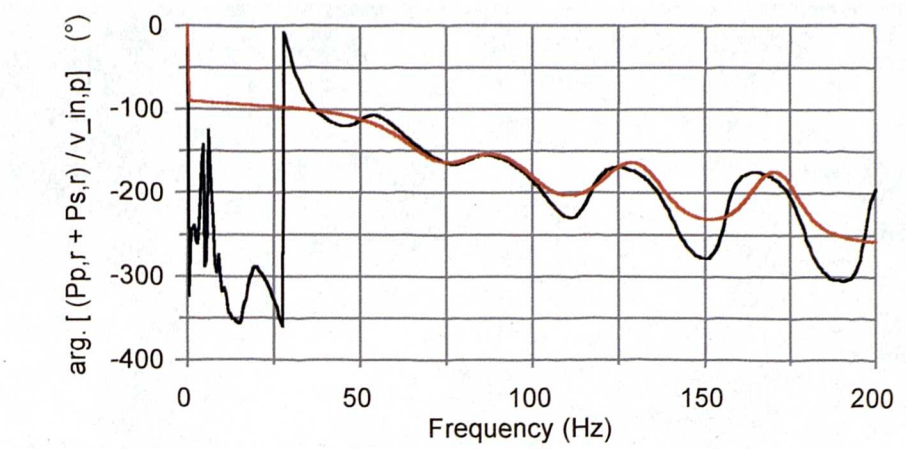

Figure 7.15 - Primary path mode fit - solution point x=0.05 - phase
a) Measured data b) 4 mode sum

Secondary				
Modal f (Hz)	75.000	107.000	140.000	179.500
Scale	4.000	-4.800	4.000	-2.800
-2Re(p)	1.946	1.942	1.932	1.908
$\|p\|^2$	0.960	0.970	0.980	0.987

Secondary path filter coefficients

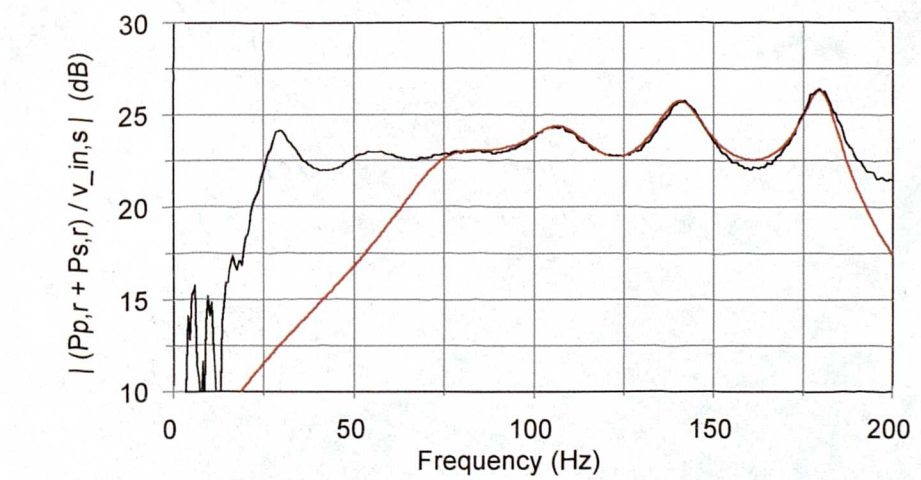

Figure 7.16 - Secondary path mode fit - solution point x=0.05 - magnitude
a) Measured data b) 4 mode sum

than four filter sections would be required in order to obtain good fit accuracy between modal frequencies. This result agrees with the modelled predictions of fit accuracy and its dependance on modal Q-factor discussed in Chapter 6. Phase fit accuracy is superior for primary path functions compared to the secondary path. The additional 'mode' present in

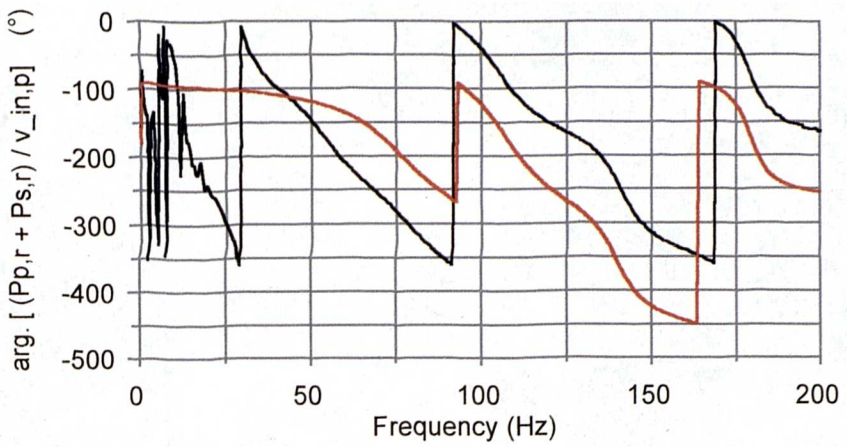

Figure 7.17 - Secondary path mode fit - solution point x=0.05 - phase
a) Measured data *b) 4 mode sum*

the latter measurement is not modelled with an additional filter section, and appears to reduce the accuracy of the model fit in phase.

The controller designed for coupled operation using a four-mode biquad fit method is compared to the optimal coupled canceller, and the optimal uncoupled canceller, in Figures 7.18 (magnitude) and 7.19 (phase). The biquad fit solution might be expected to track the response of the optimal solution over the frequency bandwidth where the fit process models measured data - namely between 70 and 180 Hz. This anticipated result is broadly observed

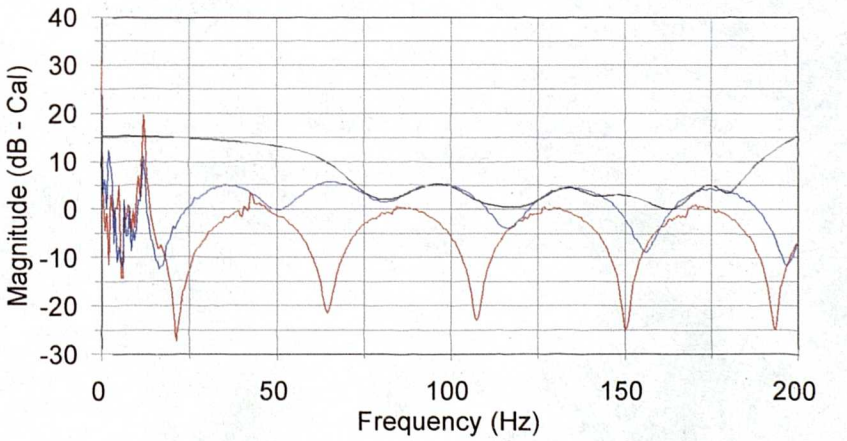

Figure 7.18 - Magnitude response of point cancellation control filter
a) Coupled biquad solution *b) Optimal coupled solution*
c) Optimal uncoupled solution

in Figure 7.18. Off-resonance however, errors in the biquad fits observed in Figures 7.14 to 7.17 mean that the magnitude responses of the biquad fit canceller and the optimal coupled filter diverge. The response of the biquad controller deviates from the optimal case by up to 10dB, and outside the bandwidth of control provided by the four filter sections in the biquad model, the controller is unable to approximate an appropriate response. The phase response (Figure 7.19) of the biquad fit controller deviates markedly from the optimal coupled solution, by as much as 100 degrees.

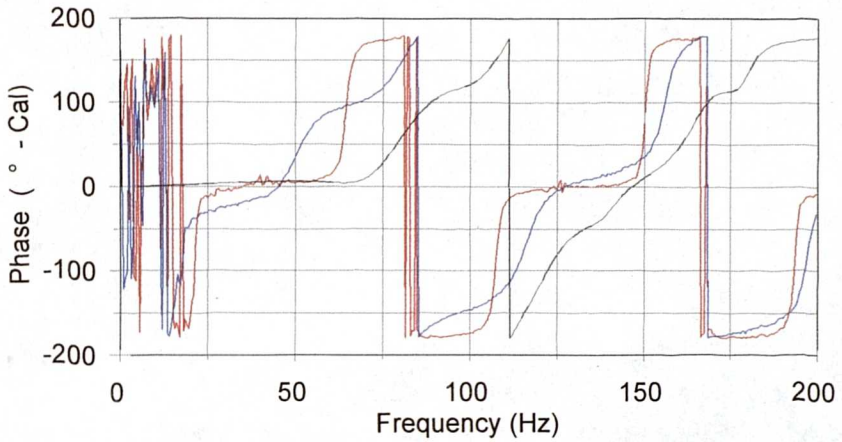

Figure 7.19 - Phase response of point cancellation control filter
a) Coupled biquad solution *b) Optimal coupled solution*
c) Optimal uncoupled solution

This is largely due to inaccuracies in the fit of the phase response of the secondary path transfer function, and in the light of these inaccuracies it is perhaps surprising that the biquad fit canceller performs as well as is indicated in Figure 7.20. Here, the performance of the biquad fit canceller in the duct is simulated using (**7.13**). Also shown is the response due to the use of the optimal *uncoupled* filter, in the presence of coupled sources.

Responses are shown in terms of the pressure at the solution point in response to a 1V primary input voltage, where the response of an uncontrolled duct is provided for reference. The optimal coupled control solution would therefore be expected to result in a pressure equal to -∞dB. As previously discussed, it is to be expected that a biquad model of the uncoupled canceller may be constructed with reasonable accuracy, since the functions on which it is based are all strictly second order bandpass sections.

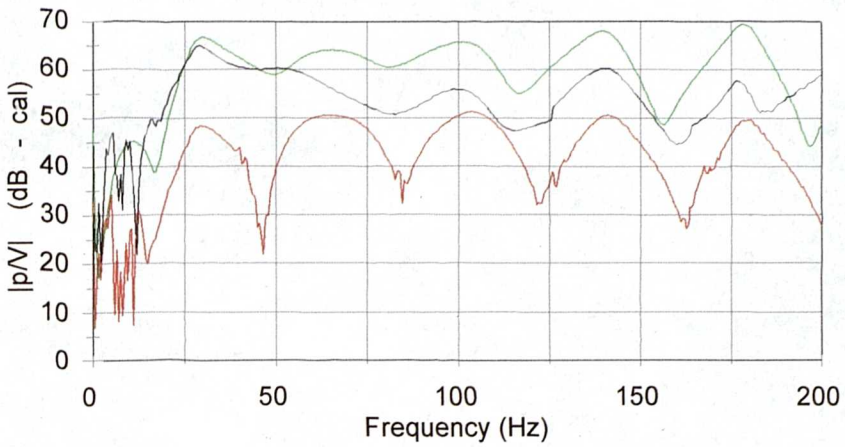

Figure 7.20 - Performance of canceller at solution point x=0.05m
a) Uncontrolled b) Biquad (4mode) controller
c) Optimal uncoupled controller

The following conclusions may be drawn from Figure 7.20 :

- Some degree of cancellation is possible using the four-mode biquad fit model of the coupled canceller. Performance is poor at frequencies where this controller response deviates from the optimal coupled canceller, and overall a reduction of approximately 10dB is predicted.
- The uncoupled optimal canceller actually performs better than the biquad model of the coupled canceller. This is due to the poor fit accuracy of the functions from which the coupled canceller is based, and occurs in spite of the uncoupled solution being simulated in operation with coupled sources.
- The biquad fit method is unsuitable for systems whose constituent components are not simple second order functions. In the duct the best cancellation strategy using a biquad fit model would appear to involve fitting measured *p/u* transfer impedances with as many filter sections as practicable, and accepting the inevitable degradation of performance due to source coupling.

7.4 Conclusions on the use of Biquad fit control in one dimension

In attempting to replicate the model of Biquad Fit control in the duct introduced in Chapter 6, the difficulties presented by the limited source impedance of practical sources and the strongly modal nature of the in-duct radiation load have been investigated. An approach has been outlined which enables the specification of a feedforward control filter in these

circumstances, and which incorporates non-real termination impedance and sources of low impedance into the design of a run-time control filter. However, since the biquad fit technique was designed to exploit the second-order bandpass characteristic of the normal modes of a space, its use is no longer appropriate where the functions describing a particular system do not follow this pattern. If other control filter structures were used, the coupled analysis remains useful in providing the optimal controller - the pursuit of alternative feedforward filter structures forms one suggested avenue of further investigation, and in Chapter 10 the subject is discussed at some length.

Models of active control in a duct predicted that the biquad fit technique would be subject to errors introduced by modelling the system with a limited number of second order sections. Additionally, the validity of a modal model of the duct was called into question where the desired or actual termination impedance was very small. The practical realisation of this model has been defeated, not by either of these difficulties, but by the nature of the coupling between the practical electrodynamic sources used to drive the duct with the required velocities.

One possible solution to this problem would be to employ very 'stiff' electroacoustic sources with high source impedance compared to changes in the modal radiation load. The analysis of uncoupled sources suggests that such a scheme would yield a practically realisable system which would enable comparison with the mathematical models - the transfer functions required for system characterisation would then follow the anticipated second order bandpass form. Salava [67] suggests a number of approaches to designing such sources in practice, and limitations on the range of load impedances over which they can be assumed to have constant volume velocity.

However, the primary aim of the project is not to implement control in a one-dimensional environment; the duct merely provides a useful starting point in a comparison between the behaviour of the two alternative control systems. It remains entirely possible that in a three dimensional room, changes in the radiation load will not be so dramatic as in the enclosed duct, and the biquad fit method may yield useful results. The performance of a biquad fit controller in a room is reported in Chapter 9.

Chapter 8

Impedance control techniques in a three dimensional environment

8.0 Introduction

The active control of acoustic impedance has been shown to be a useful tool in manipulating steady-state and decay artefacts of the soundfield enclosed in a one-dimensional environment. To some degree the success of the technique is due to the ease with which the target impedance of the system may be specified in one dimension - the realisation of a characteristic termination is easy to visualise from theory and the resulting changes in the acoustics of the system are those which follow using the mathematics of Chapter 3.

In a three dimensional environment, the relationship between the control source surface impedance and the modal behaviour of the room is not simple. The soundfield in the room is not plane, although it can be considered to result from the sum of a number of normal modes which individually are plane waves [11,25]. There exist three orthogonal coordinate axes for particle velocity rather than the single axis of the duct, and the velocity of the controlling driver may lie in the plane of one coordinate, or perhaps none of the three. The meaning of a 'characteristic impedance' is therefore no longer clear, and it does not follow that the characteristic impedance solution for the duct will result in the optimal control of the modal behaviour of the room.

Unlike the one dimensional case where careful secondary source placement could ensure a degree of control over all the modes of the system, in the room it is expected that only a limited number of modes may be suppressed [12]. This restriction is in part a function of the chosen target impedance, but before alternative targets are considered the behaviour of an impedance-controlled source in a three dimensional environment is investigated. The

controlled source is identified as a potential sound absorber, and the formation of models for, and transduction of, surface impedance in three dimensions are briefly discussed.

Then, two control strategies are investigated comparing measurements and numerical predictions. This comparison is made in terms of the control of frequency, time and spatial artefacts associated with a modal soundfield, and forms the main aim of this chapter. The work comprises part of the novel contribution made by this Thesis, as previously published active impedance control data has been concerned with one-dimensional waveguides.

8.1 Global control using one secondary source in three dimensions

In the introductions to Chapters 6 and 7 it has been noted that for control in one dimension, careful placement of the secondary control source can result in a degree of suppression of all acoustic modes within the system. This result is obtained by Nelson and Elliot [12] in an attempt to minimise the acoustic potential energy in a duct, where the control and primary sources are located at opposite ends. Where the ratio of dominant mode to residual components is high, a large degree of cancellation may be achieved. Between modal peaks, the requirement to match the conflicting phase of adjacent residues which flips between modes of odd and even order means that little or no pressure reduction is observed.

For a pressure minimisation control task this places a clear limit on the levels to which loudness may be reduced. In the applications of this Thesis, where modal *damping* rather than overall sound pressure defines the control target, this restriction does not necessarily limit the control performance. It has been shown in Chapter 4 that for a duct, a single controlled characteristic termination may effectively remove the modal character of the soundfield and leave a direct field due to the primary source. The resulting flat pressure response follows a similar form to that obtained by Nelson and Elliot [12] for the best-case duct pressure minimisation. However, the results must not be regarded as equivalent since damping by characteristic termination is accompanied by associated reductions in modal decay time, which are not reported in the pressure minimisation work.

In three dimensions, axial, tangential and oblique modes populate the space and it is yet more difficult to match the complex velocity of the control source with the requirements of

a number of modal residues. For the pressure minimisation task Nelson and Elliot note that *one* secondary source may be driven to completely remove *one* modal component - but that the presence of the remaining residues may mean that throughout the space significant pressure remains, even at the peak frequency of the cancelled mode. Bullmore [21] notes that even where modes are degenerate, they may be cancelled using a single secondary source so long as the primary modal contributions at the controller have the same relative phase and roughly equal amplitudes. These results may inform the present study, but they do not apply directly as our concern is with modal quality factor.

A direct application of the numerical analysis of Nelson and Elliot to the work presented here is inappropriate. This analysis relies on a cost function equal to total time-averaged acoustic potential energy, which is minimised to determine the theoretical limit of noise control using a single secondary source. This cost function is not appropriate for the consideration of modal damping, even though results in the duct suggest that in frequency the two control tasks may appear to have similar outcome. The derivation of an appropriate cost function forms a useful study which lies outside the scope of the present Thesis, and is discussed as an avenue for further work in Chapter 10.

In this chapter therefore, two control approaches are tested where the theoretical limit of spatial control has not been defined. The first technique uses a real controlled impedance, and could be expected to add damping to all modes whose eigenvectors exhibit high impedance at the location of the control source. This is expected to implement a global reduction in the modeshape amplitudes. In contrast, complex controlled impedances might be expected to reduce local pressures at the expense of global reductions.

For both strategies, evidence of increased modal damping rather than pressure cancellation is sought using measurements of time-domain decay of modal components. These measurements are made at a number of locations around a room, for a number of control source positions. In conjunction with steady state pressure measurements these results are used to draw conclusions regarding the ability of the controllers to implement global changes in modal quality using a single control source.

8.2 Relationship between controlled impedance and acoustic absorption

The active control of acoustic impedance has been introduced in the context of the relationship between the pressure and velocity at the surface of a controlled loudspeaker cone. The specific acoustic impedance at the cone surface is defined by the (potentially complex) ratio between pressure at the cone, and cone velocity. It is also possible to consider this relationship in terms of the power radiated by the source, which in certain circumstances becomes negative, corresponding to *absorption* of energy by the source.

When a sound source radiates acoustic power at low frequency (assuming pistonic motion and uniform pressure over the source), the power radiated is proportional to the real part of the product of velocity and total pressure :

$$W \propto \Re e[p_T u] \qquad \textbf{8.1}$$

If the velocity of the source can be controlled, such that the real part of the pressure* velocity product goes negative, the source is absorbing acoustic power. It is important to note that the pressure p_T is the sum of components from the absorbing source and some external sound source [12,35].

It can be useful to think of the impedance-controlled source as an absorber of acoustic power, but modelling the behaviour of such an absorber is not as simple as might at first be assumed. Firstly, the pressure over the surface of a practical driver is not constant, but varies considerably in magnitude and to a lesser extent phase. Secondly, the total pressure at the cone will contain components due to the direct radiation of primary and secondary sources, and in a low-frequency reverberant field will also incorporate modal contributions due to both sources. It is therefore important to consider the practical measurement of surface pressure and velocity, and how these measurements tie up with a theoretical understanding of the radiation of a pistonic source in a modal environment.

8.3 Modelling and measuring the impedance of a controlled source in a room

A discussion of the measurement of acoustic impedances and appropriate numerical models has been undertaken in section 6.1 for a plane wave environment. The direct transduction

of particle velocity in a three dimensional environment is subject to the same constraints as described in section 4.2.1 for the one dimensional duct. The transduction of pressure and the formation of an appropriate model for low-frequency radiation impedance in a room must be reconsidered.

In a three dimensional environment, the radiation load presented to a source changes from the plane wave case, and the result differs depending on whether radiation occurs in anechoic or reverberant conditions. The free field result is based on familiar series expansions [10,87,88] or 'piston functions', but in the work presented in this chapter it is necessary to model the surface impedance of a plane pistonic source radiating into an enclosed modal soundfield, and to reconcile these results with practical measurement.

The classical wave solution for a rectangular room at low frequencies has been presented in Chapter 3. The model is usually quoted as applying to point sources (**3.5**), which presents a problem when using the analysis to predict the impedance at the surface of a radiator in an enclosure. When the distance between source and receiver $r - r_0$ is small, all modal residues add in-phase, and the summation may not converge [8].

Different authors have approached this problem in a variety of ways. Bullmore adopts rectangular piston sources of finite area [21], but errors in the calculated impedance are still significant in the modelling and implementation of active acoustic absorption [45]. Maa suggests the explicit addition of a term representing the direct field radiated by the source [91,24]. As stated in his paper, Maa's approach is actually wrong since the addition of the extra term defeats the normal solution of the wave equation by the addition of orthogonal modal components. However, the technique provides a useful approximation for the pressure field close to the surface of a source in a modal environment, as is shown below.

As a microphone location approaches a source in modal environment, individual modes appear to be suppressed and peaks in pressure are smoothed. This is shown in Figure 8.1, which plots a series of magnitude transfer impedance measurements ($|p_r / u_{r0}|$) made over a range of perpendicular distances between 5 and 200mm from a control source located in the reverberant room described in Appendix F.

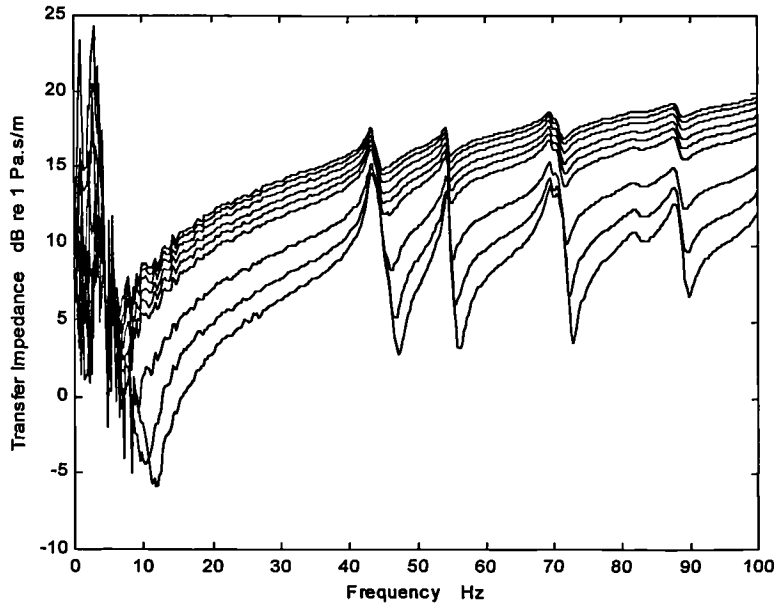

Figure 8.1 - Magnitude transfer impedances measured away from a source. Distances from cone (top to bottom trace) = 5, 10, 20, 30, 40, 50, 100, 150, 200mm

The number of modal components needed to model a transfer impedance depends on the measurement distance. At a distance of 200mm resonant peaks are clearly defined and pressure may be modelled with reasonable accuracy using a modal decomposition which only includes modes of low order - the changing polarity of higher order modeshapes means they add incoherently, and may therefore be omitted.

The practical implementation of an impedance controller incorporates a microphone which is positioned far closer to the cone of the control loudspeaker - the distance averages around 5mm, corresponding to the top trace of Figure 8.1. In this case the modal decomposition takes far longer to converge, since modal residues add coherently right up until a very high natural frequency where the wavelength becomes small compared to 5mm. Because modal density increases dramatically with frequency, the summation of (**3.5**) must be expanded to much higher orders if a good model of the measured transfer impedance is to be obtained so close to the source.

Figure 8.2 displays a series of black traces representing the modelled pressure very close to a controlled source with unit velocity, showing the effect of increasing the order of modal summation in a three dimensional enclosure. Order [N,N,N] modes are used where N takes values of 5 (bottom trace) through 10, 20 and 40 to 80 (top trace). As the number of

included modes increases the coherent residues form a sum which approaches the measured data asymptotically (blue trace) - in other words the residues themselves add to approximate the direct field. However, the computational cost entailed in large summations is high. The time taken to perform a calculation increases with the cube of the increase in mode order, and each successive black trace represents an eight-fold increase in calculation time.

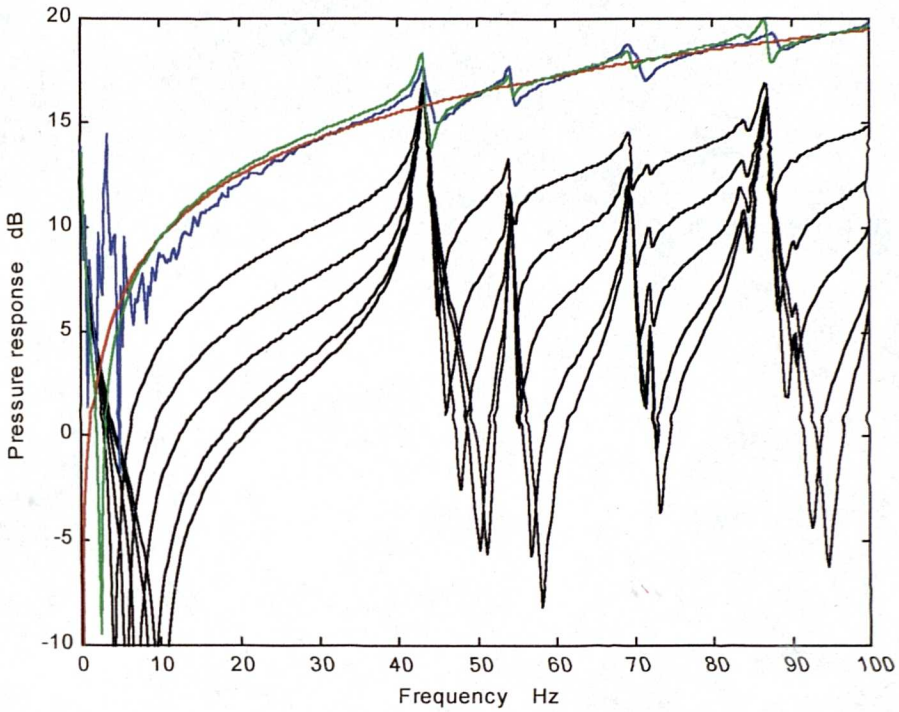

Figure 8.2 - Magnitude pressure response at a source (arbitrary reference)
a) Measured data b) Direct term only c) Maa solution (N=5)
d) (bottom to top) N=5,10,20,40,80 (no direct term)

Also shown in Figure 8.2 is a model of the direct field radiated by the source (red trace). As anticipated by Maa, this approximates the measured data quite closely, although some detail due to the resonant nature of the radiation load on the device is lost. Maa's approach of the addition of a modal decomposition (N=5) to a directly radiated term is shown as a green trace, and demonstrates a pragmatic solution to the problem of large computation times associated with the calculation of a radiation impedance close to the source.

An attempt to suppress the modal component of pressure in an enclosure using the approach of Maa has been reported by Avis and Darlington [52]. However, the method relies on using the addition of a direct radiated component at some distance from the source, and the results are therefore unreliable. The identification of alternative target impedances for the

active control of a modal soundfield has been attempted, and their performance evaluated in changing the modal response in a three dimensional environment.

8.4 Impedance control techniques 1 - Real controlled impedances in a room

As has been noted, the meaning of a 'characteristic termination' is unclear in the context of a three dimensional environment. However, the encouraging results obtained using impedance control in the one-dimensional waveguide need not be entirely disregarded when designing a controller to work inside a room. Although the 'ρc' solution may not be applicable, theory (eg. section 3.3) suggests that *real*, finite impedances at room boundaries will reduce the Q-factor of the natural modes in that space, leading to lower spatial- and frequency- domain variance in the soundfield together with shorter modal decay times.

Darlington [44] and Darlington and Avis [92] have considered the operation of real impedance controllers in terms of the Active Absorber concept introduced in section 8.2. Since the impedance very close to the radiating source is transduced by the controller (section 4.1), a model for the pressure at the control source cone based on the work of Maa has been adopted. It is noted [44] that if it were possible to cover one entire wall of an enclosed volume with controlled loudspeakers, the problem would reduce (at least for axial modes terminated by the controlled boundary) to something analogous to the one-dimensional duct case. Consideration of the simple case when the system terminates an acoustic waveguide of cross sectional area equal to the active surface area of the absorber is useful in formulating a more generally valid strategy for impedance control in a room.

In this simple case, acoustic plane waves, lowpass limited to frequencies below the "plane wave cut-off" frequency of the waveguide, are normally incident upon the active surface of the control source. The total acoustic pressure at the cone has three components; incident pressure $p_{incident}$, blocked reflected pressure (which equals $p_{incident}$), and the radiated pressure caused by motion of the loudspeaker. The total pressure at the cone is

$$p_{total} = 2p_{incident} + S.Z_{rad}\, u(t) \qquad \textbf{8.2}$$

Z_{rad} is the radiation impedance presented to the absorber by the waveguide (for example $\rho c/S$ for an infinite waveguide), S is the radiating area and $u(t)$ is the velocity of the

loudspeaker diaphragm. The specific acoustic impedance at the surface of the control source is then:

$$Z=\frac{2p_{incident} + S.Z_{rad}u(t)}{u(t)} \qquad \textbf{8.3}$$

Rearranging (**8.3**), control laws relating the cone velocity to acoustic pressures may be defined which force the impedance at the surface to the characteristic value appropriate to an impedance controller in this application, and which have been adopted in the one-dimensional work reviewed in Chapter 4. If incident pressure $p_{incident}$ can be transduced then:

$$u(t)=\frac{2p_{incident}}{(\rho_0 c + S.Z_{rad})} \qquad \textbf{8.4}$$

If a single microphone is used to transduce *total* pressure, then:

$$u(t)=\frac{p_{total}}{\rho_0 c} \qquad \textbf{8.5}$$

In the special case of a control source terminating an anechoic waveguide with normally incident plane waves, (**8.4**) and (**8.5**) are equivalent as $p_{total} = p_{incident}$ when the active termination implements characteristic acoustic impedance and removes the reflected pressure component. If a smaller number of individual controlled sources are used in a room, the one-dimensional approximation does not apply and the pressure set up in the space is modelled as described in Figure 8.3. Here, the pressure field close to the source has three components - plane incident and reflected waves comprising the modal soundfield, and a spherically-divergent term radiated by the source. Figure 8.3 models radiation at a frequency which strongly excites an axial mode compared to the residues of other modes with differing spatial distribution, and

$$p_{incident}(x,t) = P_{incident}e^{j(\omega t+kx)} \qquad \textbf{8.6}$$

$$p_{reflected}(x,t) = P_{incident}e^{j(\omega t-kx)} \qquad \textbf{8.7}$$

$$p_{radiated}(r,t) = \rho_0 c\ U\ \frac{a}{r}\cos(\theta_a)\ e^{j(\omega t-k(r-a)+\theta_a)} \qquad \textbf{8.8}$$

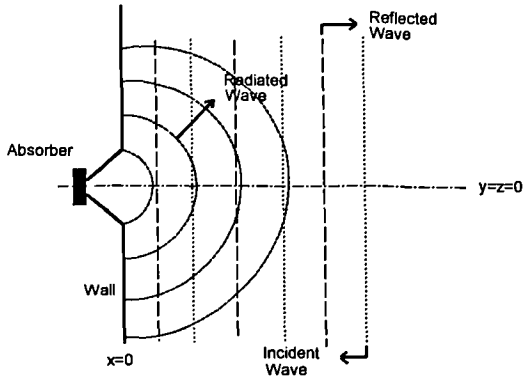

Figure 8.3 - Circular source on reflecting boundary with incident plane waves

The radiated pressure is thus modelled as that from a monopole [10], where U is the velocity amplitude, a is the driver radius, r is the distance from the acoustic centre and θ_a describes the normalised frequency

$$\theta_a = \tan^{-1}\left(\frac{1}{ka}\right) \qquad \textbf{8.9}$$

The total pressure at the control source is

$$p_{total} = 2p_{incident} + \rho_0 c\ U\ [\cos^2(\theta_a) + j\cos(\theta_a)\sin(\theta_a)]\ e^{j\omega t} \qquad \textbf{8.10}$$

and the power flow into the control source or absorber is given by

$$W_{absorber} = \frac{1}{2}\ \pi a^2\ \Re e[\ p^*_{total} \cdot\ U\ ] \qquad \textbf{8.11}$$

where the asterisk denotes conjugation. Substituting for the total pressure gives :

$$W_{absorber} = \frac{1}{2}\pi a^2 \Re e[(2P_{incident} + \rho_0 c\ U\ (\cos^2(\theta_a) + j\cos(\theta_a).\sin(\theta_a))^*.U] \qquad \textbf{8.12}$$

The conventional setup of the active impedance control system allows no differentiation between the soundfield in the room resulting from the operation of a primary sound source, and that due to the controller itself. Therefore, the detected pressure signal is proportional to the *total* pressure at the cone. Where the desired admittance of the device F_d **(4.1)** is specified by a real scalar control coefficient I_R, then:

$$I_R = \frac{U}{P_{total}} \qquad \textbf{8.13}$$

The power at the controller surface is found from (**8.11**) as

$$W = I_R \frac{\pi a^2}{2} |P_{total}^2| \qquad \textbf{8.14}$$

The magnitude squared of P_{total} can be calculated by substituting for velocity (**8.13**) into (**8.10**), which then allows the expression of W in terms of I_R.

$$|P_{total}|^2 = \frac{4|P_{incident}|^2}{(1-\rho_0 c\ I_R\ \cos^2\theta_a)^2 + (\rho_0 c\ I_R\ \cos\theta_a\ \sin\theta_a)^2} \qquad \textbf{8.15}$$

Darlington [44] solves (**8.14**) and shows that maximum power is absorbed when I_R takes value

$$I_{R,opt} = -\frac{1}{\rho_0 c\ \cos\theta_a} \qquad \textbf{8.16}$$

Nelson, Elliot *et al.* [eg 12,36] make extensive comment on the propriety of an approach which aims to maximise the power flow into an actively absorbing device. In an active noise control context, it is suggested that maximum power absorption leads to potential *increases* in sound pressure within the space. With reference to (**8.11**), it is evident that the dependance of power flow on pressure at the control source means that an increase in the magnitude of such pressure may lead to an increase in power absorbed. In energy terms, it is suggested that the presence of a control source changes the radiation impedance acting on the primary radiator with the result that greater electroacoustic efficiency is achieved. The secondary source therefore appears to 'suck' more energy from the primary, and both absorbed power, and pressure, are increased.

This phenomenon occurs when a full modal model of the pressure at the control source is adopted, but the application of (**8.16**) differs from this situation on two counts. Firstly, the absorption has only been maximised within the constraint of a *real* control law - the true maximum absorption impedance is complex, and is derived in section 8.5. Secondly, the scenario represented in Figure 8.3 is not the complete modal description of the controlled,

enclosed soundfield. The primary source is not represented, and only the direct field radiated by the controller and an incident and reflected plane wave are considered. Within these limitations, **(8.16)** is shown in the following section to specify a real impedance which reduces the Q-factor of the modes to a minimum value compared to other possible real solutions. Corresponding spatial and time-domain effects are likewise observed.

8.4.1 Modelled and practical results with a real impedance controller

Figure 8.4 shows the dependance of $I_{R,opt}$ on normalised frequency **(8.16)**. It is seen that as long as very low values of *ka* are avoided, the variance of the control parameter is weak.

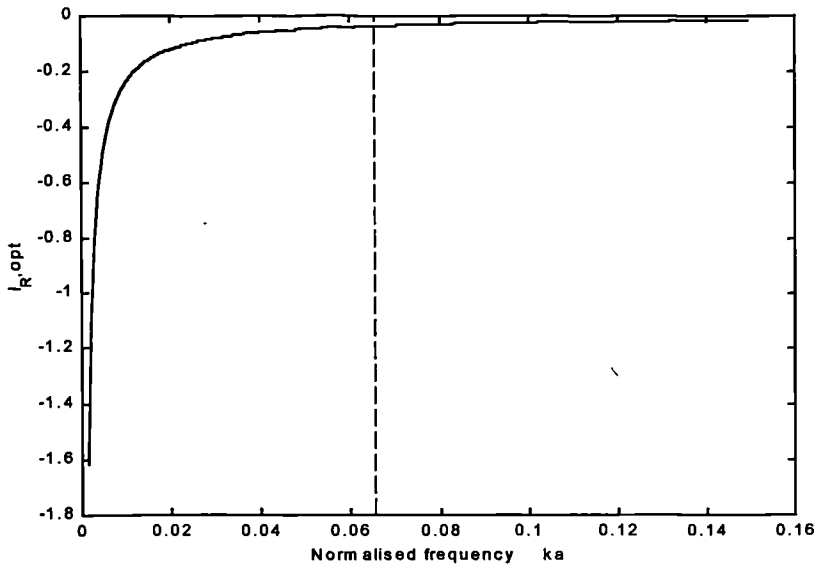

Figure 8.4 - Variation in $I_{R,opt}$ with frequency

Practical measurements based on this work use an 8" nominal diameter Peerless driver with a radius of 0.0815m. In the (3.95 x 3.15 x 2.38)m test room described in Appendix F the lowest axial mode occurs at 44Hz, resulting in a figure for normalised frequency of *ka=0.065*. At the frequencies at which the performance of the controller was investigated, changes in the desired value of $I_{R,opt}$ are small compared to those changes which could be observed to produce a measurable change in the soundfield in the test room. Therefore a simple controller topology was adopted which maintained a real relationship between pressure and velocity at the cone regardless of the frequency of excitation. A number of target values have been chosen, including the optimal value at the frequency of the lowest axial mode such that

$$I_{R,opt}|_{ka=0.065} = -0.0374$$

This approach was replicated in a FORTRAN model of the test room; an approximation after Maa of the surface impedance of the control source (using a limited modal summation in conjunction with a 'direct field' term) was used together with a modal simulation of the pressure at the same point due to a primary source, located elsewhere. Examples of the FORTRAN routines are included in Appendix E.

Examples of the results of these simulations are given in Figures 8.5 to 8.8. The primary and control sources were located at positions (3.95,1,1) and (0.1,1,1) respectively. Figure 8.5 clearly indicates the modelled change in modal quality factor resulting from the action of a number of values of I_R. The graph is in terms of the variation of the magnitude of the specific radiation impedance at the primary source, and shows that the calculated optimal target impedance corresponds to a maximum reduction in the quality factor of the mode.

Interestingly, as damping is added the apparent resonant frequency of the mode *increases*, rather than decreasing which might be expected from the usual action of the addition of damping to a resonant system. If the control coefficient is larger than the optimal value the apparent resonant frequency increases by up to 0.3Hz, and the Q-factor approaches that expected for the uncontrolled case. Q-factor reductions of around one-half are predicted.

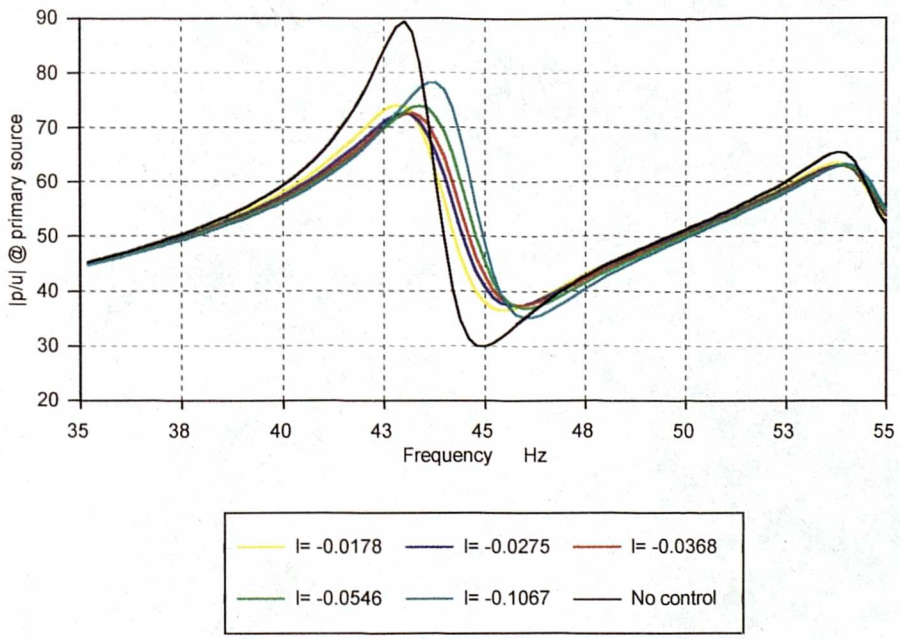

Figure 8.5 - Simulated primary source specific radiation impedance as a function of frequency and control parameter 'I'

It is worth noting that the first 'height' resonance at 54Hz experiences a much smaller degree of control, due partly to the initial lower Q-factor and partly to the lower coupling of the controller with the respective mode shape.

These results are closely mirrored in practice; Figure 8.6 shows a measured result using the same source locations, in terms of the pressure at the room location (3.95, 0.1, 0.1). The quality factor of [1,0,0] is reduced from an uncontrolled value of 80.5 to an optimally controlled value of 43.75. This reduction in quality factor may also be expressed as a reduction in the variability of sound pressure with respect to both frequency and space.

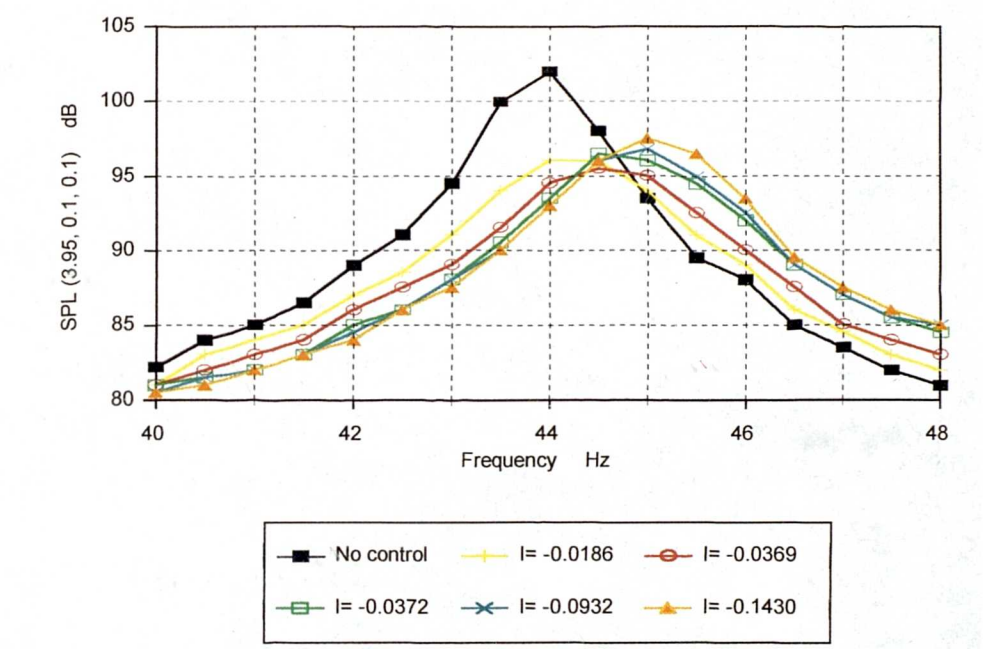

Figure 8.6 - Measured control data for fundamental x-mode

Darlington and Avis [92] have calculated such metrics, firstly in terms of the frequency domain irregularity for a complex function of frequency $G(\omega)$:

$$J_{frequency} = \sigma^2(20\log(|G(\omega)|)) \;|_{\omega_{min}<\omega<\omega_{max}} \qquad \textbf{8.17}$$

This metric is shown (Figure 8.7) against the control variable I_R, for the first axial mode of the test room using the usual source locations. A 20Hz averaging-bandwidth was employed.

The frequency domain variability of the soundfield is a minimum very close to the calculated optimum value of the control variable $I_{R,opt}$. It would be expected that this smoothing in frequency would correspond to a reduction in the spatial variability of the soundfield at

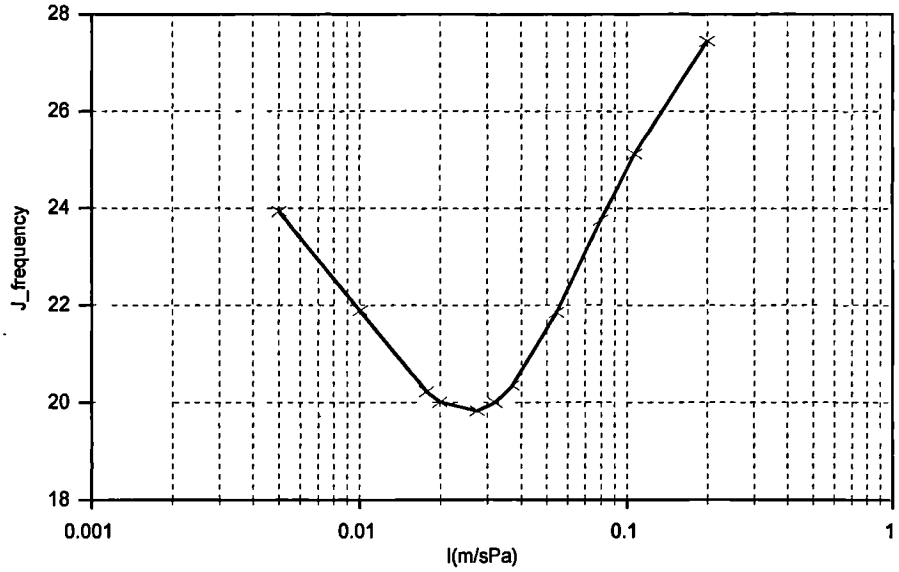

Figure 8.7 - Modelled variance with frequency of SPL at location (1,1,1.5) against control variable 'I'

resonance also. Corresponding figures for the spatial variability of the soundfield were obtained using the FORTRAN model with a spatial variance metric defined by:

$$J_{space} = \sigma^2 [20\log\left(\frac{\left|\frac{p_x}{U_0}\right|}{p_{ref}}\right)] \qquad \textbf{8.18}$$

Figure 8.8 shows the function J_{space} evaluated on the horizontal plane including primary and control sources. Local irregularities in the sound field around the control sources were neglected by limiting the spatial area over which the evaluation was made. The frequency of the first axial mode was chosen, and it can be seen that the field is flattest with respect to space when the controller is adjusted to implement $I_{,R,opt}$.

Measured pressure distributions over the controlled volume show a very similar pattern. Figures 8.9 and 8.10 detail the changes in the spatial soundfield measured over the same horizontal plane as that modelled for Figure 8.8. The pressures shown are for the uncontrolled and optimal real control cases. It can be seen that control results in a reduction of pressure at the room boundaries corresponding to the lower quality factor of the mode, and the spatial distribution of pressure is also more smooth. If, as a first approximation, it is assumed that a spatial decomposition into cosine eigenvectors is still valid (even though the boundary impedance of the space can no longer be assumed to be close to infinite), then

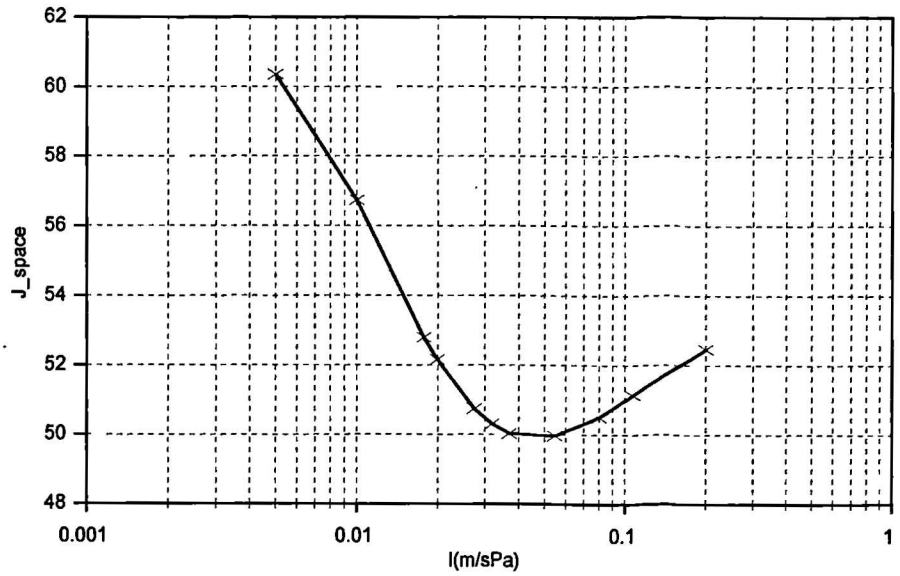

Figure 8.8 - Modelled variance with space of SPL against control variable 'I'

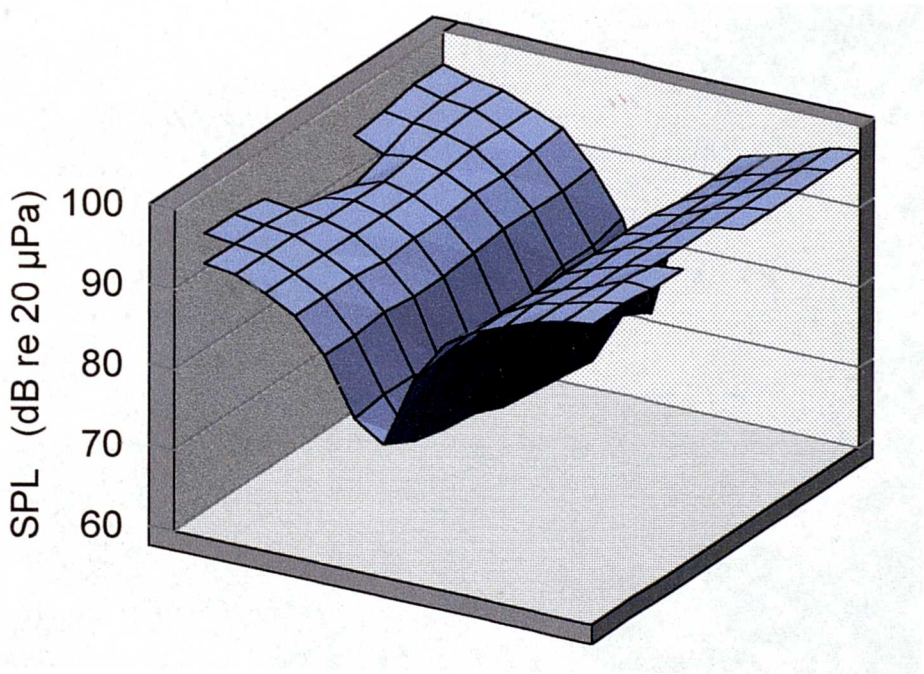

Figure 8.9 - Uncontrolled pressure contour over y=1m plane, f=44.5Hz

the results can be interpreted as a reduction in the scaling of the cosine modeshape, leading to lower spatial pressure variability.

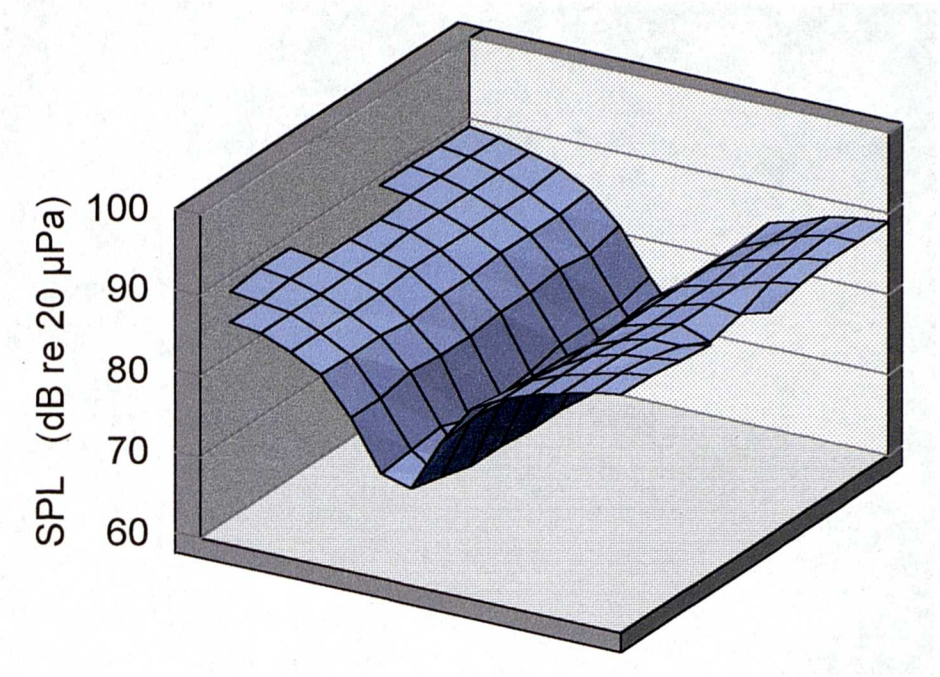

Figure 8.10 - Pressure contour with optimal real control over y=1m plane, f=44.5Hz

Quality factor reductions are directly related to changes in modal decay time, since

$$Q = \frac{\omega_n}{2\delta_n} \qquad \textbf{8.19}$$

Using a 60dB decay definition (usually employed for diffuse reverberation time)

$$p^2(t) = p^2(0)e^{-\delta_n t}$$

and so

$$T_{60} = \frac{13.8}{\delta_n} \qquad \textbf{8.20}$$

Figure 8.11 shows quality factor modifications by various real controllers, reported as changes in modal decay time. A single 8 inch loudspeaker is seen to be capable of almost halving the decay time of the 44 Hz (first axial length) mode.

The changes in modal decay time shown above are calculations based on measurements of the modal quality factor. A direct measurement of a decay time is possible at low frequencies where modes are widely spaced, by a simple sinusoidal excitation of a resonance which is subsequently switched off, and the decay captured [94]. Although the turn-off

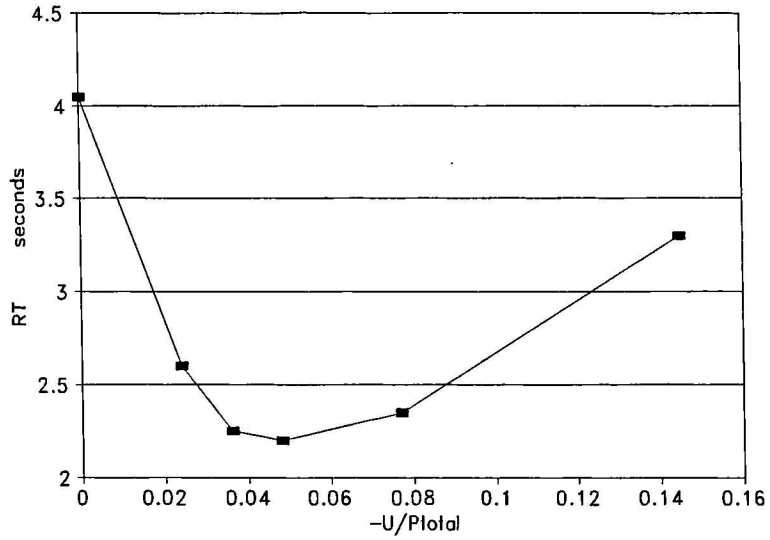

Figure 8.11 - -60dB decay time of first axial (44 Hz) mode

transient is a step function which has frequency content which may excite all modes in the space, the amount of energy in the primarily excited mode is comparatively large and so a clear decay of this one mode can usually be visualised. Figure 8.12 illustrates the decay of a 44Hz test tone at location (1,1,1.5). Primary and secondary sources were located at (3.95,1,1) and (0.1,1,1) respectively. It is seen that the modelled and measured changes in modal quality factor (Figures 8.5 and 8.6) are also in evidence in the time domain. The secondary source controlled to exhibit surface impedance $I_{R,opt}$ reduces the modal decay time

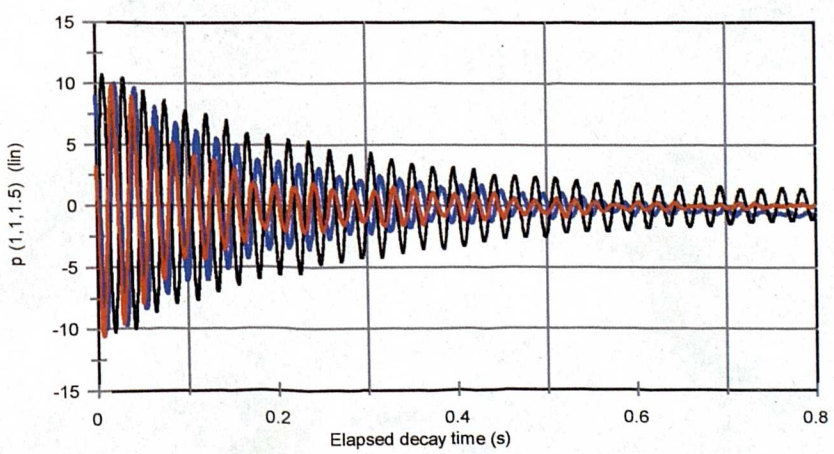

Figure 8.12 - Decay of [1,0,0] mode with real impedance control
a) Uncontrolled *b) Single peerless driver, $I_{R,opt}$*
c) 4 driver cabinet

noticeably. The decay time is further reduced by the adoption of a four-driver loudspeaker array. Target impedance $I_{R,opt}$ is modified by a suitable factor proportional to the increase in area of the composite source (since **(8.16)** contains source diameter a); a further reduction in steady-state Q-factor is also observed. The relationship between the performance of real impedance controllers and their radiating area forms one part of a forthcoming Masters thesis [95].

Using the same source locations, the modification in decay time of mode [0,1,0] was investigated. A small reduction was achieved for a truncated 54.5 Hz test tone (Figure 8.13), corresponding to the small reduction in steady-state Q-factor anticipated in Figure 8.5. The calculation of $I_{R,opt}$ takes no account of the location of the two sources, but intuitively it seems reasonable to imagine that the performance of the controller may be enhanced by a secondary source location which couples maximally into the modeshape over which control is desired. The secondary source was therefore moved into the centre of the test room floor, and the decay of the test tone measured with and without control.

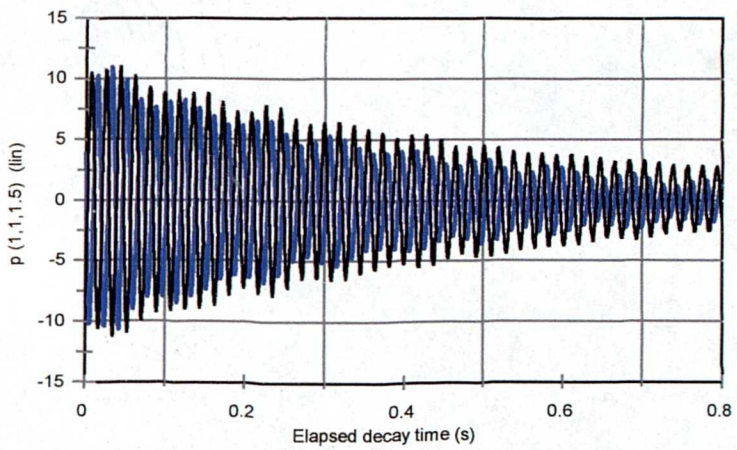

Figure 8.13 - Decay of [0,1,0] mode with real impedance control
a) Uncontrolled b) Single peerless driver, $I_{R,opt}$

No modification was made to the target impedance - results are shown in Figure 8.14. Given the result for mode [1,0,0] it is not surprising that when the area of the control source is increased (with appropriate target impedance modification) the decay performance of the controller is improved. The decaying test tone is amplitude-modulated by a residue of mode [1,0,0] excited by the turn-off transient - this is clearly seen with the latter secondary source location of Figure 8.14 which does not couple strongly into the modeshape of [1,0,0].

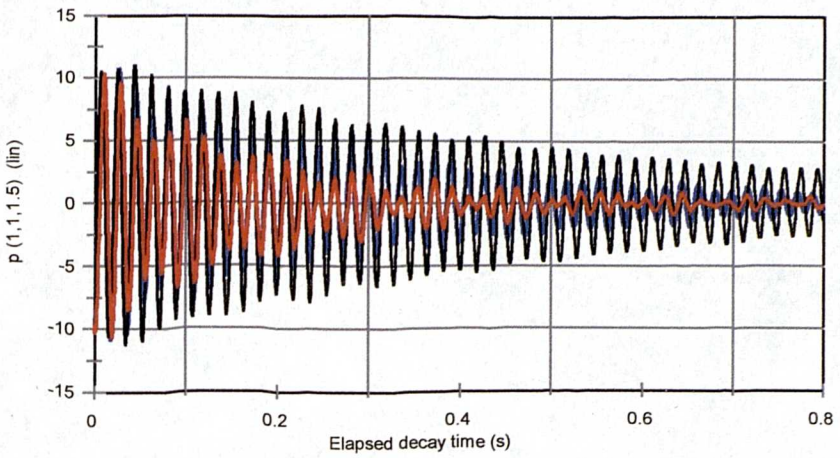

Figure 8.14 - Decay of [0,1,0] mode with real impedance control
a) Uncontrolled *b) Single peerless driver, $I_{R,opt}$ in floor centre*
c) 4 driver cabinet, $I_{R,opt}$ in floor centre

In addition to adding the damping required to reduce the reverberation time of a mode, it has been shown that a real impedance controller causes a significant reduction of the acoustic potential associated with room modes. Although this effect occurs when the absorber is adjusted to absorb maximum power within the constraint of a real control law, greater reductions in averaged pressure levels across a space can be achieved when a single controller is configured to implement other more explicitly reactive impedances. The investigation of these impedances forms the basis of the following section.

8.5 Impedance control techniques 2 - Complex controlled impedances in a room

Darlington [44] and Avis [53] do not restrict the design of an absorber to a real control law, but include the case where a complex solution may be selected. The acoustics of Figure 8.3 are applied where the cone velocity is designed to maximise power flow into the absorber, defining the true negative extremum of **(8.12)**. The controller impedance is then no longer limited to real values and may become reactive. The room model is still limited to incident and reflected plane waves, and is not a full modal expression of the soundfield. Incident pressure and cone velocity are related by the generalised complex transfer function H:

$$U = H.P_{incident} \qquad \textbf{8.21}$$

and the acoustic power at the absorber, from **(8.12)**, reduces to:

$$W_{absorber} = \frac{\pi a^2}{2} |P_{incident}|^2 [\, 2\, \Re e(H) + \rho_0 c\, \cos^2(\theta_a)\, |H|^2] \qquad \textbf{8.22}$$

Darlington [44] states that "*...Limiting the control law H to be a real scalar does not limit the power which can be absorbed at a single frequency...*", from which it follows that

$$W_{absorber} = \frac{\pi a^2}{2} |P_{incident}|^2 [2.H + \rho_0 c\, \cos^2(\theta_a)\, H^2\,] \qquad \textbf{8.23}$$

Differentiating the contents of the square brackets w.r.t H, the scalar controller (**8.24**) resulting in maximum acoustic power absorption, and that power itself (**8.25**), are obtained:

$$H_{opt} = \frac{-1}{\rho_0 c.\cos^2(\theta_a)} \qquad \textbf{8.24}$$

$$W_{opt} = H_{opt} \frac{\pi a^2}{2} |P_{incident}|^2 \qquad \textbf{8.25}$$

This specification of a maximum power absorber relies on the transduction of incident pressure alone. In the more general case when total pressure is detected, an expression for the optimum relationship between total pressure and cone velocity, I_{opt} is required. For optimum absorption, P_r is cancelled by the real part of the radiated hemispherical field, leaving only P_i and the imaginary part of the radiated field. Therefore after (**8.10**)

$$P_t = (P_i + j\rho c\, U.\cos\theta_a \sin\theta_a).e^{j\omega t} \qquad \textbf{8.26}$$

Substituting for velocity

$$P_t = (P_i + j\rho c P_i H_{opt}.\cos\theta_a \sin\theta_a).e^{j\omega t} \qquad \textbf{8.27}$$

and so

$$\frac{P_t}{P_i} = 1 + jH_{opt}\rho c.\cos\theta_a \sin\theta_a \qquad \textbf{8.28}$$

Therefore

$$\frac{u}{p_t}|_{opt} = I_{opt} = \frac{1}{\frac{1}{H_{opt}} + j\rho c.\cos\theta_a \sin\theta_a} \qquad \textbf{8.29}$$

H_{opt} is known from (**8.24**), and it follows that

$$I_{opt} = H_{opt}\left[\frac{1 + j\tan\theta_a}{1 + \tan^2\theta_a}\right]$$
$$= \frac{H_{opt}}{\sqrt{(1 + \tan^2\theta_a)}}.e^{j\theta_a} \qquad \textbf{8.30}$$

8.5.1 Maximum absorption controllers and the free-field radiation load

It is instructive to compare the implementation of (**8.30**) with a solution designed to absorb maximum power from a *modal* radiation load. The surface impedance required of a controller in order to implement a true maximum power absorber is defined by Mazzola [42] as the negative conjugate of the radiation load 'seen' by that source when driving the acoustics of the space in which it is placed. In an enclosed acoustic system, this radiation load is by definition modal. Preliminary investigations with this solution in a duct and within a room have shown that the power absorbed is indeed maximised [53].

The mechanism involves the maximisation of the total pressure at the controller (and hence cone velocity, since the two are related via I), which is seen in (**8.11**) to result in a maximisation of the absorbed power. However, because the pressure at the controller is maximised, the solution has the effect of actually reinforcing the modal behaviour of the space, rather than giving the desired reduction in modal quality factor. As an example, Figure 8.15 shows the uncontrolled acoustic potential in a rigidly terminated waveguide, and with an impedance controller configured for maximum absorption.

With no control, resonances at $k_nL = n\pi$ are clearly seen. When the maximum power absorber is implemented the original modes are still present but new modes are created, such that there are now modes when $k_nL = n\pi/2$. The active absorber has added resonances at the set of "quarterwave" frequencies by implementing an extremely low acoustic impedance at these frequencies (making the pipe look "open" at $x=L$) whilst maintaining high impedance at the original halfwave frequencies. This maintains the pressure at the controller at a maximum, ensuring maximum power absorption. The findings of Nelson and Elliot [36] are supported, and a controller designed to absorb maximum power from a modal radiation load is unsuitable for reducing the modal artefacts of an enclosed system.

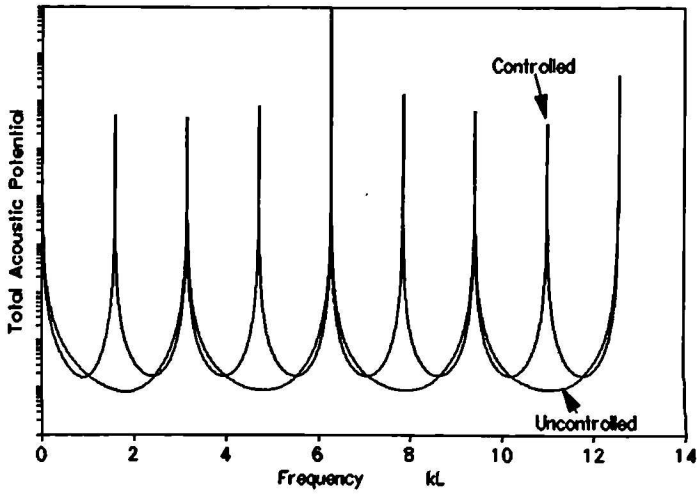

Figure 8.15 - Total Acoustic Potential (arbitrary reference) in a waveguide with active controller configured for maximum absorption.

In contrast, I_{opt} **(8.30)** has been arrived at using a maximum power argument, but rather than considering a modal radiation load the simplified acoustics of Figure 8.3 have been employed. Figure 8.16 shows the magnitude and phase of I_{opt} compared to the calculated $-Z_{RAD}^{*}$ (true maximum power) solution for the usual controller location in the test room. I_{opt} is identical to the negative conjugate of the *free-field* radiation load experienced by the control source. The impedance solution given by **(8.30)** is therefore equal in magnitude and phase to the familiar piston impedance functions [10], and only differs in that the sign of the

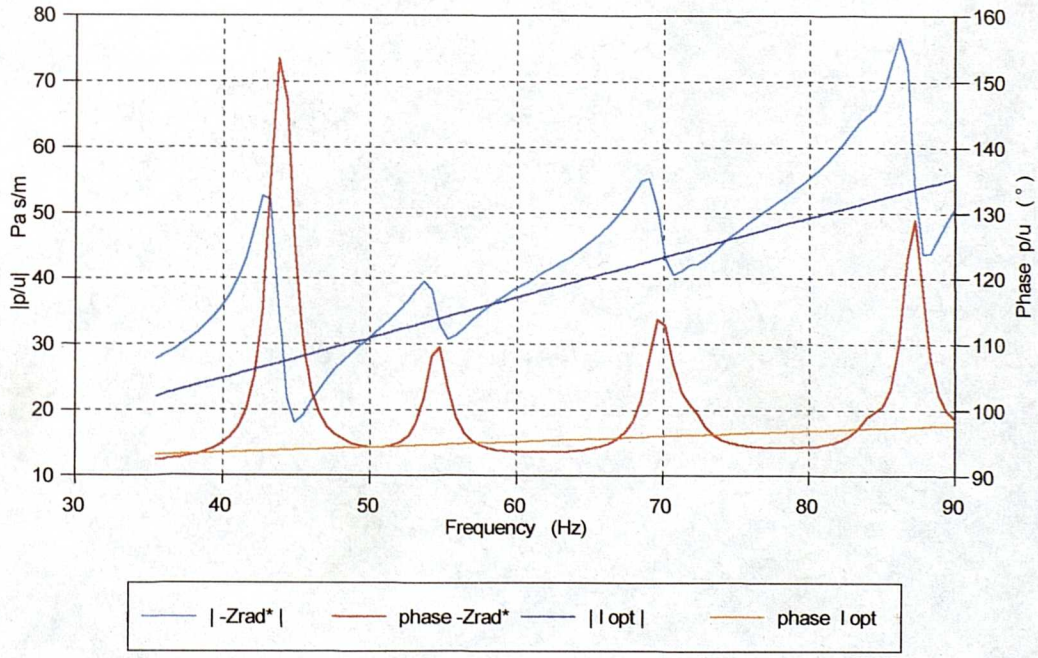

Figure 8.16 - Modelled maximum power absorption impedance solutions from modal and free-field radiation loads

real part is inverted. I_{opt} can be said to implement that impedance which would absorb maximum power from an acoustic environment containing no modes whatsoever - which in the limit is the environment which the control system attempts to produce in the room.

It may at first appear strange that this impedance could be useful in reducing the influence of modal artefacts within a three dimensional space. However, if the optimal *characteristic* termination applied to the one-dimensional duct is interpreted in this way, it is seen to represent the negative (conjugate) of the radiation load which would be experienced in an infinitely long waveguide. This represents a one-dimensional "free-field" - the characteristic termination implements an impedance equal to the negative (conjugate) of the free field radiation impedance which is experienced by the source at the end of an infinitely long duct.

In a three dimensional application it is feasible to configure a small impedance-controlled source to implement the *negative conjugate of the radiation load it would experience in free field.* In practice the controller is mounted against a wall, such that the radiation load considered is that experienced when driving a half-space. Such a configuration has been reported [44,53,54,50] and tested in the laboratory.

8.5.2 Modelled and practical results with a complex impedance controller

The implementation of I_{opt} is considered in Figure 8.17, which displays the modelled action of an impedance-controlled source in the test room. The usual primary and control source locations have been chosen, and the impedance at the controller set to a number of target values equal to the complex solution of **(8.30)** at six particular frequencies. The resulting pressure magnitude at a test location (1,1,1.5) is shown.

The pressure is minimised for each solution of **(8.30)** at a frequency very close to the respective value used in the calculation of I_{opt} in each case. Because I_{opt} changes rapidly with frequency in both magnitude and phase (Figure 8.16) compared to the real values of $I_{R,opt}$ (Figure8.4), it appears that it will be necessary to drive the controller towards the desired surface impedance across a range of frequencies, rather than assuming an average fixed value as in the case of the real solution. This is as expected, since it is only a purely real solution which can be specified by a filter which has no frequency dependance.

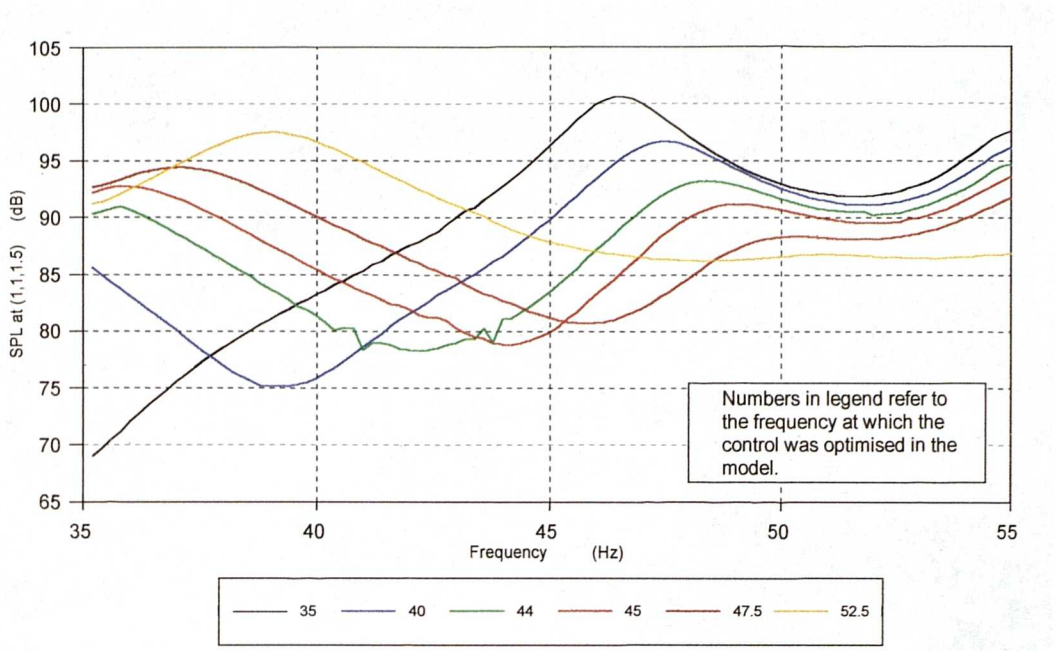

Figure 8.17 - Controlled pressure with action of complex impedance controller

The uncontrolled modal response has peaks at 44.5 Hz (fundamental axial x-mode) and 54.5Hz (fundamental axial y-mode) in this bandwidth. These are shown in Figure 8.18 together with the modelled pressure at the test point when a controller is used which matches I_{opt} across the entire bandwidth. The usual primary source location was employed, and two alternative control source locations are indicated.

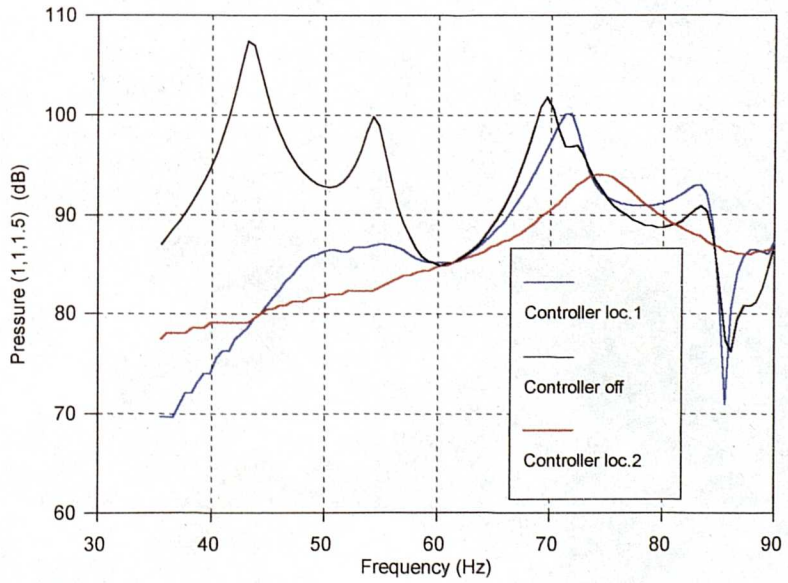

Figure 8.18 - Optimal control in test room. Location 1 - (0.1,1,1)
Location 2 - (1.98,1.58,0.1)

It can be seen that good performance is anticipated with the controller at location 1 on the fundamental axial x [1,0,0] and y [0,1,0] modes (44.5 and 54.5 Hz), but around 69 and 71 Hz two almost degenerate resonances ([1,1,0] and [0,0,1]) conspire to produce a poor result, and the controller actually increases the modelled pressure. Moving the controller to a new location can ameliorate this effect, but as the mode order increases extreme care is required in choosing the appropriate combination of primary and secondary source location - a common constraint on effective active control in an enclosed volume [eg 18,21,22]. The spatial corollary to the pressure reductions shown above is displayed in Figure 8.19 for excitation at 44 Hz - the peak frequency of x-mode [1,0,0].

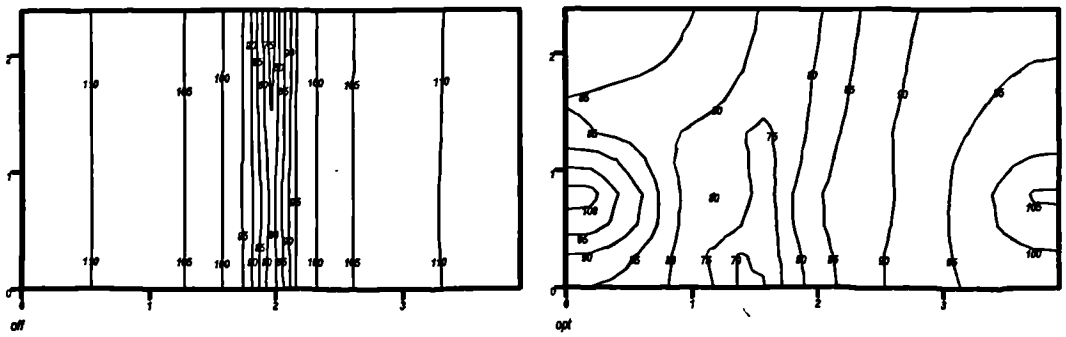

Figure8.19 - Modelled pressure distribution at 44 Hz in test room
a) Uncontrolled
b) with optimal complex control

Both plots incorporate constant (5 dB) pressure increments as a contour interval. The room is excited by a constant velocity source near the centre of the left-hand wall. In the room section on the left, the primary source alone is operating; the clear halfwave resonance is seen. In the right hand section the control source, near the centre of the opposite wall, is driven such that its surface impedance is the negative conjugate of the radiation load the source would experience firing into half space; the analogy of the one-dimensional "characteristic termination". The pressure field shows a much smoother spatial dependence. This smoothing would normally be interpreted as a reduction in the quality factor of the resonance, as was suggested for the real control impedance solution.

Measured results support the models of Figures 8.17 to 8.19. Control and primary source locations at (1.0,1.0,1.5) and (3.85,1.0,1.5) were chosen in the test room of dimensions (3.95m*3.15m*2.38m). The control solution I_{opt} **(8.30)** was implemented using the absorber

system of Figure 4.1. The frequency dependence illustrated in Figure 8.16 was approximated by a first-order FIR model for F_d which was set to control mode [1,0,0] optimally, but whose response became increasingly arbitrary at higher frequencies. The adaptive control filter was set up in a feedforward configuration, and allowed to converge using a band-limited pink noise stimulus. Following convergence, adaptation was halted and the pressure at different field locations was recorded.

In Figure 8.20, the pressure at a test location (1,1,1.5) is shown uncontrolled, and controlled where the stimulus is band-limited to 0-100Hz, and 25-100Hz. Superior performance results from the exclusion of very low frequencies, since the adaptive filter (FIR length 256 taps, f_s=*3kHz*) does not misplace zeros in an attempt to minimise l.f. errors at sub-sonic frequencies and can more closely achieve the desired response in the modal bandwidth.

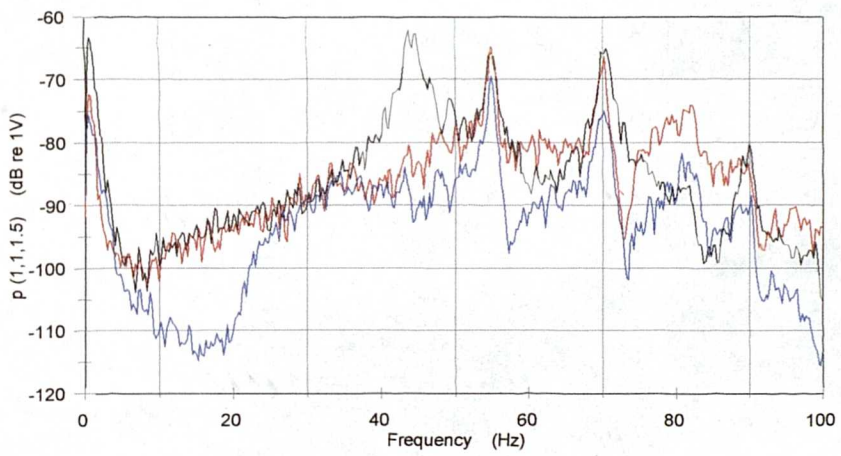

Figure8.20 - Measured pressure response at (1.0,1.0,1,5)
a) Uncontrolled b) I_{opt}, 0-100Hz
c) I_{opt}, 25-100Hz

Similar performance differences are noted at a second location (3.15,0.75,2.25) (Figure 8.21). In addition to the suppression of mode [1,0,0], the rapid transition in frequency at around 55Hz between [0,1,0] and [0,0,1] / [1,1,0] is smoothed due to the increased damping presented to all resonances. The latter combination of two degenerate modes is most resistant to control, supporting other findings that control is most effective when modal density is low [21].

The pattern is repeated in Figures 8.22 and 8.23, for measurement locations (1.0,2.2,1.5) and (2.95,1.0,1.5) respectively. At the latter location, mode [0,1,0] proves especially

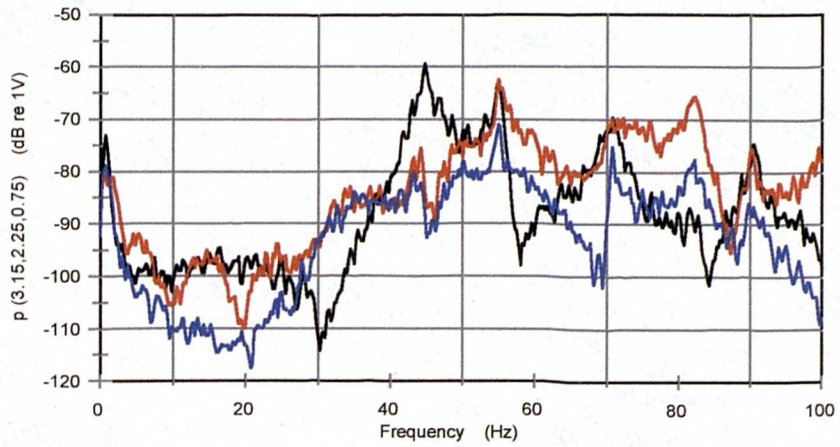

Figure8.21 - Measured pressure response at (3.15,2.25,0.75)
a) Uncontrolled *b) I_{opt}, 0-100Hz*
c) I_{opt}, 25-100Hz

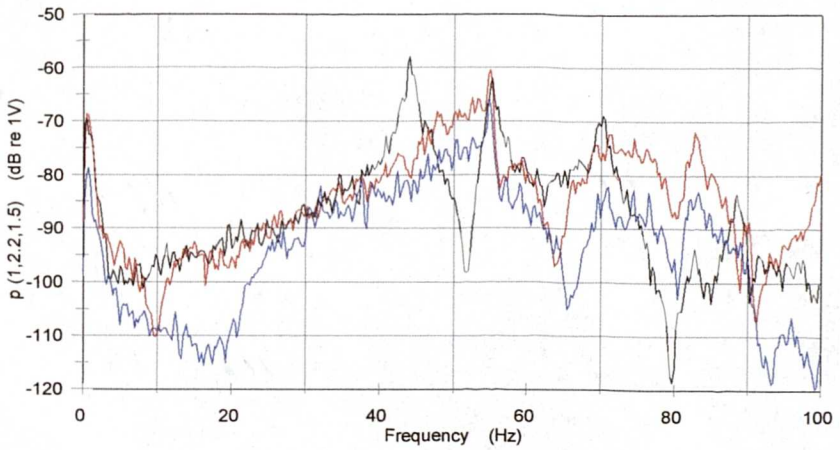

Figure8.22 - Measured pressure response at (1.0,2.2,1.5)
a) Uncontrolled *b) I_{opt}, 0-100Hz*
c) I_{opt}, 25-100Hz

resistant to control, and the rapid transitions in pressure magnitude with respect to frequency may be expected to incorporate inherently long decay response characteristics. Since Olive and Schuck [3] identify decay performance as of primary subjective significance, this gives some cause for concern.

Both the modelled pressure distribution in Figure 8.19 and the measured results in Figures 8.20-8.23 are derived for one particular combination of source and controller location. The fact that great care must be taken with these locations, especially for modes of higher order, points towards the possibility that rather than adding damping to the room (which might be

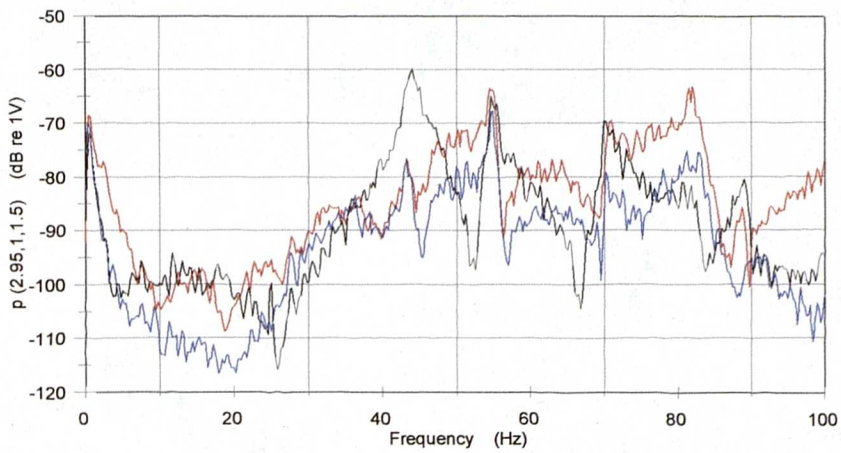

Figure8.23 - Measured pressure response at (2.95,1.0,1.5)
a) Uncontrolled *b) I_{opt}, 0-100Hz*
c) I_{opt}, 25-100Hz

expected to produce soundfield modifications which are less strongly related to source location), the complex impedance solution may be implementing something more analogous to pressure cancellation. If this were the case, useful steady-state pressure reductions would not necessarily translate into reductions in modal decay time.

This idea is investigated by looking at the decay performance of control, since genuine reductions in Q-factor implying an increase in modal damping *will* be accompanied by corresponding reductions in modal decay time. The energy-time-frequency approach introduced in the context of the one-dimensional waveguide (section 4.4.2) [54] is used to analyse the complex impedance control solution in the room. Simulations and measurements of the time/frequency response of rooms subjected to broadband excitation are presented.

8.5.3 Energy-Time-Frequency response of a room with optimal impedance control

Time / frequency responses have been measured using a sub-optimal implementation of the active acoustic absorber. The experimental hardware was able to achieve the optimal surface impedance at only one frequency. The optimal impedance is frequency dependant, and the hardware implements an impedance specified by a first order digital filter for F_d; the first order filter could represent the target function at any one frequency.

A raw measure of the time / frequency response of the uncontrolled room is shown as Figure 8.24, and as expected clear modal decay 'tails' are evident.

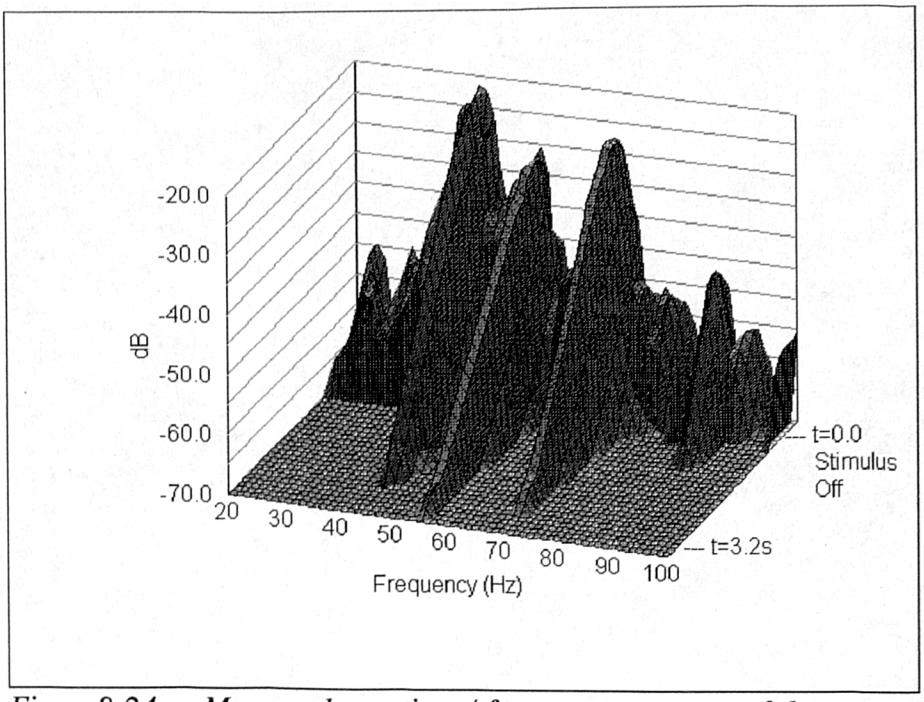

Figure8.24 - Measured raw time / frequency response of the test room

The time / frequency response of the sub-optimally controlled room is shown in Figure 8.25. This controller has been optimised for the 44.5 Hz mode, and can be seen to reduce the steady state level in the room compared to the uncontrolled case. The length of the modal decay associated with the 44.5 Hz resonance is reduced, suggesting that the Q-factor of that

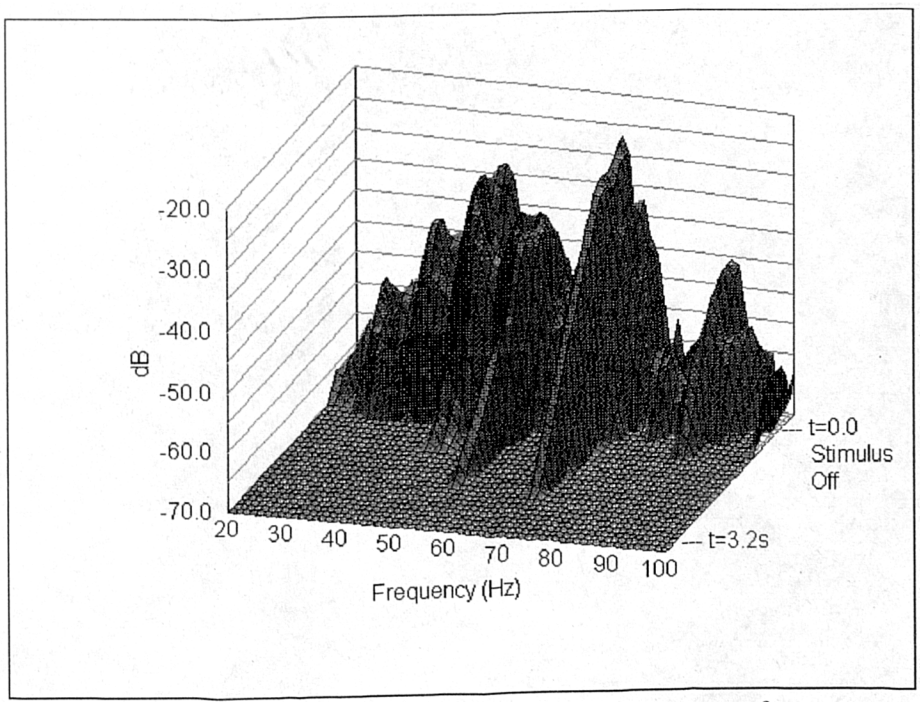

Figure8.25 - Measured raw time / frequency response of a room controlled by a single sub-optimal active acoustic absorber

mode has indeed been controlled. The second mode (at 54.5 Hz) also decays faster, despite the errors in the surface impedance implemented at that frequency. The third mode (70 Hz) is not significantly influenced by the controller. This is due to a combination of factors - the error in the impedance specification due to the hardware limitation is more significant than in the case of the two modes with lower frequency, and the control source is poorly coupled into what are actually two degenerate modes very close to one another in frequency.

The control of degenerate modes by a single secondary source is the subject of further comment by Bullmore *et al.* [21] in the context of the minimisation of acoustic potential energy. If the secondary source is located at a point such that the residues of each mode in the primary soundfield are out of phase, then it is suggested that control cannot occur. As the controller tries to suppress the residue of one mode, it actively reinforces the residue of the other, and so although the spatial characteristic of pressure may change no global reductions are possible. The two modes in question in Figure 8.25 are [0,0,1] and [1,1,0], and for the source locations chosen the phase of both primary modal residues is actually consistent at the secondary source. However, the secondary source lies close to a nodal line for mode [0,0,1] but not for [1,1,0], and the large source strengths required to influence the former must inevitably disturb the latter in non-optimal fashion. Although Bullmore makes these comments for a controller designed as a pressure canceller, they are still of relevance in a consideration of active acoustic absorption.

The decay characteristics evident in Figure 8.25 are perhaps more clearly illustrated using a simple level-vs-time presentation. The two figures overleaf represent the decay of the resonant phenomena *a) [1,0,0]*, *b) [0,1,0]* and *c) [1,1,0] plus [0,0,1]*. Whilst the initial part of the decay is very rapid suggesting a very significant reduction in modal quality factor, after about 0.5 seconds the decay "rebounds". A new, slower rate is seen which is similar to the uncontrolled rate of decay.

Investigation of the structure of the adaptive control filter reveals the reason for the change in decay rate. The measurements presented in this section were all made using band-limited noise, and the filter was allowed to adapt during a steady-state training phase. Following successful convergence of the filter response (minimisation of mean-square error) the adaption was turned off. When attempting to implement the complex solution I_{opt} the

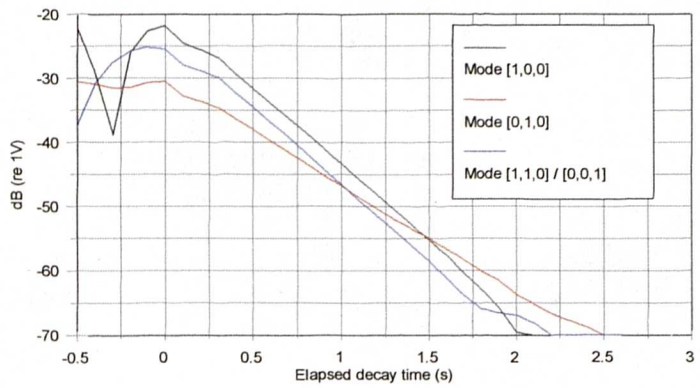

Figure8.26 - Measured modal decay of test room - uncontrolled

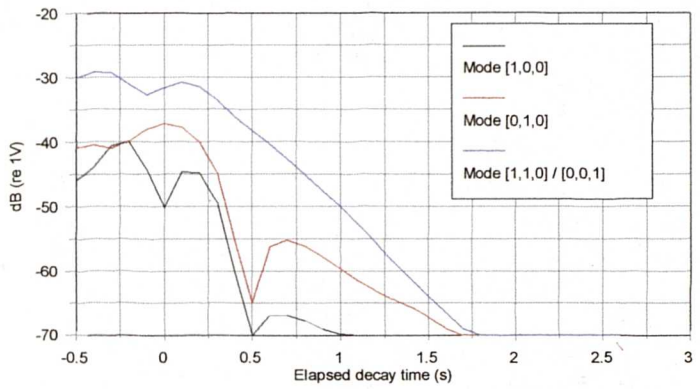

Figure8.27 - Measured modal decay of test room - controlled using single sub-optimal absorber

controller was not stable in a feedback configuration. This is due to the fact that in order to implement the correct impedance on- resonance, the first-order FIR filter used to specify desired impedance F_d gave a feedback loop gain contravening the Nyquist stability criterion, resulting in instability at some other frequency. Accordingly, a feedforward approach was chosen. The adaptive filter was 253 taps long, and even with a sample frequency as low as 512 Hz the controller was effectively turned off after 0.5 seconds.

In order to build a filter with a longer impulse response to control the decay phase of room modes, a longer adaptive filter might be used. A more efficient approach would employ a more sophisticated filter structure (FIR or IIR) to specify F_d, which could be expected to rectify the stability problem and allow feedback operation, without incurring the increased expense of a long adaptive filter. The design of such a filter structure for F_d is suggested as an avenue of further work in section 10.4.3.

8.7 Conclusions on real and complex impedance controllers in a room

Real impedance controllers can be configured to produce small steady state reductions in the soundfield, corresponding to four or five dB level changes at modal antinodes. If an appropriate target impedance is chosen, the pressure reduction corresponds to a genuine modification of modal quality factor. The hardware implementation of a real controller used in this project is stable in a feedback configuration, with the result that useful and predictable changes in modal decay times corresponding to measured changes in quality factor may be achieved. The placement of the control source relative to the modeshape over which control is desired has a significant effect, and controllers located at modal pressure nodes will not be able to control the particular mode in question.

Complex controllers can be configured to produce large changes in the steady state soundfield - frequently greater than 20dB at modal antinodes. The performance of the complex controller is such that it is difficult to argue that the large pressure reductions result from genuine reductions in modal quality factor, and it is possible that an element of cancellation is responsible rather than simply an addition of damping. The hardware implementation of the complex controller used in this project is not stable in a feedback configuration, with the result that modifications to modal decay phases result in a somewhat unpredictable decay performance. The placement of the control source relative to the primary source has a potentially large effect, and controllers located at modal pressure nodes will not be able to control the particular mode in question.

Both control strategies are most effective for axial modes which are widely separated in frequency from each other. Effectiveness is increased when the control source is coupled as strongly as possible into the resonant modeshape over which control is required. Modes which are closely spaced in frequency or degenerate present a problem to the controller, and neither steady-state nor decay performance modifications are particularly significant. This finding echoes that of Nelson and Elliot [12] from a pressure minimisation context, where it is suggested that *"very little global reduction can be produced in enclosure energy...if the modal bandwidth approaches the frequency spacing between the modes."*

Chapter 9

Feedforward IIR control techniques in a three dimensional environment

9.0 Introduction

The Feedforward IIR (or 'biquad fit') control techniques introduced in Chapter 5 and investigated in a duct in Chapters 6 and 7 were found to suffer problems when applied to the problem of control of modes in a one-dimensional waveguide, since the coupling between sources in run-time meant that the transfer functions between sources and solution point could not adequately be described by off-line measurements fitted with second-order bandpass IIR filter sections. It was postulated in section 7.4 that in a three dimensional environment, these fit problems would not be so significant, with the result that the biquad fit technique could be expected to produce useful results.

This chapter is concerned with the application of Biquad fit techniques to the control of resonant behaviour in a three dimensional environment, and draws upon the mathematical framework for mode-fitting and the subsequent design of control filters laid out in Chapters 5 and 6. Practical IIR models of measured transfer impedances are demonstrated, and the effects of limited source impedance which defeated control in one dimension are considered. The comments of section 8.1 regarding a theoretical limit for control in a room using a single secondary source apply here also, and the performance of controllers is assessed at a number of locations in terms of both steady state and decay performance.

Two main control techniques are investigated - modal cancellation / replacement and the direct modification of modal Q-factor introduced in Chapter 5. This chapter forms part of the novel contribution of this Thesis, in that it reports attempts to apply a novel control technique in a new acoustic environment.

9.1 Fitting measured room transfer functions with biquad sections

It was established in Chapter 5 that an IIR model of a modal system might be arrived at based on a z-plane modal decomposition into a number of parallel filter sections, of the form given in (**5.5**). Examples of 'fits' of measured transfer impedances in the waveguide, with four parallel filter sections, are given in Figures 7.14 to 7.17. The following IIR models were constructed in the test room, dimensions (3.95 x 3.15 x 2.38)m. The primary source location was (3.8, 1.0, 1.0) and the control source location, (0.15, 1.0, 1.0). A solution point at location (1.0, 1.0, 1.5) was used in the measurement of practical transfer impedances. This placed the microphone far enough away from the control source to avoid convergence problems with the modal decomposition (requiring many, many filter sections to simulate a 'direct field' due to the source) - and the location does not lie on a nodal plane or line of any of the resonances inside the 100Hz bandwidth chosen for the investigation.

Figure 9.1 describes the magnitude fit of a primary path true (*p/u*) transfer impedance. This shows that whilst a good fit is obtained on-resonance, between the modes the accuracy of the magnitude fit suffers. This is particularly clear at frequencies below the first axial x-mode at 44Hz. The addition of the zeroth mode to the model can improve the fit considerably, but as noted in section 5.3 in order to form controllers based on the resulting IIR filters, the zeroth mode must be approximated by a biquad section of similar form to the higher modes in the decomposition to preserve the structure of the control filter. The

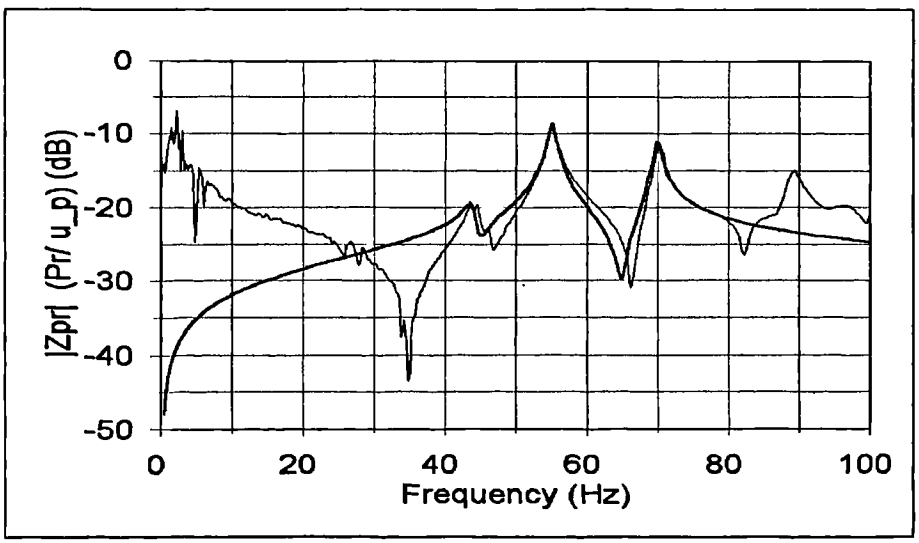

Figure 9.1 - Magnitude 3 mode fit modelled on p/u
a) measured data ***b) modal sum***

inclusion of higher frequency modes improves the off-resonance fit further still, at the expense of increased control filter complexity.

The corresponding phase data is shown as Figure 9.2. Generally good agreement is seen between measured and modelled data, and again if more higher frequency modes are included, the off-resonance fit is improved.

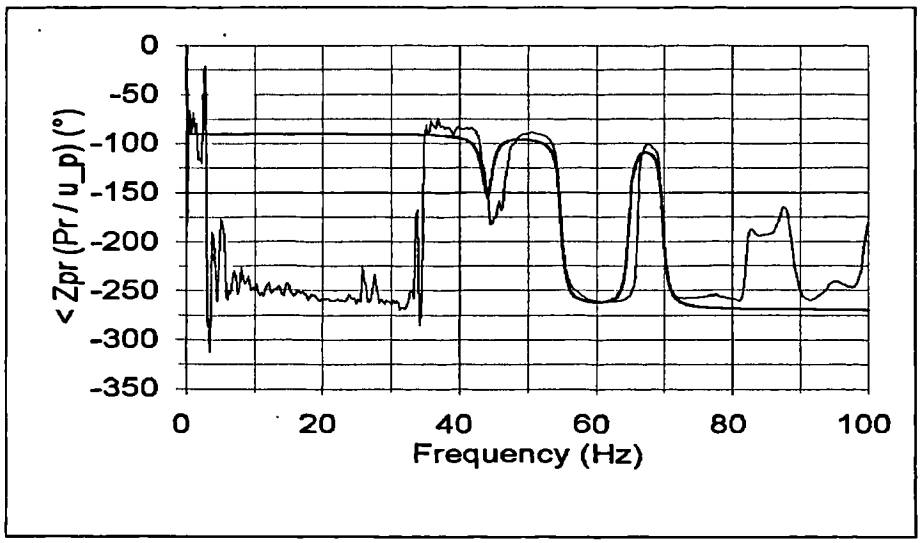

Figure 9.2 - Phase of 3 mode fit modelled on p/u
a) measured data ***b) modal sum***

It was noted in section 5.2 that rather than instrument the control source with an accelerometer and measure true transfer impedances, it is often more convenient to define the modal behaviour of the space in terms of the ratio of measured pressure to line voltage input (**5.3**). The fit in magnitude is very similar to the true transfer impedance data (Figure 9.1), and the corresponding phase plot is given in Figure 9.3.

There are similar trends in measured and modelled data, but the model is unable to track a falling phase angle with frequency. The inclusion of a 'zeroth' mode does not resolve this problem, and closer investigation reveals that the characteristic is peculiar to p/V_{in} data, and does not appear in *p/u* measurements. Because the former includes the signal voltage to cone velocity transfer function, measurements incorporate the transfer characteristic of the amplifier and the velocity response of the loudspeaker itself. In p/V_{in} measurements DC zeros from the amplifier combine with the mass-spring second order velocity characteristic of the driver to give the falling phase response, which is not catered for in the model based on (**5.5**) as this assumes a *velocity* input. The significance of this phase error depends on

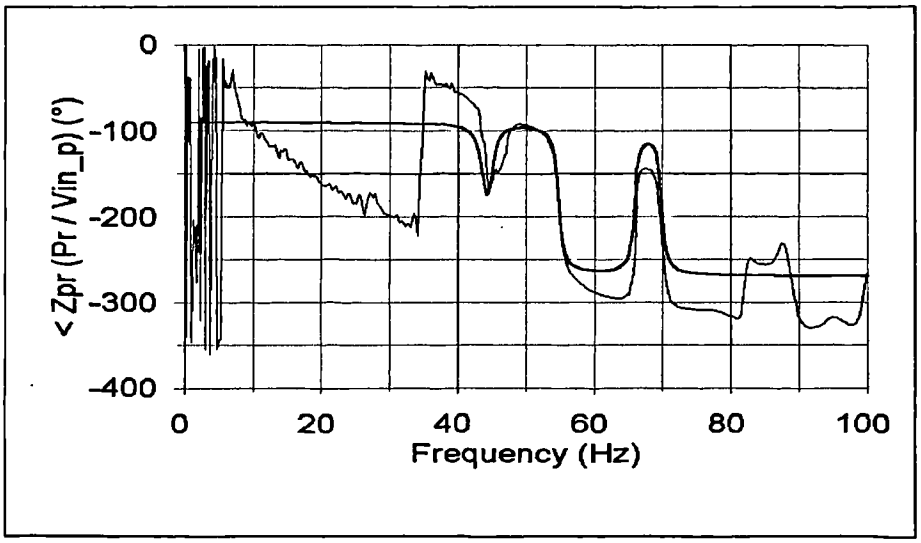

Figure 9.3 - Phase of 3 mode fit modelled on p/V_{in}
a) measured data ***b) modal sum***

the control task selected and the interaction between primary and secondary path fit errors, and is discussed further in section 9.4.4.

9.2 Biquad Fit control techniques for application in three dimensions

Having introduced a z-plane model for one-dimensional resonant systems, alternative control strategies were considered in the duct in Chapters 5 (Q-factor modification) and 7 (point cancellation). The original motivation for the development of the point canceller was for use in the following prototype feedforward control system.

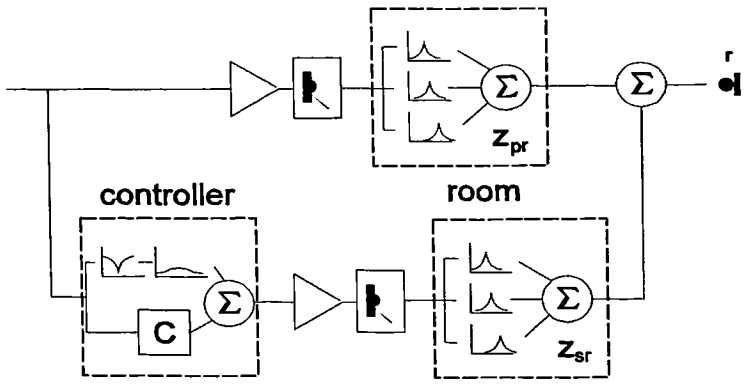

Figure 9.4 - Prototype feedforward modal control system

The primary signal is amplified and fed through a loudspeaker. The primary soundfield at *r* is set up through the modal transfer impedance Z_{pr}. Any signal reproduced via the

secondary path is subject to the same function, modified by the alternative secondary source location *s*. The controller features two parallel branches; '*C*' represents a canceller which is designed to reduce the pressure at *r* due to the primary source to zero. If required, a new mode can then be 'replaced' by first deconvolving the particular original mode from the secondary path, and then introducing a new mode of suitably reduced Q-factor.

The mathematics defining the biquad point cancellation filter are given in equations (**7.13**) to (**7.15**). The cancellation / replacement system has been measured in operation in the test room. Results for cancellation at a point only, and cancellation of one mode followed by modal replacement, are described in section 9.3.

As an alternative to cancellation or cancellation / modal replacement, a technique for the modification of modal Q-factor has been introduced in Chapter 5, with mathematics presented in equations (**5.18**) to (**5.22**). Again, the approach translates directly from a one-dimensional environment to a room.

9.2.1 Effects of limited source impedance in a three dimensional environment

It was shown in Chapter 7 that for a one-dimensional duct, Biquad fit control is defeated by the coupling which occurs between primary and control sources of limited source impedance. The reactive, non-rigid nature of the duct termination provided by the uncontrolled drivers makes fitting measured transfer impedances with biquad section responses extremely difficult. An approach has been identified which incorporates the coupling issues into the control filter by superposition, and it has been postulated that in a three dimensional environment, the coupling between sources will not be so strong, and the biquad fit technique might be expected to produce useful results.

The difference between duct and room is evident from a comparison of Figure 9.5 overleaf, with Figure 7.4. Whereas in the duct the anticipated bandpass characteristic of the voltage - velocity transfer function through the loudspeaker is entirely dwarfed by the influence of the modal radiation load on the driver, in the room the bandpass function is dominant for both primary and secondary sources. Only at frequencies very close to the normal modes of the space (44.5 Hz, 54.5 Hz, 70 Hz, 89 Hz) is the transfer function seen to deviate from the anticipated form, due to the influence of a strongly varying radiation load.

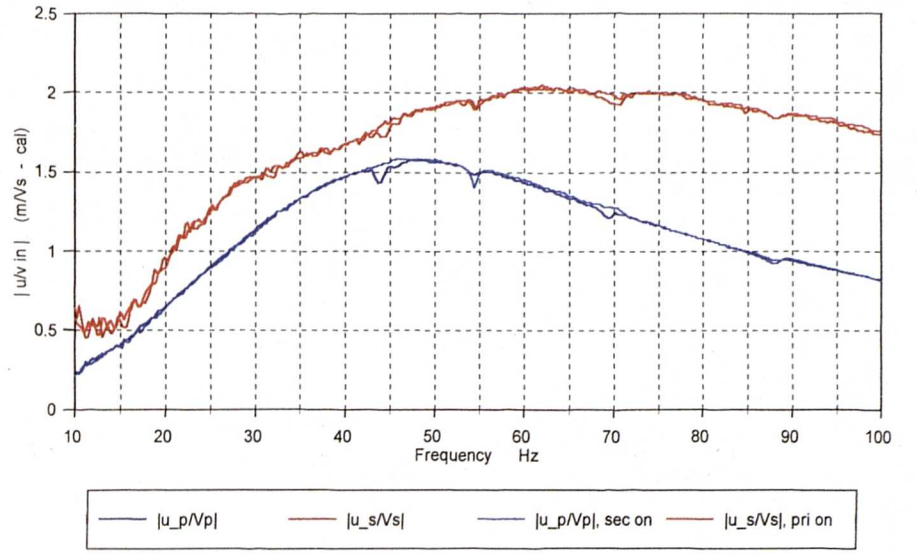

Figure 9.5 - Measured voltage-velocity transfer functions of Primary and Secondary sources in test room, with and without other source operating in canceller configuration.

The local reductions in the magnitude of u/V_{in} are smoothed out when both sources are run simultaneously in a canceller configuration. The magnitude changes in radiation load are effectively scaled-down, becoming small in comparison with the electro-mechanical source impedance of each driver which then dominates the observed transfer function. Figure 9.5 thus contains a measurement of the changing factors responsible for the difference between the magnitude of off-line system characterisation transfer impedance measurements, and the run-time transfer impedances which determine the operational behaviour of the controller. In comparison with the one-dimensional environment, these changes are small.

Figure 9.6 overleaf shows a series of measurements of p/V_{in} for primary and secondary path transfer functions in the presence and absence of the other acoustically-driven source, following the A,B,C,D matrix form of (**7.6**) and (**7.7**). As with measurements in section 7.2, the source not electrically connected had its voice-coil shorted to simulate connection to the low output impedance voltage amplifier used during run-time control experiments. Not only are the effects of the acoustically driven source marginal and confined to the resonant peaks in the measured transfer functions; their effect on the canceller solution computed directly from the measured data (after (**7.12**)) are practically indistinguishable.

Figure 9.7 demonstrates this comparison for the same set of source and solution point locations as used for the measurements in Figure 9.6. The 'uncoupled solution' is that design

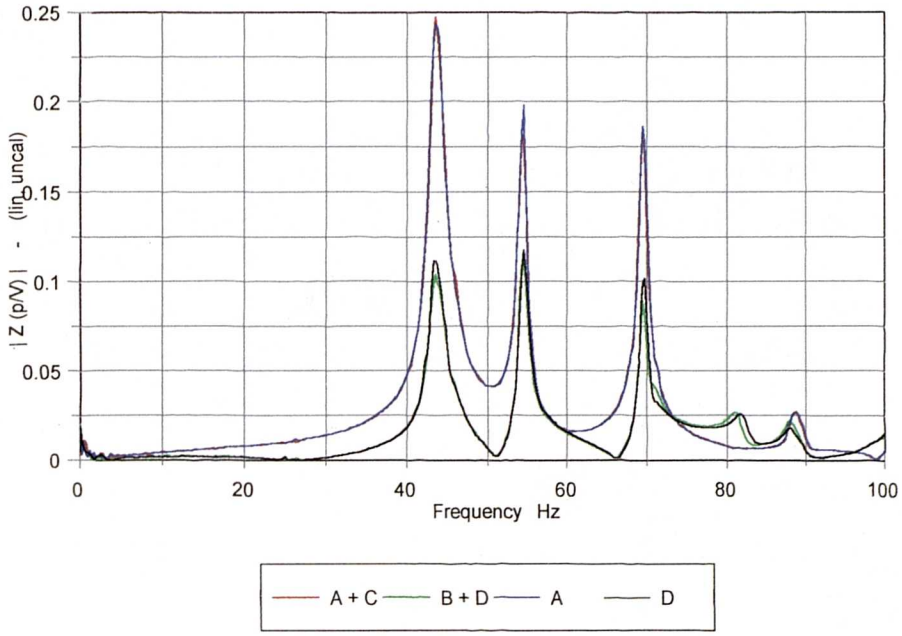

Figure 9.6 - Magnitude transfer function (p/V_{in}) measurements

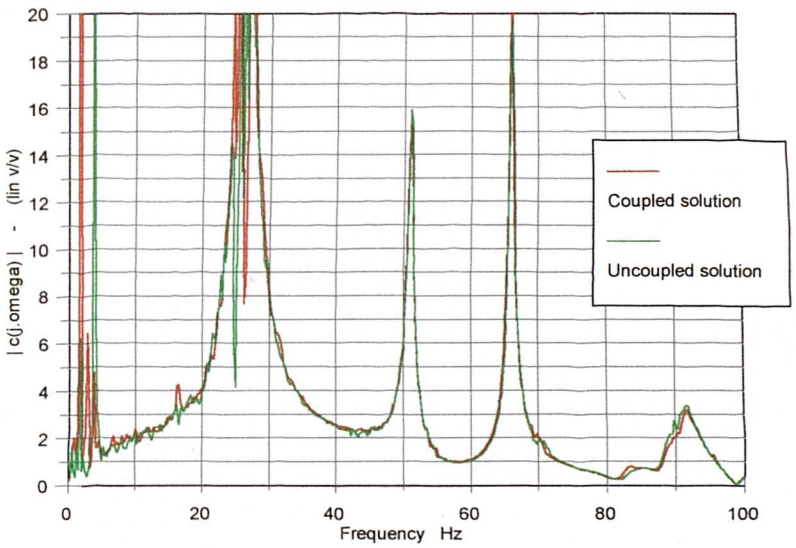

Figure 9.7 - Comparison of point canceller derived with coupling
a) neglected b)compensated using matrix approach

which will completely cancel the pressure at the solution point, designed purely from calculations using the measured transfer functions and with no attempt to make it practically realisable by the use of biquad section fits.

Further experimentation with source location produces results which support the statement that contrary to results in the one-dimensional waveguide, coupling due to limited source

impedance between sources in the three dimensional room is not a factor which limits the utility of biquad fit control in that environment. Limitations in the accuracy of the fit of measured transfer impedances with biquad models are far more significant, and are discussed in relation to specific control tasks in sections 9.3 and 9.4.

9.3 Results - Point cancellation and direct modal replacement

The control approaches outlined in section 9.2 have been tested, based on biquad fits of practical measured room transfer functions and with control performance measured in the same test room. Measured transfer impedances (in terms of p/u or p/V_{in}) were manually fitted with biquad filter sections in a spreadsheet, where the pole locations of the filter sections were adjusted whilst viewing magnitude and phase comparisons of the digital model and measured data. Following appropriate calculations depending on the control task selected, the control filter was implemented in assembly language using the same DSP32C boards used in the implementation of active impedance control. Results associated with the prototype controller of Figure 9.4 are reported below, in terms of the operation of canceller C and its use in conjunction with a modal replacement strategy.

9.3.1 Working with a single mode

Equation (**7.15**) has been used in conjunction with single mode fits of measured primary and secondary path transfer functions (p/V_{in}) to produce a point cancellation filter designed to remove the lowest axial mode from the rectangular test room. Primary and control source locations were chosen at (3.8,1.0,1.0) and (0.15,1.0,1.0), and the solution point was positioned at (1.0,1.0,1.5). Figure 9.8 overleaf shows a 12dB reduction in the pressure magnitude on the first axial x-mode at the solution point. Cancellation is incomplete, and that part of the pressure at 44Hz remaining has a resonant Q which appears similar to that of the uncontrolled mode.

Tests to establish the decay time of the controlled mode confirm that whilst the pressure magnitude has been substantially reduced, the slope of the decay is not modified. Although only the 44Hz mode [1,0,0] is selected for control, some modification of 55Hz [0,1,0] and 70 Hz ([1,1,0] and [0,0,1]) modes has also taken place. This results from the interaction of

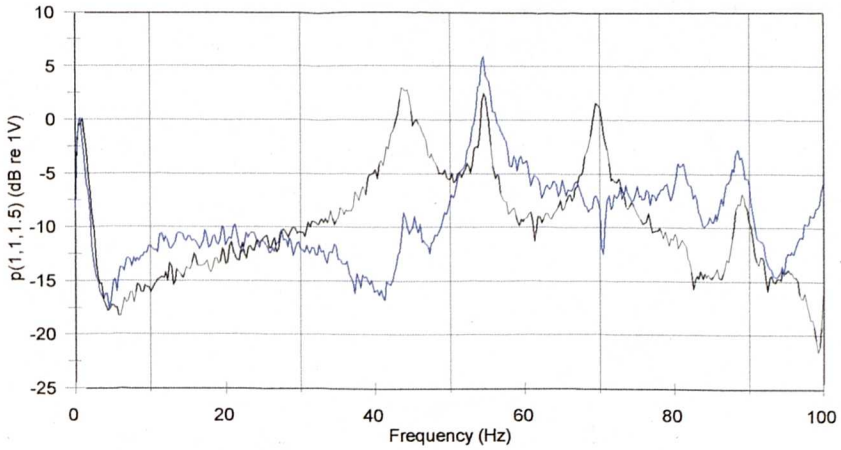

Figure 9.8 - Cancellation of 44Hz mode at sol^{n} pt. (1.0,1.0,1.5)
a) Uncontrolled b) Controlled

the control filter transfer function (arbitrary at these frequencies) with the respective modeshapes (scale factors). In this case, the set of source and receiver locations results in an enhanced 55 Hz mode, whilst the degenerate pair at 70 Hz are attenuated.

The pressure response at a location remote from the solution point (1.0,1.0,1.5) (location *A*) is plotted in Figure 9.9. A new location at (3.0,2.24,0.65) (location *B*) was selected purposefully, since at this point all dominant modeshapes in the bandwidth of interest will have opposite polarity relative to their value at the original position. In a sense this makes the two positions 'distant' in terms of the modeshapes governing the spatial distribution of the enclosed soundfield. All solution points and source locations used in these measurements are indicated on a map of the test room, in Appendix F.

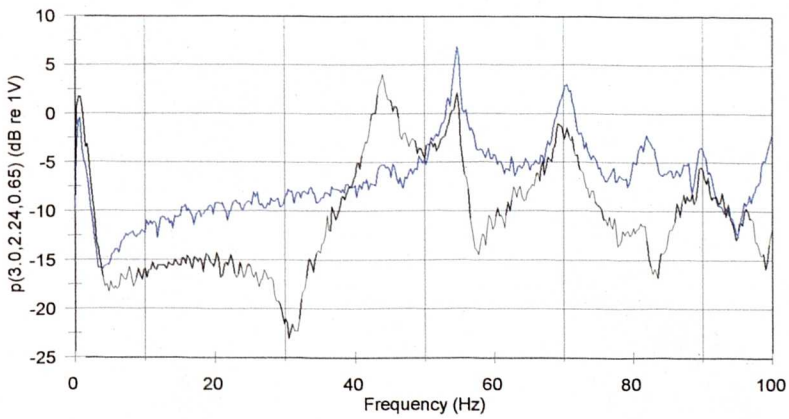

Figure 9.9 - Cancellation of 44Hz mode, remote from sol^{n} pt.
a) Uncontrolled b) Controlled

Whilst the controlled mode is still attenuated relative to the uncontrolled measurement, the performance at other frequencies shows an increase in pressure level. Once again, the interaction of the control filter transfer function with the respective modeshapes results in an increase in measured pressure. It therefore seems that whilst there is some claim for the global cancellation of the mode under control, this unavoidably results in unwanted increases in modal pressure at other frequencies. This result is unsurprising in that the dominant modes at these other frequencies are not incorporated into the design of the control filter.

These observations are not restricted to the particular mode under control in Figure 9.9. Figure 9.10 demonstrates the same finding for control of the [0,1,0] mode, and Figure 9.11 for the [0,0,1] mode. A solution point at location *A* was used in both cases, and the Figures

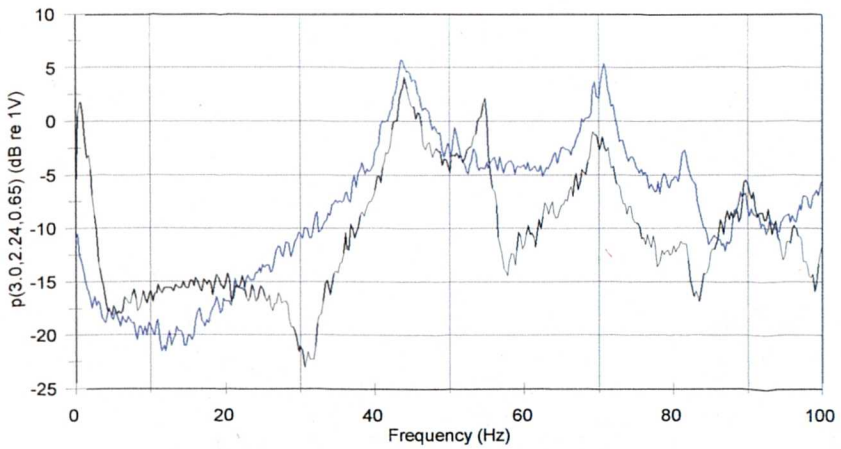

Figure 9.10 - Cancellation of 54.5Hz mode, remote from sol^{n} pt.
a) Uncontrolled b) Controlled

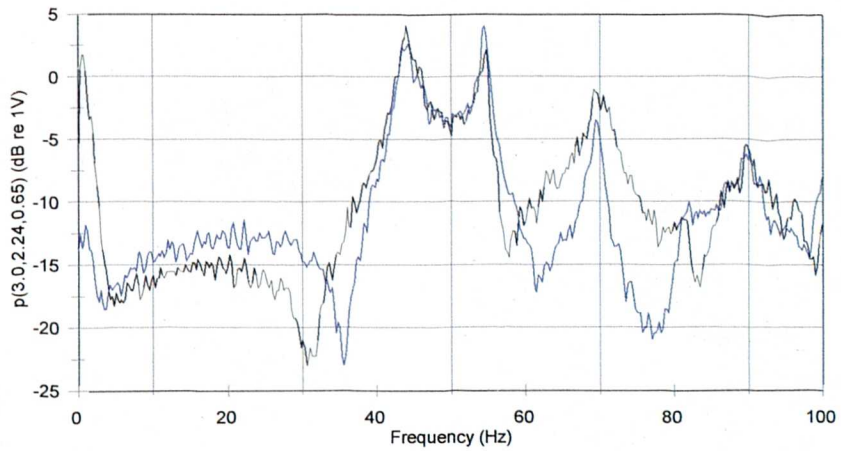

Figure 9.11 - Cancellation of 70.1Hz mode, remote from sol^{n} pt.
a) Uncontrolled b) Controlled

show a comparison between controlled and uncontrolled pressure at the remote location *B*. It is interesting to note that in the latter case, the degeneracy of the mode over which control is desired means that the controller performance is poor. This result holds true at the solution point, and at the remote location illustrated above.

Having examined the performance of the canceller alone, it was used as part of a filter based on the schematic of Figure 9.4 in an attempt to replace an existing mode in the room with a new resonance of lower quality factor. In addition to the canceller, two other filter specifications are required: the inverse of the mode due for replacement, and a low-Q substitute resonance. The inverse of the existing mode was arrived at by a manual measurement of resonant frequency and Q-factor. Pole locations were then calculated based on the one-dimensional optimisation approach shown in Figure 5.1 and using **(5.8)** and **(5.9)**. The inverse of this mode fit simply results from the reversal of pole and zero locations. A low-Q replacement was designed by moving the pole locations of the measured mode along z-plane radii, so that they lay further from the unit circle.

A result of this process, where filter coefficients have been measured for the [1,0,0] mode and the appropriate filter characteristics have been calculated, is shown in Figure 9.12. The uncontrolled mode has a measured Q of 46, and the control filter is designed around a target Q of 10. When the low-Q mode is substituted following the schematic of Figure 9.4, the measured peak in the frequency response is noticeably curtailed. It also appears that in

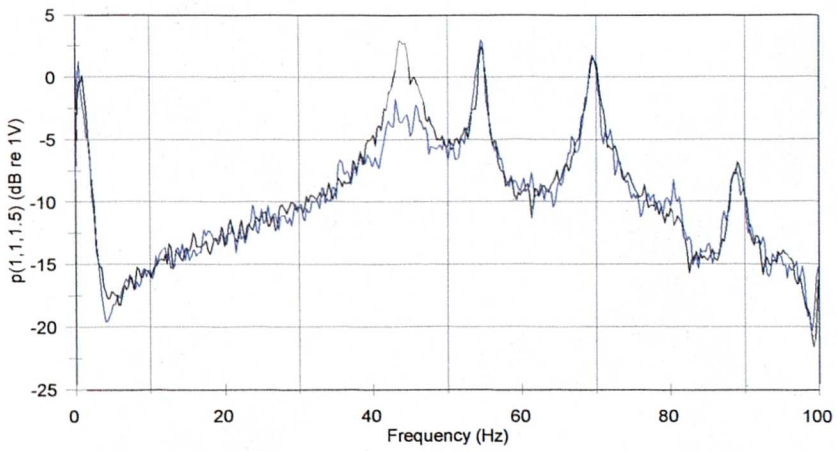

Figure 9.12 - Modal replacement (Q=10) of 44Hz mode at sol^{n} pt. (1.0,1.0,1.5)
a) Uncontrolled b) Controlled

comparison to the cancellation scenario illustrated in Figure 9.8, arbitrary interactions of the control filter with uncontrolled modes result in a controlled field which does not differ markedly from the uncontrolled case.

If the pressure field is sampled away from the solution point (Figure 9.13), then the same type of variation in the amplitude of other modes occurs as one moves along the respective modeshapes. Since interactions between the controller and the other modes are not as significant as for the point cancellation filter, the amplitudes of modes not included in the control filter remain very similar to their uncontrolled value. Similar results were recorded for control of [0,1,0], but the control of [1,1,0] / [0,0,1] was hampered by the poor performance of the canceller at this frequency, documented in Figure 9.11.

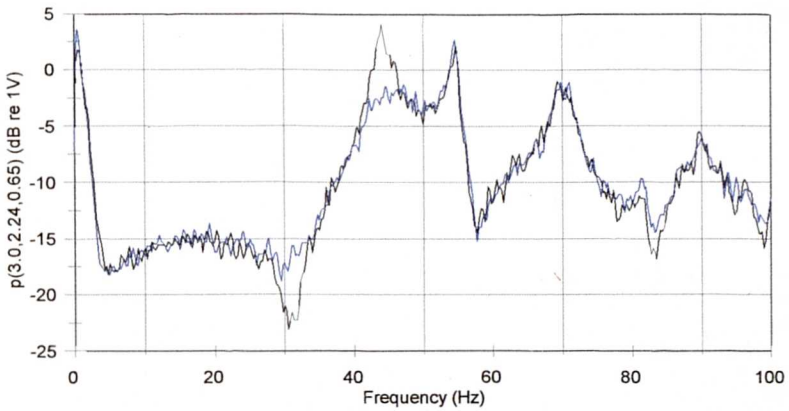

Figure 9.13 - Modal replacement (Q=10) of 44Hz mode remote from sol^n pt.
a) Uncontrolled b) Controlled

It can therefore be concluded that where modes are not degenerate, a single-mode canceller works well at the solution point. Where controller transfer function and primary/secondary source-receiver modeshapes interact fortuitously, the steady-state pressure at other locations may also appear to be controlled, but at other locations modes may actually be enhanced. The mode which is the subject of control *may* be attenuated globally, but this depends on the proximity of other modes in frequency, which is itself a function of damping and mode order. The replacement of the cancelled mode with a resonance of lower quality-factor has the byproduct of reducing the impact of control at frequencies remote from the mode under consideration, and means that the global soundfield is less subject to unpredicted and unwanted interactions between primary and secondary sources.

So far only one mode has been considered at a time. A filter which is able to modify the Q-factor of a number of adjacent modes simultaneously would be highly desirable, and attempts at realising such a filter are reported in section 9.3.2

9.3.2 Working with multiple modes

As a pre-requisite for a modal replacement strategy which operates on more than one mode simultaneously, let us first consider a cancelling filter *'C'* designed on the basis of **(5.21)** and the schematic of Figure 7.13. Transfer impedance measurements were made in the room and manually fitted with biquad filter sections. P/V_{in} data was used, and the three lowest modes of the space were modelled along with an approximation for the zeroth mode. The primary source location was (3.8, 1.0, 1.0) and the control source location, (0.15, 1.0, 1.0). A solution point at location *A* was selected, and an example of the resulting fit parameters for a filter sample rate f_s=*3 KHz* are shown below in table 9.1.

	Z_{pr} model parameters				Z_{sr} model parameters			
Freq Hz	0^{th}	43.6	54.5	69.6	0^{th}	43.6	54.5	69.6
Scale	-2e-4	4e-4	-2e-4	2.3e-4	2e-4	1.7e-4	1.3e-4	1.05e-4
$2re(P_i)$	1.98997	1.98868	1.98502	1.97681	1.98997	1.98868	1.98502	1.97681
$\|P_i\|^2$	0.990	0.997	0.998	0.998	0.990	0.997	0.998	0.998

Table 9.1: Example pole locations for IIR room model

The resulting controlled pressure reconstructed at the solution point in practice is shown in Figure 9.14 overleaf. Although the steady-state frequency response at the solution point is attenuated by around 12 dB on the modes, the remaining pressure is still modal and the quality factor of the resonances appear similar to that of the uncontrolled soundfield. Further tests indicate that the decay times of the modal remnant have not been modified compared to the uncontrolled field. Inspection of Figure 9.3 (the phase of the biquad fit) suggests that errors in the fit of the transfer impedances are responsible for some increases in pressure, most notably at 30Hz but also around 50Hz.

These results are obviously limited, in that they relate to one particular solution point and are concerned with the reconstruction of the controlled field at that location. A degree of steady-state attenuation which is subject to errors in the fit of the measured transfer

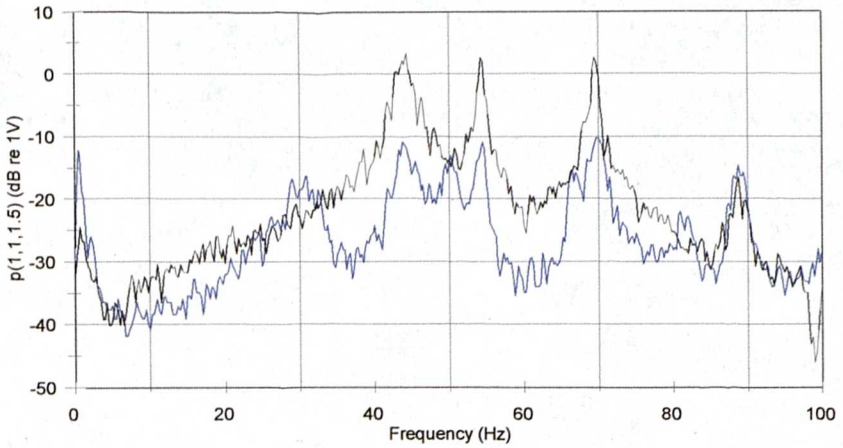

Figure 9.14 - Cancellation of lowest 3 + 0th mode at solⁿ pt. (1.0,1.0,1.5)
a) Uncontrolled *b) Controlled*

functions has been demonstrated, but no generality can yet be claimed with reference to either the performance of that solution at positions remote from the original solution point, or the stability and performance of a solution formed at other locations. To look for answers to these questions, the controller designed at location (1.0,1.0,1.5) was tested at location (1.0,2.2,1.5) (location *C*). This position was selected in order to move to a point where the polarity of the mode [0,1,0] is inverted in comparison to its value at the solution point *A*. The value taken by the other dominant modeshapes is unchanged. Figure 9.15 shows the measured pressure at the new measurement location.

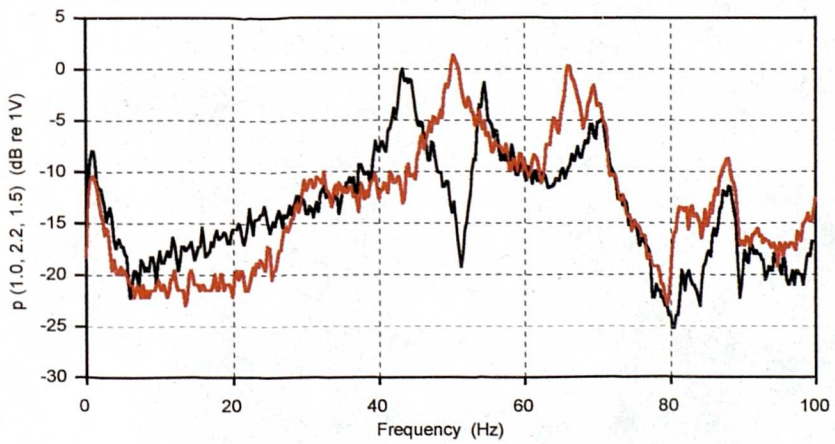

Figure 9.15 - Point canceller designed at 'A', tested at 'C'
a) Uncontrolled *b) Controlled*

Although the modes [1,0,0] and [0,1,0] are attenuated, the Figure is dominated by peaks in the measured controlled pressure at 50 Hz and 68 Hz which are even more pronounced than

the original modal maxima. The origin of these peaks is evident if one considers the magnitude response of the cancelling filter '$C(j\omega)$'. The implementation of this filter based on IIR sections has magnitude response very similar to the optimal version displayed in Figure 9.7. Referring to this response, the origin of the peaks in Figure 9.15 can clearly be discerned - they correlate with the peaks in the magnitude of the cancelling control filter.

A measurement of the controlled pressure due to the multiple-mode canceller designed at *A* was also made at a third position, *D* (2.95,1,1.5) (Figure 9.16). This position is mirrored in the [1,0,0] nodal plane compared to *A*, implying a change in polarity of this mode whilst maintaining the polarity of all other dominant axial modeshapes, and leaving all magnitudes unchanged. Peaks in the controlled pressure appear again at 50 and 68 Hz which are of comparable magnitude to the uncontrolled modes, despite a degree of control being evident over at least the mode [1,0,0] at its own natural frequency. It therefore appears that at both locations *C* and *D* the original canceller solution is ill-specified. Changes in the modeshapes between solution point *A* and the new measurement locations mean that the peaks in $C(j\omega)$ at the noted frequencies are no longer matched to the transfer impedances from the sources out to these positions. The interference of primary and secondary fields cannot then result in the desired attenuation across the full bandwidth of interest.

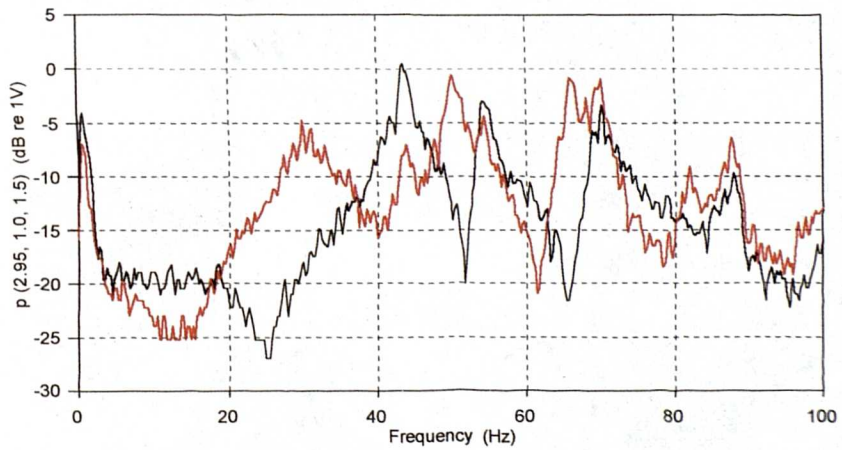

Figure 9.16 - Point canceller designed at 'A', tested at 'D'
a) Uncontrolled b) Controlled

Part of the mismatch between control filter and measurement location is contained within the formation of the admittance $1/Z_{sr}$. The peaks at 50 Hz and 68 Hz coincide with minima in the transfer function Z_{sr} measured between a control source at (0.15,1.0,1.0) and the

solution point (1.0,1.0,1.5), and occur as a result of the phase interference between adjacent modal residues in the decomposition of the total pressure. Modes adjacent in frequency and sharing a common eigenvector polarity have residues which interfere *destructively* at some point between their two natural frequencies, since the complex frequency dependence of each resonance contains a 180° phase reversal as one moves from below the peak frequency, to above it. Their complex sum is therefore very close to zero, and the pressure at this frequency merely consists of the sum of in-phase higher residues with very low amplitude.

At location *A*, all modes in the IIR model of Z_{sr} are in-phase, as evidenced by the polarity of the scale factors shown in Table 9.1. The inverse of the Z_{sr} model therefore contains maxima at frequencies between the eigenvalues of the constituent sections - and these appear at 50 and 68 Hz. In contrast, the polarity of certain modeshapes at locations *C* and *D* are dissimilar, with the result that *constructive* interference occurs around the frequencies previously marked by strong minima in the magnitude transfer impedance. An example of this change is shown in Figure 9.17, which displays the measured transfer function Z_{sr} for locations *A* and *C*. Note the increase in magnitude around 68Hz for location *C*, where modes [1,0,0] and [0,1,0] now interfere constructively.

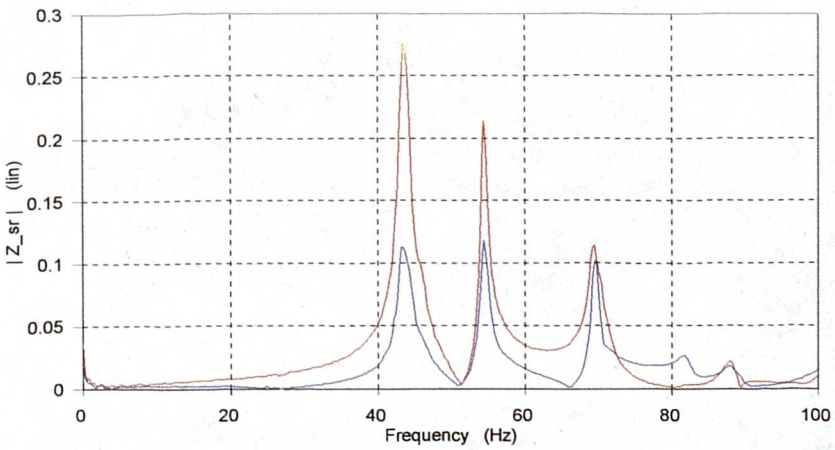

Figure 9.17 - Magnitude of secondary path transfer impedance
a) To solⁿ pt. 'A' b) To solⁿ pt. 'C'

The mismatch between the canceller design at point *A* and its resulting action at points *B* and *C* illustrates that it is a local solution, with spatial extent inexorably linked with the physics of the eigenvectors which govern the spatial behaviour of the soundfield in the enclosure. Interestingly, attempts to realise cancelling controllers with solution points specifically

located at B and C are frustrated by a failure to achieve a stable inverse to the transfer function Z_{sr}. It seems that so long as the individual sections of the filter retain a common polarity, a stable inverse exists, but where an inversion of polarity occurs for one or more of the constituent sections, the inverse contains poles which lie outside of the unit circle.

Neely and Allen [57] comment indirectly on this problem whilst looking for solutions to the deconvolution of the impulse response from a source to a listener in an enclosed space. It is suggested that where room impulse responses are non-minimum phase, a stable inverse does not exist, and that in turn the distance from source to receiver and the reflection coefficient of the boundaries determine the nature of the impulse response. The inversion in scale factor required from certain biquad filter sections in order to model the changing polarity of the room modeshapes is equivalently expressed by the introduction of 180° phase shifts to those sections. It appears that the addition of this phase shift in a parallel filter structure is analogous to the inclusion of non-minimum phase components in the overall room response, with the result that a stable inverse cannot be achieved.

Whilst within certain stability constraints a controller may be derived which is to some degree effective as a point canceller, a global solution to the multiple-mode cancellation problem appears elusive. The basis of the canceller design lies in the ratio of primary to secondary transfer impedances given in (**7.2**), and changes in these functions resulting from changes in their constituent modeshapes mean that movement around the enclosed space is bound to introduce discrepancies between a solution derived at one location, and the pressure realised at another. At first it appears logical that if the changes in Z_{pr} and Z_{sr} could in some way be spatially synchronised, a global cancellation strategy might emerge. Such synchronisation must result from the co-location of primary and secondary sources.

Two co-located sources in the room may be controlled such that their interference results in zero (or near-zero) pressure throughout the space. This begs the question - why carry out the summation in the acoustic domain at all? It might be thought more effective to complete the summation of primary and secondary path signals in the electrical domain, reducing the number of physical sources in the room to one and achieving perfect co-location. Unfortunately this implies that the strategy reduces to pressure cancellation by the electrical disconnection of the primary source!

From these arguments it appears that the prototype modal controller of Figure 9.4 is not an ideal strategy for global modifications to a number of modes, since the cancellation which must precede modal replacement is always imperfect and of local rather than global spatial extent. The approach is seen to be effective in controlling one mode at a time, in terms of a reduction in the Q-factor of that mode and a reduction in the corresponding modal decay time. However, in order to realise a controller which is able to affect changes to more than one mode at a time in the room environment, it is necessary to consider the alternative strategy of the direct specification of reductions in modal quality factor.

9.4 Results - Q-factor modification

The control approach of Q-factor modification outlined in section 5.3 has been tested, based on biquad fits of practical measured room transfer functions and with control performance measured in the same test room. Measured transfer impedances (in terms of p/u or p/V_{in}) were manually fitted with biquad filter sections in a spreadsheet following the same process as for point cancellation filters. Following appropriate calculations (**(5.18)** to**(5.22)**), control filters were implemented in assembly language using the same DSP32C boards used in the implementation of active impedance control. Results associated with the controller of Figure 5.3 are reported below, in terms of the operation of filters which change the steady-state quality factor of a mode and its associated decay time.

9.4.1 Working with a single mode

Initial attempts at Q-factor modification used biquad models of a single mode to derive a control filter. Figure 9.18 shows the steady-state spectrum with and without control; primary and secondary source locations are respectively (3.8,1.0,1.0) and (0.15,1.0,1.0), and the field is sampled at solution point *A* (1.0,1.0,1.5). The measured data was fitted with an IIR section having pole 'radius' $|p^2| = 0.998$, and a desired mode set up at the same frequency but with reduced pole radius corresponding to $|p^2| = 0.990$. Data is displayed against a nominal logarithmic axis representing dB re 1V at the analyser, and allows comparison between the controlled and uncontrolled soundfield.

The successful reduction in Q factor is mirrored by the reduction in the decay time at the solution point displayed in Figure 9.19, measured using a truncated 44Hz sine tone. The

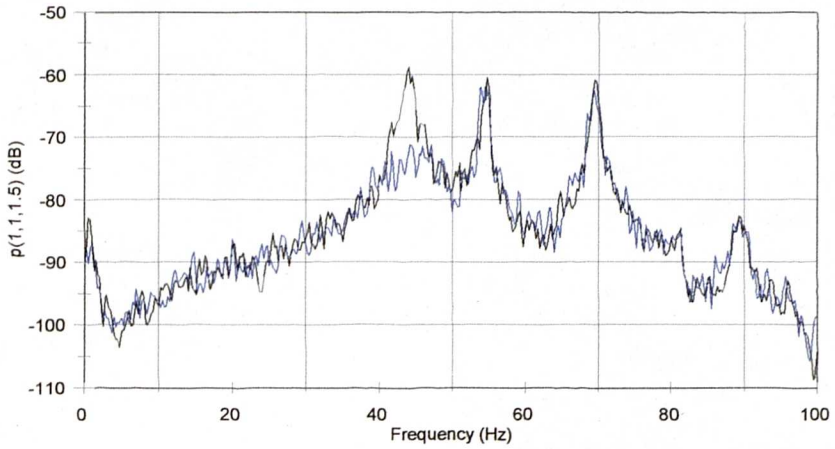

Figure 9.18 - Q-factor modification with pole radius of mode [1,0,0] reduced from 0.998 to 0.99
a) uncontrolled *b) controlled*

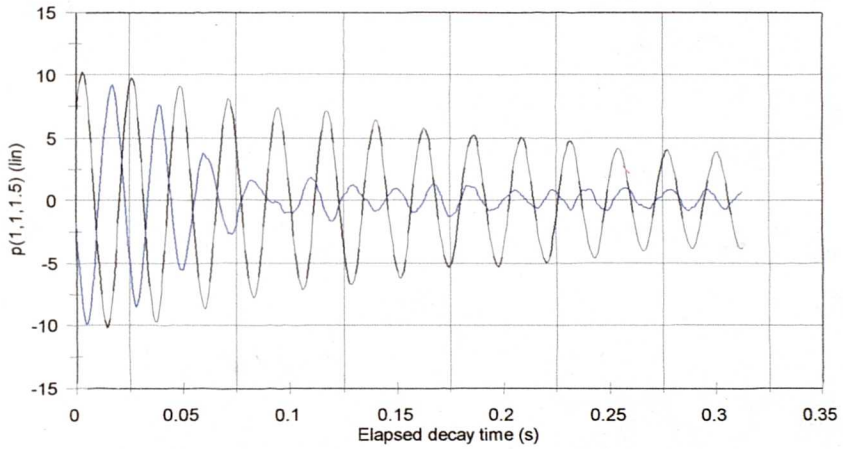

Figure 9.19 - Decay at sol^{n} pt. of mode [1,0,0] - pole radius reduced from 0.998 to 0.99
a) uncontrolled *b) controlled*

data is plotted against a linear axis showing mV input to the analyser, and allows comparison between controlled and uncontrolled decays. Despite the presence of an uncontrolled residual decay after an elapsed decay time of 100mS, the subjective impression is one of a 'boomy' decay being replaced with a more anechoic acoustic. Similar measurements were made at locations distant from the solution point. Figure 9.20 shows the steady-state control resulting from the solution at *A*, measured in a corner location (3.95,0.1,0.1), and Figure 9.21 the corresponding decay characteristic. There is some evidence to suggest that if modal overlap is low then similar performance may extend throughout the room volume.

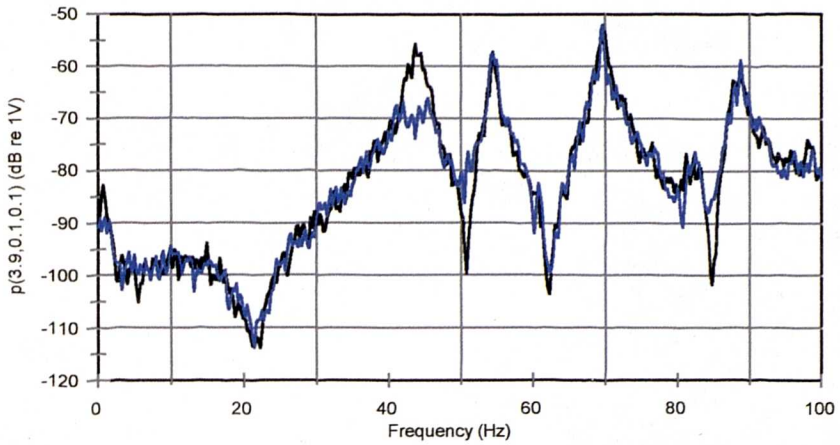

Figure 9.20 - Pressure at remote location - pole radius for mode [1,0,0] reduced from 0.998 to 0.99 at sol^{n} pt. 'A'
a) uncontrolled *b) controlled*

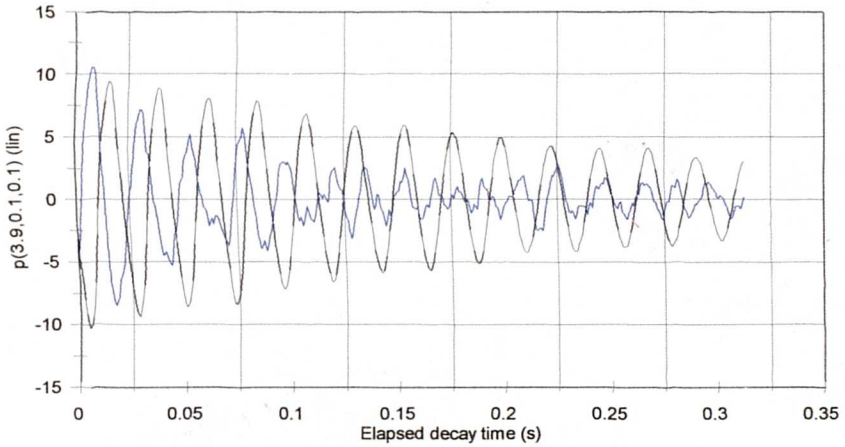

Figure 9.21 - Decay at remote point of mode [1,0,0] - pole radius reduced from 0.998 to 0.99 at sol^{n} pt. 'A'
a) uncontrolled *b) controlled*

The turn-off transient does excite modes which are not excited by the steady-state tone, and the magnitude of these in the decay depends on the location of the pressure measurement relative to those particular modeshapes. At the corner location illustrated in Figure 9.21, there are clearly a number of uncontrolled modal residues at comparatively high frequency, initiated by the turn-off transient of the test tone, which corrupt the uncontrolled remainder of the test tone and result in an angular waveform rich in frequency content. It is to be expected that these residues would be more in evidence in Figure 9.21 than in 9.19, since the former location is positioned at a maximum of all axial, and near a maximum for many tangential and oblique, modeshapes.

The prominence of uncontrolled modal artefacts in the measured decay in the test room during controller operation also turns out to be a factor of the severity of the imposed control task. The desired pole locations for mode [1,0,0] were moved from their original locations at $|p|^2 = 0.998$ through the already noted location $|p|^2 = 0.990$, and on to a very low-Q specification at $|p|^2 = 0.950$. The steady-state consequences of the resulting filter operation are shown in Figure 9.22.

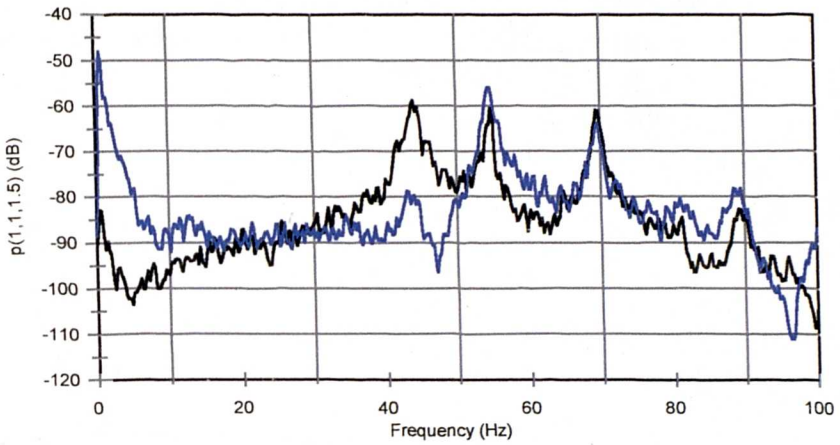

Figure 9.22 - Pressure at sol^n pt. 'A' - pole radius for mode [1,0,0] reduced from 0.998 to 0.950
a) uncontrolled b) controlled

The controlled pressure bears close resemblance to the response observed during the attempted *cancellation* of the [1,0,0] mode (Figure 9.8); the two tasks are rather similar given the extremely low-Q desired mode in the Q-factor modification filter, which could be interpreted as an attempt to remove that mode altogether. As in the case of the cancelling controller, the controller results in an *increase* in the amplitudes of the [0,0,0] and [0,1,0] modes - both uncontrolled by this filter. These increases were not observed when the control task only required a pole radius reduction to $|p|^2 = 0.990$.

The amplification of uncontrolled modal artefacts is also clearly evident in Figure 9.23, which shows the corresponding decay of a 44.5 Hz test tone. The 'controlled' decay exhibits a complicated waveform which does not seem to have shortened the modal decay time as anticipated. Closer inspection suggests that the decaying 44.5 Hz test tone is amplitude modulated by a decaying residue of the [0,1,0] mode (natural frequency = 54.5 Hz), excited by an appropriate frequency component of the turn-off transient. The question

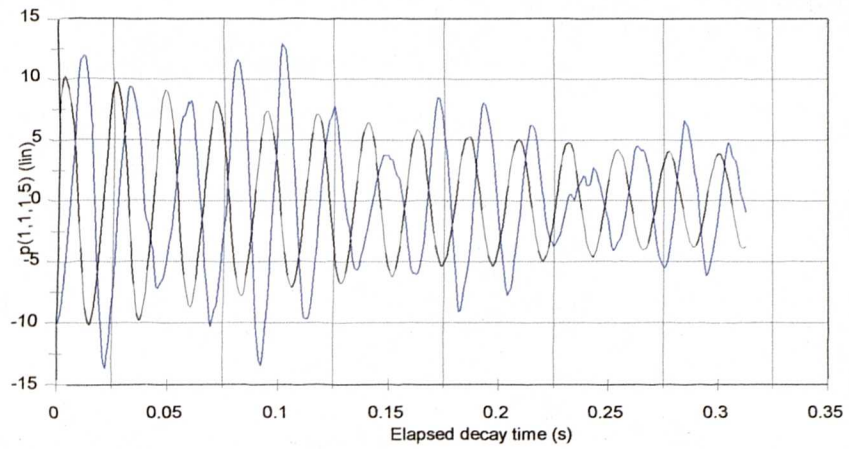

Figure 9.23 - Decay at sol^{n} pt. 'A' of mode [1,0,0] - pole radius reduced from 0.998 to 0.950
a) uncontrolled b) controlled

emerges as to why, when a more stringent control task is specified, do uncontrolled residual artefacts of other modes feature more strongly in the steady-state and decay responses measured in the test room?

Equation **(5.22)** shows that the Q-factor modification filter introduces poles into the secondary path which are those *specified by the desired pole locations.* This means that as the desired Q-factor of a controlled mode is reduced, poles are introduced into the secondary path which lie further and further from the unit circle. The magnitude response of *C(z)* is therefore broadened in frequency, which has two important implications.

Firstly, during steady state operation the broader filter will enable an increased secondary path excitation of other modes adjacent to that principally under control. This factor is responsible for the increase in measured pressure at 54.5 Hz and 70 Hz. Secondly, during the decay phase of the mode the step function implied by the test signal truncation is filtered by the broader *C(z),* and significant frequency content may be passed at the natural frequencies of adjacent modes. Therefore the secondary path excites adjacent decaying modes more strongly than would have been the case had a more modest reduction in quality factor been specified. It can thus be seen that it may not be desirable to attempt bold reductions in the Q-factor of the uncontrolled room. Depending on the proximity in frequency of adjacent resonances, a more modest objective can give results which in steady-state and decay terms suggest a more effective application of damping.

So far these results have concerned the control of mode [1,0,0]. A Q-factor modification filter was also designed for the mode [0,1,0], where the uncontrolled z-plane pole radius of $|p|^2 = 0.998$ was replaced by a mode modelled with a pole radius of *0.990*. Figure 9.24 shows the steady state frequency response measured at solution point *'A'*, where it can be seen that a good degree of control over the 54.5 Hz resonance has been attained.

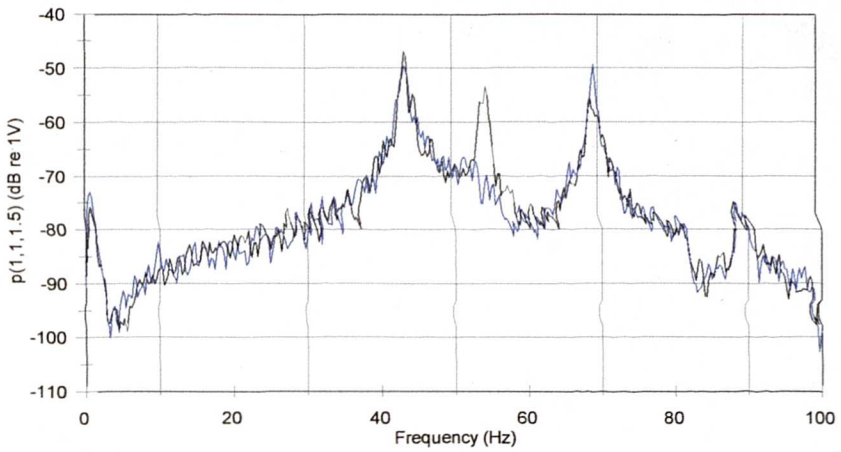

Figure 9.24 - Q-factor modification for mode [0,1,0] - pole radius reduced from 0.998 to 0.99 at sol^n pt. 'A'
a) uncontrolled b) controlled

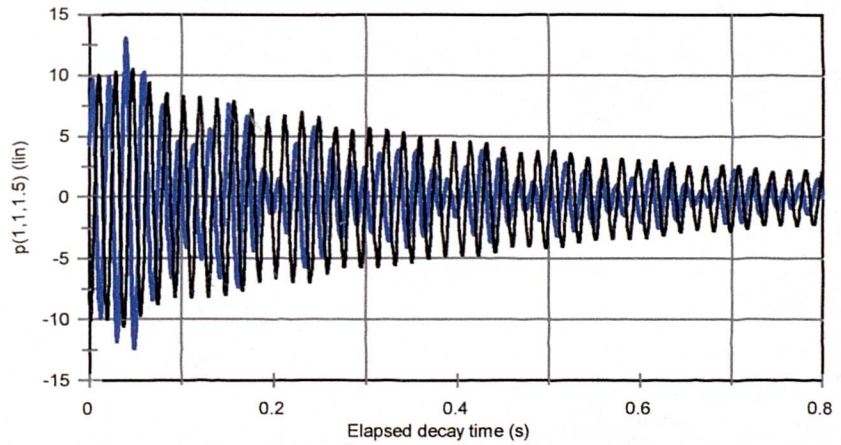

Figure 9.25 - Decay at sol^n pt. 'A' of mode [0,1,0] - pole radius reduced from 0.998 to 0.99
a) uncontrolled b) controlled

Corresponding control over the decaying [0,1,0] mode has been measured and results are presented in Figure 9.25. It can be seen that the controlled decay appears to be amplitude modulated by a signal with frequency close to that of the test tone (54.5 Hz), and close inspection of the uncontrolled trace suggests a lesser degree of modulation also. The

periodicity of the modulation reveals that the turn-off transient of the decaying test tone used to excite the [0,1,0] mode is also responsible for the excitation of the [1,0,0] mode. The controlled 54.5 Hz tone has amplitude comparable to that of the residual 44 Hz decay, and their interaction results in the decay shown above. This result supports the conclusion that control over a single mode in the room is unlikely to produce satisfactory decay characteristics, even if the steady-state control over one mode appears convincing. Simultaneous control over a number of resonances is evidently required, and results of tests to establish such a scheme are reported in section 9.4.2.

9.4.2 Working with multiple modes

The initial experiment with simultaneous control over two modes was set up so as to incorporate modes [1,0,0] (44 Hz) and [0,1,0] (54.5 Hz) into controller *C(z)*, and the resulting steady-state control at the solution point (*A*) is shown in Figure 9.26.

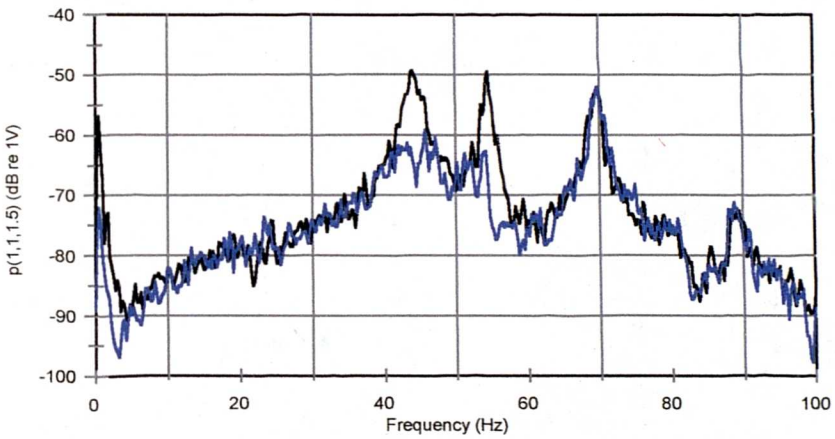

Figure 9.26 - Q-factor modification for modes [1,0,0] and [0,1,0] - pole radii reduced from 0.998 to 0.99 at sol^{n} pt. 'A' a) uncontrolled b) controlled

Both modes had desired target models specified with pole radius reduced to $|p|^2=0.990$, and following a modal fitting process the appropriate control filter was derived. It can be seen that large pressure reductions are obtained at the natural frequencies of the two modes incorporated into the controller. Of more interest is the resulting decay performance at the two relevant frequencies, displayed in Figures 9.27 and 9.28.

Figure 9.27 suggests that the two-mode controller is almost as efficient in shortening the decay of mode [1,0,0] as that controller designed specifically to operate on this mode alone

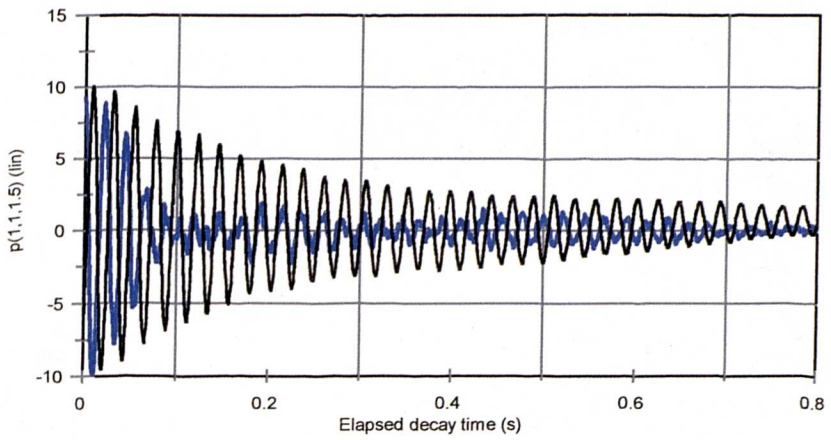

Figure 9.27 - Decay at sol^{n} pt. 'A' of mode [1,0,0] - pole radius reduced from 0.998 to 0.99
a) uncontrolled *b) controlled*

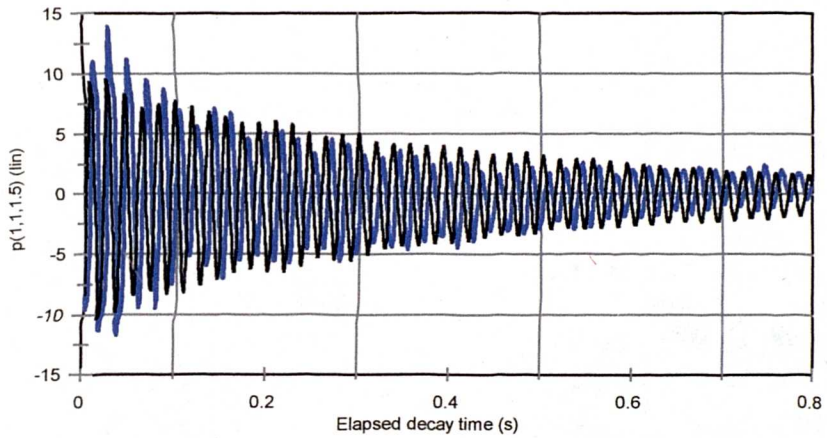

Figure 9.28 - Decay at sol^{n} pt. 'A' of mode [0,1,0] - pole radius reduced from 0.998 to 0.99
a) uncontrolled *b) controlled*

(the result for the latter case is illustrated in Figure 9.19). The increased complexity of the controller appears to have resulted in some excitation of higher modal residues, since the decay after 100mS has a somewhat angular waveform. The Fourier transform of this decay confirms the presence of these residues excited by the test tone turn-off transient. However, the subjective impression of the change in the room acoustic is similar to that created by the control of one mode only, and can be considered to be a useful reduction in decay time.

Figure 9.28 stands in contrast to this result, since little apparent reduction in decay time for mode [0,1,0] appears to have been bought by the inclusion of this mode into the controller.

In contrast to Figure 9.25, amplitude modulation of [0,1,0] by a decaying residue of mode [1,0,0] has been suppressed by the inclusion of the latter into the controller. However, the expected reduction in decay time of mode [0,1,0] is not in evidence. The steady state reduction of [0,1,0] (Figure 9.26) has not been coupled to a corresponding decay phase benefit, and it was hypothesised that the non-inclusion of the higher adjacent modes [1,1,0] and [0,0,1] might be responsible. Including the higher modes into the biquad fit model could be expected to marginally improve the fit at the natural frequency [0,1,0] itself, and lessen the influence of uncontrolled decaying modal artefacts at frequencies around 70 Hz, which could be excited by the turn-off transient of the 54.5 Hz test tone.

To investigate this possibility, equations **(5.18)** to **(5.22)** have been implemented with three modes built into the model (at 44, 54.5 and 70Hz). All modes were subject to an attempt to decrease their z-plane pole radius from around 0.998 to near 0.99. The two degenerate room modes at 69-70 Hz were incorporated as one biquad section, since they were considered to be inseparable during the frequency-domain fitting process. Measured p/V_{in} data was used in the fitting process, as described in section 9.1.

Figure 9.29 shows that the steady-state modal amplitudes have all been attenuated at the solution point (*A*), but the associated decay characteristics are not all straightforward. The decay of mode [1,0,0] in Figure 9.30 shows that control is to some degree effective over

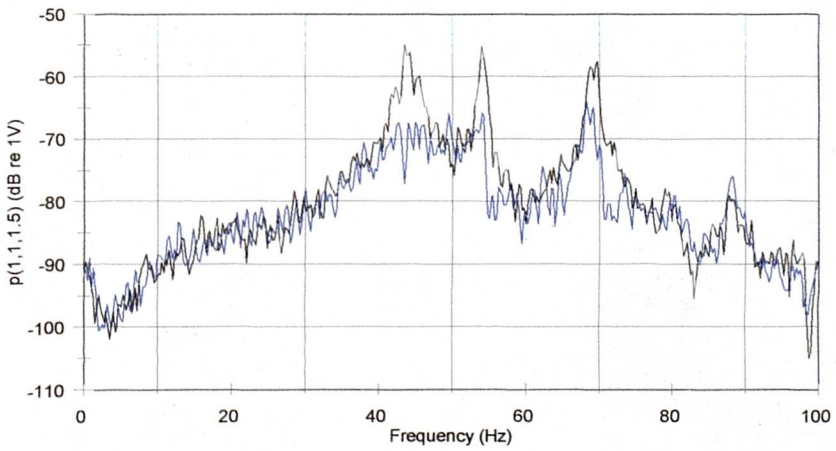

Figure 9.29 - Q-factor modification for modes [1,0,0], [0,1,0] and [1,1,0] / [0,0,1] - pole radii reduced from 0.998 to 0.99 at sol^{n} pt. 'A'
a) uncontrolled b) controlled

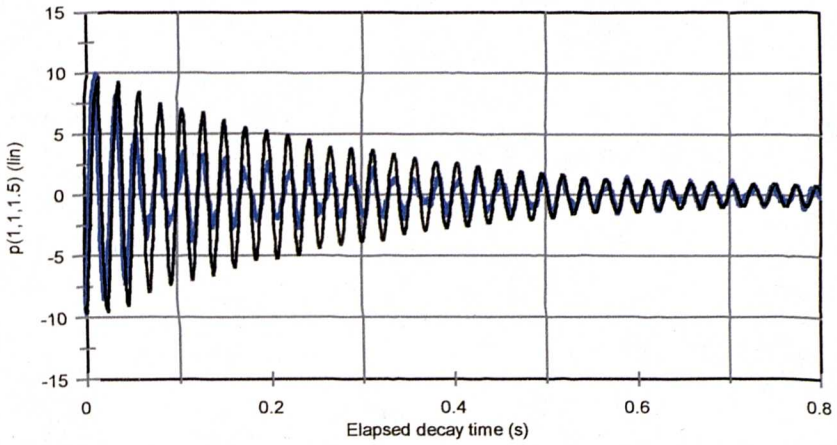

Figure 9.30 - Decay at sol^{n} pt. 'A' of mode [1,0,0] - pole radius reduced from 0.998 to 0.99 by 3-mode controller
a) uncontrolled *b) controlled*

modal decay. The inclusion of more modes into the controller means that the broader frequency response of *C(z)* excites yet more residues, and the controlled decay performance is to some degree compromised compared to that designed for one mode alone. However, a useful initial reduction in decay time remains which creates an audible effect. It is worth noting the findings of Toole and Olive [65], who suggest that the energy in the first few cycles of decay of a resonator output may be a more reliable cue to the detection of resonance than the duration of ringing itself.

Some increase in initial decay rate is also seen for modes [1,1,0] / [0,0,1] (Figure 9.31) despite their degenerate nature, but mode [0,1,0] still appears to be invulnerable to alterations in its decay time. However, the Fourier transform of the respective truncated sine response contains a predominant frequency component which lies not at the natural frequency of the original mode (which equals the frequency of the truncated test tone), but at the frequency of the 'notch' present in the steady state controlled spectrum located around 54.5 Hz (Figure 9.29). The notch frequency differs subtly from the natural frequency by several tenths of one Hertz. This notch results from the addition of primary and secondary fields rather than from either path alone, and it is to be expected that a steady-state spectrum incorporating a rapid magnitude transition at a particular frequency will be associated with a ringing frequency component within the corresponding impulse response.

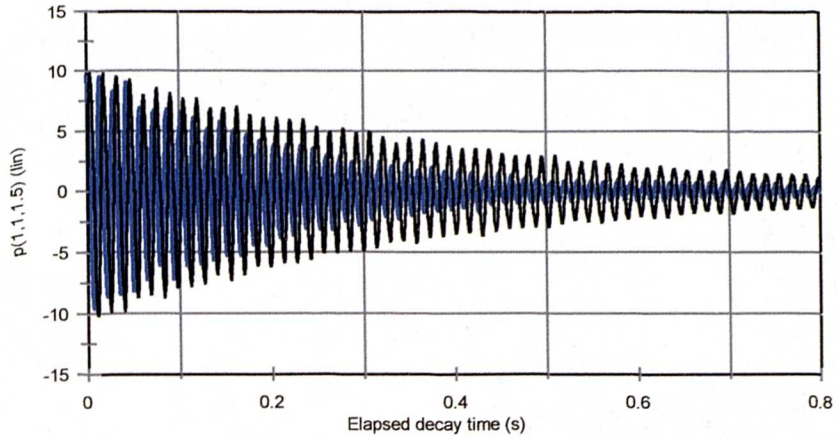

Figure 9.31 - Decay at sol^{n} pt. 'A' of modes [0,0,1] / [1,1,0] - pole radii reduced from 0.998 to 0.99 by 3-mode controller a) uncontrolled b) controlled

The performance of the multiple mode Q-factor modification filter in controlling the decay of mode [0,1,0] is therefore not improved by the inclusion of adjacent modes into the model. This problem appears to be related to a notch in the steady-state spectrum, created at the solution point where a smooth reduction in modal Q-factor had been anticipated. It is instructive to consider the use of alternative source locations; results using new locations point to an explanation for the failure to control the decay of mode [0,1,0] and to a technique for overcoming the problem.

9.4.3 Using alternative source locations

A naive interpretation of the results reported in section 9.4.2 might suggest that the failure of decay control over mode [0,1,0] results from a controllability problem. This cannot be true, as the steady state response is modified by the action of the secondary source. However, moving primary and secondary sources to locations where mode [0,1,0] is symmetrically excited by both (as has been measured for mode [1,0,0]) provides a useful insight into the mechanisms mitigating against successful decay control.

Primary and secondary sources were moved to the centre of the room floor, at locations (1.9,0.30,0.86) and (1.9,0.23,1.73). These points were chosen to minimise the influence of mode [1,0,0] whilst maximising [0,1,0] in the measured transfer functions, and will be referred to as source location set 2. The previous locations at (0.15, 1.0, 1.0) and (3.8, 1.0, 1.0) are referred to as source location set 1. Both sets of source locations are shown

on a map of the test room in Appendix F. p/V_{in} transfer functions were measured, and desired pole radii chosen. Uncontrolled, the three modes [1,0,0], [0,1,0] and [1,1,0] / [0,0,1] had $|p|^2 = 0.9975$, 0.9985 and 0.9985 respectively. Desired modal pole radii were selected with $|p|^2 = 0.990$, 0.994 and 0.992, which gave a smooth frequency characteristic in the biquad room model. Desired pole radius $|p|^2 = 0.990$ was also used for mode [0,1,0], and in all cases coefficients for the modal Q-factor modification filter were calculated.

The resulting steady-state control at the solution point *A* is shown in Figure 9.32. Using source location set 2, the 'notch' problem has not occurred for mode [0,1,0] around 54-55Hz, and both desired pole radii modifications have resulted in a visible and appropriate reduction in modal quality factor. Decay performance is likewise successfully modified, as shown in Figure 9.33. It appears that the more ambitious Q-factor reduction results in a greater excitation of uncontrolled higher modal residues, as previously noted. However, useful reductions in the decay time of mode [0,1,0] are obtained.

The Q-factor modification filter is not only effective in controlling modal decay. Figure 9.34 shows the change in the excitation of a mode resulting from the application of the controller when the test tone is switched on. The attack of the mode is greatly increased, since the rate of energy build-up is directly related to quality factor in the same way as the decay. The improvement in controller performance resulting from the adoption of new source locations may result from a number of different factors. These include the dominance of mode [0,1,0]

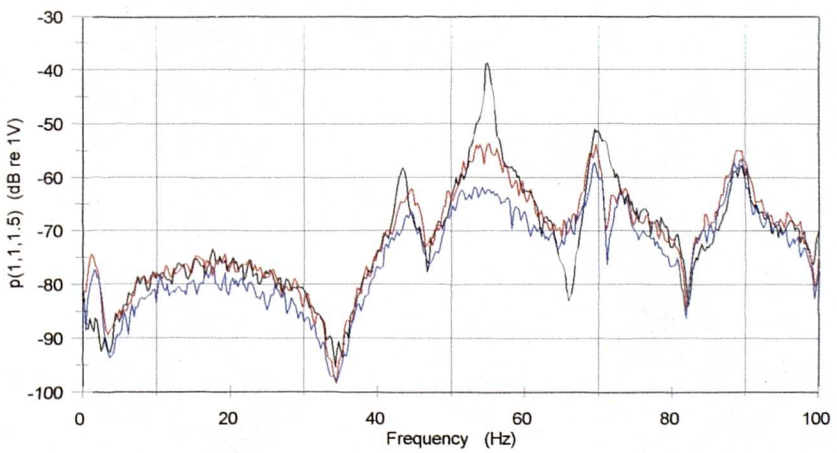

Figure 9.32 - Q-factor modification for three modes.
a) Uncontrolled b) $|p|^2 = 0.994$ for [0,1,0]
c) $|p|^2 = 0.990$ for [0,1,0]

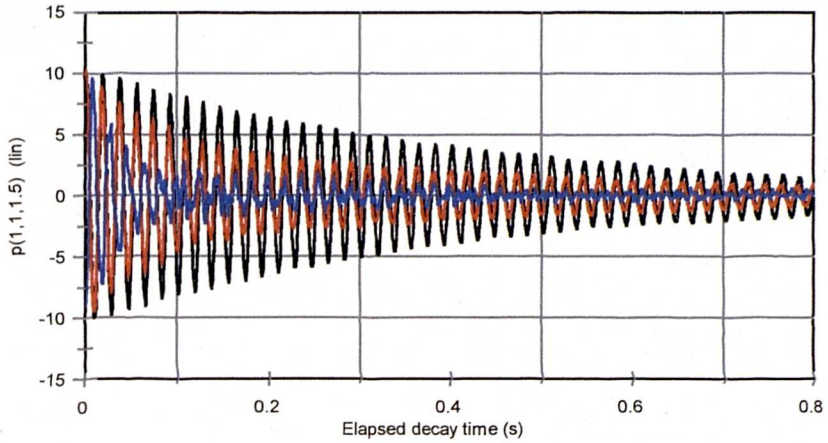

Figure 9.33 - Decay at sol^{n} pt. 'A' of mode [0,1,0]
a) Uncontrolled *b) $|p|^2 = 0.994$ for [0,1,0]*
c) $|p|^2 = 0.990$ for [0,1,0]

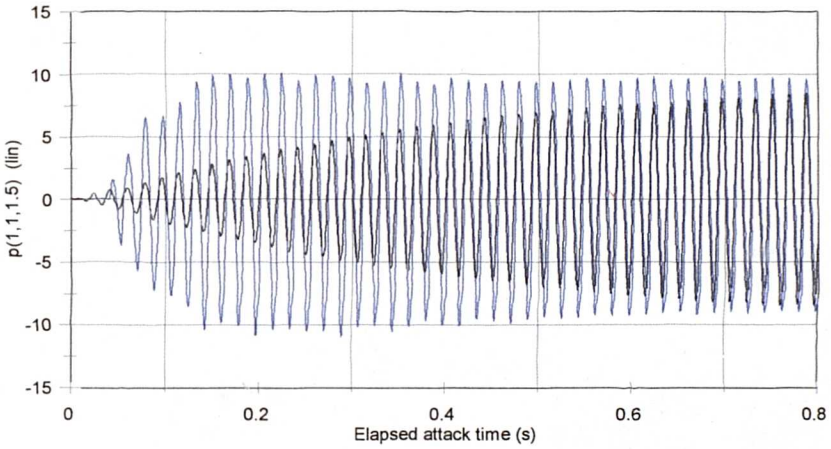

Figure 9.34 - Attack at sol^{n} pt. 'A' of mode [0,1,0]
a) Uncontrolled *b) $|p|^2 = 0.990$ for [0,1,0]*

in transfer functions measured using source location set 2 rather than set 1, which will have a bearing on the ratio of the amplitude of the dominant mode to that of the modal residues. Additionally, coupling effects between the two sources are modified by new locations, as is the fit accuracy of the measured data with the biquad model.

In order to investigate these factors further, another set of source locations were considered ('set 3' - see Appendix F), with primary and secondary sources located at (1.9, 0.3, 0.86) and (0.18, 0.23, 1.0) respectively. The primary source is in the same position as for set 2, but the control source has been repositioned in order to maximally excite *both* modes

[1,0,0] and [0,1,0]. Biquad fits of the three modes were used with an approximation of the zeroth mode to form models of the primary and secondary path transfer functions, and pole radii were modified from uncontrolled values of 0.9975 and 0.9985 to a uniform value of $|p|^2 = 0.990$ in the desired mode model. Figure 9.35 shows control at solution point *A*.

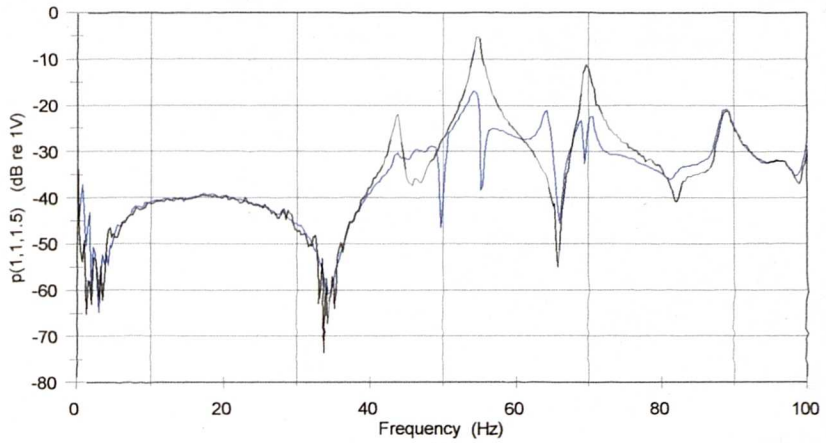

Figure 9.35 - Q-factor modification for three modes.
a) Uncontrolled b) $|p|^2 = 0.990$

Once again, decay control is hampered by the presence of a notch at around 55Hz in the steady-state frequency response. The turn-off transient of the test tone excites this notch and unpredictable control of the decay of mode [0,1,0] results. The pressure is actually *increased* by control at frequencies around 65Hz, and the anticipated smooth reduction of modal quality factor is not realised.

The question arises as to why the notch is set up with source location sets 1 and 3, but not set 2? An examination of the biquad fits of the measured transfer functions used to define the digital room model suggests that it is the fit accuracy which is responsible for errors in the steady state and decay performance of the controller. Because the notch problems and associated unpredictable control performance are due to both sources operating simultaneously rather than either path alone, we can conclude that the notch results from an unfortunate interaction of fit errors in primary and secondary paths, which has a particularly noticeable effect with the source location sets 1 and 3.

These fit errors are illustrated in Figures 9.36 and 9.37 for the secondary path of source location set 3. Errors in magnitude and particularly phase are visible around 55 and 65 Hz, which are compounded by similar errors in the primary path model and which appear to be

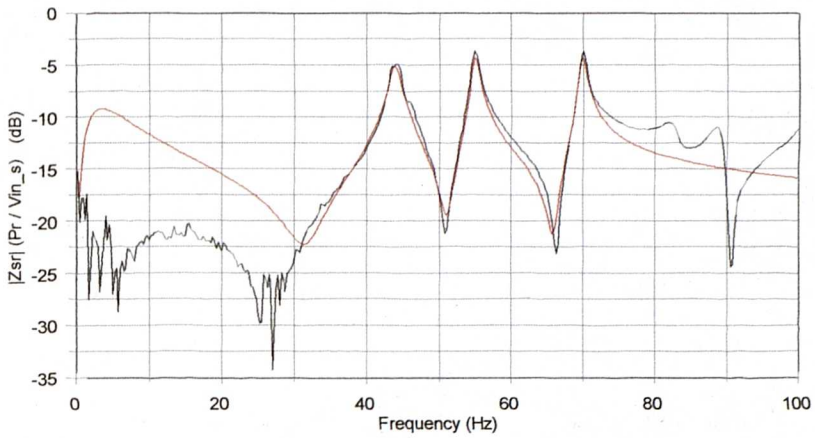

Figure 9.36 - Magnitude biquad fit of secondary path transfer function
a) Measured data *b) Biquad model*

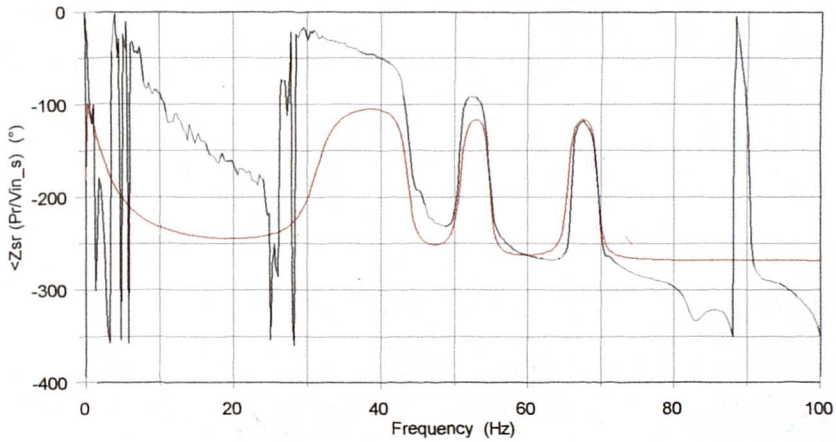

Figure 9.37 - Phase of biquad fit of secondary path transfer function
a) Measured data *b) Biquad model*

responsible for the problems with control noted in Figure 9.35. The largest cause of error between measured data and biquad models is the lack of incorporation of the transfer characteristics of the power amplifier and loudspeakers. These functions prevent the room from acting simply as the parallel sum of a number of second order sections, as assumed by the biquad model. They are responsible for the 'falling phase' characteristic noted in the measured data which is not replicated by the model. The incorporation of these transfer functions into the controller is considered in section 9.4.4 as a means of obtaining successful steady-state and decay control with source locations which otherwise give rise to unwanted characteristics in the controlled soundfield.

9.4.4 Incorporating loudspeaker bandpass functions

Primary and secondary paths both incorporate a voltage transfer function due to the power amplifier $G(j\omega)$, and loudspeaker voltage / velocity transfer functions $L(j\omega)$. If these functions were merely resistive scaling terms, then within the constraints applied by source impedance and loading / coupling the system should operate as anticipated. However, all functions are frequency dependant, and their compensation must therefore be attempted either by a) making secondary and primary path functions $G_s(j\omega)$ equal to $G_p(j\omega)$ and $L_s(j\omega)$ equal to $L_p(j\omega)$ or b) the incorporation of an appropriate compensation network into $C(j\omega)$.

In practice, it can be assumed that power amplifier voltage transfer functions $G_s(j\omega)$ and $G_p(j\omega)$ are indeed equal, and the DC zeros contained therein may be neglected. However, the electromechanical transfer characteristics of the two sources may differ significantly, and a compensation network is required. The total pressure at some receiver ***r*** is found from:

$$P_r = v_1 . \left[C(j\omega) . G_s(j\omega) . L_s(j\omega) . Z_{sr} + G_p(j\omega) . L_p(j\omega) . Z_{pr} \right] \qquad \textbf{9.1}$$

Let $G_s = G_p = G$. Then,

$$P_r = v_1 . G(j\omega) . \left[C(j\omega) . L_s(j\omega) . Z_{sr} + L_p(j\omega) . Z_{pr} \right] \qquad \textbf{9.2}$$

If measured *p/V* room transfer functions Z_{pr} and Z_{sr} have the loudspeaker responses L_p and L_s divided out from them, good biquad fits of form equivalent to true *p/u* transfer impedances are possible. In the room L_p and L_s take the form of Figure 9.5 - second order bandpass functions - rather than the complex behaviour dominated by the modal radiation load shown in Figures 7.4 and 7.5 for a loudspeaker driving the duct. It is this simple form of L_p and L_s that makes their compensation possible. One method would simply incorporate the inverse of L_p and L_s into primary and secondary path respectively, using biquad approximations for the bandpass loudspeaker functions L_p`and $L_s$`.

$$P_r = v_1 . G(j\omega) . \left[C(j\omega) . \frac{1}{L_s'(j\omega)} . L_s(j\omega) . Z_{sr} + \frac{1}{L_p'(j\omega)} . L_p(j\omega) . Z_{pr} \right] \qquad \textbf{9.3}$$

This would mean including a filter in the primary signal path where none as yet exists. Alternatively, multiplying through by L_p`

$$P_r . L_p'(j\omega) = v_1 . G(j\omega) . \left[C(j\omega) . \frac{L_p'(j\omega)}{L_s'(j\omega)} . L_s(j\omega) . Z_{sr} + L_p(j\omega) . Z_{pr} \right] \qquad \textbf{9.4}$$

By incorporating a filter into the secondary path with zeros provided by the pole locations of L_s` and poles by the pole locations of $L_p$`, the simple structure of $C(j\omega)$ should operate correctly in a room driven by real loudspeakers with bandpass electromechanical transfer characteristics. The resulting pressure on the LHS of (**9.4**) is modified from a simple modal response by function $L_p`(j\omega)$, but the additional phase implied by this modification is immaterial and the Q-factor of $L_p`(j\omega)$ compared to the Q of the room modes means the modification is acceptable in magnitude.

Functions L_p`and $L_s$` are designed using biquad fits of measured loudspeaker voltage-velocity transfer functions. The primary path data is displayed by way of example in Figures 9.38 and 9.39, and the fit parameters for a sample frequency $f_s = 4kHz$ are given in table 9.2. The improvement in fit accuracy is shown in Figure 9.40 where the biquad model for the primary path is multiplied by the loudspeaker model. In magnitude the model shows an improvement in fit at the extremes of the bandwidth of interest, and in phase (Figure 9.41)

Table 9.2 - Loudspeaker model parameters

	V/u_p parameters	V/u_s parameters
Freq Hz	40.0	40.5
Scale	2.7e-3	5.5e-3
$2re(P_i)$	1.93524	1.87237
$\|P_i\|^2$	0.94	0.880

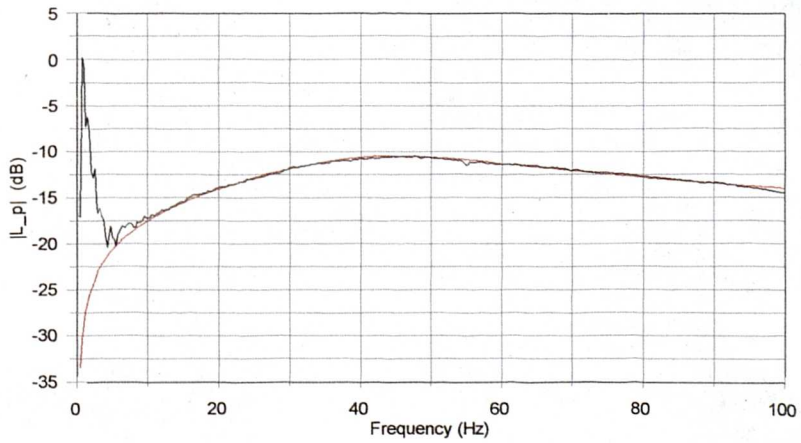

Figure 9.38 - Magnitude biquad fit of primary source voltage-velocity transfer function
a) Measured data b) Biquad model

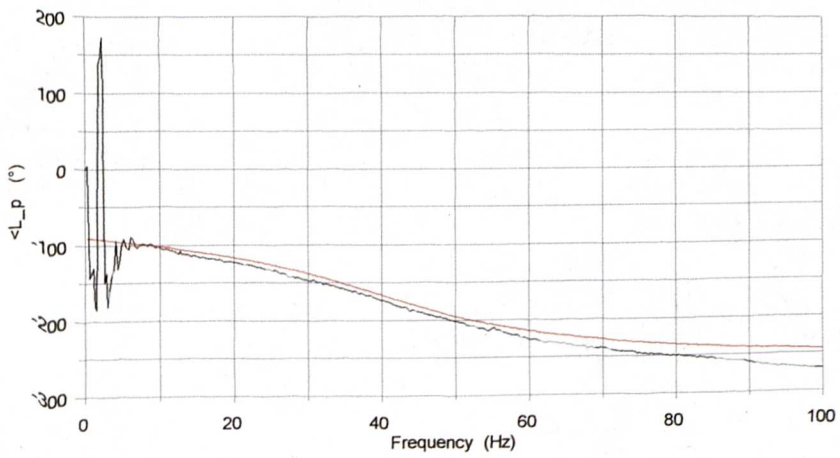

Figure 9.39 - Phase of biquad fit of primary source voltage-velocity transfer function
a) Measured data *b) Biquad model*

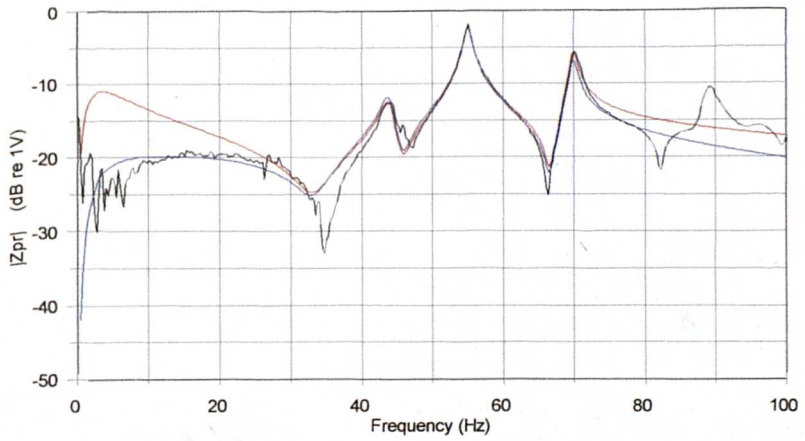

Figure 9.40 - Magnitude biquad fit of primary path transfer function
a) Measured p/V data *b) Basic Biquad model*
c) Biquad model plus driver compensation

the effect is even more evident. The falling phase characteristic of the measured data is replicated, and the accuracy of the phase fit is improved across the full bandwidth of interest. The measured data still incorporates power amplifier function $G_s(j\omega)$, which is responsible for some of the remaining discrepancy from the model. This same discrepancy is seen in the secondary path data and does not reduce the efficiency of control.

A Q-factor modification filter incorporating loudspeaker compensation after **(9.4)** was tested in the room using source location set 3. Control performance at solution point *A* is shown in Figure 9.42, and may be compared with performance without loudspeaker compensation

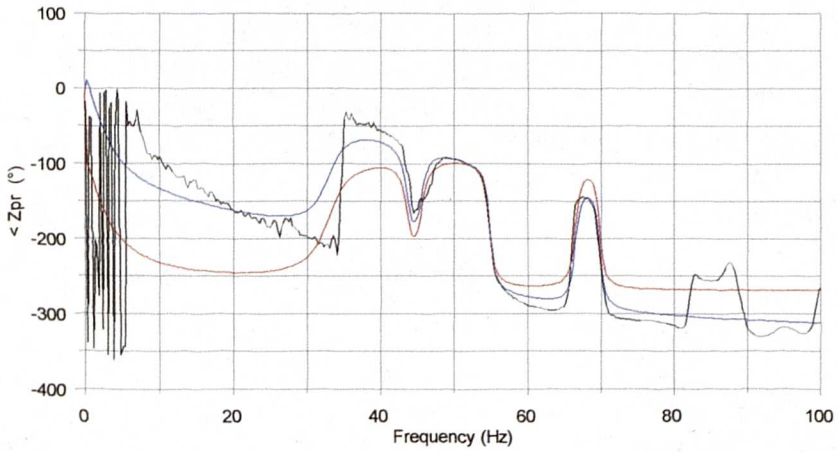

Figure 9.41 - Phase of biquad fit of primary path transfer function
a) Measured p/V data *b) Basic Biquad model*
c) Biquad model plus driver compensation

(Figure 9.34). The notch at around 55 Hz has been removed, and the resulting smooth reduction in modal quality factor is as anticipated. The control filter is able to set up a field with a smooth decay characteristic, and the problems of ringing at frequencies near that of mode [0,1,0] are removed. A new notch visible at 50Hz and an increase in pressure around 65Hz are due to fit inaccuracies in the secondary path. The filter which resulted in Figure 9.42 was a design constructed with no approximation for the zeroth mode built in; the improvement this modification makes to the secondary path biquad fit around 50 Hz and 65 Hz means that a filter incorporating the zeroth mode would be expected to substantially ameliorate the irregularities in the controlled field.

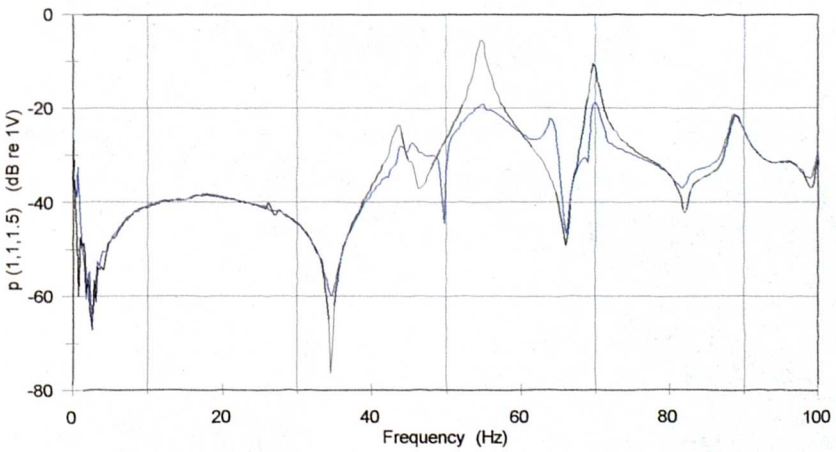

Figure 9.42 - Q-factor modification for three modes incorporating loudspeaker compensation
a) Uncontrolled *b) $|p|^2 = 0.990$*

9.5 Conclusions on Biquad Fit control in three dimensions

It has been shown that point cancellation has some effect on steady-state frequency response, but control is specific to the solution point with the exception of fortunate interactions of modal shape functions and controller transfer function. Source coupling problems experienced in the duct are very much less significant in the three-dimensional room and do not limit the utility of biquad fit control in that environment. However, complete cancellation is prevented by errors in the biquad fit, and remnant energy decays at a rate equal to that of the uncontrolled soundfield. The design of an efficient canceller using IIR sections becomes increasingly more difficult as more modes are incorporated into the filter, and this limits the application of a modal cancellation / replacement strategy to situations where only one mode is manipulated at the one time.

Q-factor modification works well in modifying time and frequency domain modal behaviour in the room. Arguably the best results are obtained when only one mode is controlled at a time, although as one attempts to reduce the impact of the mode more strongly the steady-state pressure starts to resemble the cancellation case and the decay performance suffers. Modal Q-factor reduction works for more than one mode controlled simultaneously, although the increased width of the control filter in frequency means that the secondary path may excite uncontrolled modal residues.

The practical performance of Q-factor modification in a room is limited by the accuracy of the fit of the biquad model to measured transfer impedances, and especially by the omission of loudspeaker electromechanical transfer functions. These functions distort the response (especially in phase) of the measured room transfer functions away from the anticipated parallel sum of second order bandpass sections. Depending on the choice of source locations these errors in the primary and secondary path models may create variations in the steady-state controlled sound fields which are rapid with respect to frequency, and which in turn result in long decay characteristics. Some improvement is possible by building IIR models of loudspeaker voltage-velocity transfer characteristics into the controller, and since in the three-dimensional case these functions broadly follow a bandpass form their incorporation into the IIR control filter is not difficult.

Chapter 10

Conclusions and further work

10.0 Introduction

The active control of low frequency modes has been approached in terms of adaptive Active Impedance Controllers, and non-adaptive Biquad Fit Controllers. Impedance controllers have been taken from their previous development applications in one dimensional ducts and applied in the new environment of the three dimensional room. Biquad fit controllers are a novel technology exploiting an analytical modal decomposition of a soundfield, and have been applied to both one- and three-dimensional environments.

The performance of both systems has been investigated using models and practical measurements. Conclusions regarding the outcomes of these studies are presented first in terms of the performance of each system individually, in each test environment. A comparison is then made between the systems, and recommendations suggested as to which is the most suitable control strategy in each environment. Finally, avenues for further research are suggested in terms of a number of specific recommendations together with preliminary investigative material.

10.1 Active impedance control

It has previously been shown that in the one-dimensional duct, active impedance control works successfully and in a way which ties up well with modelled predictions of system behaviour. The control task is greatly simplified in one dimension by the ease with which the requisite target impedance (which is real and frequency independent) may be specified and controlled, but in three dimensions the problem is considerably more complex.

In a room, measuring and modelling radiation impedances very close to a piston-like source presents some difficulty. The mathematics suggest that a true modal decomposition will model the measured soundfield accurately, but at low frequencies the measured pressure tends towards the familiar piston-function free field solution, perturbed by the presence of modal peaks. A true modal solution suffers convergence problems when source and receiver locations are very close together, and it is found that adding an explicit term for the direct field gives results which agree reasonably well with those measured in practice.

Active impedance controllers implementing real target impedances can be configured to produce small steady state reductions in the soundfield, corresponding to level changes of seven or eight dB at modal antinodes. The hardware implementation of a real controller used in this project is stable in a feedback configuration, with the result that useful and predictable changes in modal decay times corresponding to measured changes in quality factor may be achieved. The placement of the control source relative to the modeshape over which control is desired has a significant effect, and controllers located at modal pressure nodes are not able to control the particular mode in question.

Impedance controllers implementing a complex target impedance equivalent to the negative conjugate of the free-field radiation load on the source can be configured to produce large changes in the steady state soundfield - frequently greater than 20dB at modal antinodes. The decay performance of the complex controller is such that it is difficult to argue that the large pressure reductions result from genuine reductions in modal quality factor, and it is possible that an element of cancellation is responsible rather than simply an addition of damping. The hardware implementation of the complex controller used in this project is not stable in a feedback configuration, with the result that modifications to modal decay phases lead to somewhat unpredictable decay performance.

Since this hardware implementation is sub-optimal and can only match the desired target impedance across a narrow frequency bandwidth, it is possible that an improved filter design may overcome these limitations, and such designs are discussed in section 10.4.2 as one avenue for further investigation. At the same time, the placement of the control source relative to the primary source has a large effect - this is a feature of the eigenvectors governing the spatial distribution of sound pressure, and is unlikely to be influenced by

changes in the filter structure. As with real impedance controllers, sources located at modal pressure nodes are not able to control the particular mode in question.

Both control strategies are most effective for axial modes which are widely separated in frequency from each other. Effectiveness is increased when the control source is coupled as strongly as possible into the resonant modeshape over which control is required. Modes which are closely spaced in frequency, or degenerate, present a problem to the controller, when neither steady-state nor decay performance modifications are particularly significant.

10.2 Biquad fit control

In a duct, theory suggests that the performance of Biquad fit control is predictable for small desired reductions in modal Q-factor, and may be compromised as the desired termination impedance approaches characteristic value. The modelled performance of the controller is to some extent governed by the number of built-in modes. More significantly, fundamental limitations in the accuracy of a modal decomposition with non-rigid boundary conditions limit the success of models of Biquad fit control. The applicability of cosine modeshape functions is called into question, and distortions in z-plane bandpass transfer functions with low Q-factor also come into play. In a theoretical investigation of Biquad fit control in a one-dimensional duct it appears that these factors will limit the applicability of the control technique as the desired Q-factor of the modes is made smaller and smaller.

In practice, Biquad fit control in the duct is not defeated by these problems with the modal decomposition, but by characteristics of the practical sources used to implement control in the laboratory. Limited source impedance and the strongly modal nature of the in-duct radiation load result in coupling between primary and secondary paths in such a way that off-line system characterisation measurements do not follow a simple bandpass form. Since the biquad fit technique was designed specifically as a novel exploitation of the second-order bandpass characteristic of the normal modes of a space, its use is no longer appropriate where the functions describing a particular system do not follow this pattern.

In a room, these fit problems are less significant. It is possible to reduce the impact of modal artefacts by a cancellation / replacement strategy, or by the direct specification of

desired modal Q-factors. Point cancellation has some effect on steady-state responses, but control is specific to the solution point with the exception of fortunate interactions of modal shape functions and controller transfer function. Complete cancellation is prevented by errors in the biquad room model, and remnant energy decays at a rate equal to that of the uncontrolled soundfield. The design of an efficient canceller becomes increasingly more difficult as more modes are built into the filter; this limits the modal cancellation / replacement strategy to applications where only one mode is manipulated at the one time.

Q-factor modification works well in modifying time and frequency domain modal behaviour in the room. Arguably the best results are obtained when only one mode is controlled at a time, although as one attempts to reduce the impact of the mode more strongly the steady-state pressure starts to resemble the cancellation case and the decay performance suffers. Modal Q-factor reduction works for more than one mode controlled simultaneously, although the increased bandwidth of the control filter in frequency means that the secondary path may excite uncontrolled modal residues.

Practical performance in the room is limited by accuracy of the fit of the biquad model to measured transfer impedances, in terms of the inclusion of residues of higher modes and especially by the omission of loudspeaker electromechanical transfer functions. These functions change the response (especially in phase) of the measured room response, away from the anticipated parallel sum of second order bandpass sections. Depending on the choice of source locations these errors in the primary and secondary path models may create variations in the steady-state controlled soundfields which are rapid with respect to frequency, and which in turn result in long decay characteristics. Some improvement is possible by building IIR models of loudspeaker voltage-velocity transfer characteristics into the controller, and since in the room these functions broadly follow a bandpass form their incorporation into the IIR control filter is not difficult.

It has been suggested that system identification methods may offer a route by which IIR filters may be fitted to simulated transfer impedances. The aim is to improve the accuracy of the model and therefore control performance, while maintaining simplicity and efficiency in real-time operation. This refinement is discussed in section 10.4.2 as a suggestion for further investigation, along with the results of preliminary models using the technique.

10.3 Comparison between active impedance and biquad fit control

In the duct, the best performance results from the use of Active Impedance Control with real target impedances. This impedance is easily specified and controller performance is predictable in both frequency and time domains. In contrast, Biquad fit control suffers from limitations due to finite source impedance which make its application impracticable. One obvious application for an actively controlled duct is for the testing of small electroacoustic transducers such as hearing aids. Passive techniques require terminations built from successive layers of absorbent of increasing density, and carry high space penalties.

In the room, Active Impedance and Biquad Fit techniques offer alternative methods for the reduction of modal artefacts in steady state and decay responses. Biquad fit control has the advantage of a very modest hardware requirement - simply a number of IIR filter sections - and has been shown to offer useful performance in steady-state and decay phases. The fixed filtering technique exhibits no problems associated with filter convergence, and provided the solution is formed at a location at which a stable secondary path inverse exists there are no stability issues. The performance is however subject to errors in the biquad room model, and is to some extent spatially limited to the solution point at which this model is formed.

Simultaneous control over a number of modes is possible using Q-factor modification, and typical performance data is given in Chapter 9. Where narrow notches in the steady-state controlled response are avoided by careful source placement and /or the incorporation of electromechanical source characteristics into the controller, modal pressure reductions of more than 20dB have been demonstrated with corresponding reductions in modal decay time of the order of a factor of ten.

Active impedance control can also give large steady state pressure reductions with complex target impedances, but this risks unpredictable decay performance and the controller may exhibit cancellation rather than absorption. Measurements suggest similar steady-state reductions may be achieved as those obtained using biquad fit control (around 20dB on the modes), although the sub-optimal nature of the impedance control implementation means that the bandwidth over which control is effective is reduced. Limitations in the filter implementation also make it difficult to draw a direct comparison between the decay

performance of the two techniques. It has been shown that complex impedance control is capable of large, measurable reductions in modal decay time, but the controlled decays exhibit irregularities which are not present in the biquad fit results.

At this stage of development it appears that biquad fit systems offer more predictable steady-state and decay control. Impedance controllers implementing real target impedances offer smaller steady-state reductions (around 8dB), but decay performance is more predictable than for the complex case, and where larger controlled surfaces are practicable it appears that the benefit of control may be significant. With a controlled surface area four times that of the secondary source used with the biquad fit controller, modal decay time may be reduced by a factor of around 3. This compares unfavourably to the reduction obtained using biquad fit control - however further measurements are required to compare the spatial extent over which the two systems operate. It appears likely that optimum decay performance for the biquad fit controller may be limited to an area surrounding the solution point - an investigation into the theoretical spatial limit of damping control using a single secondary source is suggested as one avenue of further work.

10.4 Further work

10.4.1 Optimum control of damping using a single secondary source

In section 8.1 the results of Nelson and Elliot [12] were discussed, which show that in a three-dimensional pressure minimisation context a single control source may only be expected to completely cancel one modal contribution to the sound field. This is in contrast to the one-dimensional case, where with careful placement a degree of control may be exerted over all modes. These results inform the present study, but do not apply directly as our concern is with *damping* control whose aim is the reduction of modal quality factor.

In deriving a theoretical spatial limit of control, Nelson and Elliot's analysis is based on the minimisation of a cost function equal to total time-averaged acoustic potential energy. This cost function is not directly applicable to a consideration of modal damping, even though results in the duct suggest that in frequency the two control tasks may appear to have similar outcome. What is required then is the specification of an appropriate cost function related to the performance of a damping controller. This might take the form of an expression related to the Q-factor or decay time of a number of modal contributions, summed in some

manner to reflect the spatial distribution of modal pressure throughout the room volume. The cost function will be minimised to determine the theoretical spatial limit of damping control resulting from the use of a single control source.

Some preliminary work (section 8.4.1) has involved attempts to minimise the spatial variance of pressure throughout the room volume (rather than its absolute magnitude). This relates to the control of damping, since reductions in modal Q-factor will result in reduced scaling of eigenvectors and therefore lower spatial pressure variance. A variance of zero throughout a room volume cannot be achieved, but the function has potential in defining the optimal spatial control of damping achievable using one control source.

10.4.2 Using System Identification methods

In certain environments such as the duct, it has been shown that the Biquad fit technique is defeated by changes in the radiation load on the sources between system characterisation and run-time. This means that the filter structure can no longer exploit a second-order modal decomposition of the soundfield into parallel biquad sections, and so the technique fails. However, the optimal source strength relationships derived in Chapter 7 and the mathematics concerned with the accommodation of source coupling are still valid, and it would not seem unreasonable to pursue an alternative feedforward filter structure which incorporates this work without relying exclusively on second order bandpass functions.

The technique of System Identification [eg. 96] has been suggested as a way forward, where measured complex transfer functions are fitted with an n^{th} order filter approximation. This fit process follows a least-squares method, such that the expression (**10.1**) is minimised by the optimisation of zero and pole coefficient vectors *b* and *a*.

$$\sum_{k=1}^{n} wt(k) \left| h(k) - \frac{B(w(k))}{A(w(k))} \right|^2 \qquad \textbf{10.1}$$

$A(w(k))$ and $B(w(k))$ are the Fourier transforms of the polynomials a and b at frequency $w(k)$

n is the number of frequency points

$h(k)$ is the k^{th} point in the measured complex transfer function

$wt(k)$ is a vector allowing error weighting in the frequency domain

This process has been carried out for the primary duct transfer function shown in Figure 7.14 - results are shown in Figure 10.1. It can be seen that the model is far superior to that achieved using four biquad sections in the earlier work, and it might be hoped that such a model could form the basis for a more effective control filter. This may be so, but a number of caveats apply, which must be considered before such a controller can be designed.

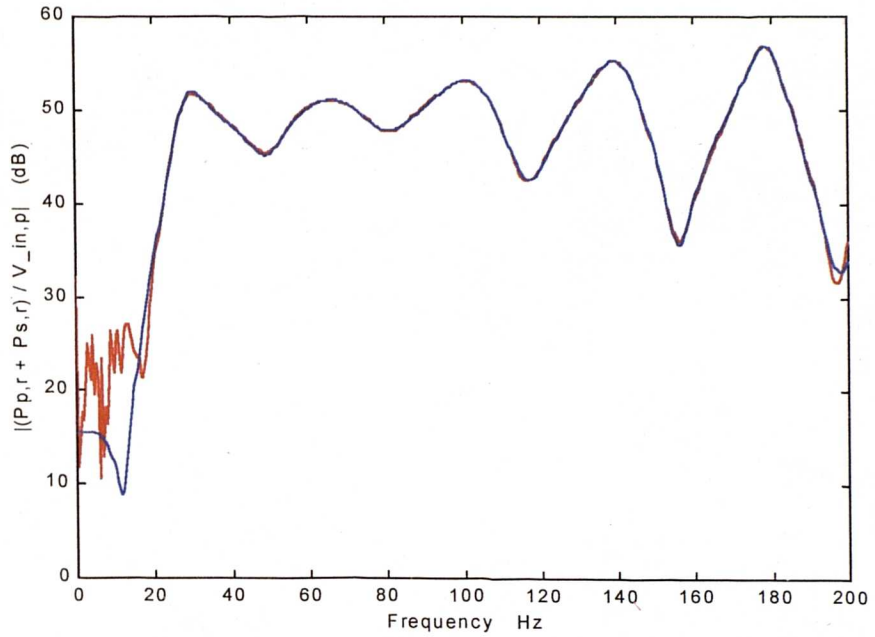

Figure 10.1 - Duct primary transfer functions P/V_{in}
a) measured b) fitted with 14th order IIR filter

It must first be noted that the polynomials defining the filter in Figure 10.1 are of order 14, compared to the 8th order design of Chapter 7. This increase in complexity accomplishes the desired improvement in model accuracy; however as well as an increase in Filter *order*, the *structure* of the model has been altered. Whereas the biquad fit models exploit an analytical modal decomposition to derive a parallel filter structure, the order 14 polynomials implemented in Figure 10.1 form a cascade. An eighth order cascade design optimised using **(10.1)** has performance inferior to the parallel biquad design of Figure 7.14 - in the latter filter the exploitation of a physical model of the measured transfer function enables a more intelligent placement of the small number of available poles and zeros.

The adoption of a cascade design also means that the Q-factor modification scheme introduced in Chapter 5 is no longer appropriate. The solution of equations **(5.18)** to **(5.22)** requires that the soundfield is described by a number of parallel filter sections with distinct

conjugate poles and common zeros at DC and $f_s/2$.(It is however possible that in some circumstances the high-order polynomials resulting from the minimisation of **(10.1)** may be broken up into the addition of a number of partial fractions representing a parallel bank of filters of lower order).

Figure 10.2 shows the locations of the poles and zeros resulting in the response of Figure 10.1 . One strongly negative real zero has been omitted, so as to preserve appropriate scaling for the remainder of the data. The distribution of poles and zeros is no longer derived using a physical model of the acoustic space - their location is simply that most appropriate for the minimisation of **(10.1)**. Whilst this filter format is no longer suitable as a basis for Biquad fit control as introduced in Chapter 5, it may form a useful model for an alternative controller; similar techniques are used in the work of Mourjopoulos [eg 62] to name only one instance. One immediately apparent use for these filters is in the description of the desired impedance filter F_d required for complex active impedance control.

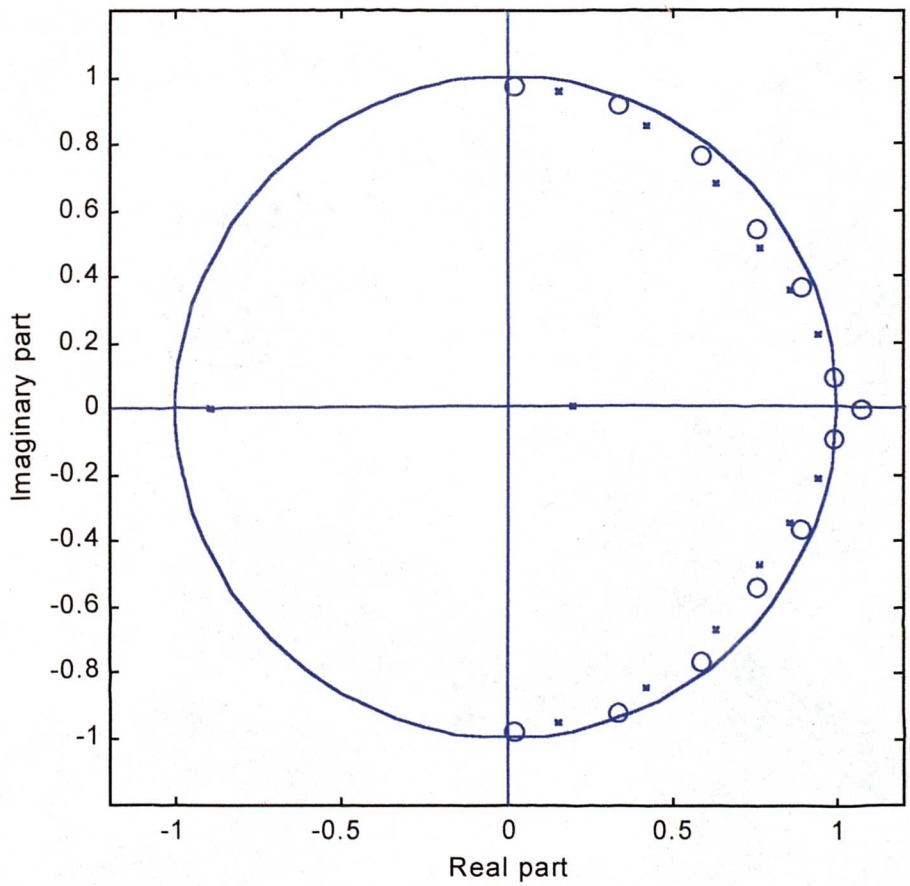

Figure 10.2 - Pole/Zero locations resulting in filter response of 10.1

10.4.3 Further investigations using active impedance controllers

The complex impedance control implementations introduced in this Thesis are limited, since they only allow correct impedance specification across a very narrow frequency bandwidth. As a result, control filters are not stable in a feedback configuration, and it has not been possible to quantify the optimal decay performance of the filter. A more sophisticated (ie longer) FIR or IIR design for the desired impedance filter F_d could be expected to rectify the stability problem and allow feedback operation, giving control over a broader bandwidth and allowing controlled decay comparisons with Biquad fit controllers.

Filter F_d might be efficiently defined using the system identification techniques introduced in section 10.4.2. Decay comparisons should be made throughout the room volume and not simply in the vicinity of the solution point used to design the Biquad fit controller. A theoretical appreciation of the possible extent of global damping control using a single secondary source (section 10.4.1) would then prove useful.

This theoretical limit of control would also define maximum performance objectives for real controllers. Preliminary investigations have shown that real impedance controllers do not have to follow an adaptive filter topology. Because the desired outcome of control is a real transfer function relating cone pressure and velocity, it should be possible to base a controller around a simple feedback network where cone pressure is used as the input to a filter which derives a signal to drive the cone to the appropriate in-phase velocity. This idea bears some resemblance to published work by Clark and Cole [46]. Such a system is obviously subject to stability requirements and the feedback loop gain must be carefully controlled to ensure the Nyquist criterion is obeyed. Initial attempts at an implementation have resulted in unstable operation, but if such a filter could be realised it would give all the benefits of the real Active Impedance Controller with significantly reduced hardware cost.

Sources with active impedance control which radiate directly should be compared to hybrid passive / active porous devices such as those introduced by Furstoss *et al* [55]. The hardware necessary for their construction already exists as a product of this research, and it would be interesting to examine the performance of hybrid systems in a test room and to establish if simplification of the control filter is possible whilst retaining good low-frequency performance.

The combination of the results presented here with those of Mercy [95] should be attempted when the latter become available, in relation to the importance of controller active area to performance. It may be that real impedance controllers covering a significant proportion of the room boundary offer the best spatial control over room modes, and the models introduced in this work could be employed to determine optimum target impedance for the best steady-state and decay performance.

10.4.4 Further investigations using Biquad controllers

Biquad fit controllers have been produced which offer useful performance, and the importance of the inclusion of models for driver electromechanical response and the zeroth mode model has been established. Further work should be undertaken to investigate the ensuing benefit to controller performance if large numbers of higher modal residues are included in the room models, as a function of source location and control task. To this end, a numerical optimisation of the biquad fit parameters would be useful to replace the present manual procedure, possibly using an adaptation of the least-squares method introduced in section 10.4.2.

Following this investigation, it would be beneficial to establish whether controller performance can be improved by adoption of Morse and Bolt - type cosh scale factors, with a resulting requirement to design filter sections with phase delays based on the complex-valued modeshapes. A refinement of the treatment of source coupling may offer a more profitable route to improving controller performance, and might be simultaneously investigated. The ultimate goal might be the construction of a compact low-frequency radiator containing primary and control source, with a measurement microphone incorporated for system characterisation and automated mode fitting / desired pole specification.

References

[1] 'Sound System Equipment, Part 13 : Listening tests on Loudspeakers,' International Electrotechnical Commission IEC 268-13 (1985)

[2] Newell, P.R., Holland, K.R., Hidley, T. 'Control Room Reverberation is Unwanted Noise.', *Proc. IOA* 16(4) (1994) pp365-373

[3] Olive, S.E., Schuck, P.L., Ryan, J.G., Sally, S.L., Bonneville, M.E. 'The Detection Thresholds of Resonances at Low Frequencies', *J. Audio Eng. Soc.*, 45(3) (1997) pp116 - 127

[4] Morse, P.M., Bolt, R.H., 'Sound waves in rooms', Reviews of modern physics 16(2) (1944) pp 69-150

[5] Bullmore, A.J., 'The active minimisation of harmonic enclosed sound fields with particular application to propeller induced cabin noise', PhD. Thesis, Southampton (1987)

[6] Morse, P.M., 'Vibration and Sound', McGraw-Hill (1948) pp389-413

[7] Morse, P.M., Feshbach, H., 'Methods of Theoretical Physics', McGraw-Hill, (1953)

[8] Morse, P.M., Ingard, K.U., 'Theoretical Acoustics', Princeton, New Jersey (1986)

[9] Doak, P.E., 'Fluctuations of the Sound Pressure Level when the Receiver position Is Varied', Acustica 9(1) (1959) pp1-9

[10] Kinsler, L.E., Frey, A.R., 'Fundamentals of Acoustics' (2nd ed.) Wiley, New York (1962)

[11] Kuttruff, H., 'Room Acoustics', (2nd ed.) Applied Science Publishers, Barking (1973)

[12] Nelson, P.A., Elliott, S.J., 'Active Control of Sound', Academic Press, London, (1993)

[13] Leug, P., 'Verfahren zur Dämpfung von Schallschwingungen', DRP (German Patent) No. 655 508 Filed: 27 January 1933 Patented: 30 December 1937

[14] Guiking, D., 'On the invention of active noise control by Paul Leug', J.Acoust.Soc.Am. 87(5) (1990) pp2251-2254.

[15] de Heering, P., 'Comments on 'On the invention of active noise control by Paul Leug' ', J.Acoust.Soc.Am. 93(5) (1993) p2989

[16] Warnaka, G.E., Zalas, J.M., Tichy, J., Poole, L.A., 'Active control of noise in interior spaces', Proc. Internoise 83 (1983) pp 415-418

[17] Curtis, A.R.D., Nelson, P.A., Elliot, S.J., Bullmore, A.J., 'Active suppression of acoustic resonance', J.Acoust.Soc.Am.81(3) (1987) pp 624-631

[18] Nelson, P.A., Curtis, A.R.D., Elliot S.J., Bullmore A.J., 'The active minimisation of harmonic enclosed soundfields 1. Theory', JSV 117(1) (1987) pp 1-13

[19] Aitken, A.C., 'Determinants and matrices', Oliver and Boyd, London (1951)

[20] Schroeder, M.R., Kuttruff, K.H., 'On frequency response curves in rooms', J.Acoust.Soc.Am.34 (1962) pp 76-80

[21] Bullmore A.J., Nelson, P.A., Curtis, A.R.D., Elliot S.J., 'The active minimisation of harmonic enclosed soundfields 2. A computer simulation', JSV 117(1) (1987) pp 15-33

[22] Elliot S.J., Curtis, A.R.D., Bullmore A.J., Nelson, P.A., 'The active minimisation of harmonic enclosed soundfields 3. Experimental verification', JSV 117(1) (1987) pp 35-58

[23] Nelson, P.A., Hammond, J.K., Elliot, S.J., 'Analytical approaches to the active control of stationary random enclosed sound fields', Proc. Internoise 88 (1988) pp 959-962

[24] Maa, D.Y., 'Potential Active Noise Control in Enclosures', Proc. Inter-Noise 91 (1991) pp 629-632

[25] Maa, D.Y., 'Soundfield in a room and its active noise control', Applied Acoustics 41 (1994) pp 113-126

[26] Johnson, M.E., Elliot, S.J., 'Measurement of acoustic power output in the active control of sound', J.Acoust.Soc.Am. 93(3) (1993) pp1453-1459

[27] David, A., Elliot, S.J., 'Numerical Studies of Actively Generated Quiet Zones', Applied Acoustics 41 (1994) pp63-79

[28] Joseph, P., Elliot, S.J., Nelson, P.A., 'Near field zones of quiet', JSV 172(5) (1994) pp602-627

[29] P. Herzog, A. Soto-Nicolas, F. Guery, 'Passive and active control of the low-frequency modes in a small room,', Presented at 98th AES Convention, Preprint 3951(D1), Paris (1995)

[30] Ferekidis, C., Kempe, U., 'Room Mode Excitation of Dipolar and Monopolar Low-Frequency Sources', Presented at 100th AES Convention, Preprint 4193, Copenhagen (1996)

[31] Kuo, S.M., Morgan, D.R., 'Active Noise Control: A Tutorial Review', Proc. IEEE 87 (6) (1999) pp 943-973

[32] Olson, H.F., May, E.G., 'Electronic sound absorber', J.Acoust.Soc.Am.25 (1953) pp1130-1136

[33] Ford, R.D., 'Where does the power go?', Proc. Of 11th ICA, Paris Vol 8 (1983) pp277-280

[34] Guiking, D., Karcher, K., Rollwage, M., 'Active control of the reflection coefficient at low frequencies', Proc. Internoise 83 (1983) pp 419-422

[35] Guiking, D., Karcher, K., Rollwage, M., 'Coherent active methods for applications in room acoustics', J.Acoust.Soc.Am.78 (1985) pp1426-1434

[36] Elliot, S.J., Joseph, P., Nelson, P.A., Johnson, M.E., 'Power output minimisation and power absorption in the active control of sound', J.Acoust.Soc.Am.90 (1991) pp 2501-2512

[37] Nicholson, G.C., Darlington, P., 'Smart Surfaces for Building Acoustics', Proc. IOA 13(8) (1991) pp 155-164

[38] Darlington, P., Nicholson, G.C., 'Theoretical and practical constraints on the implementation of active acoustic boundary elements', Proc. Second Intl. Congress on Recent Developments in Air- and Structure-Borne Sound and Vibration. (1992) pp 1011-1018

[39] Orduna-Bustamante, F., Nelson, P.A., 'An adaptive controller for the active absorption of sound', J.Acoust.Soc.Am. 91 (1992) pp 2740-2747

[40] Chung, J.Y., Blaser, D.A., 'Transfer function method of measuring in-duct acousic properties', J.Acoust.Soc.Am. 68 (1980) pp907-921

[41] Nicholson, G.C., Darlington, P., 'Active control of acoustic absorption, reflection and transmission', Proc.IOA 15(3) (1993) pp 403-409

[42] Mazzola, C.J., 'Active Sound Absorption', NAMLAK, New York, 1993.

[43] Snyder, S.D., Tanaka, N., 'To absorb or not to absorb: Control source power output in active noise control systems', J.Acoust.Soc.Am. 94(1) (1993) pp185-195

[44] Darlington, P. 'Suppressing room modes using active absorbers', Proc. IOA 16(4) (1994) pp 389-401

[45] Darlington, P., Nicholson, G.C., Mercy, S.E., 'Input transduction errors in active acoustic absorbers', Acta Acustica 3 (1995) pp 345-349

[46] Clark, R.L., Cole, D.G., 'Active damping of enclosed sound fields through direct rate feedback control', J.Acoust.Soc.Am.97(3) (1995) pp1710-1716

[47] Clark, R.L., Gibbs, G.P., 'Analysis, testing, and control of a reverberant sound field within the fuselage of a business jet', J.Acoust.Soc.Am.105(4) (1999) pp 2277-2286

[48] Schroeder, M., 'Die Statistischen Parameter der Frequenzkurven von Grossen Räumen', Acustica 4 (1954) pp 594-600

[49] Schroeder, M., Kuttruff, K.H., 'On Frequency Response Curves in Rooms. Comparison of Monte Carlo Results for the Average Frequency Spacing between Maxima', J.Acoust.Soc.Am.34(1) (1962) pp 76-80

[50] Darlington, P., Avis, M..R., 'Noise control in resonant soundfields using active absorbers', Proc. Internoise 96 (1996) pp1121-1126

[51] Darlington, P., 'Active boundary control of enclosed sound fields', Proc. Internoise 96 (1996) pp1127-1132

[52] Avis, M.R., Darlington, P., 'Modifying Low Frequency Room Acoustics 1: Local Active De-Reverberation', Proc. IOA 17(7) (1995) pp 77-86

[53] Darlington, P., Avis, M.R., 'Modifying low frequency room acoustics 2: global control using active absorbers', Proc. IOA 17(7) (1995) pp 87-96

[54] Darlington, P., Avis, M.R., 'Time Frequency Response of a Room with Active Acoustic Absorption', Presented at 100th AES Convention, Preprint 4192(H-5), Copenhagen (1996)

[55] Furstoss, M., Thenail, D., Galland, M.A., 'Surface impedance control for sound absorption: direct and hybrid passive/active strategies', JSV 203(2) (1997) pp219-236

[56] Gentry, C.A., Guigou, C., Fuller, C.R., 'Smart foam for applications in passive-act radiation control', J.Acoust.Soc.Am. 101(4) (1997) pp1771-1778

[57] Neely, S.T., Allen, J.B., 'Invertibility of a room impulse response', J. Acoust. Soc. Am. 66(1) (1979) pp 165-169

[58] Mourjopoulos, J., 'On the variation and invertibility of room impulse response functions', JSV 102(2) (1985) pp217-228

[59] Mourjopoulos, J., Paraskevas, M.A., 'Pole and zero modelling of room transfer functions', JSV 146(2) (1991) pp281-302

[60] Elliot, S.J., Nelson, P.A., 'Multiple-Point Equalisation in a Room Using Adaptive Digital Filters', J.Audio.Eng.Soc. 37(11) (1989) pp899-907

[61] Elliot, S.J., Bhatia, L.P., Deghan, F.S., Fu, A.H., Stewart, M.S., Wilson, D.W., 'Practical Implementation of Low-Frequency Equalisation Using Adaptive Digital Filters', J. Audio Eng. Soc. 42(12) (1994) pp988-998

[62] Mourjopoulos, J., 'Digital Equalisation of Room Acoustics', J. Audio Eng. Soc. 42(11) (1994) pp884-900

[63] Haneda, Y., Makino, S., Kaneda, Y., 'Multiple-Point Equalisation of Room Transfer Functions by Using Common Acoustical Poles', IEEE Transactions on Speech and Audio Processing 5(4) (1997) pp 325-333

[64] Bücklein, R., 'The Audibility of Frequency Response Irregularities' (1962) reprinted in English in J. Audio Eng. Soc., 29, (1981) pp 126-131

[65] Toole, F.E., Olive, S.E., 'The Modification of Timbre by Resonances: Perception and Measurement', J. Audio Eng. Soc., 36(3) (1988) pp122-141

[66] Olive, S.E., Schuck, P.L., Sally, S.L., Bonneville, M.E., 'The Effects of Loudspeaker Placement on Listener Preference Ratings', J. Audio Eng. Soc., 42(9) (1994) pp651-669

[67] Salava, T., 'Sources of the Constant Volume Velocity and their use for Acoustic Measurements', J. Audio Eng. Soc., 22(3) (1974) pp146-153

[68] Salava, T., 'Acoustic Load and Transfer Functions in Rooms at Low Frequencies', J. Audio Eng. Soc., 36(10) (1988) pp763-774

[69] Davies, P.O.A.L., 'An Introduction to Dynamic Analysis and Automatic Control', Wiley, London, (1965)

[70] Abramowitz, M., Stegun, I.A., 'Handbook of Mathematical Functions', Dover, New York, (1965)

[71] Widrow, B., Stearns, S.D., 'Adaptive Signal Processing', Prentice Hall, Englewood Cliffs, (1985)

[72] Nicholson, G.C., 'The Active Control of Impedance', PhD Thesis, University of Salford, (1995)

[73] Boucher, C.C., Elliot, S.J., Nelson, P.A., 'The Effects of Modelling Errors on the Performance and Stability of Active Noise Control Systems', Recent Advances in Active Control of Sound and Vibration, Virginia State University, Technomic Publ. (1) pp291-301

[74] 'Technical notes on the use of the BU1771 accelerometer cartridge', Knowles Electronics Company, Burgess Hill (1982)

[75] Ericksson, L.J., Allie, M.C., 'Use of random noise for on-line transducer modelling in an adaptive active attenuation system', J.Acoust.Soc.Am. 85(2) (1989) pp797-802

[76] Elliot, S.J., Stothers, I.M., Nelson, P.A., 'A Multiple Error LMS Algorithm and Its Application to the Active Control of Sound and Vibration' IEEE Trans. Acoust., Speech, Sig. Proc. Vol. ASSP-35, (1987) pp 1423-1434

[77] Lynn. P.A., Fuerst, W., 'Introductory digital signal processing', Wiley Chichester, (1994)

[78] N.A. Halliwell, "Laser-Doppler Measurement of Vibrating Surfaces: A Portable Instrument", J. Sound and Vibration, 62 (1979) pp.312 - 315

[79] Elliot, S.J., Anthony, D.K., 'A Comparison of Three methods of measuring the Volume velocity of an Acoustic Source', J. Audio Eng. Soc., 39(5) (1991) pp355-365

[80] Bies, D.A., Hansen, C.H., 'Engineering Noise Control', Unwin Hyman, London (1988)

[81] Beranek, L.L., 'Acoustic Measurements', Wiley, New York (1949)

[82] ISO 10534 - 1:1996 , 'Acoustics - Determination of sound absorption coefficient and impedance in impedance tubes - Part 1 : Method using standing wave ratio'

[83] Walker, R., 'The measurement of time-frequency responses in small rooms', Proc. IOA 20(5) (1998) pp 59-69

[84] Bergman, J.M., Fincham, L.R., 'The Application of Digital Techniques to the measurement of Loudspeakers', J. Audio Eng. Soc., 25 (1977) pp370-384

[85] Silcox, R.J., Elliot, S.J., 'Applicability of superposition and source impedance models of active noise control systems', Proc. Internoise '85 (1985) pp587-590

[86] Small, R.H., 'Closed Box Loudspeaker Systems Part 1: Analysis', J. Audio Eng. Soc., (Dec.1972) reprinted in AES 'Loudspeakers' anthology pp271-281

[87] Beranek, L.L., 'Acoustics', McGraw-Hill, New York (1954)

[88] Crandall, I.B., 'Theory of Vibrating Systems and Sound', MacMillan and Co., London, (1927)

[89] Lyon, R.H., 'Statistical analysis of power injection and responses in structures and rooms', J.Acoust.Soc.Am. 45 (1969) pp 545-565

[90] Harris, N., Hawksford, M.O., 'The Distributed-Mode Loudspeaker (DML) as a Broad-Band Acoustic Radiator', Presented at 103rd AES Convention, Preprint 4526(D-6), New York (1997)

[91] Maa, D.Y., 'Formulae of sound field in enclosures', Letter, Chinese Journal of Acoustics 8(4) (1989) pp373-375

[92] Darlington, P., Avis, M.R., 'Improving listening conditions in small built spaces using active absorbers', Proc. Active '95 (1995) pp 519-528

[93] Roederer, J.G., 'The Physics and Psychophysics of Music', Springer-Verlag New York, (1995)

[94] Zha, X, Fuchs, H.V., Nocke, C., Han, X. 'Measurement of an effective absorption coefficient below 100 Hz', IOA Bulletin v24 no1 (1999) p5-10

[95] Mercy, S.E., 'The modelling of active impedance surfaces', M.Phil Thesis, University of Salford (1999)

[96] Dennis, J.E., Schnabel, R.B., 'Numerical methods for unconstrained optimization and nonlinear equations', Prentice Hall, Englewood Cliffs NJ, (1983)

Appendix A

Drive unit characteristics

KEF B200 Velocity / Voltage Transfer Functions

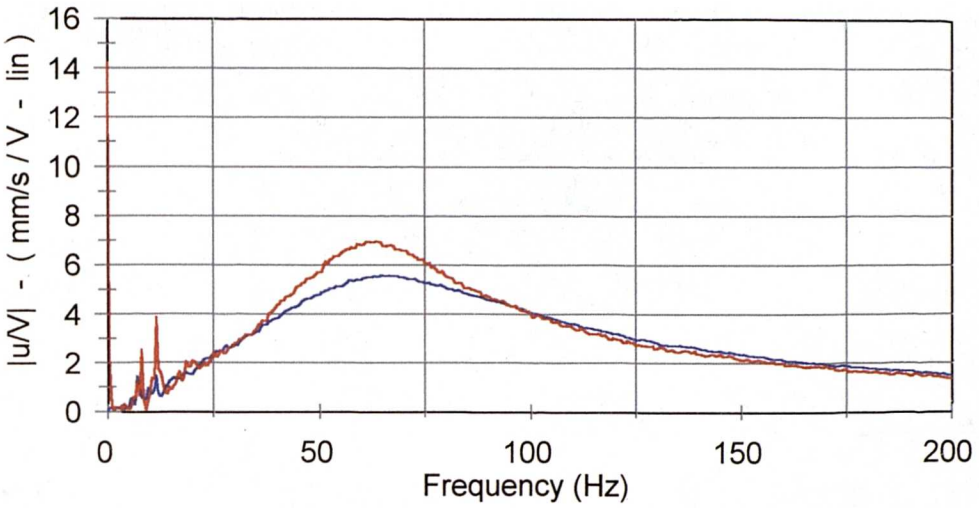

Figure A1: - Magnitude velocity / voltage transfer function: a) Unit 1 b) Unit 2

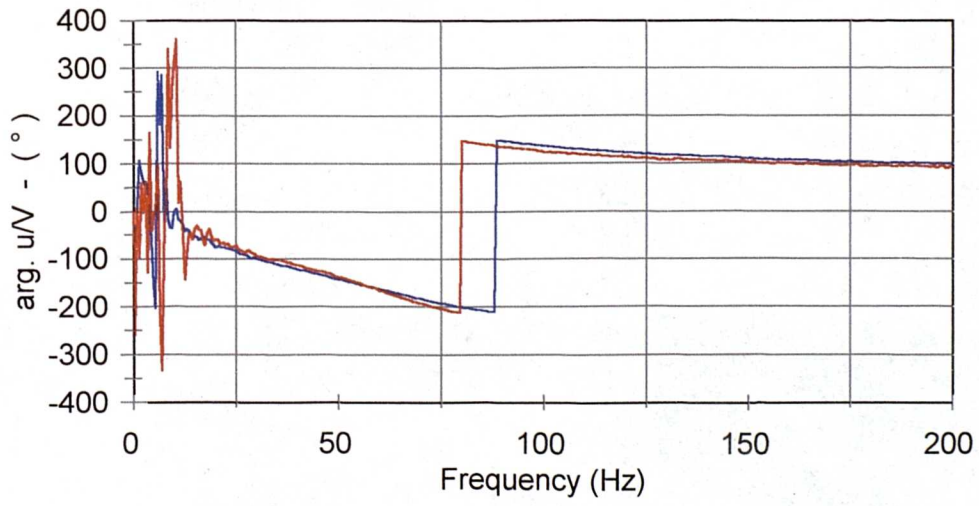

Figure A2: - Phase of velocity / voltage transfer function: a) Unit 1 b) Unit2

KEF B200 Small Signal Parameters

Measurements were made using the MLSSA maximum-length sequence signal analyser, using an added-mass method. Although this method gives results which can differ from measurements made using sinusoidal excitation, variation in the values of parameters such as the driver-suspension resonance f_s with MLS stimulus amplitude suggest differences are due to the higher power embodied within one pure-tone signal. Small-signal parameter measurements are only indicative as a model of practical driver behaviour, and are included here to facilitate comparison between the two drive units.

Unit1		**Unit2**	
Title: Measured Data		Title: Measured Data	
Method: Mass-loaded (8.00 grams)		Method: Mass-loaded (8.00 grams)	
DCR mode: Measure (-0.13 ohms)		DCR mode: Measure (-0.13 ohms)	
Series resistance: 75.00 ohms		Series resistance: 75.00 ohms	
Stimulus level: 1.00 volts		Stimulus level: 1.00 volts	
0.255	RMSE-free Ohms	0.558	RMSE-free Ohms
65.178	Fs Hz	64.568	Fs Hz
6.783	Re Ohms[dc]	6.888	Re Ohms[dc]
23.041	Res Ohms	63.951	Res Ohms
4.29	Qms	13.845	Qms
1.263	Qes	1.491	Qes
0.976	Qts	1.346	Qts
0.513	L1 mH	0.472	L1 mH
0.831	L2 mH	0.884	L2 mH
2.503	R2 Ohms	3.124	R2 Ohms
0.191	RMSE-load Ohms	0.317	RMSE-load Ohms
21.254	Mms grams	20.979	Mms grams
280.54	Cms µM/Newton	289.616	Cms µM/Newton
6.837	Bl Tesla-M	6.27	Bl Tesla-M
0.04	Rub-index	0.017	Rub-index
2.02875609	$R_{MS}=Bl^2/R_{ES}$	0.61473472	$R_{MS}=Bl^2/R_{ES}$

These measurements were carried out with the drivers mounted in 25.6*l* cabinets. Cms therefore incorporates a series capacitance due to the compliance of the volume of air in the cabinet, where that compliance C_{MB} (in units of force/velocity) can be found from the expression

$$C_{MB} = \frac{C_{AB}}{S_D^2} = \frac{V}{\rho c^2 S_D^2}$$

Appendix B

Standing wave ratio methods for determining acoustic impedance

It has been shown in Chapter 3 that the standing-wave pressure field in a duct can be represented by its two travelling components

$$p = \boldsymbol{A}e^{j[\omega t + k(L-x)]} + \boldsymbol{B}e^{j[\omega t - k(L-x)]} \qquad \textbf{B1}$$

from which it can be shown that the (mechanical) duct termination impedance is given by

$$Z_{mL} = \rho_0 c S \frac{\boldsymbol{A}+\boldsymbol{B}}{\boldsymbol{A}-\boldsymbol{B}} \qquad \textbf{B2}$$

The normal-incidence impedance of a sample of material placed at the end of a duct and subjected to an incident plane-wave can then be determined [10,80,82]. If the amplitudes of incident and reflected waves are given as

$$\begin{aligned} \boldsymbol{A} &= A \\ \boldsymbol{B} &= Be^{j\theta} \end{aligned} \qquad \textbf{B3}$$

where θ represents a phase change on reflection, then it follows that

$$\frac{Z_{mL}}{\rho_0 c S} = \frac{1 + \frac{\boldsymbol{B}}{\boldsymbol{A}} e^{j\theta}}{1 - \frac{\boldsymbol{B}}{\boldsymbol{A}} e^{j\theta}} \qquad \textbf{B4}$$

Where the incident and reflected wave interfere constructively, the pressure at the resulting antinode is equal to $\boldsymbol{A} + \boldsymbol{B}$. Where destructive interference occurs, the resulting pressure node has amplitude $\boldsymbol{A} - \boldsymbol{B}$. The standing wave ratio can be measured where

$$SWR = \frac{A+B}{A-B} \qquad \textbf{B5}$$

Rearranging:

$$\frac{B}{A} = \frac{SWR - 1}{SWR + 1} \qquad \textbf{B6}$$

Beranek [81] shows that for practical impedance tubes where losses may occur along the length of the duct, the standing wave ratio is not constant as might be imagined from the above analysis, but decreases as one moves away from the plane of the surface under examination. As long as such losses are small, the surface impedance may conventionally be approximated by measuring a ratio between the minimum *closest* to the sample and the following maximum. The subject of (**B6**) may then be substituted back into (**B4**) in order to determine the surface impedance of the sample. This of course is a potentially complex quantity, which necessitates the measurement of the distance of the first minimum from the sample surface. If (**B3**) is modified so that the θ shift between A and B is achieved by delaying A by $\theta/2$ and advancing B by $\theta/2$, then by substitution into (**B1**) :

$$|p| = \left[(A + B)^2 \cos^2(k(L-x) - \theta/2) + (A - B)^2 \sin^2(k(L-x) - \theta/2)\right]^{1/2} \qquad \textbf{B7}$$

The first minimum then occurs when the cosine term goes to zero at $(k(L-x) - \theta/2) = n\pi/2$, *n odd* and so

$$\theta = 2k(L-x) - \pi \qquad \textbf{B8}$$

This result completes the solution of (**B4**) and the surface impedance can be found.

Appendix C

Pressure and velocity transduction - signal conditioning and calibration

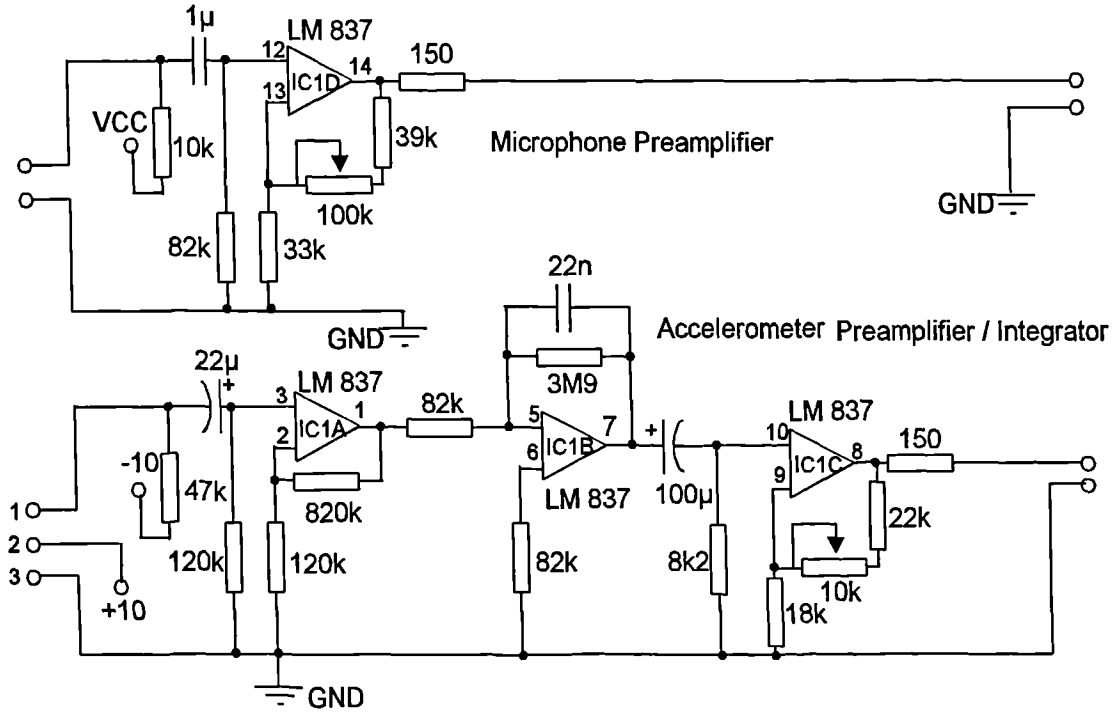

Figure C1 - Signal conditioning circuitry for Senheiser KE4-211-2 and Maplin Electret pressure microphones, and Knowles BU1771 Accelerometer.

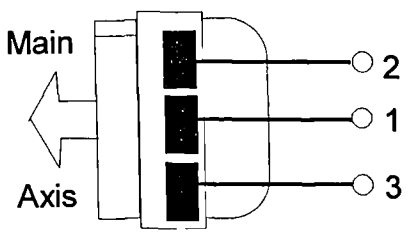

Figure C2 - Accelerometer connection

Refer also to Knowles technical data [74].

The following calibration data use experimental transducers connected to the signal conditioning circuitry illustrated. A reference accelerometer (D.J.Birchall type A/23/E s/n 6168) has charge sensitivity - 7.55 pC/ms^{-2}, and was connected to a charge amplifier (B&K type2635 s/n768919) set to give a velocity sensitivity of 1V/ms^{-1} . The miniature Birchall device was compared to a number of larger B&K units, and was concluded to have a flat response (+- 0.01dB) in the frequency range 20-200 Hz.

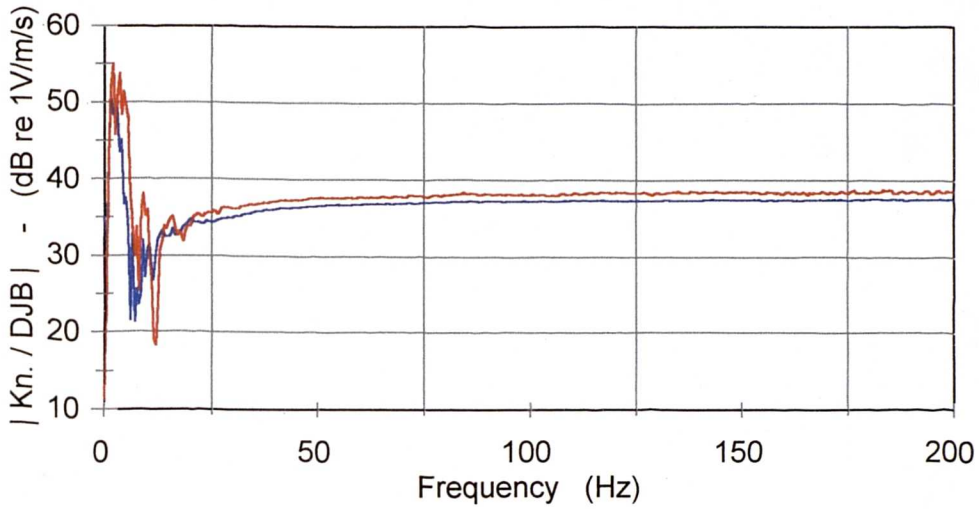

Figure C3: - Magnitude velocity response re: 1V/ms^{-1} *a) BU1771 Unit 1*
b) BU1771 Unit2

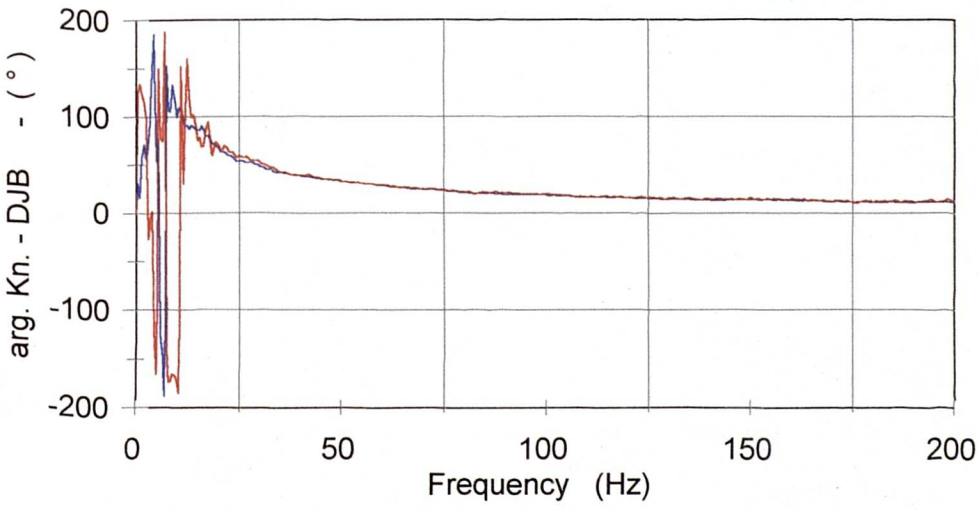

Figure C4: - Phase of velocity response *a) BU1771 Unit 1*
b) BU1771 Unit2

Pressure calibrations compare a proprietary 1/4" electret capsule connected to the above preamplifier with a reference microphone GRAS type 40AF (B&K 4165 equivalent) s/n8881 with B&K type 2619 preamplifier s/n503697. Measurements were made under anechoic conditions (fully anechoic above 100Hz - highly damped modal behaviour at lower frequencies) in a reactive field 5mm from the moving cone of an 8" peerless driver.

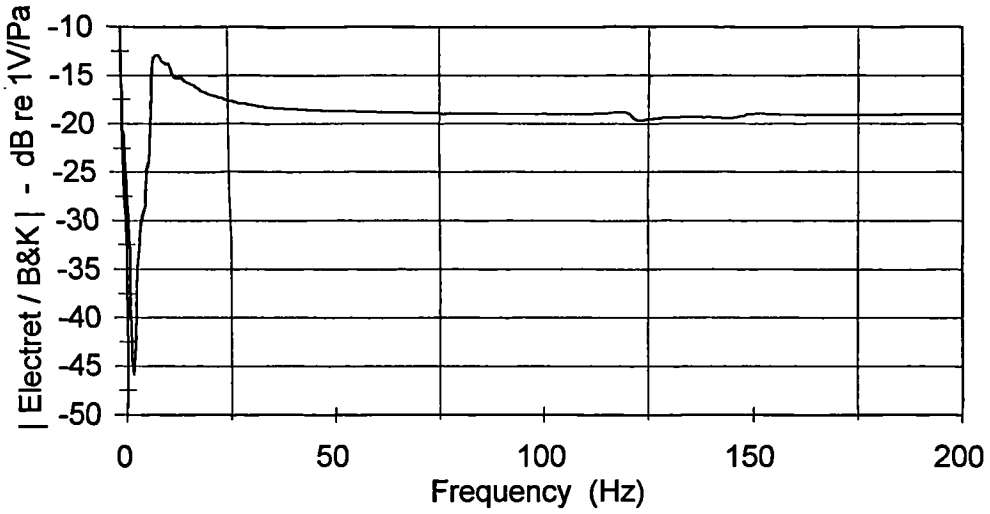

Figure C5 - Magnitude pressure calibration of electret capsule normalised to 1V/Pa

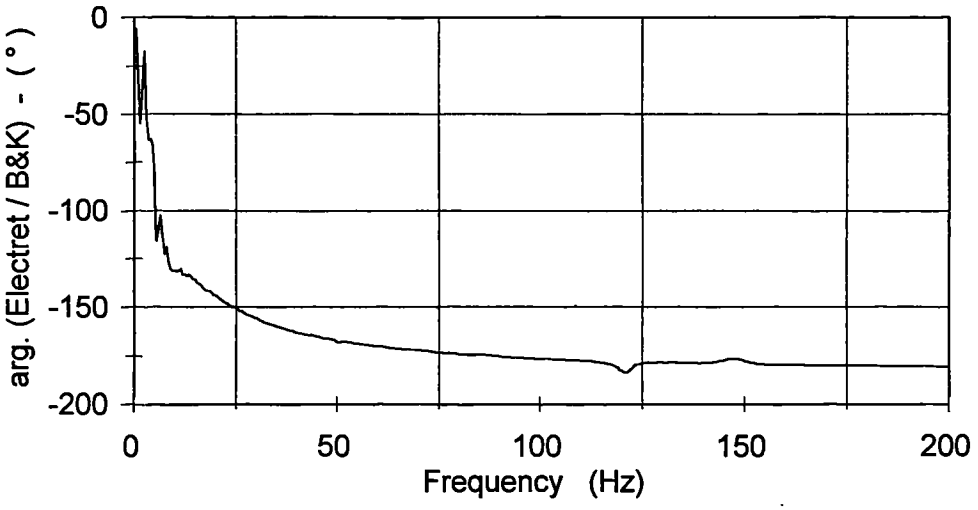

Figure C6 - Phase of pressure calibration of electret capsule

Appendix D

Power amplifier V_o / V_i transfer functions - Quad 306 S/N023461

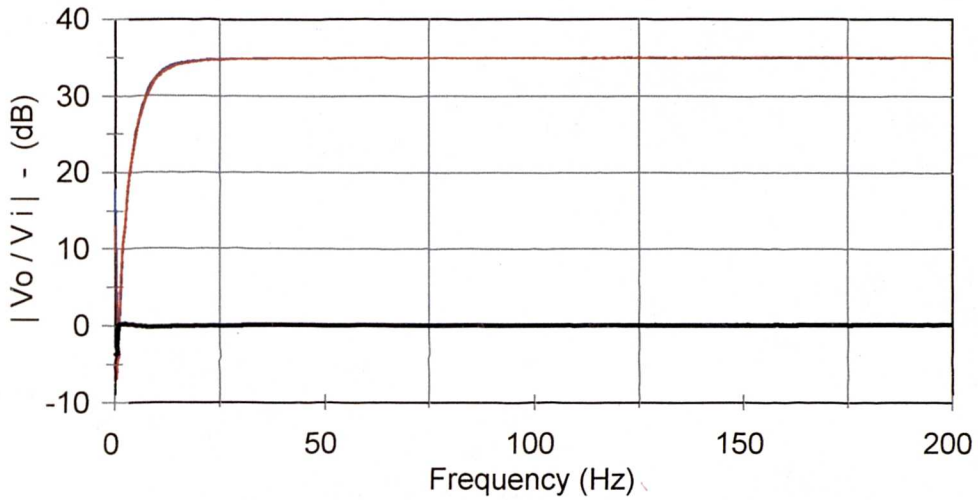

Figure D1: - Magnitude T.F. a) Left Channel b) Right Channel c) Left / Right

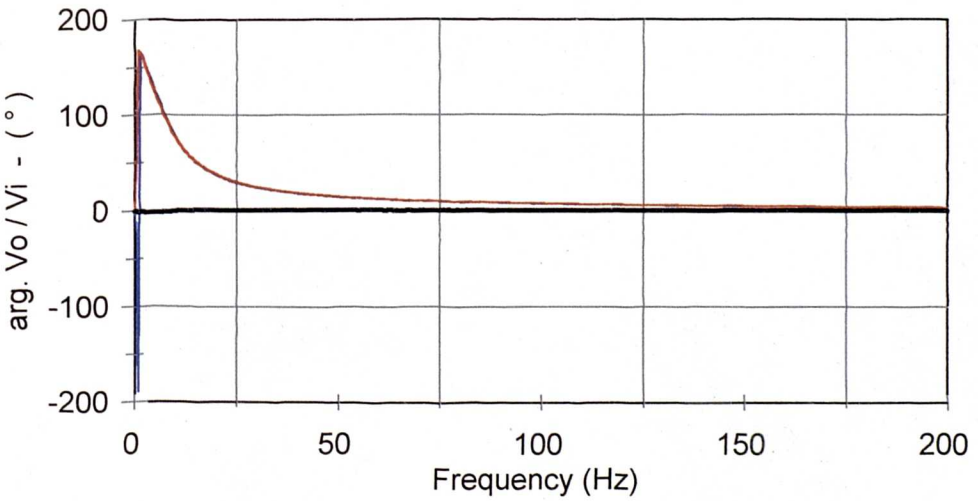

Figure D2: - Phase of T.F. a) Left Channel b) Right Channel c) Left / Right

Appendix E

FORTRAN models

```
cccc  Program to model absorber operation in rectangular room
cccc  This revision detects TOTAL pressure
      real f,u,Q,ro,w,wn(6,6,6),pi,V,Impmag,Imppha,
     >     Ax,Ay,Az,alpx,alpy,alpz,xs,ys,zs,
     >     lx,ly,lz,xa,ya,za,xas,XSS,amag,apha,
     >     sMAG,sPHA,tmag(300),tpha(300),ra,rs,
     >     thi,totmag,totpha,Energy,var,
     >     signflag,Magu(300),AngU(300),omega(300)
      integer i,j
      complex Source,Absorb,Totpres,Ua,Us,tot,Imp
      complex source1,absorb1,totpres1,tot1,ux,uy,uz
      complex SpaceU

cccc  Some intitial variable values
      Energy=0.0
      signflag=1.0
      pi=4*atan(1.0)
      absorb=(0,0)
      source=(0,0)
cccc  a and b are re and im parts of Ua - optimisation start loc.
cccc  These numbers work for our maximum pressure reduction case
      a=-1.148e-2
      b=5.8689e-3
cccc  Try these ones for a fast run with a REAL absorber
c      a=4.33e-2
c      b=3.754e-3

      alpx=0.1
      alpy=0.1
      alpz=0.1
cccc  Radii of source and absorber speakers
      rs=0.105
      ra=0.0815

cccc  First guess at speed of convergence
cccc  (Outside of 'converge' routine so that a successful speed
cccc   can be worked out over a range of frequencies)
      speed=1E-2

cccc  READ IN USER DEFINED VARIABLES

      call input(f,lx,ly,lz,xs,ys,zs,xa,ya,za,j)

cccc  SET UP VARIABLES FROM USER DEFINED INPUT
      W=2.*PI*F
      ro = 1.21
      xas=xa+0.05
      XSS=XS-0.05
      V=LX*LY*LZ
      AX=2.*LY*LZ
      AY=2.*LX*LZ
```

```
      AZ=2.*LX*LY
      AX=ALPX*AX
      AY=ALPY*AY
      AZ=ALPZ*AZ

cccc     To determine possible room resonances
         call natfreq(pi,lx,ly,lz,wn)

cccc     To send program to loop for realising desired impedance
cccc     If requested in input routine

      if (j.eq.1) then
          call Idef(pi,Impmag,imppha,imp,Us)
      else
          call Udef(pi,Us,Ua)
      endif


cccc  Now calculate the source IMPEDANCE  over a range
cccc  of frequencies

      do 10 i=219,300,1

         w=2.*pi*(35.+165.*real(i)/300.)
         omega(i)=w
cccc     use these coordinates for the source location...
c         x=xsS
c         y=ys
c         z=zs
cccc     use these coordinates for our 'listening point'
         x=1.0
         y=1.0
         z=1.5

         if (j.eq.1) call converge(i,a,b,imp,v,pi,lx,ly,
     >   lz,w,wn,ro,ax,ay,az,xas,xa,ya,za,xs,ys,zs,
     >   Us,rs,tot,Ua,ra,speed)

         call fromplex(ua,u,thi)

cccc     Work out total pressure at the point
         print*,I
         call roompres(v,pi,lx,ly,lz,w,wn,ro,Ax,Ay,Az,
     >   x,y,z,xs,ys,zs,Us,rs,tot)
         source=tot
         call roompres(v,pi,lx,ly,lz,w,wn,ro,Ax,Ay,Az,
     >   x,y,z,xa,ya,za,Ua,ra,tot)
         absorb=tot
         totpres=source+absorb
         callfromplex(totpres,totmag,totpha)
c        print*,'totmag=',totmag
         tmag(i)=totmag
         tpha(i)=totpha


cccc           Now work out first approximation to velocity
cccc           Z+1
               z=lz*real(k)/9.
               if (k.eq.10) then
                   z=lz*real(k-2)/9.
                   signflag=-1.
               endif
               call roompres(v,pi,lx,ly,lz,w,wn,ro,Ax,Ay,Az,
     >         x,y,z,xs,ys,zs,Us,rs,tot1)
               source1=tot1
```

```
                call roompres(v,pi,lx,ly,lz,w,wn,ro,Ax,Ay,Az,
     >          x,y,z,xa,ya,za,Ua,ra,tot1)
                absorb1=tot1
                totpres1=source1+absorb1
                Uz=signflag*(-1/ro)*cmplx(0.0,(-1./w))*
     >          (totpres1-totpres)/(lz/9.)
                z=lz*real(k-1)/9.
                signflag=1.0

cccc            y+1
                y=ly*real(j)/9.
                if (j.eq.10) then
                    y=ly*real(j-2)/9.
                    signflag=-1.0
                endif
                call roompres(v,pi,lx,ly,lz,w,wn,ro,Ax,Ay,Az,
     >          x,y,z,xs,ys,zs,Us,rs,tot1)
                source1=tot1
                call roompres(v,pi,lx,ly,lz,w,wn,ro,Ax,Ay,Az,
     >          x,y,z,xa,ya,za,Ua,ra,tot1)
                absorb1=tot1
                totpres1=source1+absorb1
                Uy=signflag*(-1/ro)*cmplx(0.0,(-1./w))*
     >          (totpres1-totpres)/(ly/9.)
                y=ly*real(j-1)/9.
                signflag=1.0

cccc            x=x+1
                x=lx*real(i)/9.
                if (i.eq.10) then
                    x=lx*real(i-2)/9.
                    signflag=-1.0
                endif
                call roompres(v,pi,lx,ly,lz,w,wn,ro,Ax,Ay,Az,
     >          x,y,z,xs,ys,zs,Us,rs,tot1)
                source1=tot1
                call roompres(v,pi,lx,ly,lz,w,wn,ro,Ax,Ay,Az,
     >          x,y,z,xa,ya,za,Ua,ra,tot1)
                absorb1=tot1
                totpres1=source1+absorb1
                Ux=signflag*(-1/ro)*cmplx(0.0,(-1./w))*
     >          (totpres1-totpres)/(lx/9.)
                x=lx*real(i-1)/9.
                signflag=1.0

                spaceu=cmplx(   ( (real(ux)**2)+(real(uy)**2)+
     >                           (real(uz)**2)   )**0.5,
     >                          ( (aimag(ux)**2)+(aimag(uy)**2)+
     >                           (aimag(uz)**2)   )**0.5   )
                call fromplex (spaceu,totmag,totpha)
                MagU(i,j,k)=totmag
                AngU(i,j,k)=totpha*180./pi
                Energy=0.5*ro*(magu(i,j,k)**2)+0.5*(tmag(i,j,k)
     >                 **2)/(ro*(343.**2))

10      continue

cccc    to workout variance with frequency

        call variance(pi,tmag,var,Us)
        call outimp(pi,tmag,tpha,omega,Us,var)

100     format (10(1x,f7.2))
200     format (1x,8(a,f8.1))
        end
```

```
      subroutine converge(count,a,b,imp,v,pi,lx,ly,lz,w,wn,ro,
     > ax,ay,az,xas,xa,ya,za,xs,ys,zs,Us,rs,tot,Ua,ra,speed)

      real ro,w,wn(6,6,6),pi,V,Ax,Ay,Az,xs,ys,zs,
     >     lx,ly,lz,xa,ya,za,xas,ra,rs,newa,newb,
     >     thi,a,b,totmag,totpha,impmag,imppha
      real Esq,da,db,Edsq,REALslope,IMAGslope,speed,
     > OLDRSL,OLDISL,d2rsl,d2isl,D2TOT
      integer i,count,nO UP
      complex Source,Absorb,Totpres,Ua,Us,tot,Imp
      oldrsl=0.0
      oldisl=0.0
      d2tot=0.0
      NO UP=0
cccc  da and db are the small increments to find error slope
      da=1.E-6
      db=1.E-6


cccc     Loop to find converging value for Ua, so that ratio of total
cccc     resulting pressure with Ua agrees with Impmag and Imppha

      do 5  i=1,10000,1

cccc     To determine the pressure at the absorber

         call roompres(v,pi,lx,ly,lz,w,wn,ro,Ax,Ay,Az,
     >   xas,ya,za,xs,ys,zs,Us,rs,tot)

         source=tot

cccc     To determine the pressure at the absorber DUE TO
cccc     Qa

         Ua=cmplx(a,b)
         call roompres(v,pi,lx,ly,lz,w,wn,ro,Ax,Ay,Az,
     >   xas,ya,za,xa,ya,za,Ua,ra,tot)

         absorb=tot
c         call fromplex(absorb,amag,apha)

         totpres=source+absorb
         call fromplex(totpres,totmag,totpha)
         call fromplex(Ua,u,thi)
         call fromplex(imp,impmag,imppha)

         print*,'*******************************************'
         print*,'Impmag=',impmag,'Imppha=',Imppha*180./pi,
     >   'Actual Ua/totp mag.=',U/totmag,'Actual u-p phase=',
     >   (thi-totpha)*180./pi,'count=',count,'a=',a,'b=',b


        Esq=(REAL(Ua/totpres)-REAL(Imp))**2+
     >  (aimag(Ua/totpres)-AIMAG(Imp))**2

cccc  Now step a up by da, hold b

        a=a+da
        Ua=cmplx(a,b)

        call roompres(v,pi,lx,ly,lz,w,wn,ro,Ax,Ay,Az,
     >   xas,ya,za,xa,ya,za,Ua,ra,tot)
        absorb=tot
        totpres=source+absorb
```

```
         Edsq=(REAL(Ua/totpres)-REAL(Imp))**2
     >   +(AIMAG(Ua/totpres)-AIMAG(Imp))**2

         print*,'error diff =',edsq-esq,da,db

         IF(NO UP.EQ.2) OLDRSL=REALSLOPE

         REALslope=(Edsq-Esq)/(da)

         print*,oldrsl,realslope
cccc  Step up b by db, return a to original value

         b=b+db
         a=a-da
         Ua=cmplx(a,b)


          call roompres(v,pi,lx,ly,lz,w,wn,ro,Ax,Ay,Az,
     >    xas,ya,za,xa,ya,za,Ua,ra,tot)

         absorb=tot
         totpres=source+absorb
         Edsq=(REAL(Ua/totpres)-REAL(Imp))**2
     >    +(AIMAG(Ua/totpres)-AIMAG(Imp))**2

         print*,'error diff=',Edsq-esq,da,db

         If(NO UP.EQ.2) oldisl=Imagslope
         IMAGslope=(Edsq-Esq)/(db)
         print*,'OLD A SL.=',oldRsl,'OLD B SL.=',OLDISL
         PRINT*,'ASLOPE=',REALSLOPE,'BSLOPE=',IMAGSLOPE

         b=b-db

cccc     before 27/3/95, convergence limits were 5e-4
cccc     now narrowed for greater accurancy
         if (abs(real(ua/totpres)-real(imp)).lt.1e-4.and.
     >      abs(aimag(ua/totpres)-aimag(imp)).lt.1e-4) then
            goto 6
         endif

c        print*,'Real u/p',real(ua/totpres),'real I',
c     > real(imp),'Imag u/p',aimag(Ua/totpres),'Imag I',
c     > aimag(imp)


cccc First goes at Auto-speed adjustment

      if(NO UP.NE.0) then
         if(realslope*oldrsl.lt.0.
     >   OR.imagslope*oldisl.lt.0) then
            A=a+speed*(OLDRSL)
            B=b+speed*(OLSISL)

            speed=speed/1.01
            print*,'going down'
            NO UP=1
         ELSEif(realslope*oldrsl.GT.0.
     >   or.imagslope*oldisl.GT.0) then
            IF(ABS(REALSLOPE)+ABS(IMAGSLOPE).LT.0.1) THEN
               SPEED=SPEED*(1.+1.E-5/(ABS(REALSLOPE)+
     >          ABS(IMAGSLOPE)))
               PRINT*,'GOING UP'
            ELSE
```

```
     >          SPEED=SPEED/(1.+(ABS(REALSLOPE)+
                 ABS(IMAGSLOPE))/10.)
                PRINT*,'GOING DOWN'
                IF(SPEED.LT.5E-3) SPEED = 5E-3
              ENDIF
              A=a-speed*(REALslope)
              B=b-speed*(IMAGslope)
              NO UP=2
            ELSE
              print*,'Gradients = 0'
              speed=speed/10.0
              a=a/1.1
              b=b/1.1
              NO UP=0
            endif
          else
            A=a-speed*(REALslope)
            b=b-speed*(IMAGslope)
            NO UP=2
          endif
          PRINT*,'SPEED=',SPEED

5         continue

          print*,'Did not converge'
          stop

6         return
          end

          subroutine intocplx(smag,spha,source)
          real smag,spha,sR,sJ
          complex source
          sr=smag*cos(spha)
          sj=smag*sin(spha)
          Source=cmplx(sr,sj)
          return
          end

          subroutine fromplex(source,smag,spha)
          real smag,spha
          complex source
          smag=((real(source)**2)+(aimag(source)**2))**0.5
          spha=atan2(aimag(source),real(source))
          return
          end

          subroutine roompres(v,pi,lx,ly,lz,w,wn,ro,Ax,Ay,Az,
         >x,y,z,xs,ys,zs,U,r,tot)
          real ro,w,wn(6,6,6),pi,V,lamdan,Kn,
         >     Ex,Ey,Ez,Ax,Ay,Az,xs,ys,zs,
         >     lx,ly,lz,theta,x,y,z,DIST,RE,IM,nx,ny,nz,
         >     Rrevac,Jrevac,r
          integer l,M,N
          complex direct,tot,U
          rrevac=0.0
          jrevac=0.0

CCCC      TO FIND STRAIGHT LINE DIST FROM SCE TO MEAS. POINt
          DIST=( (X-XS)**2+(Y-YS)**2+(Z-ZS)**2) **0.5

          RE=(SIN(W*DIST/343.))/(4.*PI*DIST)
          IM=(COS(W*DIST/343.))/(4.*PI*DIST)

          DIRECT=CMPLX(RE,IM)
```

```
      do 40 L=1,6,1
         nx=real(l)-1.
         do 50 M=1,6,1
            ny=real(m)-1.
            do 60 N=1,6,1
               nz=real(n)-1.
               IF (WN(L,M,N).gt.0.01)
     >                THEN
                EX=1.
                EY=1.
                EZ=1.
                IF (L.NE.1) EX=2.
                IF (M.NE.1) EY=2.
                IF (N.NE.1) EZ=2.
                LAMDAN=1./(EX*EY*EZ)
                KN=(343./(8.*V))*(0.5*EX*AX+0.5*EY
     >             *AY+0.5*EZ*AZ)

cccc            To evaluate shape func for source
                call shapefnc(nx,ny,nz,pi,lx,ly,lz,
     >                  xs,ys,zs,theta)
                re=2.*wn(l,m,n)*kn*theta
                im=-(w**2-wn(l,m,n)**2)*theta

CCCC            To evaluate shape function for point we're at
                call shapefnc(nx,ny,nz,pi,lx,ly,lz,
     >                     x,y,z,theta)

                re=re*theta
                im=im*theta

                re=re*(1/lamdan)/( ((2.*wn(l,m,n)
     >          *kn)**2)+((w**2)-(wn(l,m,n)**2))**2)

                im=im*(1/lamdan)/( ((2.*wn(l,m,n)
     >          *kn)**2)+((w**2)-(wn(l,m,n)**2))**2)

                rrevac=rrevac+re
                Jrevac=jrevac+im
                ENDIF
60           continue
50        continue
40     continue

       rrevac=(real (direct)+((343**2)
      >       /v)*rrevac)
       jrevac=(aimag(direct)+((343**2)
      >       /v)*jrevac)

       tot=cmplx(rrevac,jrevac)
c       print*,u*2*pi*r**2
       tot=tot*(U*2*pi*r**2)*w*ro
       return
       end


       subroutine natfreq(pi,lx,ly,lz,wn)
       real pi,lx,ly,lz,wn(6,6,6),w,nx,ny,nz
       do 10 i=1,6,1
          nx=real(i)-1.0
          do 20 j=1,6,1
             ny=real(j)-1.0
             do 30 k=1,6,1
                nz=real(k)-1.0
                w=pi*343.*( ( ((nx/lx)**2)+((ny/ly)**2)+
```

```
     >           ((nz/lz)**2)  )**0.5)
                wn(i,j,k)=w
c                print*,w
30            continue
20          continue
10       continue
         return
         end


         subroutine shapefnc(nx,ny,nz,pi,lx,ly,lz,xs,ys,zs,theta)
         real pi,lx,ly,lz,nx,ny,nz,xs,ys,zs,theta
         theta=cos(pi*nx*xs/lx)*cos
        >(pi*ny*ys/ly)*cos(pi*nz*zs/lz)
         return
         end


         subroutine outimp(pi,tmag,tpha,omega,Us,var)
         real omega(300),tmag(300),tpha(300),Z
         real umag,upha,pi,var
         integer i
         complex us
         character magname*12,phaname*12,pathname*6
         pathname='c:\ep\'

         print*,'Enter a filename for mag. output'
         read 300,magname
         print*,'Enter a filename for phase output'
         read 300,phaname
         magname(8:)='.imp'
         phaname(8:)='.imp'
         OPEN(5,FILE =magname)
         OPEN(6,FILE=pathname//phaname)
         magname(8:)='.vll'
         phaname(8:)='.vll'
         OPEN(7,FILE=pathname//magname)
         OPEN(8,FILE=pathname//phaname)

         call fromplex(Us,Umag,Upha)
         do 10 i=1,300,1
            z=tmag(i)/Umag
            write(5,100) omega(i)/(2.*pi),tmag(i)

 10      continue
         print*,var
         write(5,*) 'variance=',var

         print*,'Total energy in the room (NOT corrected for'
         print*,'elemental vol.) =',energy

         close (5)
         close (6)
         close (7)
         close (8)
 100     format (10(1x,f7.2))
 200     format (10(1x,f6.5))
 300     format (a)
         return
         end
```

```
      subroutine input(f,lx,ly,lz,xs,ys,zs,xa,ya,za,i)

      real f,lx,ly,lz,xs,ys,zs,xa,ya,za
      integer i
      pi=4*atan(1.0)
      print*,'Enter frequency of source vibration'
      read*,f
      print*,'Enter room dimensions:- x=(m)'
      read*,lx
      print*,'Enter room dimensions:- y=(m)'
      read*,ly
      print*,'Enter room dimensions:- z=(m)'
      read*,lz
      print*,'Enter location of source'
      print*,'x-coordinate =(m)'
      read*,xs
      print*,'y-coordinate =(m)'
      read*,ys
      print*,'z-coordinate =(m)'
      read*,zs
      print*,'Enter location of absorber'
      print*,'x-coordinate =(m)'
      read*,xa
      print*,'y-coordinate =(m)'
      read*,ya
      print*,'z-coordinate =(m)'
      read*,za
      print*,'Do you want to specify an impedance at the absorber'
      print*,'(u/p, mag and phase) (1), or would you rather enter'
      print*,'values for the magnitude of Us and Ua, and the phase'
      print*,'between them (2)?'
      read*,i
      return
      end



      subroutine Idef(pi,Impmag,imppha,imp,Us)
      real impmag,imppha,pi,U
      complex imp,Us
      print*,'What impedance do you want the absorber to
     >implement?'
      Print*,'Mag of u/p ='
      read*,Impmag
      Print*,'Phase of <u-<p (degrees)'
      read*,Imppha
      print*,'Enter velocity of source(m/s)'
C      read*,u
      u=0.113
      Us=u*cmplx(1,0)
      Imppha=Imppha*pi/180.

      call intoCplx(impmag,imppha,imp)
      return
      end

      subroutine Udef(pi,Us,Ua)
      real u,thi,pi
      complex us,ua
      print*,'Enter magnitude of Us (m/s)'
      read*,u
      Us=u*cmplx(1,0)
      print*,'Enter magnitude of Ua (m/s)'
      read*,u
```

```
      print*,'Enter phase of Ua-Us (deg.)'
      read*,thi
      thi=thi*pi/180.
      ua=u*cmplx(cos(thi),sin(thi))
      return
      end

      subroutine variance(pi,tmag,var,Us)
      real pi,tmag(300),mean,var,umag,upha
      complex Us
      integer i
      mean=0.0
      var=0.0
      call fromplex(us,umag,upha)

      do 10 i=1,300
c          mean=mean+tmag(i)
         mean=mean+20*log10(tmag(i)/2.e-5)
10    continue
      mean=mean/300.
c      mean=mean/umag
      do 20 i=1,300
c          var=var+((tmag(i)/umag)-mean)**2
         var=var+(20.*log10(tmag(i)/2.e-5)-mean)**2
20    continue
      var=var/300.
      return
      end
```

Subsequent duct and room models were constructed using the package 'MATLAB', using similar numerical implementations of a modal decomposition as displayed here.

Appendix F

Map of Test Room, Source and Receiver Locations

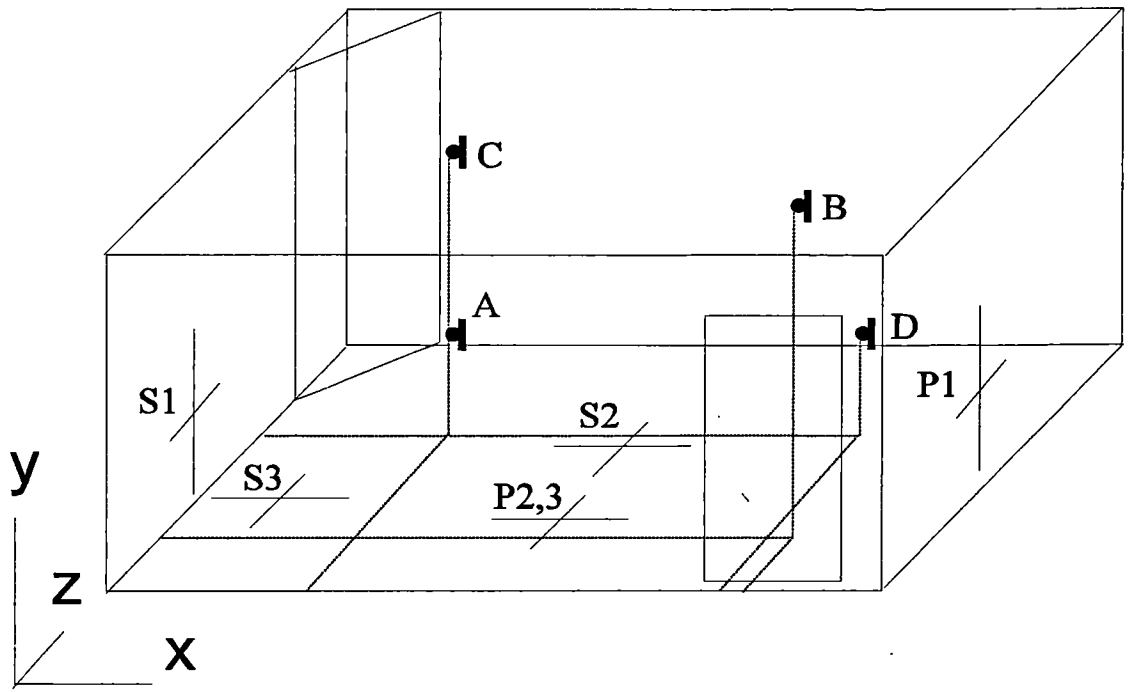

Room Dimensions - 3.95 x 3.15 x 2.38 (X by Y by Z)

Source Locations	**Primary**	**Secondary**
Set 1	(3.8,1.0,1.0)	(0.15,1.0,1.0)
Set 2	(1.9,0.3,0.86)	(1.9,0.23,1.73)
Set 3	(1.9,0.3,0.86)	(0.18,0.23,1.0)

Receiver Locations	
A	(1.0,1.0,1.5)
B	(3.0,2.24,0.65)
C	(1.0,2.2,1.5)
D	(2.95,1.0,1.5)

Appendix G

Solution for lightly damped modes according to Morse and Bolt

Morse and Bolt [4] adopt the trial solution to the wave equation

$$\psi_n(x) = \cosh(jk_n x - \phi_n) \qquad \textbf{G1}$$

This can be re-written in terms of its exponential identity [5] to give

$$\psi_n(x) = \frac{e^{(jk_n x - \phi_n)} + e^{(-jk_n x + \phi_n)}}{2} \qquad \textbf{G2}$$

The solution is now seen to represent two waves travelling in opposite directions. These waves are related to each other by

$$\begin{aligned} &\textit{amplitude ratio} = e^{-2\mathbb{R}(\phi_n)} \\ &\textit{phase change} = -2\mathbb{I}(\phi_n) \end{aligned} \qquad \textbf{G3}$$

A locally reacting boundary of specific acoustic impedance ζ can be expressed by the condition

$$\zeta\frac{\delta p}{\delta x} + jkp = 0$$

$$\textit{where } \zeta = \frac{Z_a}{\rho c S} \qquad \textbf{G4}$$

and x is the direction normal to the boundary

and substitution of (**G1**) into the boundary condition of (**G4**) at $x=0$ gives

$$\phi_n = -\coth^{-1}\left(\frac{\zeta_{x_0} k_n}{k}\right) \qquad \textbf{G5}$$

and when $x=L$,

$$\phi_n = jk_nL + \coth^{-1}\left(\frac{\zeta_{x_L}k_n}{k}\right) \qquad \textbf{G6}$$

Eliminating ϕ_n gives

$$jk_nL + \coth^{-1}\left(\frac{\zeta_{x_L}k_n}{k}\right) + \coth^{-1}\left(\frac{\zeta_{x_0}k_n}{k}\right) = 0 \qquad \textbf{G7}$$

The roots of this equation define the eigenvalues k_n. There are an infinite number of solutions, and the approach to finding the roots depends on the impedance at the boundaries. When $\zeta_x \gg 1$, the first terms of a series expansion for $\coth^{-1}$ [70] can be employed where

$$\coth^{-1}(z) = \left(\frac{1}{z} + \frac{1}{3z^2} + \ldots\right) \qquad \textbf{G8}$$

so that

$$k_n = (jk/L)^{1/2}(1/\zeta_{x_0} + 1/\zeta_{x_L})^{1/2}\left[1 - \frac{jkL}{6}\cdot\frac{(1/\zeta_{x_0}{}^3 + 1/\zeta_{x_L}{}^3)}{(1/\zeta_{x_0} + 1/\zeta_{x_L})^2} + \ldots\right] \qquad \textbf{G9}$$

$n=0$

$$k_n = \frac{n\pi}{L} + \frac{jk}{n\pi}(1/\zeta_{x_0} + 1/\zeta_{x_L}) + \frac{k^2L}{\pi^3n^3}(1/\zeta_{x_0} + 1/\zeta_{x_L})^2 + \ldots \qquad \textbf{G10}$$

$n>0$

These eigenvalues can now be substituted into (**G2**) to find the modeshapes. As long as the walls are fairly hard, terms in powers of $1/\zeta$ higher than 2 can be neglected [4]. Then, using the first term of the coth expansion from (**G8**):

$$\psi_n(x) = \cosh\left(\left[\frac{kl}{j(1/\zeta_{x_0} + 1/\zeta_{x_L})}\right]^{1/2}\frac{1}{L}(L/\zeta_{x_0} - x/\zeta_{x_0} - x/\zeta_{x_L})\right)$$

$n=0$

$$\psi_n(x) = \cosh\left(\left[\frac{jn\pi x}{L}\right] - \frac{k}{n\pi}\left[(x/\zeta_{x_0} + x/\zeta_{x_L}) - \frac{L/\zeta_{x_0}}{1 + \dfrac{jkL(1/\zeta_{x_0} + 1/\zeta_{x_L})}{n^2\pi^2}}\right]\right) \qquad \textbf{G11}$$

$n>0$

Examples of this expression for the eigenvector are shown in Figure G1, where the impedance is taken as equal on opposing walls and where *a)* $\zeta \to \infty$, *b)* $\zeta=5$ and *c)* $\zeta=2$. The modeshape is shown for mode order $n=4$, and driving frequency $k=k_4$. Case *c)* ties up

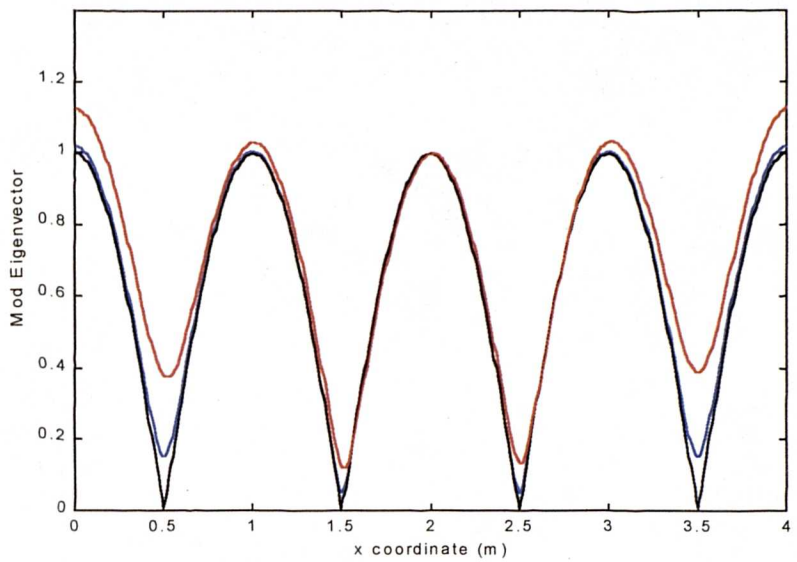

Figure G1 - Modeshapes where $n=4$, $k=k_4$
a) $\zeta \to \infty$ b) $\zeta=5$ c) $\zeta=2$

well with the plate by Kuttruff [11] mentioned in Chapter 3, although the validity of the series truncations used to derive **(G11)** must be in some doubt as the specific boundary impedance lies so close to unity. Bullmore [5] states that the main source of error in **(G11)** arises as a result of truncating the $\coth^{-1}$ expansions used in the solution of **(G7)**. Inclusion of terms in $(1/\zeta)$ up to power two in the expansions yields somewhat unwieldy expressions which have been plotted in Figure G2 for comparison with those plotted in Figure G1.

The fact that both curves lie very close in value lends weight to the idea that **(G11)** may be valid when the termination impedance is rather closer to characteristic than had originally been suggested. Figure G2 further suggests that the steep gradient of the function remote from its turning points means that the truncation error will be most significant in these frequency regions.

As ζ is reduced further and the termination becomes characteristic, the two curves start to diverge. Figure G3 shows the result of including terms in $(1/\zeta)$ up to power two in the expansions, when $\zeta=1.01$. There is now a substantial asymmetry about the centre of the

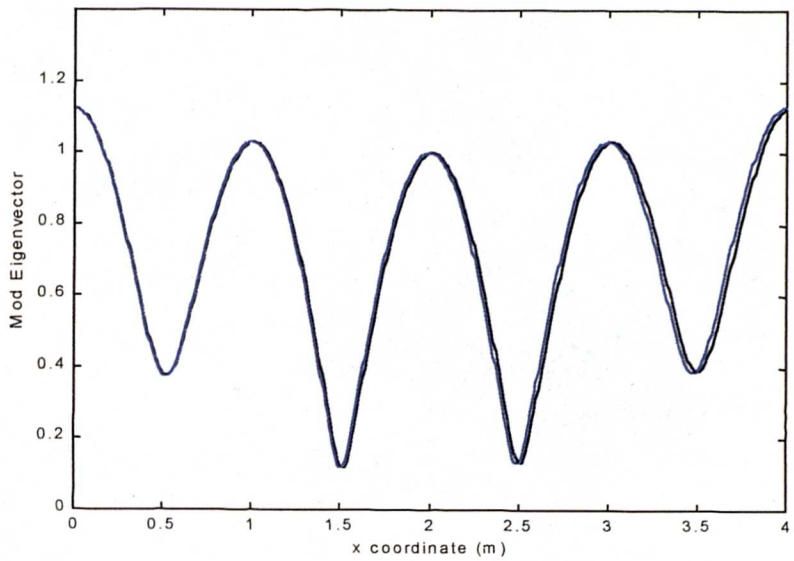

Figure G2 - Modeshapes where $n=4$, $k=k_4$, $\zeta_0 = \zeta_L = 2$.
a) incl. terms up to $(1/\zeta)^2$ b) incl. terms up to $(1/\zeta)$

duct, which is unexpected since symmetrical boundary conditions apply. This asymmetry is partially addressed by including terms in ζ^2, although it appears that substantial errors are still incorporated within the modeshape.

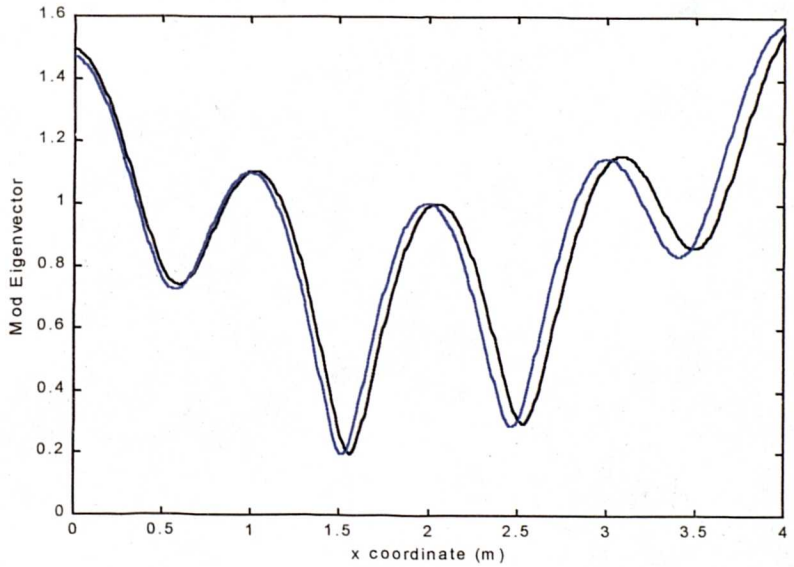

Figure G3 - Modeshapes where $n=4$, $k=k_4$, $\zeta_0 = \zeta_L = 1.01$
a) incl. terms up to $(1/\zeta)^2$ b) incl. terms up to $(1/\zeta)$